1971

Effects of system nonlinearities on synchronous machine control

Asimiyu A. Oyetunji
Iowa State University

Effects of system nonlinearities on synchronous machine control

by

Asimiyu A. Oyetunji

A Dissertation Submitted to the
Graduate Faculty in Partial Fulfillment of
The Requirements for the Degree of
DOCTOR OF PHILOSOPHY

Major Subject: Electrical Engineering

Approved:

Signature was redacted for privacy.

In Charge of Major Work

Signature was redacted for privacy.

For the Major Department

Signature was redacted for privacy.

For the Graduate College

Iowa State University
Ames, Iowa

1971

TABLE OF CONTENTS

LIST OF TABLES

LIST OF FIGURES

Figures

Figures

I. INTRODUCTION

A. Preamble

The necessity of interconnecting several power systems is becoming increasingly important. As the interconnections grow, the need to automatically control the system, particularly during transient conditions, also becomes necessary. This calls for proper and more detailed representation of the alternators for purposes of system analysis. The concern here is with a time span of a few cycles or seconds during which the system response is completely automatic, and so short a period that operator intervention is not possible.

A synchronous machine can be represented in several ways for purposes of stability or dynamic studies. The choice of a model or machine representation depends on the type of assumptions considered valid for the type of machine and on the degree of accuracy desired in the results. Thus one can start with the representation of an "ideal" synchronous machine and then include, as necessary, the effects of those elements which make the machine deviate from the ideal. An ideal machine may be defined as a machine possessing no saturation effects, whose rotor and stator surfaces are shaped, and the electrical windings are distributed in such a way as to produce only fundamental frequency currents and voltages under balanced, synchronous speed, steady state operation.

Of course, practical machines are not ideal. A major factor contributing to the departure from the ideal is the existence of several nonlinearities appearing not only in the machine but also in the associated control components.

The purpose of this thesis is to identify some of the nonlinearities in a power system and some of the assumptions commonly made in building a machine model and then to determine how they manifest themselves in the output variables of the system model.

B. Summary

A brief review of the literature pertinent to this work is given in Chapter II. Chapter III contains the development of the machine models. In Chapter IV the effects of the two major exciter nonlinearities, amplifier limiting and exciter saturation, on the nondynamic parameters of the excitation system are studied. The effects of these exciter nonlinearities on a linear model of the synchronous machine are studied in Chapter V. A nonlinear model of the machine is analyzed in Chapter VI. Here the influence of the exciter nonlinearities and machine saturation on the machine output variables are studied.

Chapter VII contains the conclusions of the studies and some suggestions for future work in this area. The list of references is in Chapter VIII. The appendices are patterned after the main body of the thesis. Thus Appendix A deals with the excitation system, Appendix B is on the linear model and Appendix C covers the nonlinear model.

II. REVIEW OF LITERATURE

A. Nonlinearity and System Modeling

Various simplifying assumptions are always made in developing a mathematical model for a system. Even though almost every physical system is inherently nonlinear, neglecting nonlinearities is about the most common assumption. As the techniques for obtaining solutions for the mathematical models improve over the years, the various assumptions made in developing earlier models are gradually being re-examined.

The power system models currently being used have been developed along the two reaction theory approach which was initiated by Park (96, 97). Synchronous machine reactances developed by Prentice (105), the per unit system developed by Rankin (106, 107) and the modified normalization developed by Lewis (74) were all in line with the two reaction theory. Several analyses of the synchronous machine are contained in the literature (5, 33, 66, 74), and some of them (5, 33) employ the modern control techniques in their analyses.

The increasing complexity, both in design and operations, of the present day power systems requires more detailed system models and one of the many ways of providing the necessary detail is to include, in one form or another, the system nonlinearities (57, 89, 91, 94, 104, 108, 109, 116, 119, 136, 142).

B. Types of Nonlinearities

The nonlinearities in a power system exist in many different forms. Those very commonly mentioned in the literature are the nonlinearities due

to machine saturation, nonlinearities due to speed, saliency and the control section, ie. nonlinearities due to amplifiers, limiters, exciter saturation (5, 6, 82, 91, 108, 121, 140). The major nonlinearities of a hydro governing system are the variation of turbine characteristics with load and constraint on the motion of the turbine wicket gates (133).

Another type of nonlinearity is that associated with the nonlinear system of equations which result whenever one models an alternator (4, 5, 6, 35, 83, 110, 116). This type of nonlinearity shows up as speed voltage terms in system equations and is interesting because it depends on the way in which the original time varying differential equations are transformed.

C. The Excitation System

Because of its direct effects on the initial operating conditions and its fast response as compared to the governor and load frequency control, the excitation system has received wide coverage in the literature (9, 12, 17, 19, 20, 26, 28, 44, 55, 91, 108, 136).

Amplifier limiting and exciter saturation are the commonly mentioned nonlinearities in the excitation system. However, several authors and machine designers in different organizations use somewhat different techniques in handling exciter saturation (13, 40, 52, 82).

D. The Alternator

Perhaps the most important nonlinearities in an alternator are those due to saturation. Among these are tooth saturation due to air gap flux, saturation due to stator slot leakage, yoke saturation, and rotor

saturation in both round rotor and salient pole machines (121). The nonlinear inductances in the machine often cause subharmonic oscillation which may lead to outages (108, 140).

At present there is no general agreement concerning representation of machine saturation. While various authors neglect saturation completely, others represent saturation only in the direct axis of the machine and a few represent saturation in both the direct and quadrature axes (14, 25, 36, 57, 72, 89, 90, 91, 94, 108, 109, 119).

However, the presence of nonlinearities in the system essentially invalidates the use of two-axis quantities which are derived by the application of the superposition principle. Hence representing saturation effects in the direct and quadrature axes is still to be considered an approximation (108, 109, 119).

E. Load Nonlinearities

Power system loads are, in general, nonlinear. However, because of their usually remote location from the machine terminals, most authors treat system loads as a constant impedance.

The stochastic load variations may be considered to be of scheduling concern and not so much a stability problem (22, 101). Where system stability and control problems are concerned, the literature contains adequate evidence showing that significant differences exist between the results obtained when load nonlinearities are neglected and when they are included in the studies (1, 18, 42, 89, 91, 132). Several methods of representing loads have been proposed (11, 60, 94, 109).

Although load nonlinearities are of direct concern in the study of system stability, no effort will be made here to improve upon techniques already proposed. Instead, our effort will be concentrated on the generator and generator controls.

F. System Damping

Damping in a control system falls into two main categories: "induced" damping and "forced" damping. In the synchronous machine the damping produced by the various machine torques may be called "induced" damping (20, 65, 81, 126). The "induced" damping is usually not enough to combat the problems of stability and control of a power system. An evidence of this is the existence of extensive literature on how to best produce "forced" damping (14, 34, 44, 57, 59, 77, 91, 111-116, 136).

A relatively new type of "forced" damping is the use of d-c link to provide damping in a parallel ac-dc power system (23, 99, 100). However, this is not an economically justifiable reason for constructing a d-c line.

Another category of damping is the fictitious damping that needs to be included in a linear model of a power system in order that the model may be more stable or in order that the response of the linear model appears similar to that of the actual system (36, 50, 70).

G. Method of Analysis

Several linear methods of analysis and synthesis such as Bode plots, eigenvalue tests, Nyquist's criterion, root locus plots and Routh Hurwitz

criterion have been applied to linear models of power systems (5, 19, 24, 58, 75, 82, 98).

Studies of power system stability and control have developed along two distinct paths. The first is the digital computer approach and is an extension of the well established network analyzer simulation (6, 35, 47, 79, 82, 90, 91, 104, 124, 125, 132, 135). The second approach, based on Park's equations (96, 97), is the use of analog computers and provides a more detailed representation of the synchronous machine (2, 3, 10, 13, 79, 87, 109, 110, 115, 116, 118, 119).

Some of the studies involving the nonlinearities in the synchronous machine have developed along the line of field theory (15, 56, 67, 68).

Recent advances in nonlinear control theory have significant impact on power system stability studies. Several texts are now available in nonlinear control theory (37, 41, 46, 69, 71, 80, 102). As a result of these developments Lyapunov's methods, Popov's method and Zubov's method have been applied to power system stability studies (31, 43, 69, 76, 95, 120, 126, 130, 131, 139, 143).

Some papers on the nonlinear nature of power system have been spurred by the latest developments in optimal control theory (122, 123, 137).

H. Scope of the Investigation

The foregoing sections A-G pose several questions with respect to the automatic control and stability analysis of a power system. Some of the questions thus raised motivate the study contained in this dissertation.

Young (142) emphasized the need to have several mathematical models of a synchronous machine with varying degrees of complexity so that, depending on the nature of the study, one can choose any model as needed. The increasing importance of stability and related studies on the power system dynamics gives this approach much credibility.

Tinney (128) mentioned the fact that many of the present day stability studies neglect complications such as limiters, saturation and other nonlinearities which cause difficulties. Reviewing the references cited under Method of Analysis (section G) leads one to support Tinney's view. This makes one wonder about the importance of including or neglecting the system nonlinearities on various system studies.

As noted earlier the commonly mentioned nonlinearities in a power system are those due to the machine saturation, the exciter saturation and the amplifier limiting. Several authors have emphasized the need to represent some or all of these nonlinearities in stability and related studies (14, 25, 36, 40, 57, 72, 89, 91, 94, 108, 109, 119, 131, 143).

All but one (72) of these references mentioned the nonlinearity represented in their work only insofar as was deemed necessary to obtain satisfactory results, that is, not with the explicit purpose of studying the effect of nonlinearities.

Lemay and Barton (72) studied the small perturbation linearization of the saturated synchronous machine equations. The purpose of their paper was "to describe the correct method of including saturation in the small perturbation equations of a synchronous generator and to use the modern concepts of modal analysis to measure the importance of the effect of saturation on the unregulated behavior of the machine." The paper

represented saturation in the direct axis. Among the conclusions reached is that the eigenvalues and eigenvectors of the system state-matrix give a quantitative measure on the effect of saturation on the modal components of the machine response.

From the foregoing considerations, it is considered appropriate to study the effects of system nonlinearity on system performance. The nonlinearities considered in this study are the exciter saturation, the amplifier limiting and the machine saturation represented in the direct and quadrature axes of the machine. Four mathematical models of a synchronous machine are developed. Using the analog computer, the effects of the excitation system nonlinearity on three of the models are studied. Studies of the fourth and the most detailed model include saturation in direct and quadrature axes.

III. MACHINE MODELS

The purpose of this chapter is to outline the different machine models which are used in the succeeding chapters. Only the basic equations used in deriving the small signal models are given in this chapter and the details of manipulating these equations to obtain the simulated form of the equations are covered in the appendices.

An ideal synchronous machine is a machine without saturation effects and a machine where the rotor and stator surfaces are shaped and their electrical windings are distributed so as to produce only fundamental frequency currents and voltages under balanced, synchronous speed, steady-state operation at synchronous speed (142).

For any studies involving the synchronous machine, the complete set of machine equations of an ideal machine may be used with a correction for saturation effects. However, this requires considerable detail in representing the system; otherwise, the results may be misleading. A rigorous solution of the problem would require that the machine representation, the transformers, the transmission lines and even the loads would have to be represented by their differential equations. This approach would rapidly increase the complexity of the computation to the extent that only a relatively simple system would be represented either on an analog computer or even on a large-scale digital computer.

Therefore the type of studies to be made should be carefully considered, following which the appropriate simplifying assumptions can be made. In general the fewer the simplifying assumptions, the more complex the machine representation.

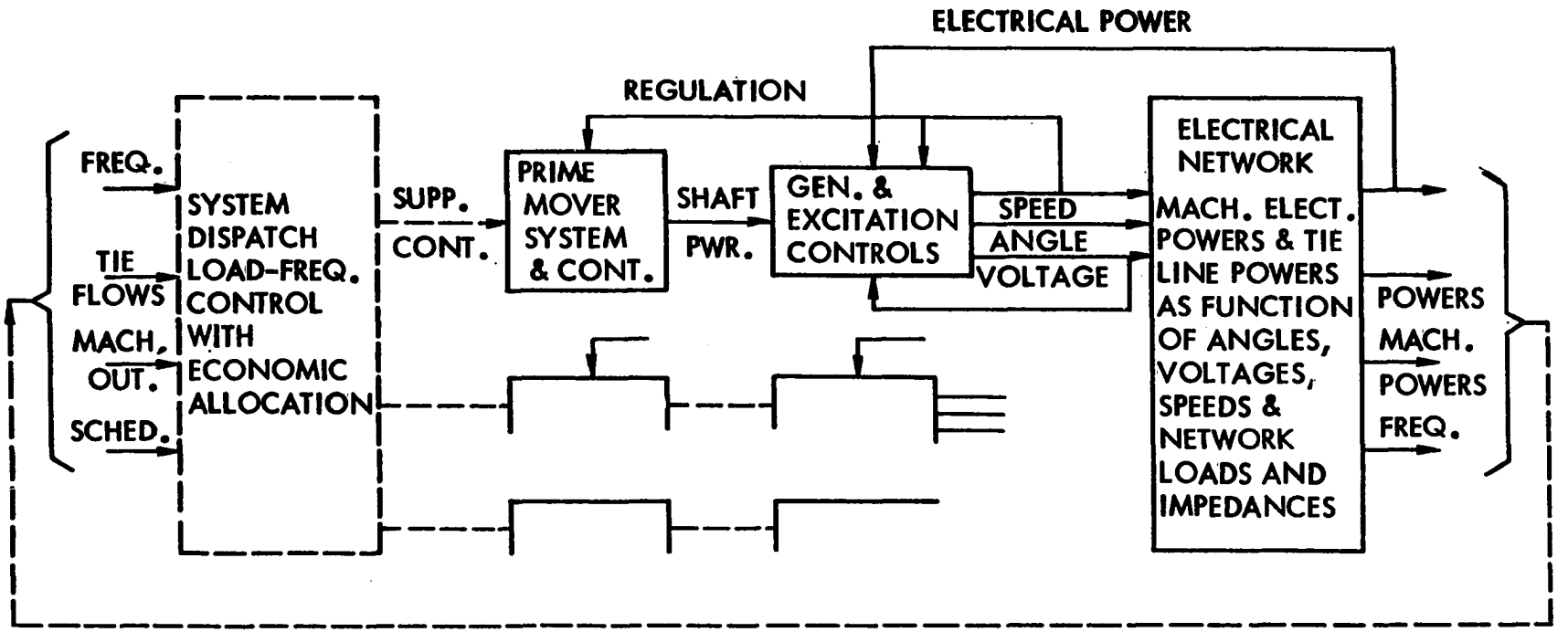

Figure 1. Schematic of power system and controls

The dimensions and complexity of a power system dynamics can be visualized from Figure 1 which shows a schematic diagram of power system and controls (23). Similar figures are contained in references 5 and 16. Several hundreds of interacting elements, including the generators with their prime movers, energy supply systems and control, are involved in the system. A mathematical representation of each element generally involves a set of high order nonlinear differential equations. However, it is not often that all areas need to be represented simultaneously in equal detail. Various opportunities for simplifications arise in several ways:

1) Since the several elements of the power system have different time constants, the duration of effects and resolution in time over which the effects are of significance can be used to simplify a model. For example, it is not necessary to represent boiler transients which develop over several minutes if the transient stability phenomena over a second or two are the primary effects under investigation. Extremely fast transients such as switching transients of high frequencies need not be represented for this same problem.
2) Some simplifications arise from the range of variables under consideration. For example, the assumption of constant speed in the generated voltage equations and constant frequency for the network impedance parameters is perfectly justified in normal power system transients where frequency excursions are small (Chapter 2, section 2.1 of reference 5).

3) The number of elements of a kind that need to be represented sometimes form a basis for simplification. An example of this is the study of the case of the single machine against an infinite bus. Many concepts about a power system can be developed from this study. However, there are a few fundamental effects, such as the study of detailed control effects, that cannot be studied better on a one- or ten-machine system representation than on a 100-machine representation.
4) The loading of a system may offer opportunities for simplification. For example, effect of saturation is less at low voltage or at leading power factor operation.

A. Modeling Philosophy

Using somewhat different simplifying assumptions, four machine models are developed. The philosophy used in developing the models from the control theory and power system points of view is presented in this section.

Basically the synchronous machine with its associated control equipment may be considered to be a multiple input and multiple output control system. Depending upon which output variable is to be corrected, the corresponding input variable can be varied appropriately. Sometimes varying one input affects all the output variables but, in general, the effect of changing an input variable is always more pronounced on some output variables than the others.

The mechanical torque, τ_m, and the exciter voltage, v_f, are probably the most important input variables of a synchronous machine. The load torque primarily determines the mechanical or megawatt output of the machine while the field voltage primarily determines the reactive or megavar output of the machine.

Many output variables of a synchronous machine are observable. Of these the most important, at least from the system operator's point of view, are the machine power output, P, or the electrical torque, τ_e, the rotor speed, ω, or the frequency and the machine terminal voltage, v_t.

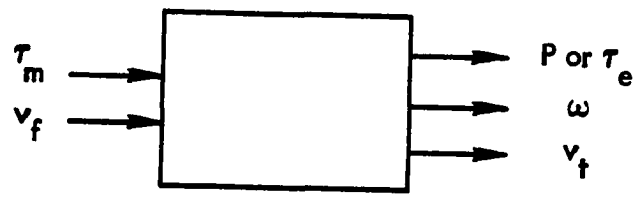

Figure 2. A general synchronous machine block diagram

The foregoing is summarized in Figure 2. The field voltage, v_f, is an output variable of the excitation system. Apart from the system feedback and compensating signals, the main input of the excitation system is the reference voltage, v_{ref}. A change in v_{ref} therefore leads to a corresponding change in v_f.

In terms of the introductory statements made at the beginning of this chapter, the foregoing focuses attention on the fact that it is not only the detail or time region of interest which determines the model to be used but also the kind of response desired. The response due to a step

change in the reference voltage, v_{ref}, is not necessarily the same as that resulting from a step change in the mechanical torque, τ_m.

The choice of simplifying assumptions and the type of response desired lead to different mathematical models for the synchronous machine.

B. Model I - A First Order Approximation

Model I, which is a first order approximation of the synchronous machine, is the simplest of the four models discussed. The assumptions used in developing this model and their comparison with the assumptions used in the remaining models are shown in Table 1 (see end of the chapter).

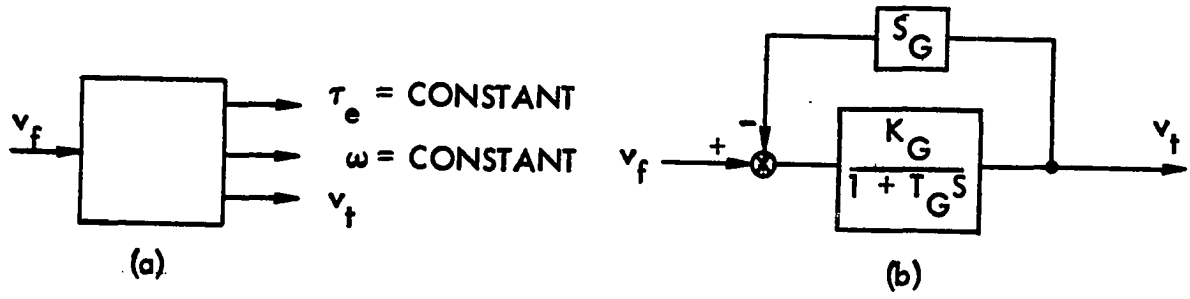

Figure 3. Block diagrams for model I
(a) Model I in terms of the general block diagram shown in Figure 2
(b) Model I showing transfer function

Figure 3(a) shows model I in terms of multiple input multiple output block diagram discussed in section A of this chapter. The mechanical torque, τ_m, the electrical torque, τ_e, and the rotor speed are all assumed to be constant and are not represented in the model.

Figure 3(b) is a more detailed block diagram for model I. K_G represents the generator gain, T_G is the generator time constant and it can be the same as the direct axis transient open-circuit time-constant, T'_{do},

S_G is the generator saturation function and S denotes the Laplace transformation variable. This model is derived in Appendix A, part A. In general, K_G is not always specified in machine data. The data required for this model and the other models are shown in Table 2 (see end of the chapter). Also, since most of the symbols are introduced in this chapter, the list of principal symbols are given in Table 3 (see end of the chapter).

This model is often used whenever a detailed study of the excitation system is being conducted (5, 33, 98). In its application, the saturation term S_G is usually neglected. The first order approximation of the generator voltage response is very crude, but it allows us to concentrate on the characteristics of the excitation system without added complexity of the generator. The model is investigated with the excitation system in Chapter IV.

C. Model II - The Classical Swing Equation

Model II represents an opposite view of the synchronous machine as compared to model I in that v_f is now assumed constant and τ_m is the only variable input quantity. Figure 4 is a block diagram representation of this model in terms of the general block diagram discussed in section A of this chapter.

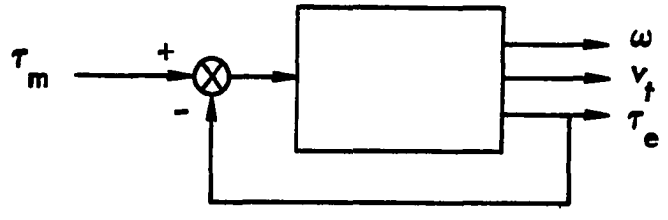

Figure 4. Block diagram for model II

The assumptions used in developing this model are compared with the assumptions used in developing the other models in Table 1. Using the same order of numbering as in Table 1, the assumptions used for model II are:

1) The currents and voltages in the stator and the connected system are of fundamental frequency only. All harmonic and dc offset currents and voltages are neglected.
2) Machine speed variations do not affect the generated voltage (by this we mean that the speed is assumed to be constant).
3) The unbalanced conditions are represented by symmetrical components.
4) The field flux linkages remain constant in magnitude.
5) Amortisseur currents and their effects are negligible.
6) Transient saliency is negligible. This is the same as saying that the field flux linkages ($\overline{e}'_q$) have the same magnitude as the voltage behind the transient reactance and that the angle of the quadrature axis is the same as the angle of the voltage behind the transient reactance. Mathematically this means that X_q and X'_q are both equal to X'_d in the system equations.
7) The armature resistance is negligible.
8) The $d\psi/dt$ or $d\lambda/dt$ terms are negligible.
9) Saturation is neglected.
10) The load torque, τ_m, is constant.

The first three assumptions are the basic assumptions usually made for all stability studies, regardless of the detail of representation of the control systems, the loads, or the machines (142). As a consequence

of the first assumption, the machine and system voltages and currents can be represented by phasors. The existence of dc offset current, particularly for faults near the machine terminals, offers a major restriction to the first assumption. If the machine speed is constant and only fundamental frequencies are permitted, the system would be solved by phasor algebra for any steady state condition or at any given instant of time. Under these conditions, symmetrical components may be used to represent unbalanced conditions as noted in the third assumption.

The resulting machine equations obtained with the three basic assumptions are still complex and further simplifying assumptions become necessary. The additional assumptions necessary for model II are given above. Usually the stator resistance is neglected in applying this model.

The only differential equation that needs to be solved for this model is the acceleration equation:

$$\frac{d^2\delta}{dt^2} = \frac{p}{2}\frac{180f}{H}(\tau_m - \tau_e) \qquad [1]$$

This model is particularly suitable for studying first-swing transient stability and should not be used for dynamic or steady-state stability. The model has been included here because of its historical importance.

D. Model III - Linear Model

Model III is more detailed than either models I or II. In this model, the synchronous machine is considered to be a two input system with

τ_m and v_f as the input variables. The output variables observable in this model are e_q', ω, δ and v_t. A block diagram comparing this model with the general block diagram discussed in section A of this chapter is shown in Figure 6 which is drawn directly above a more detailed block diagram for purposes of comparison. With this model the effect of varying both τ_m and v_f on the output variables can be studied.

The mathematical development of model III requires fewer simplifying assumptions than those used for model II (see Table 1). Only eight of the ten assumptions used for model II are necessary for model III. The assumptions that the field flux-linkages, λ_F, and the mechanical torque, τ_m, are constant are not used here. This implies that model III will be more complicated than model II.

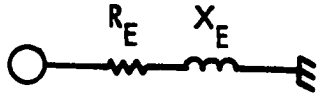

Figure 5. A single machine against infinite bus

Consider a machine connected to an infinite bus, with a voltage v, through an external impedance $R_E + jX_E$ as in Figure 5. Then using the above assumptions, the following equations expressed in per unit apply (24):

$$v_t^2 = v_d^2 + v_q^2 \qquad [2]$$

$$-v_d = \lambda_q = -X_q i_q \qquad [3]$$

$$v_d = \lambda_d = e_q' - X_d' i_d \qquad [4]$$

$$e_q = e_q' + (X_q - X_d') i_d \qquad [5]$$

$$\tau_e = e_q i_q \qquad [6]$$

$$V_B = \sqrt{3}\, v \qquad [7a]$$

$$i_d = [e_q - V_B \cos\delta]\{[X_E + X_q]/[R_E^2 + (X_E + X_q)^2]\} - V_B \sin\delta\, \{R_E/[R_E^2 + (X_E + X_q)^2]\} \qquad [7b]$$

$$i_q = [e_q - V_B \cos\delta]\{R_E/[R_E^2 + (X_E + X_q)^2]\} + V_B \sin\delta\, \{[X_E + X_q]/[R_E^2 + (X_E + X_q)^2]\} \qquad [8]$$

$$e_q' = X_{ad} i_{fd} - (X_d - X_d') i_d \qquad [9]$$

$$T_{do}' \left(\frac{de_q'}{dt}\right) = e_{fd} - X_{ad} i_{fd} \qquad [10]$$

$$\tau_m - \tau_e = M \frac{d^2\delta}{dt^2} \qquad [11]$$

Linearizing all the equations and simplifying to retain the basic variables $v_{t\Delta}$, $e_{q\Delta}'$ and δ_Δ leads to (see Appendix B for this derivation):

$$\tau_{e\Delta} = K_1 \delta_\Delta + K_2 e_{q\Delta}' \qquad [12]$$

$$e_{q\Delta}' = \frac{K_3[e_{fd\Delta} - K_4 \delta_\Delta]}{1 + sT_{do}' K_3} \qquad [13]$$

$$v_{t\Delta} = K_5 \delta_\Delta + K_6 e_{q\Delta}' \qquad [14]$$

$$\Delta\omega_u = \frac{1}{M} \int \tau_{au}\, dt \qquad [15]$$

$$\delta_\Delta = 377 \int \Delta\omega_u\, dt \qquad [16]$$

where K_1, K_2, K_3, K_4, K_5 and K_6 are as defined in Appendix B and

Equations 15 and 16 result from the torque angle relationships for the condition of the constant flux linkages in the direct axis.

Deleting the subscript "Δ's" in Equations 12 through 16, the block diagram resulting from the equations is shown in Figure 7. The portion of the figure indicated by broken lines shows the additional block that results if Equation 11 is rewritten to include damping thus:

$$\tau_m - \tau_e = M\frac{d^2\delta}{dt^2} + D\frac{d\delta}{dt} \qquad [11']$$

Figure 6 shows model III in terms of the general multiple input multiple output system discussed in section A of this chapter.

As shown in Table 2 this model requires more system data than either model I or model II. The model is analyzed in Chapter V.

E. Model IV - The Nonlinear Model

The purpose of this model is to represent the synchronous machine with as few assumptions as possible. In terms of the general block diagram presented in section A, the two inputs v_f and τ_m are included and all the important output variables are observable.

As shown in Table 1, three of the ten assumptions listed in the table are used in developing this model. Two additional assumptions which do not necessarily belong to those considered in Table 1 but which are required for the mathematical description presented here are:

a) It is assumed that the machine can be adequately represented by six magnetically coupled windings: three stator windings, one field winding and two amortisseur or damper windings

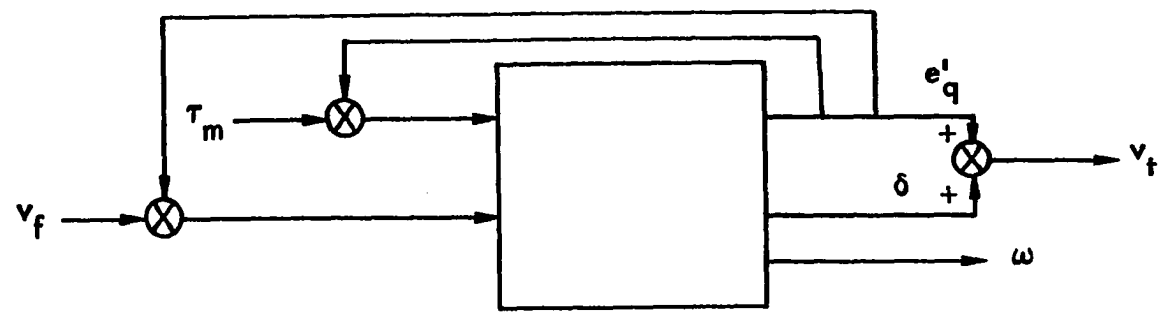

Figure 6. A general block diagram for model III

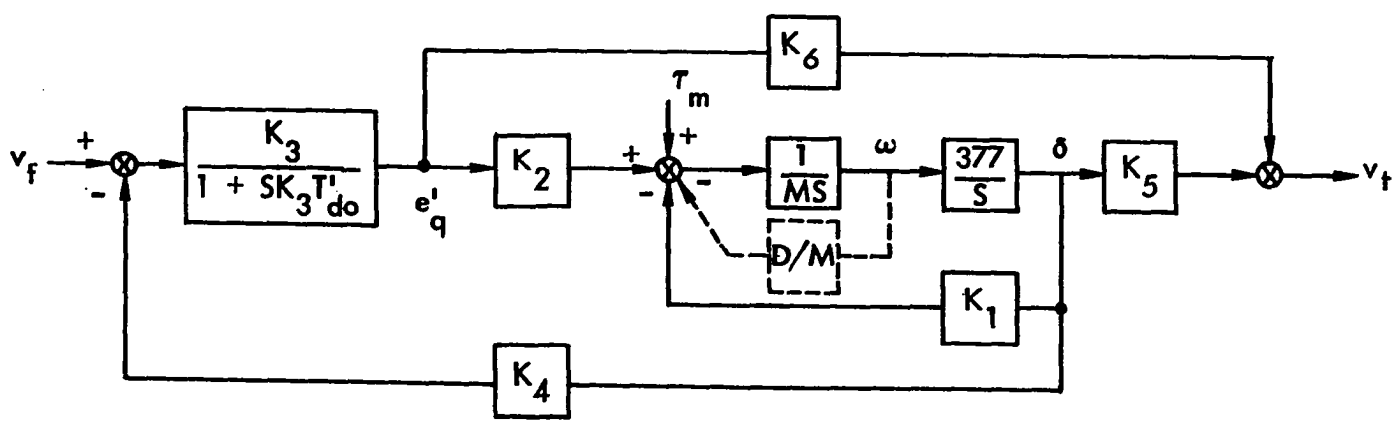

Figure 7. Detailed block diagram for model III

which represent the equivalent damping on each axis of the rotor.

b) The flux linking each winding is a function of rotor position.

The second of the three basic assumptions usually made for all stability studies has been deleted in formulating this model; that is, the assumption that the generated voltage is not affected by machine speed variations does not apply here as evidenced by the appearance of speed voltages in the transformed version of the voltage equations (see Appendix C). However, the assumption does apply to a modified form of this model (142).

Figure 8 shows the pictorial representation of a synchronous machine. If r is the resistance of the winding, i is the current flowing in the winding and λ is the flux linkage, then the instantaneous terminal voltage of any winding is of the form

$$v = \pm \Sigma\, ri \pm \Sigma\, \dot{\lambda} \qquad [17]$$

The various voltages in the machine can be written from the circuit diagram shown in Figure 9 as:

$$\begin{bmatrix} v_a \\ v_b \\ v_c \\ -v_F \\ 0 \\ 0 \end{bmatrix} = - \begin{bmatrix} r & 0 & 0 & 0 & 0 & 0 \\ 0 & r_b & 0 & 0 & 0 & 0 \\ 0 & 0 & r_c & 0 & 0 & 0 \\ 0 & 0 & 0 & r_F & 0 & 0 \\ 0 & 0 & 0 & 0 & r_D & 0 \\ 0 & 0 & 0 & 0 & 0 & r_Q \end{bmatrix} \begin{bmatrix} i_a \\ i_b \\ i_c \\ i_F \\ i_D \\ i_Q \end{bmatrix} - \begin{bmatrix} \dot{\lambda}_a \\ \dot{\lambda}_b \\ \dot{\lambda}_c \\ \dot{\lambda}_F \\ \dot{\lambda}_D \\ \dot{\lambda}_Q \end{bmatrix} + \begin{bmatrix} \underline{v_n} \\ \underline{0} \end{bmatrix} \text{ volts} \qquad [18]$$

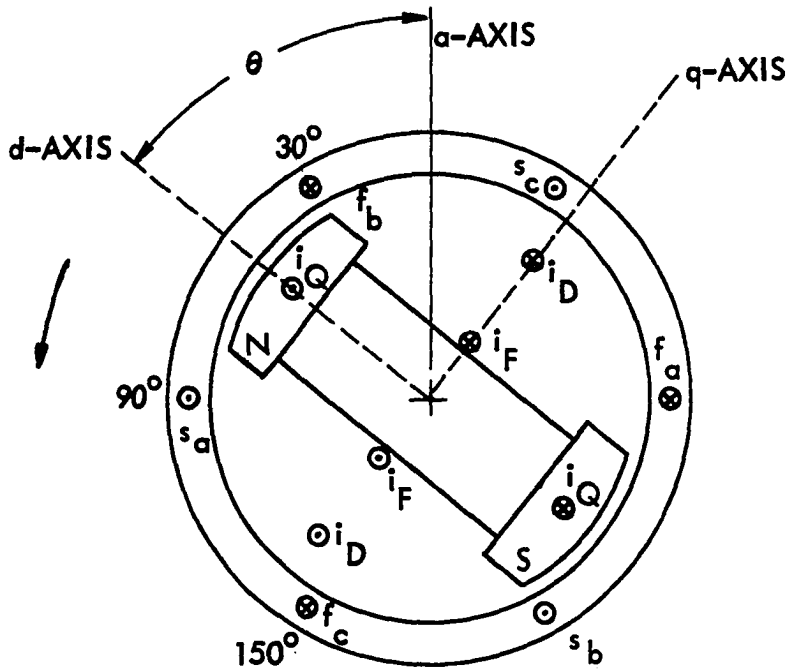

Figure 8. Pictorial representation of a synchronous machine

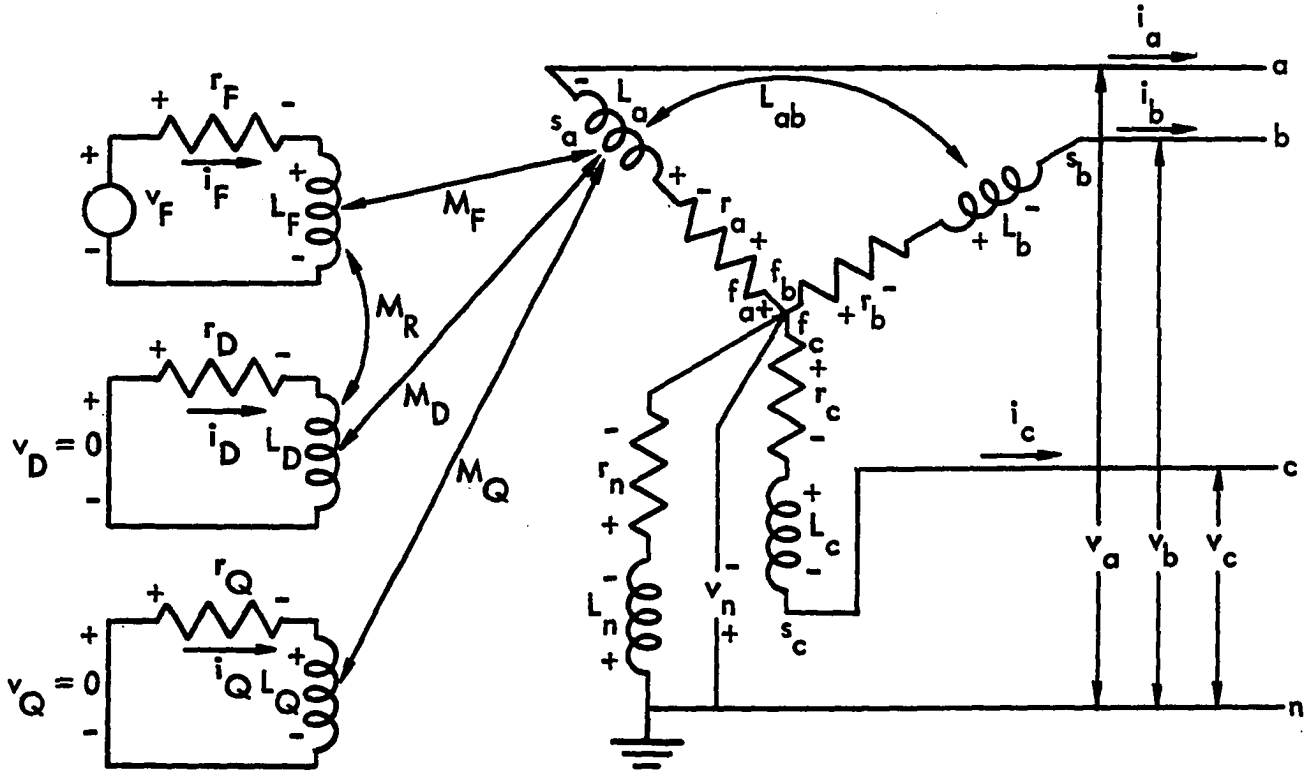

Figure 9. Circuit diagram of a synchronous machine

where

$$\underline{v}_n = - r_n \begin{bmatrix} 1 & 1 & 1 \\ 1 & 1 & 1 \\ 1 & 1 & 1 \end{bmatrix} \begin{bmatrix} i_a \\ i_b \\ i_c \end{bmatrix} - L_n \begin{bmatrix} 1 & 1 & 1 \\ 1 & 1 & 1 \\ 1 & 1 & 1 \end{bmatrix} \begin{bmatrix} \dot{i}_a \\ \dot{i}_b \\ \dot{i}_c \end{bmatrix} \text{ volts} \qquad [19]$$

$$= - \underline{R}_n \underline{i}_{abc} - \underline{L}_n \dot{\underline{i}}_{abc} \text{ volts}$$

Equations 17 and 18 include the flux linkage terms which are obtained from the flux linkage equations:

$$\begin{bmatrix} \lambda_a \\ \lambda_b \\ \lambda_c \\ \lambda_F \\ \lambda_D \\ \lambda_Q \end{bmatrix} = \begin{bmatrix} L_{aa} & L_{ab} & L_{ac} & L_{aF} & L_{aD} & L_{aQ} \\ L_{ba} & L_{bb} & L_{bc} & L_{bF} & L_{bD} & L_{bQ} \\ L_{ca} & L_{cb} & L_{cc} & L_{cF} & L_{cD} & L_{cQ} \\ L_{Fa} & L_{Fb} & L_{Fc} & L_{FF} & L_{FD} & L_{FQ} \\ L_{Da} & L_{Db} & L_{Dc} & L_{DF} & L_{DD} & L_{DQ} \\ L_{Qa} & L_{Qb} & L_{Qc} & L_{QF} & L_{QD} & L_{QQ} \end{bmatrix} \begin{bmatrix} i_a \\ i_b \\ i_c \\ i_F \\ i_D \\ i_Q \end{bmatrix} \text{ weber-turns} \qquad [20]$$

where

$$L_{jk} = \begin{cases} \text{self-inductance when } j = k \\ \text{mutual inductance when } j \neq k \end{cases}$$

As shown in Appendix C all but three of the inductances in Equation 20 are time varying. Also in Appendix C, Equations 18 and 20 are transformed to odq reference frame by a modified form of Park Transformation. The series of manipulations on the transformed equations which finally results in an analog computer representation of this model are described in Appendix C. Model IV is investigated in Chapter VI.

The list of data needed for an analog simulation of this model is shown in Table 2. The quantities X''_d, X''_q, X'_q, T''_{do}, T'_{qo} and T''_{qo} also shown in Table 2 are required only if the equations are written for a modified form of this model which is often used for a power system digital computer stability program (142).

Table 1. A comparison of the assumptions used in the models

	Assumptions	Model I	Model II	Model III	Model IV
1	Fundamental frequency emfs	✓	✓	✓	✓
2	Constant speed, ω	✓	✓	✓	
3	Symmetrical components	✓	✓	✓	
4	Constant field flux linkages		✓		
5	Neglect amortisseur effects	✓	✓	✓	
6	Neglect saliency	✓	✓	✓	✓
7	Neglect armature resistance	✓	✓	✓	
8	Neglect $d\psi/dt$ or $d\lambda/dt$ terms	✓	✓	✓	
9	Neglect saturation	_*	✓	✓	_*
10	τ_m is constant	✓	✓		

*Neglected in equations, accounted for by external feedback method.

Table 2. Data needed for the models

Constants	Model I	Model II	Model III	Model IV
r_a				X
X'_d		X	X	X
X_d			X	X
X_q			X	X
T'_{do}	X		X	X
ℓ_a				X
ℓ_f				X
H		X	X	X
R_E			X	X
X_E			X	X
L_F				X
ℓ_D				X
L_D				X
ℓ_Q				X
L_Q				X
r_F				X
r_D				X
r_Q				X
X''_d				X
X''_q				X
X'_q				X
T''_{do}				X
T''_{qo}				X
T'_{qo}				X

Table 3. Symbols used in the models

Symbol	Description
$v_f = \frac{r_f}{L_f} e_{fd}$	Generator field voltage
v_t	Generator terminal voltage
S_G	Generator saturation function
K_G	Generator gain
T_G	Generator time constant
T'_{do}	Direct axis open circuit transient time constant
$\overline{e}'_q$	Field flux linkages, per unit
$X_d = \omega L_d$	Direct axis synchronous reactance
$X_q = \omega L_q$	Quadrature axis synchronous reactance
X'_q	Quadrature axis transient reactance
X'_d	Direct axis transient reactance
δ	Angle between q axis and reference axis
H	Inertia constant, seconds
τ_m	Mechanical torque
τ_e	Electrical torque
R_E	Line resistance
X_E	Line reactance
v_d, v_q	Armature voltage, direct and quadrature axis components
λ_d, λ_q	Armature flux linkages, direct and quadrature axis components
i_d, i_q	Armature current, direct and quadrature axis components
e'_q	Voltage proportional to direct axis flux linkages
e_q	Quadrature axis flux linkages
v	Voltage at the infinite bus

Table 3 (Continued)

Symbol	Description
V_B	Transformed voltage at the infinite bus
i_f	Field current corresponding to e_{fd}
M	Inertia coefficient = 2H, seconds
D	Damping coefficient
ω	Rotor speed
λ	Flux linkages
ℓ_a	Armature leakage inductance
ℓ_f	Field leakage inductance
ℓ_D, ℓ_Q	Amortisseur leakage inductance, direct and quadrature axis components
L_D, L_Q	Amortisseur inductance, direct and quadrature axis components
X''_d, X''_q	Subtransient reactance, direct and quadrature axis components
T''_{do}, T''_{qo}	Subtransient open circuit time constant, direct and quadrature axis components
T'_{qo}	Quadrature axis transient open circuit time constant
L_f	Field inductance
r_f	Field resistance

IV. MODEL I - ANALYSIS OF THE EXCITATION SYSTEM

In this chapter the first order approximation of the generator (model I) is used to study the performance of the excitation system. Studies dealing with various aspects of excitation systems fall into two groups. The first group consists of low response ratio excitation systems while the second group contains the high response excitation systems. Even though most new large oncoming generating units will have high response, static excitation systems, the power system remains dominated by the conventional, low response, rotating exciter systems (112).

Two typical exciters, each representing one of the two groups of excitation systems, are investigated. In part A, the root locus technique is used to determine the appropriate range of values for the nondynamic parameters of the excitation system. Using some of the range of values determined in part A, the effects of the exciter saturation and amplifier limiting on the stability performance are studied in part B, using the analog computer.

A. Root Locus Analysis of the Excitation System

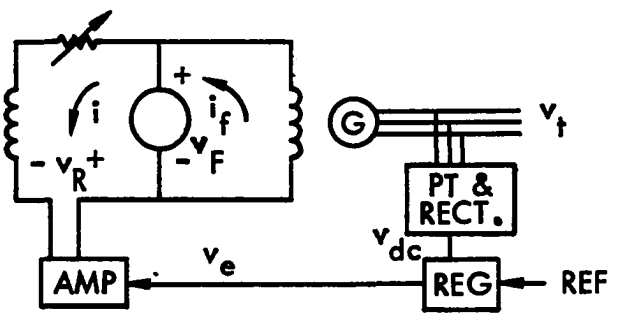

Figure 10. Simplified diagram of a boost-buck system

Consider the continuously regulated excitation system shown in Figure 10. A step-by-step analysis of each of the components of the boost-buck system leads to the following set of equations in the S-domain (see Appendix A).

Potential transformer and rectifier:
$$v_{dc} = \frac{K_R v_t}{1 + T_R S} \quad [21]$$

Comparator:
$$v_e = K(v_{ref} - v_{dc}) \quad [22]$$

Amplifier:
$$v_R = \frac{K_A v_e}{1 + T_A S}, \quad v_{Rmin} < v_R < v_{Rmax} \quad [23]$$

Exciter:
$$v_f = \frac{v_R - S_E v_f}{K_E + T_E S} \quad [24]$$

Generator:
$$v_t = \frac{K_G v_f - S_G v_t}{1 + T_G S} \quad [25]$$

The variables appearing in Equations 21-25 and in Figure 10 are defined in Table 4. Combining the equations leads to the block diagram representation of the excitation system as shown in Figure 11.

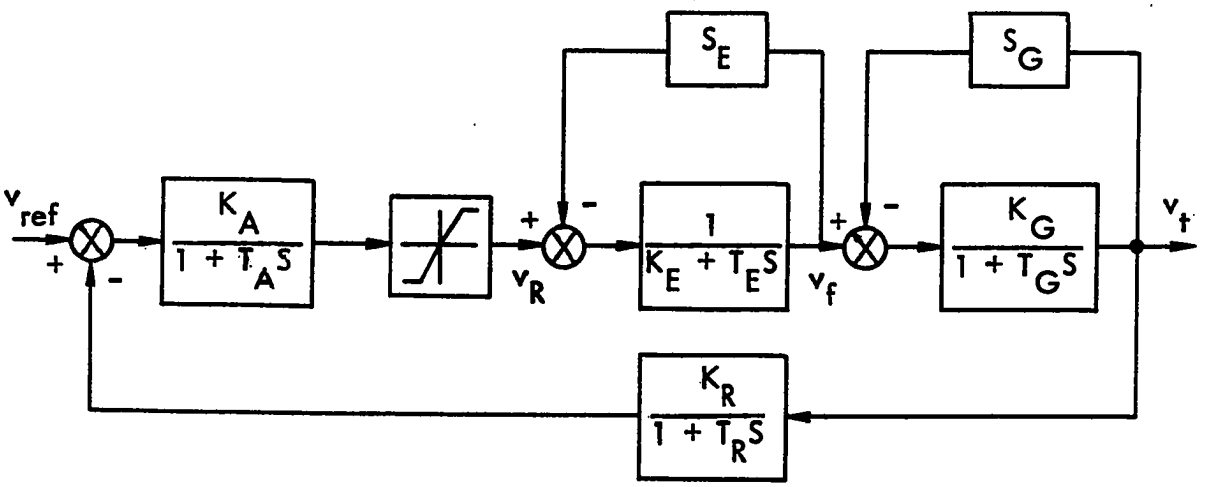

Figure 11. Block diagram of the uncompensated excitation control system

Table 4. Symbols used in the excitation system

Symbol	Description
v_{dc}	Rectifier output voltage
K_R	Regulator input filter gain
v_t	Generator terminal voltage
T_R	Regulator input filter time constant
v_e	Amplifier input voltage
v_{ref}	Regulator reference voltage setting
v_R	Regulator output voltage
K_A	Regulator amplifier gain
T_A	Regulator amplifier time constant
v_f	Exciter output voltage
T_f	Regulator stabilizing circuit time constant
S_E	Exciter saturation function
K_E	Exciter constant related to self excited field
T_E	Exciter time constant
K_G	Generator gain
S_G	Generator saturation function
T_G	Generator time constant
v_{Rmax}	Maximum value of v_R
v_{Rmin}	Minimum value of v_R

Neglecting limiting and saturation in Figure 11, the open loop transfer function KGH is

$$KGH = \frac{K_A K_G K_R}{(1 + T_A S)(K_E + T_E S)(1 + T_G S)(1 + T_R S)}$$

$$\frac{v_t}{v_{ref}} = \frac{KG}{1 + KGH}$$

$$= \frac{\frac{K_A K_G}{T_A T_E T_G}(S + \frac{1}{T_R})}{(S + \frac{1}{T_A})(S + \frac{K_E}{T_E})(S + \frac{1}{T_G})(S + \frac{1}{T_R}) + \frac{K_A K_G K_R}{T_A T_E T_G T_R}} \qquad [26]$$

Consider a system whose parameters are specified as (5):

T_A = 0.1 sec K_E = -0.05

T_E = 0.5 sec K_G = 1.0

T_G = 1.0 sec K_A = variable

T_R = 0.05 sec

These are part of the parameters of the slow exciter. The complete list of the excitation system parameters is given in Appendix A, part C. Substituting the above values into Equation 26 leads to

$$\frac{v_t}{v_{ref}} = \frac{20 K_A(S + 20)}{(S + 10)(S - 0.1)(S + 1)(S + 20) + 400 K_A} \qquad [27]$$

Applying Routh's stability criterion to the denominator of the right hand side of Equation 27 shows that the system is stable for $0.05 < K_A < 3.215$ and that the root locus plot crosses the $j\omega$ axis at $S = \pm j2.4$.

Since the system becomes unstable at very low values of gain, the excitation system requires an appropriate compensation.

A possible method of compensating the excitation system is to introduce rate feedback as shown in Figure 12 where K_F is the feedback gain and T_F is the corresponding time constant. Then the problem becomes that of choosing K_A, K_F and T_F such that a given performance criterion is satisfied. In order to study the effects of varying K_F and T_F on the root locus of the system, it is convenient to first reduce the block diagram shown in Figure 12 to the form shown in Figure 13. Then both the open loop and closed loop transfer functions of the uncompensated system are, respectively:

$$KGH = \frac{\frac{K_A K_G}{T_A T_E T_G}\left[\frac{K_F}{T_F} \cdot \frac{T_G}{K_G} S(S + \frac{1}{T_G})(S + \frac{1}{T_R}) + \frac{K_R}{T_R}(S + \frac{1}{T_F})\right]}{(S + \frac{1}{T_A})(S + \frac{K_E}{T_E})(S + \frac{1}{T_G})(S + \frac{1}{T_R})(S + \frac{1}{T_F})} \qquad [28]$$

$$\frac{v_t}{v_{ref}} = \frac{\frac{K_A K_G}{T_A T_E T_G}(S + \frac{1}{T_F})(S + \frac{1}{T_R})}{(S + \frac{1}{T_A})(S + \frac{K_E}{T_E})(S + \frac{1}{T_G})(S + \frac{1}{T_R})(S + \frac{1}{T_F}) + C} \qquad [29]$$

$$C = \frac{K_A K_G}{T_A T_E T_G}\left[\frac{K_F}{T_F} \cdot \frac{T_G}{K_G} S(S + \frac{1}{T_G})(S + \frac{1}{T_R}) + \frac{K_R}{T_R}(S + \frac{1}{T_F})\right]$$

The closed loop transfer function given by Equation 29 is particularly useful whenever the effects of varying one or two parameters within a limited range is being studied. Using the given system data and

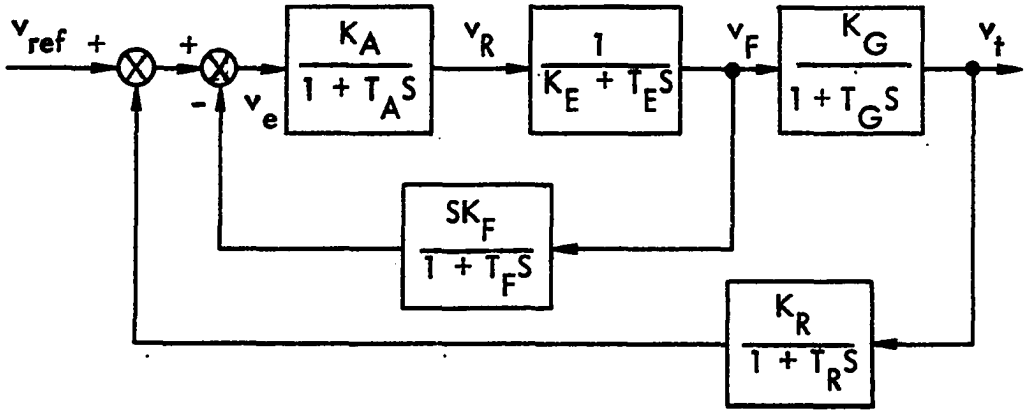

Figure 12. Block diagram of the excitation control system with rate feedback (limiting and saturation neglected)

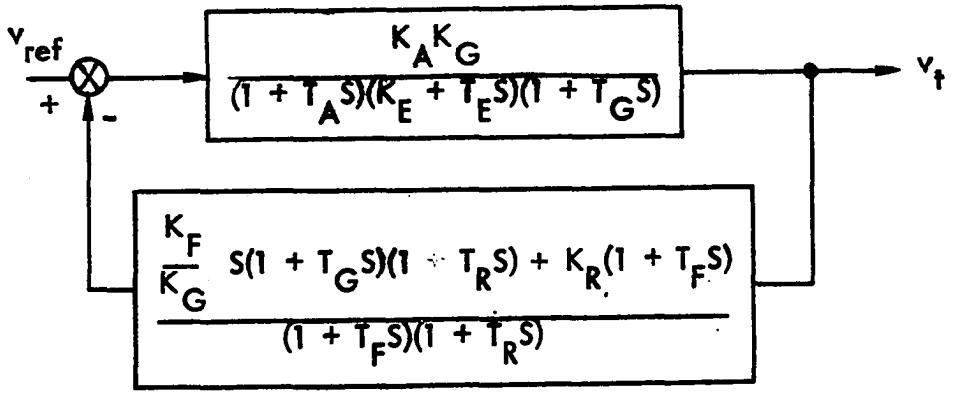

Figure 13. Reduced form of Figure 12

Equation 29, Figures 14, 15 and 16 show the time response of the system to a unit step input for various values of K_A and K_F. Table 5 compares the time response shown in Figures 15 and 16.

Table 5. A comparison of Figures 15 and 16

K_A	K_F	Settling time sec	Overshoot %	Rise time sec
200	0.015	--	--	0.15
200	0.020	1.60	100	0.15
200	0.025	0.75	75	0.15
200	0.030	0.90	52	0.15
200	0.035	1.00	42	0.15
400	0.015	2.00	145	0.10
400	0.020	0.65	75	0.12
400	0.025	0.70	45	0.12
400	0.030	0.80	40	0.14
400	0.035	1.30	35	0.20

The above approach of finding the time response of the system becomes rather expensive in terms of digital computer runs whenever several parameters or extensive range of values of a parameter are to be studied. At this point the root locus technique appears to be more appropriate.

Substituting the given system quantities which are the parameters of the slow exciter into Equation 28 leads to:

$$KGH = \frac{20K_A \left[\frac{K_F}{T_F} S(S + 1)(S + 20) + 20(S + \frac{1}{T_F})\right]}{(S + 10)(S - 0.1)(S + 1)(S + 20)(S + \frac{1}{T_F})} \qquad [30]$$

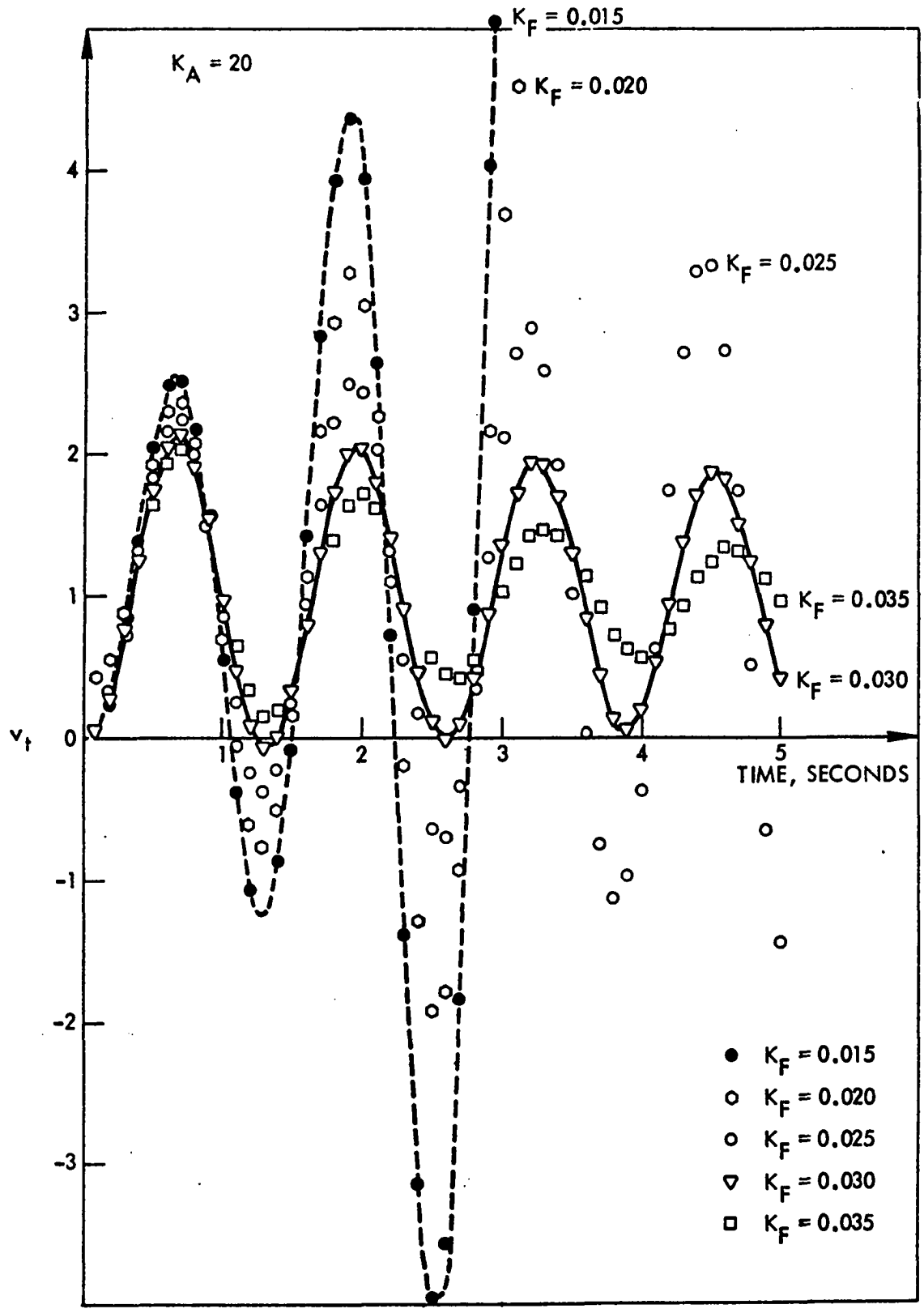

Figure 14. Time response of Equation 29 to a unit step input for $K_A = 20$

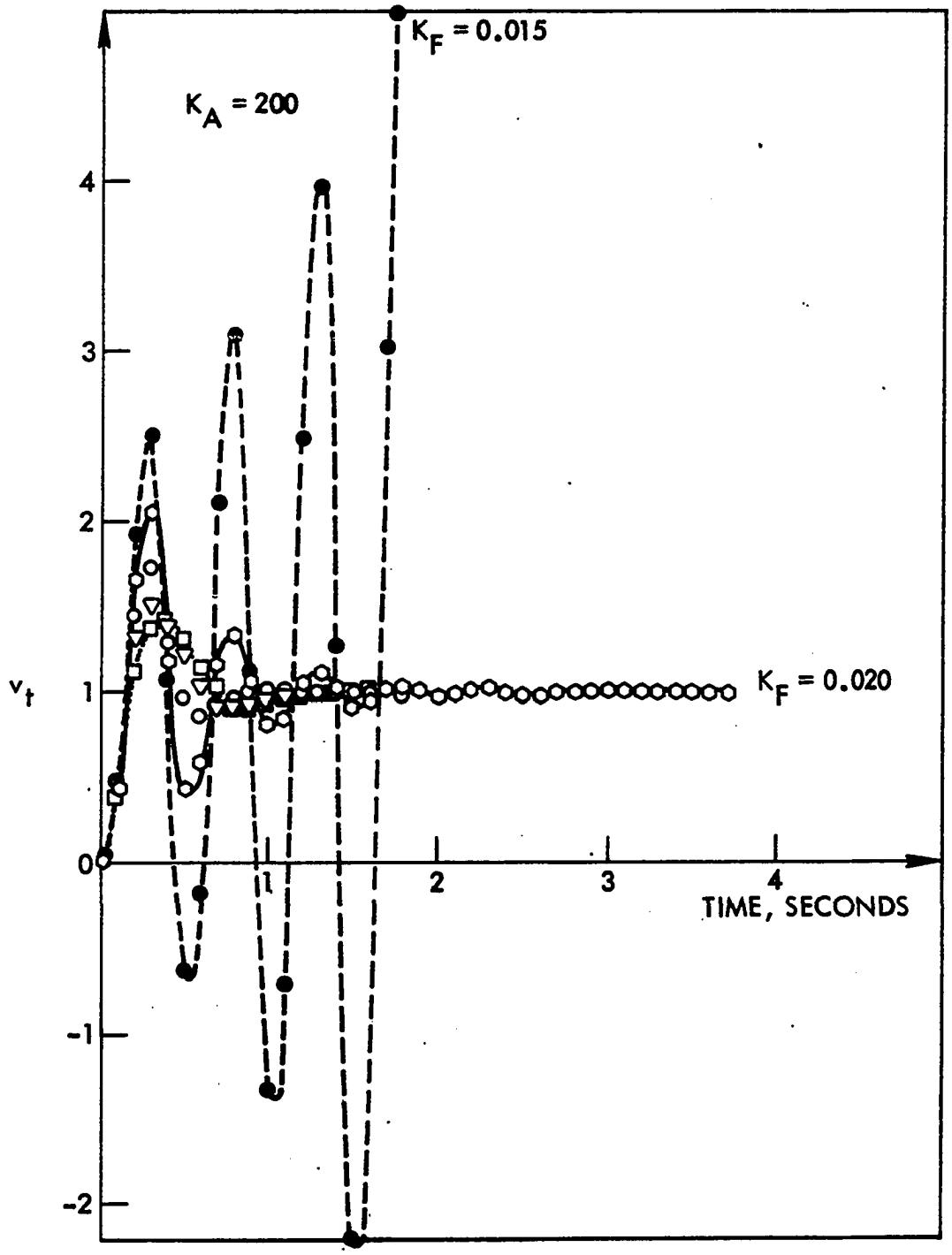

Figure 15. Time response of Equation 29 to a unit step input for $K_A = 200$

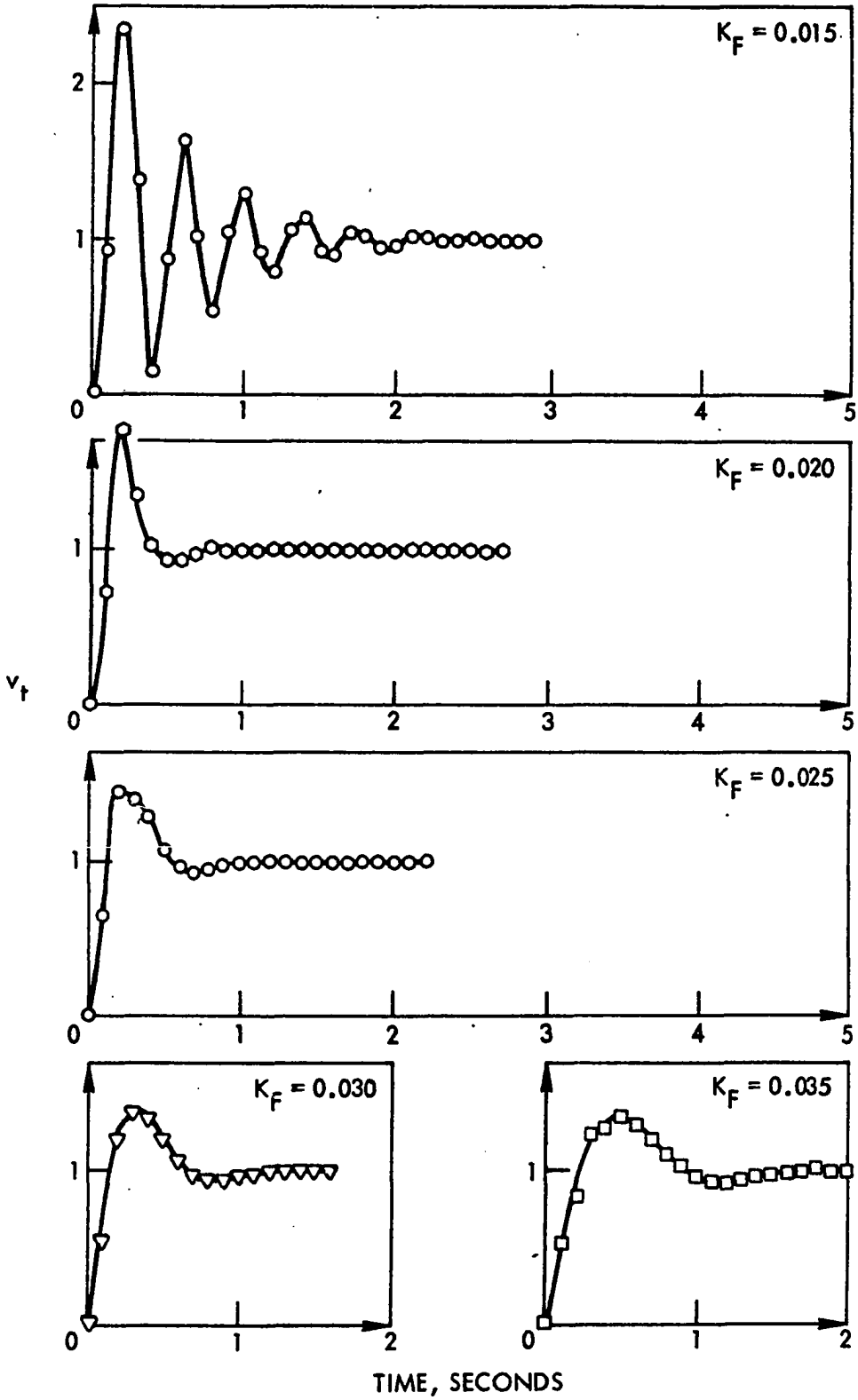

Figure 16. Time response of Equation 29 to a unit step input for K_A = 400

The root locus technique can be used to determine the appropriate range of K_F and T_F that merit further investigation. As a first step in this direction, consider the bracketed terms in the numerator of Equation 30:

$$\frac{K_F}{T_F} S(S + 1)(S + 20) + 20(S + \frac{1}{T_F}) = 0 \qquad [31a]$$

$$bs(S + 1)(S + 20) + 20(S + a) = 0 \qquad [31b]$$

$$1 + \frac{\frac{20}{b}(S + a)}{S(S + 1)(S + 20)} = 0$$

$$1 + \frac{K(S + a)}{S(S + 1)(S + 20)} = 0 \qquad [31c]$$

where

$$a = \frac{1}{T_F}$$

$$b = \frac{K_F}{T_F}$$

$$K = \frac{20}{b} = 20 \frac{T_F}{K_F}$$

Equation 31c is of the form $1 + KGH = 0$. Hence, we can plot its root locus to observe the effects of varying K. There are three cases of interest: $0 < a < 1$, $1 < a < 20$ and $a > 20$. The root loci corresponding to the three cases are sketched in Figure 17. Exact location of m and the breakaway point for each root locus depends on the value of "a" used.

Corresponding to each of the loci in Figure 17, there are two types of loci of KGH (Equation 30); one exists when all the zeros are real, and the other exists for a real zero and a complex pair of zeros. The six root loci resulting from these considerations are shown in Figure 18. Cases IA, IB, IIA, and IIIA indicate that the response will be dominated by the real root near the origin. Therefore, the system response corresponding to these cases will be sluggish. Case IIB appears to be the most promising if an appropriate damping can be determined.

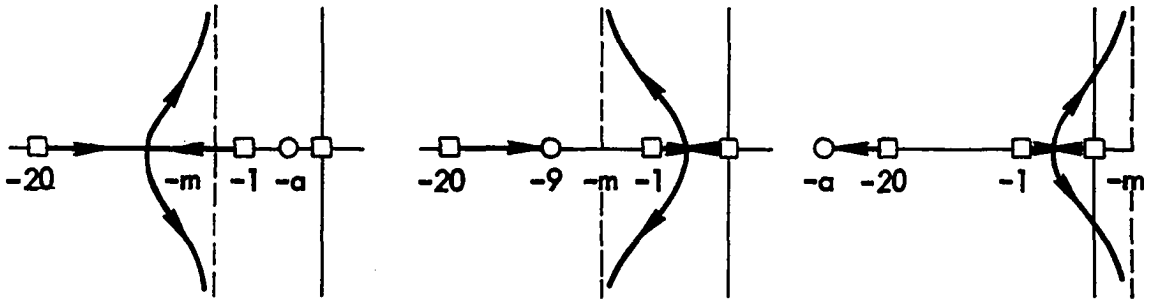

Case I: $0 < a < 1$
$-10.5 < m < -10$

Case II: $1 < a < 20$
$-10 < m < -0.5$

Case III: $a > 20$
$-0.5 < m$

Figure 17. Root loci of $1 + \frac{K(S + a)}{S(S + 1)(S + 20)} = 0$

From the above analyses, the range $1 < a < 20$ or $0.05 < T_F < 1$ merits further investigation. Thus, more detailed root loci can be prepared for several values of T_F in this range. From the root loci, appropriate sets of K_F resulting in a stable system and satisfying a specified performance can be determined. Using various sets of T_F and K_F, other sets of root loci are plotted to show the effects of varying K_A.

Case IA:	All real zeros $0 < a < 1$	Case IB:	One real, one complex pair $0 < a < 1$
Case IIA:	All real zeros $1 < a < 20$	Case IIB:	One real, one complex pair $1 < a < 20$
Case IIIA:	All real zeros $a > 20$	Case IIIB:	One real, one complex pair

Figure 18. Root loci of $KGH = 20K_A \dfrac{[bS(S + 1)(S + 20) + 20(S + a)]}{(S + 20)(S + 10)(S + 1)(S - 0.1)(S + a)}$

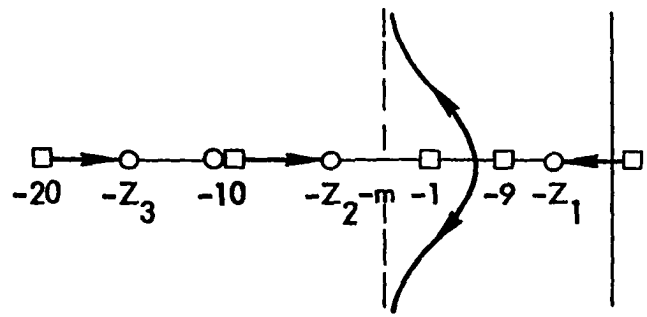

CASE IA

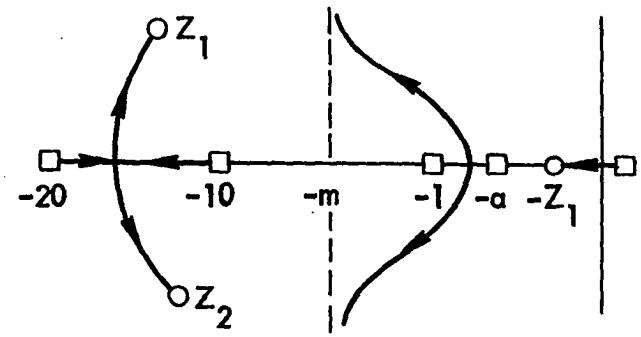

CASE IB

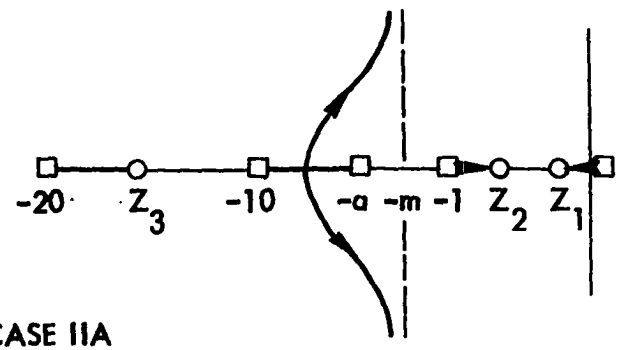

CASE IIA

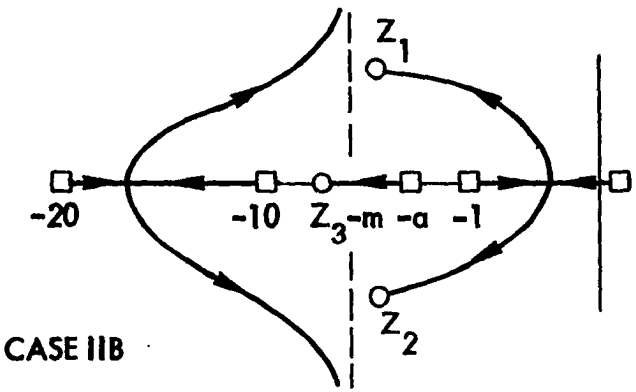

CASE IIB

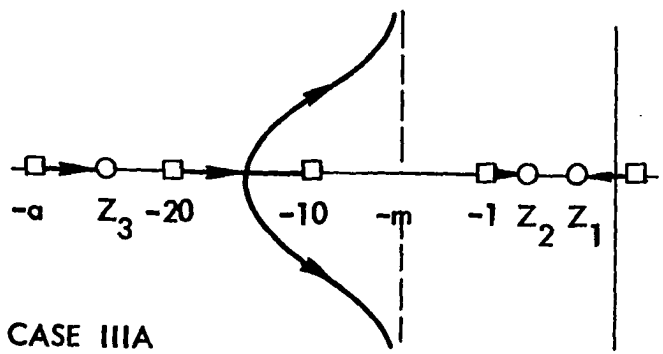

CASE IIIA

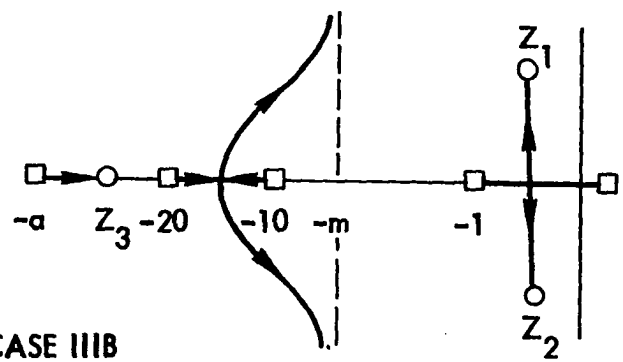

CASE IIIB

Table 6 shows the values of T_F, K_A and K_F considered suitable for further investigation. These values are used in the various studies discussed in the remaining portion of the thesis.

Table 6. Values of T_F, K_A and K_F used

T_F	K_A	K_F
0.1	400	0.015
0.2	600	0.020
		0.025
		0.030
		0.035

B. Results of Analog Computer Studies of the Excitation Control Systems

An Electronic Associates' analog computer model EAI 8812 was used to simulate the compensated excitation control system whose block diagram is shown in Figure 19.

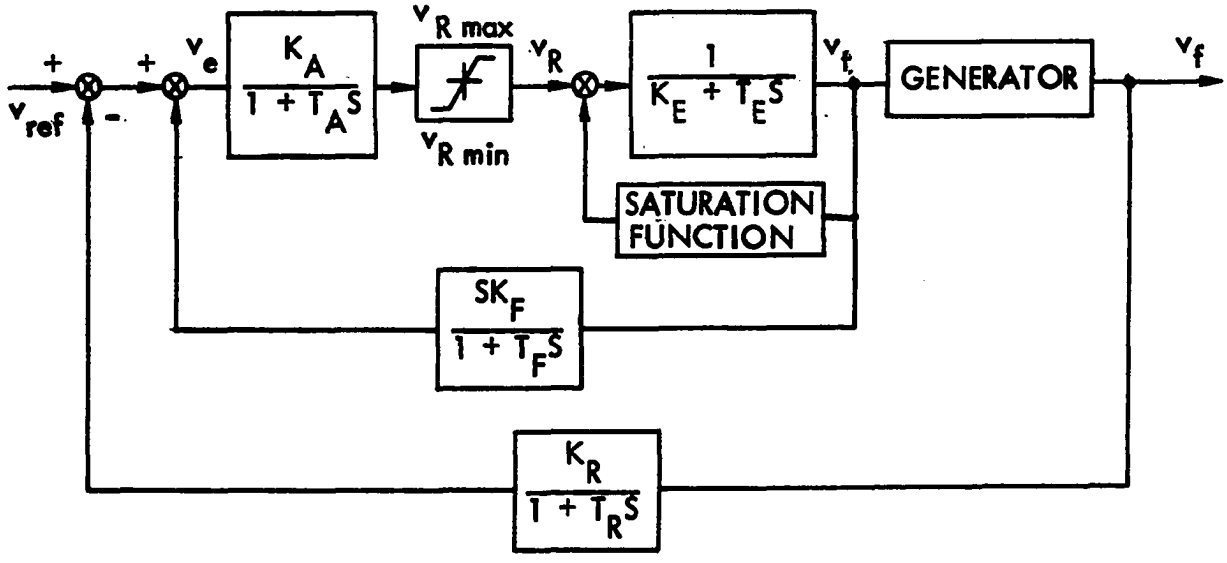

Figure 19. Block diagram of the compensated excitation control system with amplifier limiting and exciter saturation

Two types of exciters were considered for the analog computer studies. The first, a slow exciter, is the conventional rotating excitation system with 0.5 response ratio and the second, a fast exciter, is a thyristor type, high initial response system, 2.5 response ratio. The data for the two types of exciters used in the simulation are obtained from references 5 and 98 for the slow and fast exciters, respectively. The data together with the appropriate data preparations such as potentiometer settings, limiter settings and the exciter saturation are described in Appendix A.

The same range of K_F and T_F was used in the simulation of the two excitation systems. It is important to note, however, as discussed in section A of this chapter, that the set of values for K_F and T_F shown in Table 6 was chosen on the basis of the slow exciter where the exciter pole is very close to the origin (see Figure 18). The exciter pole for the fast exciter, however, lies far to the left of the origin. We have chosen to use the same range of K_F and T_F for the two exciters in order that any differences that may be noted in the results can be attributed to the fixed parameters of the excitation systems.

Four sets of readings were recorded for each of the excitation systems. Set one is the operation of the system with no limiting and no saturation, NLNS. In the second set the system is operated with limiting but no saturation, LNS. The third set is the operation of the system with both limiting and saturation, LS, while in the fourth set the system is operated with no limiting but with saturation, NLS.

In order to investigate the effects of the above on each of the values of T_F, K_A and K_F given in Table 6, each set of readings must

contain twenty analog computer runs. In each case the system is first brought to its full load steady state operating condition, then the effect of a 5% step change in the reference voltage, v_{ref}, on the output variables, particularly the terminal voltage, is recorded.

The next step is to determine a set of performance indices which can be used to compare the eighty strip chart recordings obtained for each excitation system. While several authors always give the strip chart recordings of the output variables of the systems under investigation, there is no general agreement on how to best compare two sets of output variables. In this study, we have chosen to compare the system response as if it were that of a second order system. Hence the comparison is in terms of settling time, percent overshoot and rise time -- all of which are commonly defined in control system texts (29). A sketch showing the definition of the performance indices is given in Appendix A, section E.

Tables 7 and 8 compare the system response for the two types of excitation system considered. The rise time for the system response of the slow response exciter is of the same order of magnitude for the four sets of readings. Hence the comparison shown in Table 7 does not include the rise time.

The settling time and percent overshoot shown in Tables 7 and 8 are compared graphically by plotting them against K_F.

For a fixed T_F and K_A the percent overshoot is plotted against K_F using the four sets of readings, NLNS, LNS, LS and NLS. The plots resulting from this consideration are shown in Figures 20 and 24 for the slow and the fast exciters, respectively.

Table 7. Comparison of results for model I and the low response exciter

T_F	K_A	K_F	No limiting, no saturation			With limiting but no saturation			With both limiting and saturation			No limiting but with saturation		
			Run no.	Set-tling time	% over-shoot	Run no.	Set-tling time	% over-shoot	Run no.	Set-tling time	% over-shoot	Run no.	Set-tling time	% over-shoot
				sec			sec			sec			sec	
.2	400	.015	11	2.00	125	41	5.75	120	71	4.13	110	101	1.90	125
		.020	12	0.70	75	42	1.00	85	72	0.85	85	102	0.60	75
		.025	13	0.80	47	43	0.90	61	73	0.80	60	103	0.85	47
		.030	14	1.00	43	44	1.00	41	74	1.00	40	104	1.00	41
		.035	15	1.10	39	45	1.10	37	75	1.05	37.5	105	1.10	37
	600	.015	16	0.60	100	46	2.40	110	76	1.90	100	106	0.50	100
		.020	17	0.65	55	47	0.85	80	77	0.85	72	107	0.60	57
		.025	18	0.75	43	48	0.75	53	78	0.85	49	108	0.75	43
		.030	19	0.80	39	49	1.00	39	79	1.00	38.5	109	1.00	39
		.035	20	1.05	37	50	1.00	35	80	1.15	34.5	110	1.10	37
.1	400	.015	21	1.65	80	51	1.90	75	81	2.20	80	111	2.10	80
		.020	22	1.75	70	52	2.10	67	82	2.60	65	112	2.00	70
		.025	23	2.00	65	53	2.40	63	83	2.80	61	113	2.20	65
		.030	24	2.25	61	54	2.70	61	84	2.90	59	114	2.60	61
		.035	25	2.80	58	55	2.90	59	85	2.80	57	115	2.70	59
	600	.015	26	1.75	75	56	2.10	75	86	2.05	70	116	1.70	75
		.020	27	1.85	65	57	2.00	63	87	2.10	61	117	2.50	65
		.025	28	2.00	60	58	2.30	61	88	2.30	60	118	2.80	61
		.030	29	2.20	59	59	2.65	59	89	2.30	59	119	3.10	59
		.035	30	2.40	57	60	2.70	57	90	2.50	57	120	3.30	57

Table 8. Comparison of results for model I and the high response exciter

T_F	K_A	K_F	No limiting, no saturation			With limiting but no saturation			With both limiting and saturation			No limiting but with saturation		
			Run no.	Settling time	% overshoot	Rise time	Settling time	% overshoot	Rise time	Settling time	% overshoot	Rise time	Settling time	% overshoot	Rise time
				sec		sec	sec		sec	sec		sec	sec		sec
.2	400	.015	221	0.32	11.0	.10	241	0.45	12.0 .12	261	0.50	10.5 .20	281	0.43	13.5 .10
		.020	222	0.53	15.0	.12	242	0.52	13.0 .13	262	0.60	12.0 .22	282	0.53	15.0 .13
		.025	223	0.62	18.5	.17	243	0.58	18.0 .15	263	0.70	14.0 .21	283	0.62	18.0 .15
		.030	224	0.71	19.0	.18	244	0.68	19.0 .17	264	0.75	17.0 .20	284	0.70	18.5 .19
		.035	225	0.78	20.0	.20	245	0.75	19.0 .20	265	0.80	20.0 .21	285	0.74	19.5 .20
	600	.015	226	0.42	12.0	.10	246	0.46	13.0 .11	266	0.53	13.0 .19	286	0.42	13.0 .10
		.020	227	0.52	15.0	.12	247	0.57	14.0 .13	267	0.60	14.0 .20	287	0.54	15.0 .13
		.025	228	0.61	18.0	.15	248	0.62	18.0 .15	268	0.68	16.0 .21	288	0.62	17.4 .15
		.030	229	0.71	19.0	.17	249	0.70	19.0 .17	269	0.73	18.5 .20	289	0.70	18.5 .18
		.035	230	0.79	20.0	.19	250	0.78	20.0 .19	270	0.78	20.0 .22	290	0.74	19.0 .20
.1	400	.015	231	0.88	27.0	.14	251	0.90	29.0 .12	271	0.82	21.0 .20	291	0.90	25.0 .12
		.020	232	1.06	29.0	.16	252	1.05	29.5 .14	272	1.07	24.0 .20	292	1.02	27.0 .17
		.025	233	1.20	31.5	.18	253	1.16	31.5 .17	273	1.19	28.0 .20	293	1.19	30.0 .20
		.030	234	1.30	32.0	.20	254	1.28	33.0 .20	274	1.30	31.0 .21	294	1.30	31.5 .22
		.035	235	1.43	33.0	.22	255	1.40	34.0 .22	275	1.42	33.0 .22	295	1.42	32.0 .22
	600	.015	236	0.85	27.0	.13	256	0.87	27.0 .12	276	0.90	21.0 .19	296	0.90	26.0 .12
		.020	237	1.00	30.4	.16	257	1.07	30.5 .16	277	1.03	25.0 .20	297	1.08	29.0 .16
		.025	238	1.10	31.0	.17	258	1.17	31.5 .17	278	1.20	29.0 .20	298	1.20	31.5 .18
		.030	239	1.18	32.0	.18	259	1.30	33.0 .20	279	1.32	32.0 .20	299	1.30	32.0 .20
		.035	240	1.30	33.0	.19	260	1.42	34.0 .22	280	1.42	33.0 .21	300	1.40	32.0 .22

For each set of readings, NLNS, LNS, LS and NLS AND the four different combinations of T_F and K_A, the percent overshoot is plotted against K_F. Figures 21 and 25 result from these considerations.

Using a similar approach as above, the settling time is plotted against K_F. Figures 22 and 26 parallel those of Figures 20 and 24 while Figures 23 and 27 are developed from considerations similar to those of Figures 21 and 25.

In order to facilitate visual comparison of the results, the same scale has been used in plotting the curves shown in Figures 20 to 27. Several observations can be made from Tables 7 and 8 and Figures 20 to 27. First, one can compare each figure with respect to the effects of varying T_F and K_A. Then a cross-comparison of the several figures can be made. The following are some of the possible observations:

1) For the low response exciter, the percent overshoot decreases with an increase in K_F whereas it increases slightly for the high response exciter (see Figures 20, 21, 24 and 25).
2) The percent overshoot is comparatively higher in the low response exciter than in the high response exciter (see Figures 20, 21, 24 and 25).
3) The percent overshoot does not vary significantly with NLNS, LNS, LS and NLS operations but in almost all cases the overshoot is lower when both limiting and saturation, LS, are included (see Figures 20 and 24).
4) The percent overshoot varies more significantly with T_F than with K_A for constant K_F (see Figures 21 and 25).

5) The settling time increases with an increase in K_F (see Figures 22, 23, 26 and 27).

6) For similar operating conditions the settling time is lower in the high response excitation system than in the low response system (see Figures 22, 23, 26 and 27).

7) The settling time is greater when both limiting and saturation, LS, are considered than in the other runs NLNS, LNS and NLS (see Figures 22 and 26).

8) For constant K_F, the settling time is more dependent on T_F than on K_A (see Figures 23 and 27).

From the studies described in this chapter it can be said, in general, that

1) Inclusion of saturation and limiting lower overshoot but tend to sustain oscillations longer.

2) The faster response system has better overall performance in the range of K_F, T_F and K_A considered.

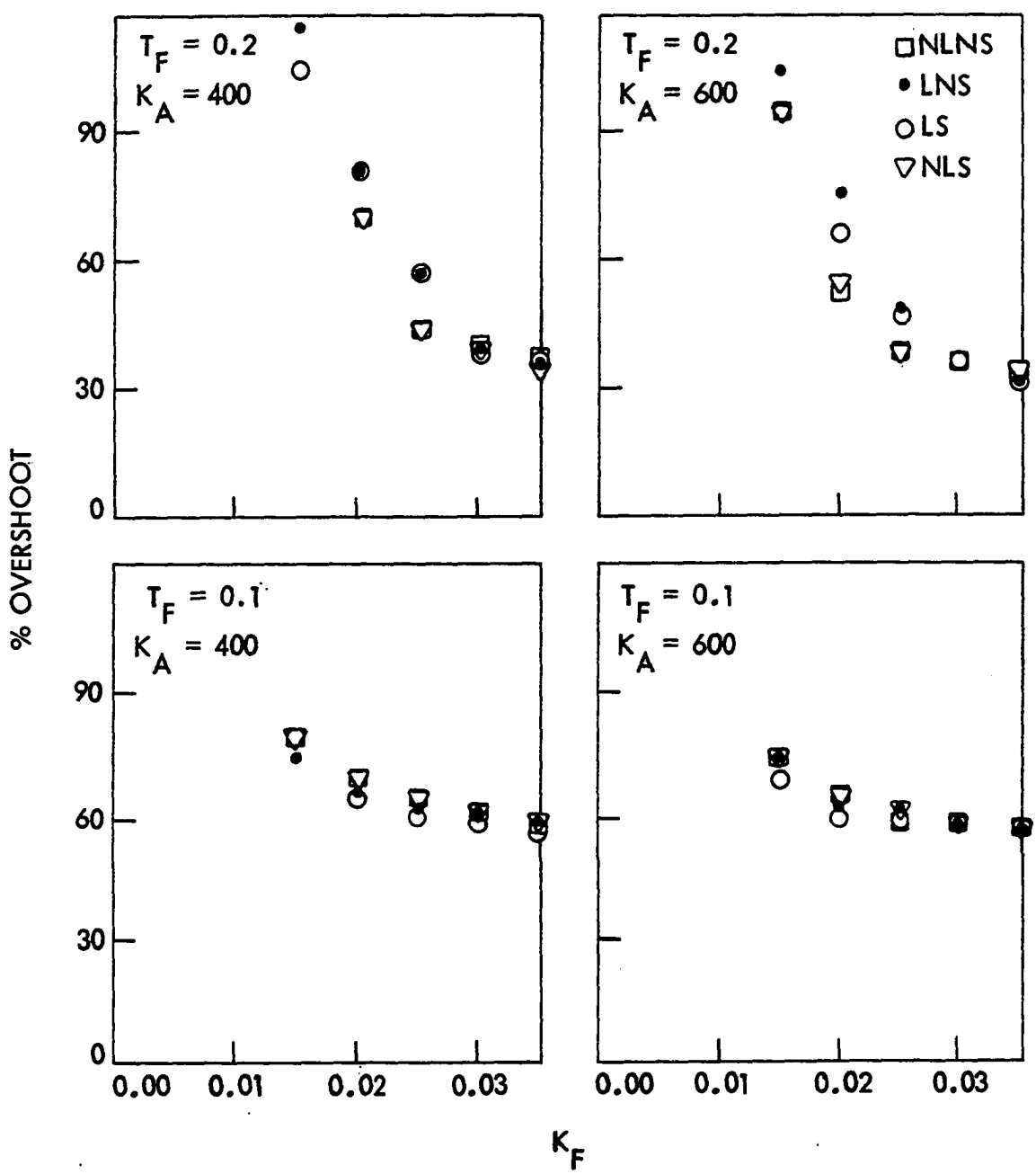

Figure 20. Percent overshoot vs K_F for NLNS, LNS, LS and NLS with low response exciter and model I

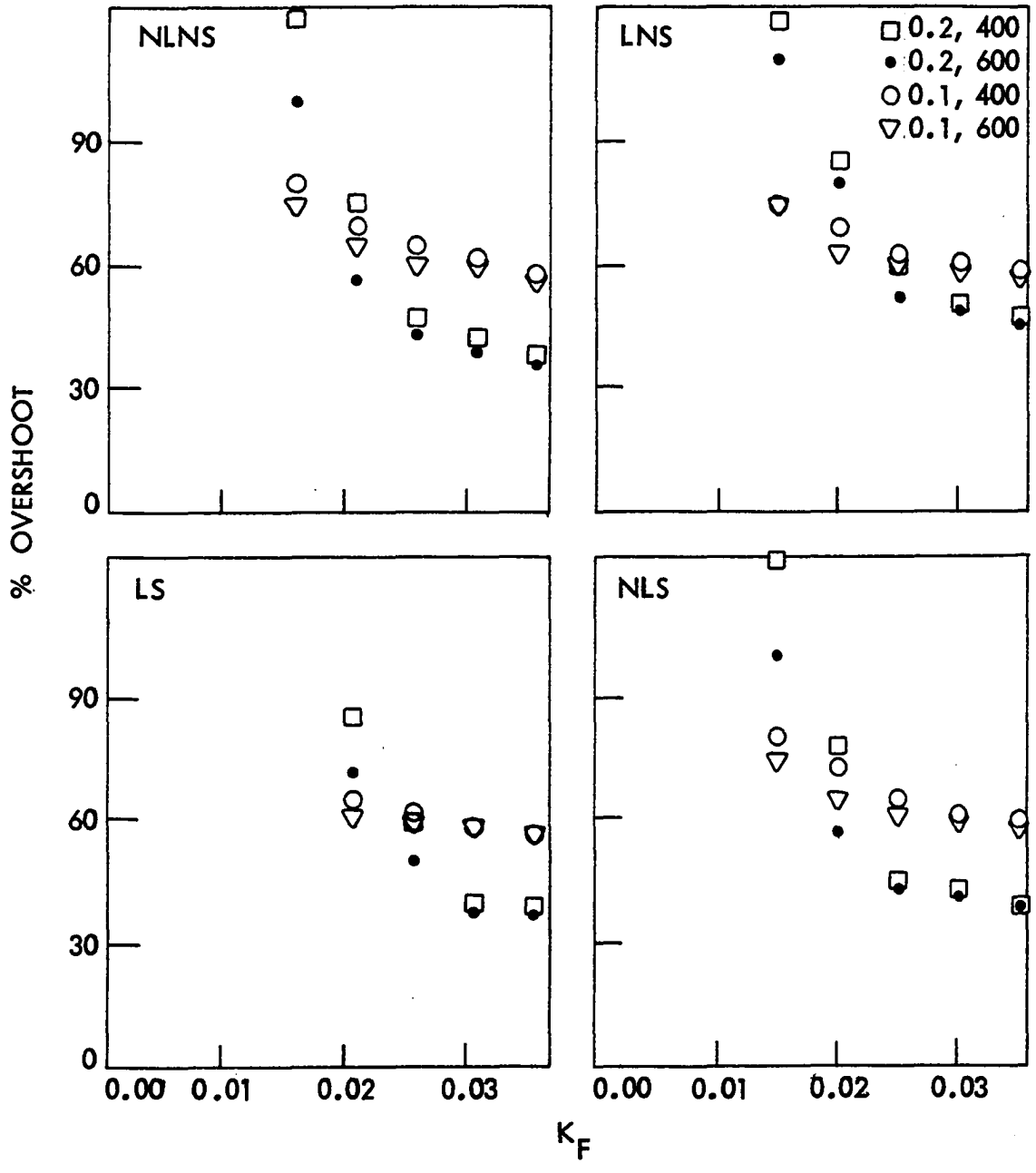

Figure 21. Percent overshoot vs K_F for T_F and K_A of .2/400, .2/600, .1/400 and .1/600 with low response exciter and model I

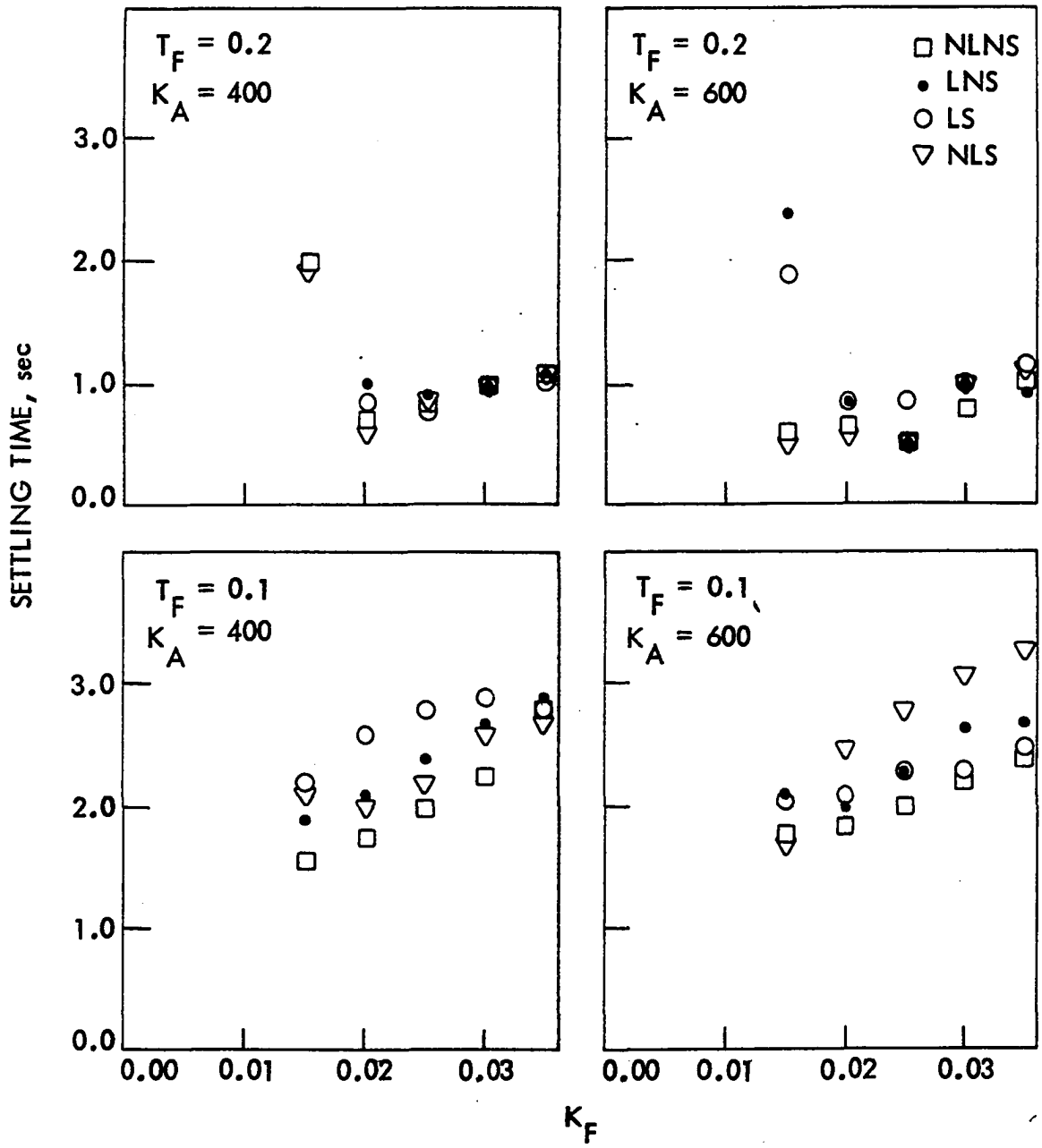

Figure 22. Settling time vs K_F for NLNS, LNS, LS and NLS with low response exciter and model I

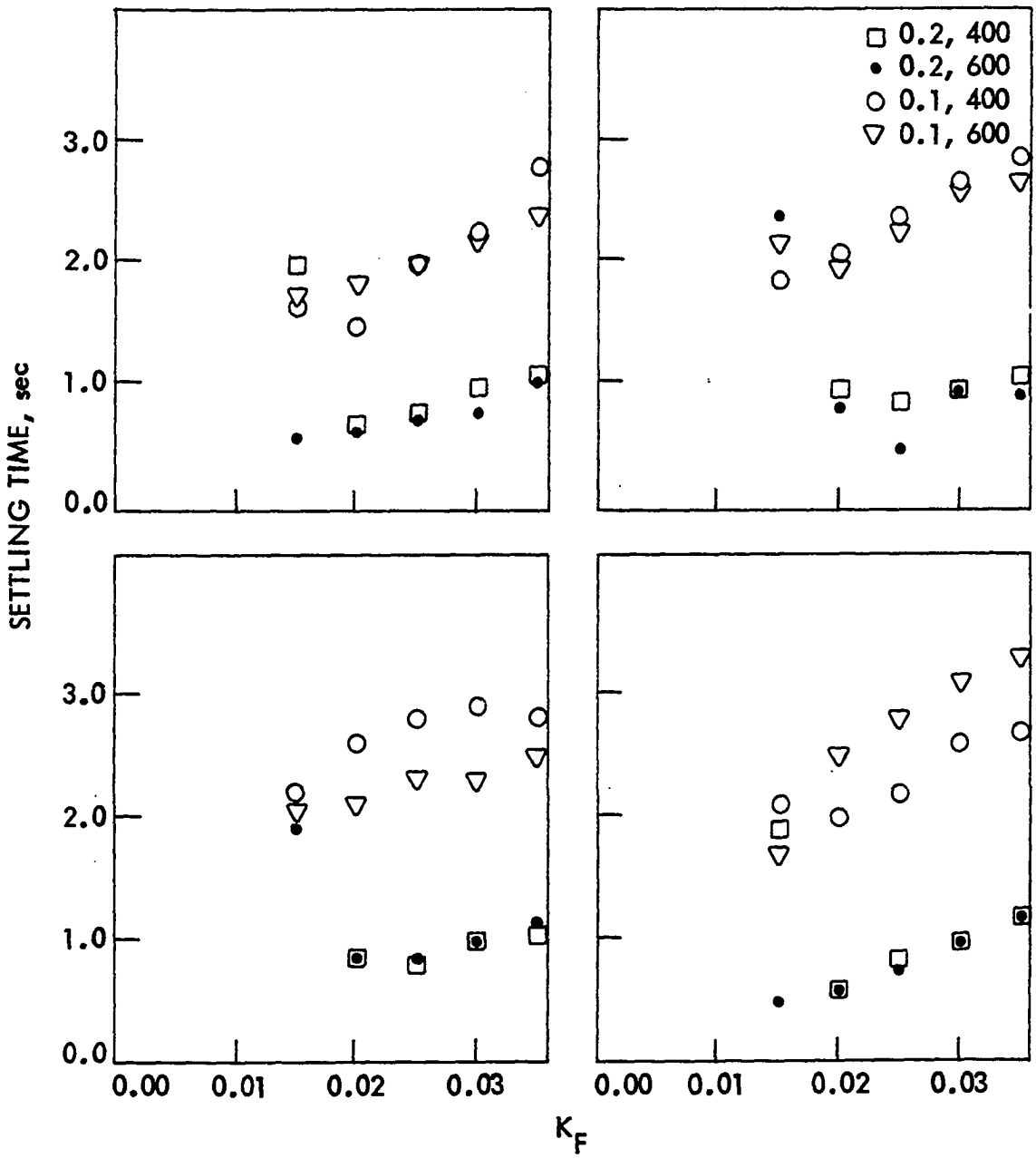

Figure 23. Settling time vs K_F for T_F and K_A of .2/400, .2/600, .1/400 and .1/600 with low response exciter and model I

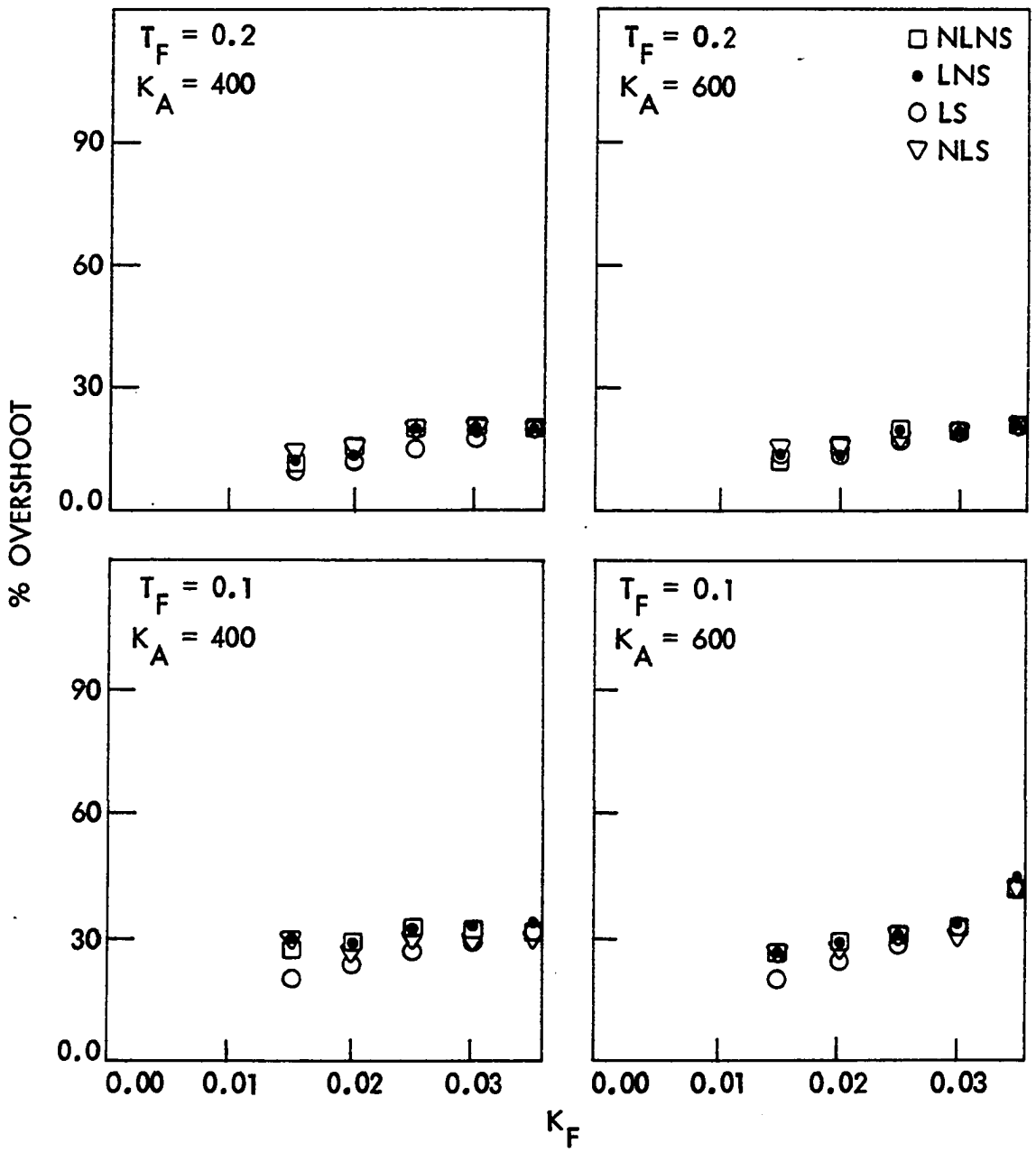

Figure 24. Percent overshoot vs K_F for NLNS, LNS, LS and NLS with high response exciter and model I

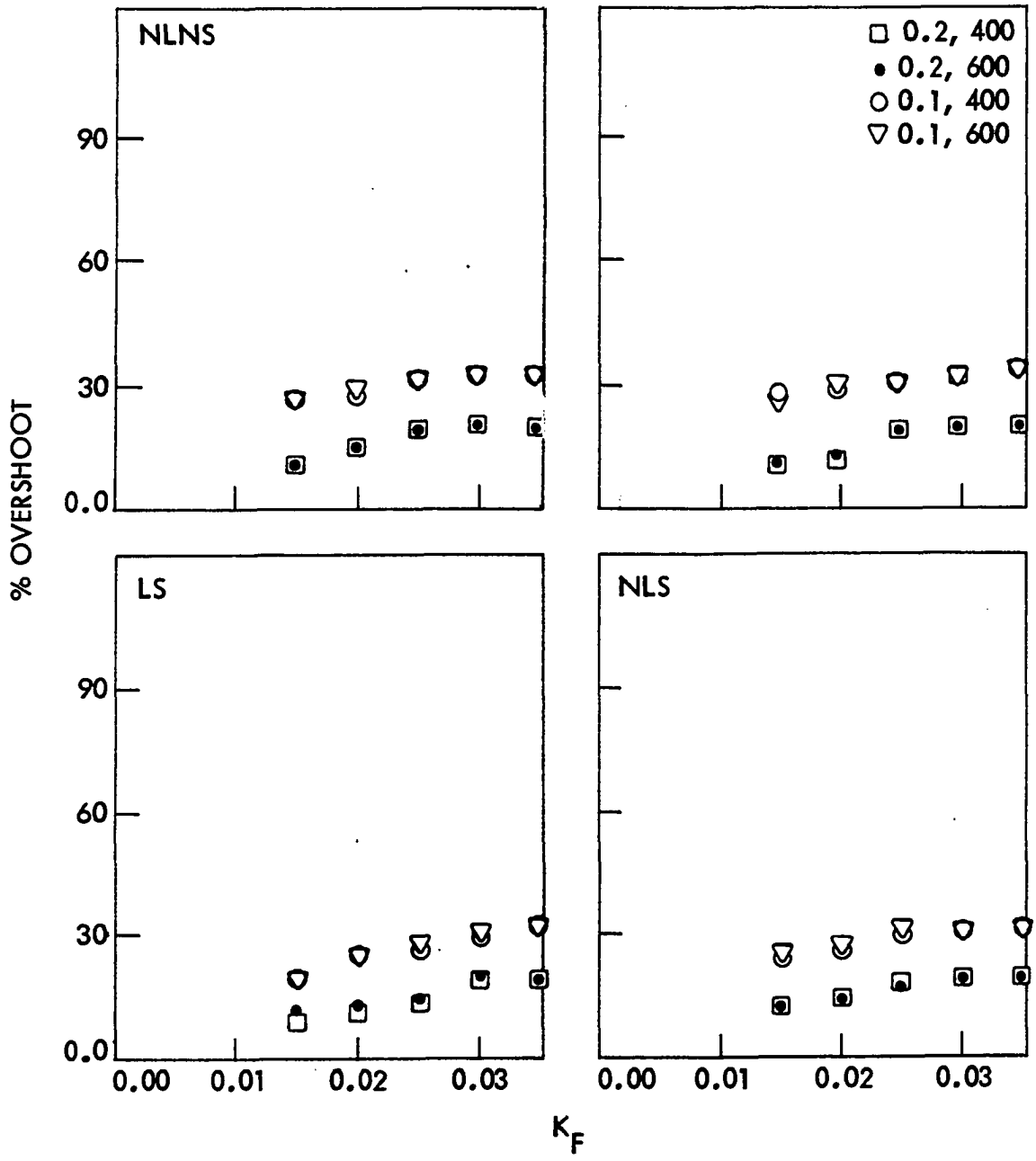

Figure 25. Percent overshoot vs K_F for T_F and K_A of .2/400, .2/600, .1/400 and .1/600 with high response exciter and model I

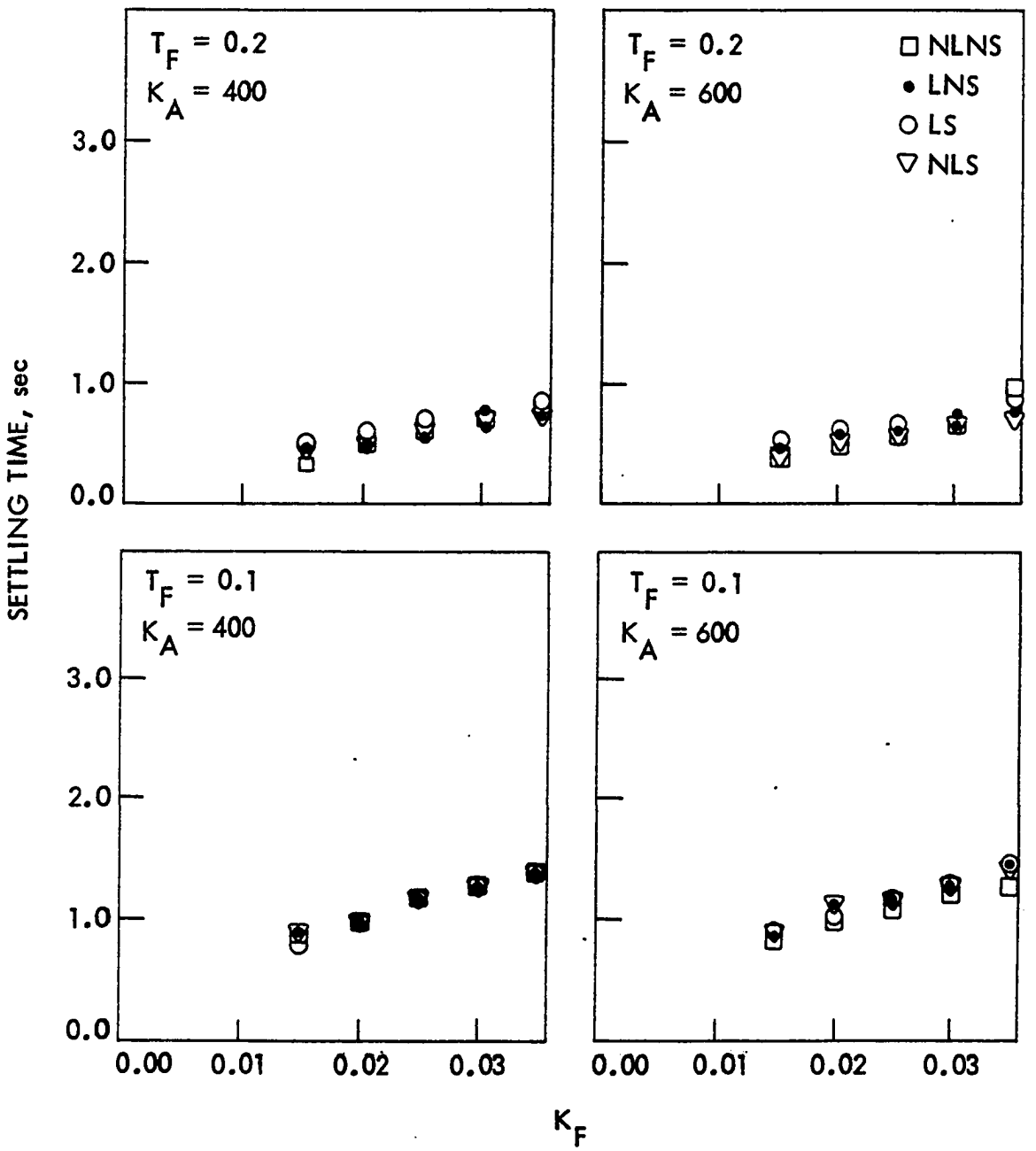

Figure 26. Settling time vs K_F for NLNS, LNS, LS and NLS with high response exciter and model I

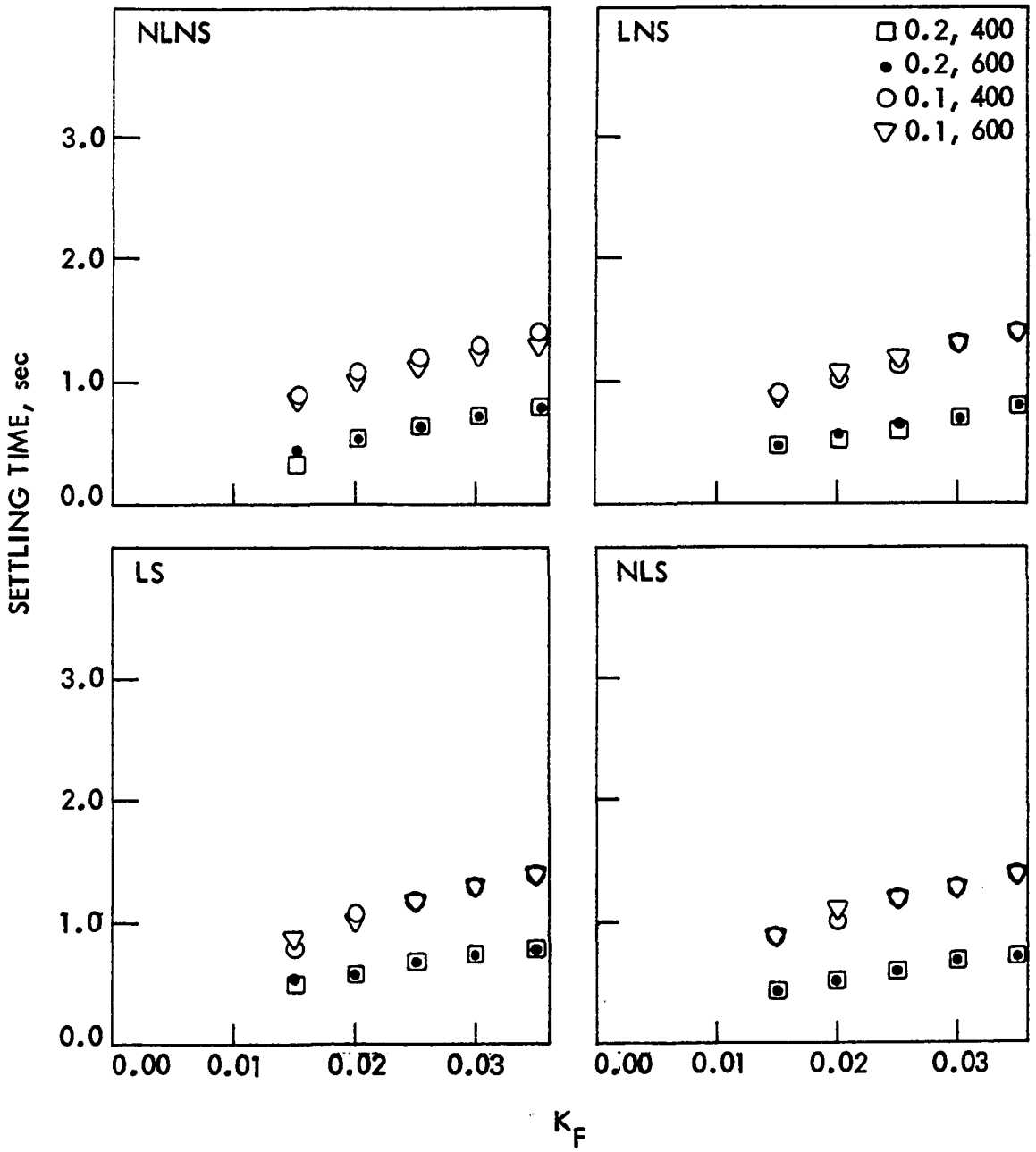

Figure 27. Settling time vs K_F for T_F and K_A of .2/400, .2/600, .1/400 and .1/600 with high response exciter and model I

V. MODEL III - SIMPLIFIED LINEAR MODEL

In this chapter the performance of the simplified linear model, model III, is studied using the two excitation systems, the low and high response exciters discussed in Chapter IV. After observing the need to include damping in the model in section A, machine model IV is simulated in section B to determine the amount of damping needed and, with the damping thus determined, the performance of model III is studied in section C. Section D presents the conclusions that can be drawn from the studies in this chapter.

A. Simulation of Model III Without Damping

Both the theoretical development of model III and the accompanying detailed block diagram have been discussed in section D of Chapter III. The analog computer simulation diagram and the potentiometer settings used for this model are presented in Appendix B.

The model was first simulated without the damping feedback path indicated by the dashed lines shown in Figure 7 (see Chapter III).

An analog computer time scaling, a, of 100 was used and the system was operated, whenever possible, in slow millisecond (SMS) analog mode. Thus one second of the analog computer time corresponds to one second of the synchronous machine operation.

Figures 28 and 29 show the response of model III for the slow and fast response exciters, respectively. The extreme left and right portions of the chart recordings indicate zero voltages. At A the system is switched to operate. The load was applied at point B. Since interest in Δv_t is

centered around the system response to step changes in τ_m and v_{ref}, the channel for recording Δv_t was off prior to point C. A step change in τ_m was applied at D and removed at E. Similarly, a step change in the reference voltage v_{ref} was applied and removed at F and G, respectively. Finally, the recorder channels were turned to zero at H.

Figure 30 shows the response of model III without damping to $\Delta\tau_m$ and Δv_{ref}. In this case the system was at steady state operation prior to point A but the chart recorder was off. Thus the values indicated between points A and B show the steady state operating condition. A step change in τ_m was applied at B and removed at C. Points D and E show the application and removal of Δv_{ref}. The recorder was returned to zero at F. This figure also shows the response of the accelerating torque, τ_a.

As shown in Figures 28, 29 and 30, the response of model III, particularly to the step change in the load torque clearly indicates the need for the damping feedback path shown in Figure 7 (see Chapter III) since the actual machine does not exhibit the oscillations visible in these runs.

B. Simulation of Model IV with the Assumptions of Model III

The amount of damping required in simulating the simplified linear model, model III, can be determined by simulating the nonlinear model, model IV, under the assumptions used in model III. For convenience, the assumptions which are not common to the two models are restated here:

1) Amortisseur effects are negligible.

2) Armature resistance is negligible.

3) The flux linkages are constant, i.e. $p\psi$ or $p\lambda$ terms are negligible.

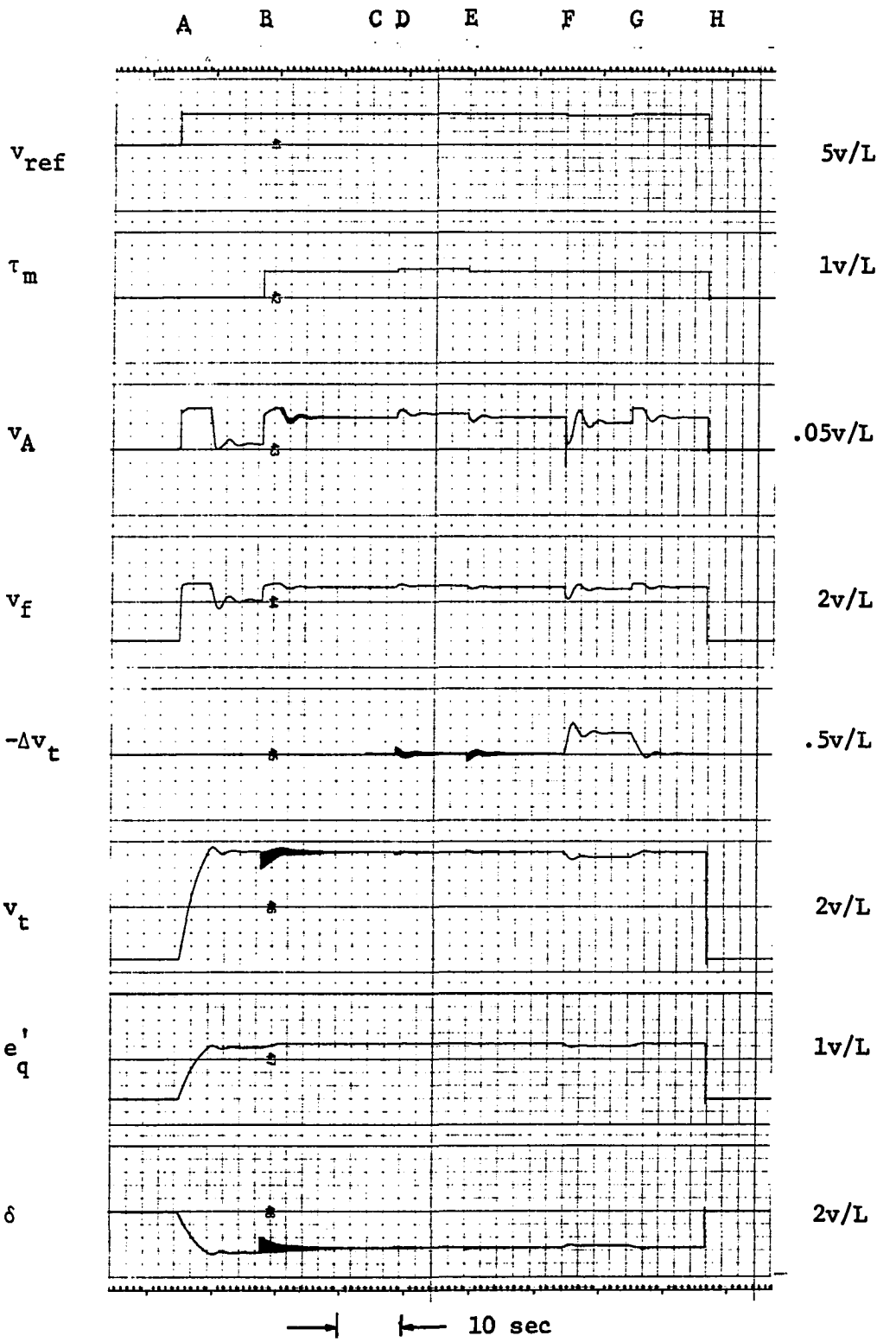

Figure 28. Response of model III to $\Delta\tau_m$ and Δv_{ref} without damping - slow exciter

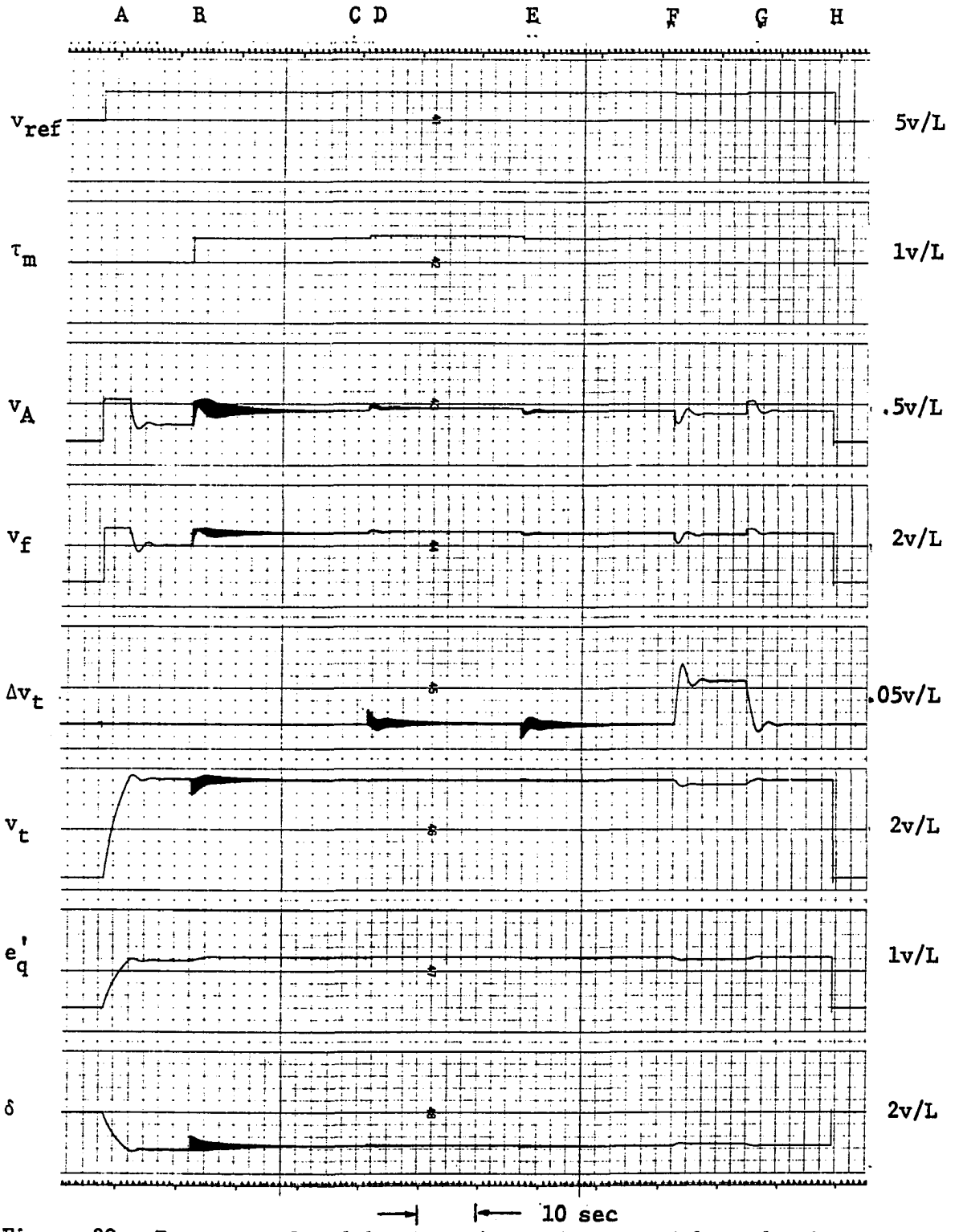

Figure 29. Response of model III to $\Delta\tau_m$ and Δv_{ref} without damping - fast exciter

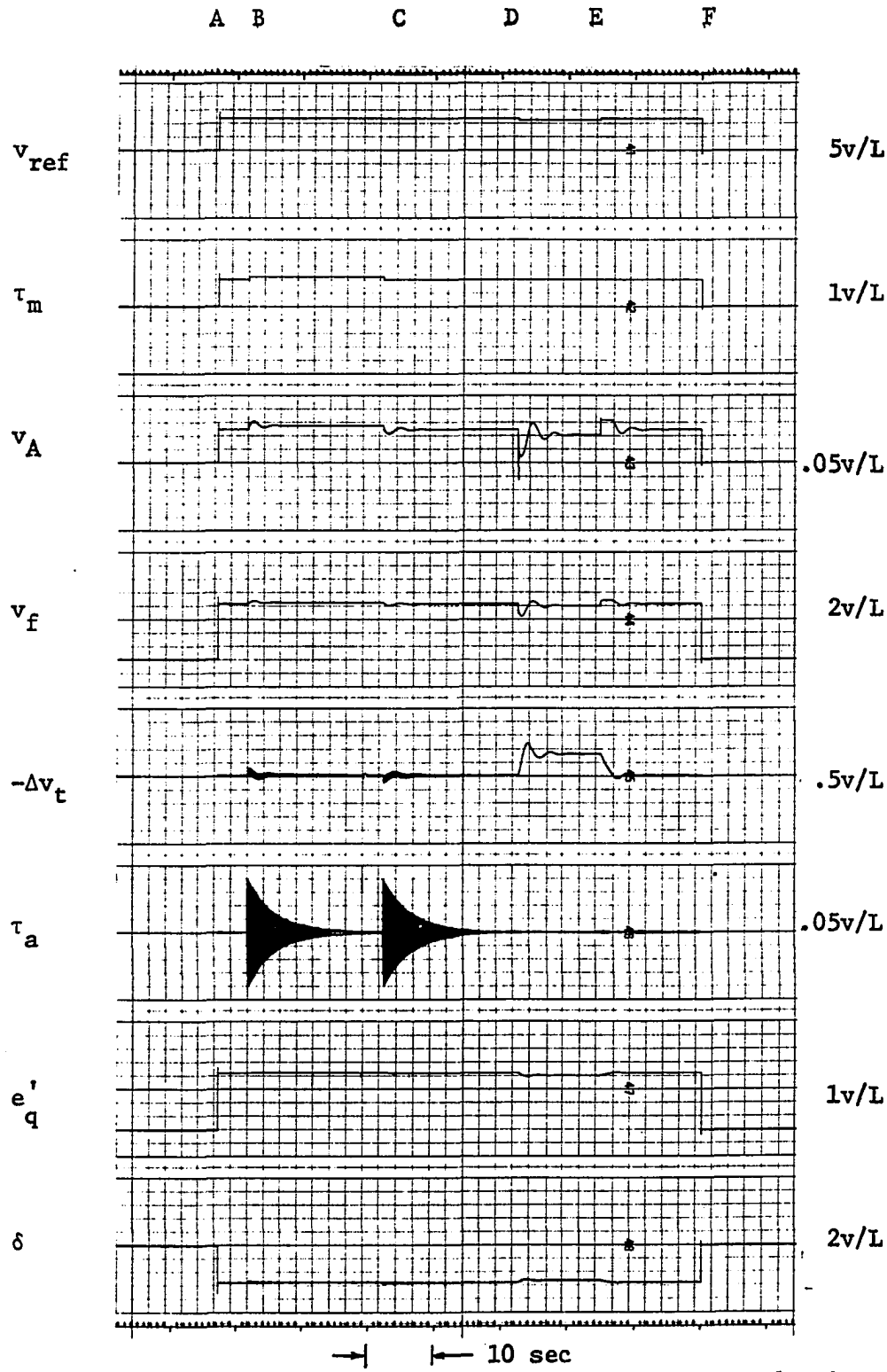

Figure 30. Effect of $\Delta\tau_m$ and Δv_{ref} on model III without damping - slow exciter

Since the above assumptions were not used in developing model IV, the model can be simulated with and without these assumptions. The analog computer representation of model IV and the analog patching changes necessary for measuring the damping are discussed in Appendix C.

1. Simulation of model IV without amortisseur effects

The simulation of the nonlinear model, model IV, without amortisseur effects was performed by making the direct and quadrature axes amortisseur resistances, R_D and R_Q, very large. In this case R_D and R_Q were increased by 100 times their normal values.

Figure 31 indicates the steps followed to determine the damping required. The system was operated in the Fast Second (F Sec) analog mode (1.0 second of real time represented by 10 seconds on chart). Point A shows when the recorder was turned to operate. At points B and C, $\Delta\tau_m$ was applied and removed, respectively. Just before point D the recorder was stopped and the values of R_D and R_Q were increased to 100 times their normal values. Then at points D and E, $\Delta\tau_m$ was again applied and removed. Then with R_D and R_Q still 100 times their normal values, a mechanical switch connecting appropriate damping into the feedback path was turned on and $\Delta\tau_m$ was again applied and removed at F and G, respectively. The system response observed after connecting the damping was about the same as that observed before the assumption of no amortisseur effects was made. This indicated that a correct potentiometer setting, from which the damping can be calculated, has been determined.

As shown in runs discussed in Chapter VI, Δv_{ref} has negligible effect on change in rotor speed, $\Delta\omega$.

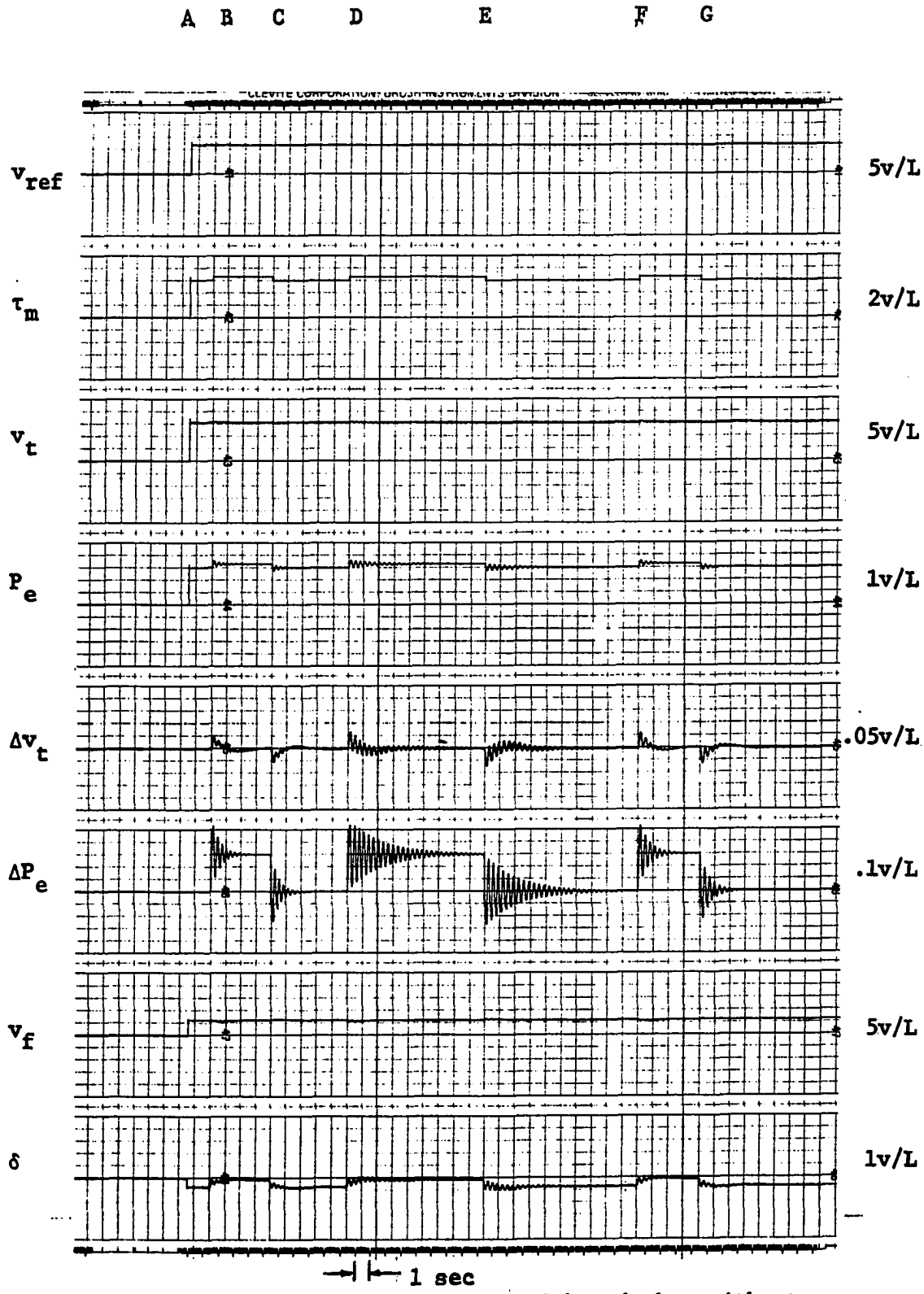

Figure 31. Response of model IV to $\Delta\tau_m$ with and then without amortisseur effects - fast exciter

2. Simulation without armature resistance

The condition of negligible armature resistance, r_a, is simulated by resetting the appropriate potentiometers (see Appendix C) to zero. Figure 32 shows the results. In this case the system was operated in the Fast Second analog mode. The chart recorder was turned on at A and off at H while points B-G have similar meaning as their counterpart in Figure 31. In this case, however, potentiometers containing armature resistance, r_a, were set to zero just before point D and, retaining the conditions used at points D and E, an arbitrarily small damping was introduced before point F. The figure indicates that armature resistance, which is actually very small, has negligible effect on the system response to $\Delta\tau_m$.

3. Simulation with no amortisseur effects and no armature resistance

Combining the assumptions of no amortisseur effects and negligible armature resistance led to a system response identical to that shown in Figure 31. This follows from section 2 where it was noted that neglecting armature resistance has little or no effect on the system response. Thus the damping determined in section 1 for the condition of no amortisseur effects survived for the two combined assumptions.

4. Simulation with constant flux linkages

Model IV could not be simulated with the assumption of constant flux linkages without saturating several analog computer summing amplifiers and integrators.

The direct axis equivalent circuit of the synchronous machine can be represented as shown in Figure 33 (see Appendix C). If $p\lambda_d$ shown in the figure equals to zero, then:

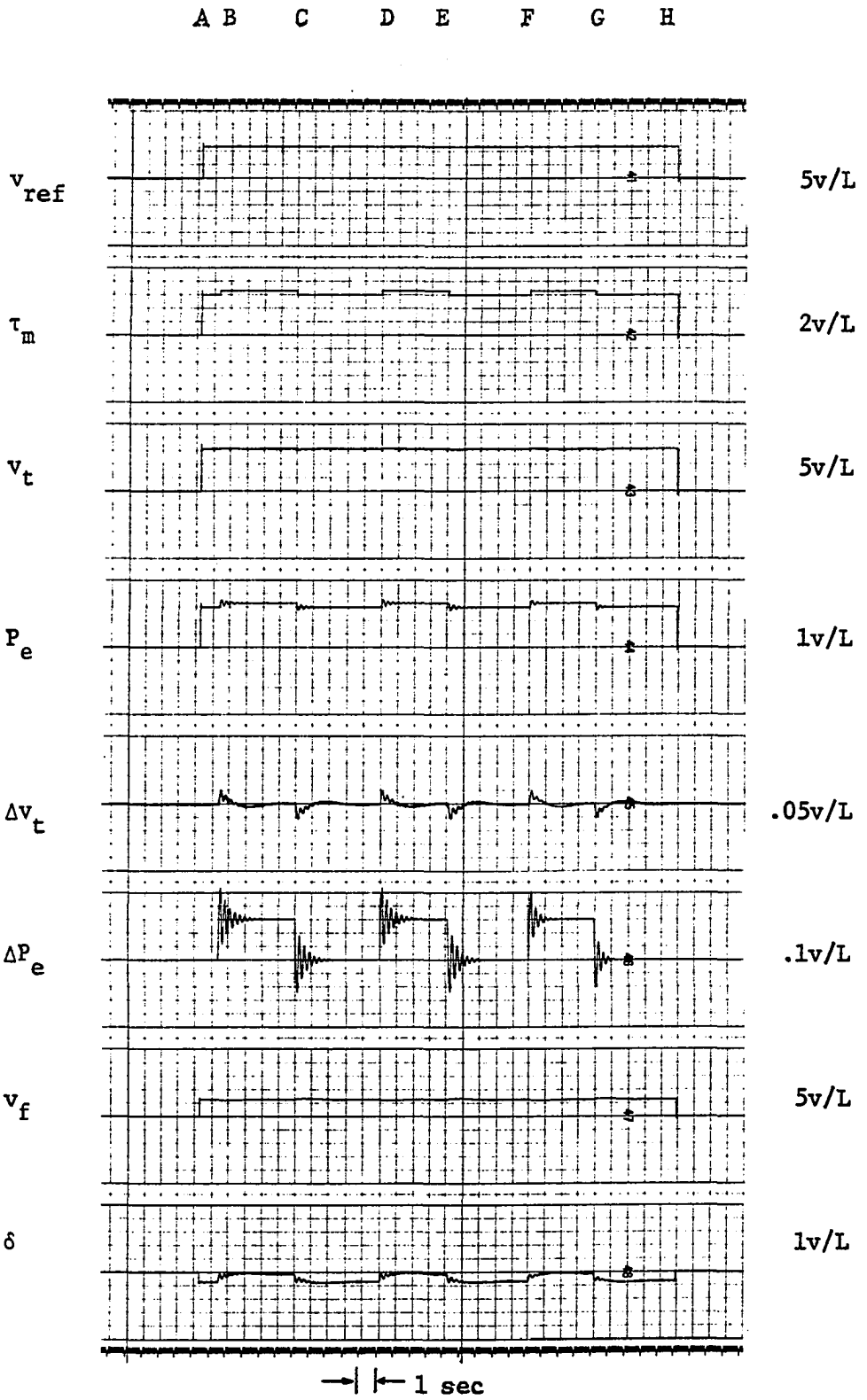

Figure 32. Response of model IV to $\Delta\tau_m$ with and without armature resistance - fast exciter

$$v_d = r_a i_d + \omega\lambda_q \qquad [32a]$$

or

$$i_d = \frac{v_d - \omega\lambda_q}{r_a} \qquad [32b]$$

Thus, since r_a is small, i_d may become very large.

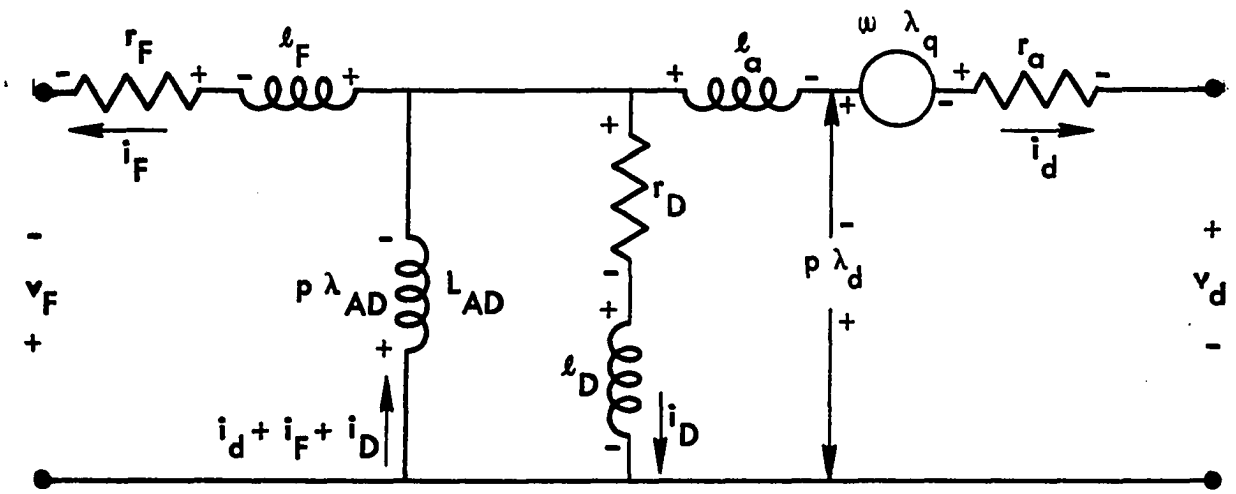

Figure 33. The direct axis equivalent circuit for synchronous machine

The operation of the nonlinear model, model IV with and without the assumption of constant flux linkages is shown in Figures 34 and 35. The model was operated in slow millisecond analog mode. After the system has reached steady state, the recorder was switched to operate at A and the step change in load torque was applied at B and removed at C. The recorder was stopped at D and, using an electronic switch, the integrators for computing λ_d and λ_q were switched to hold. Immediately after this,

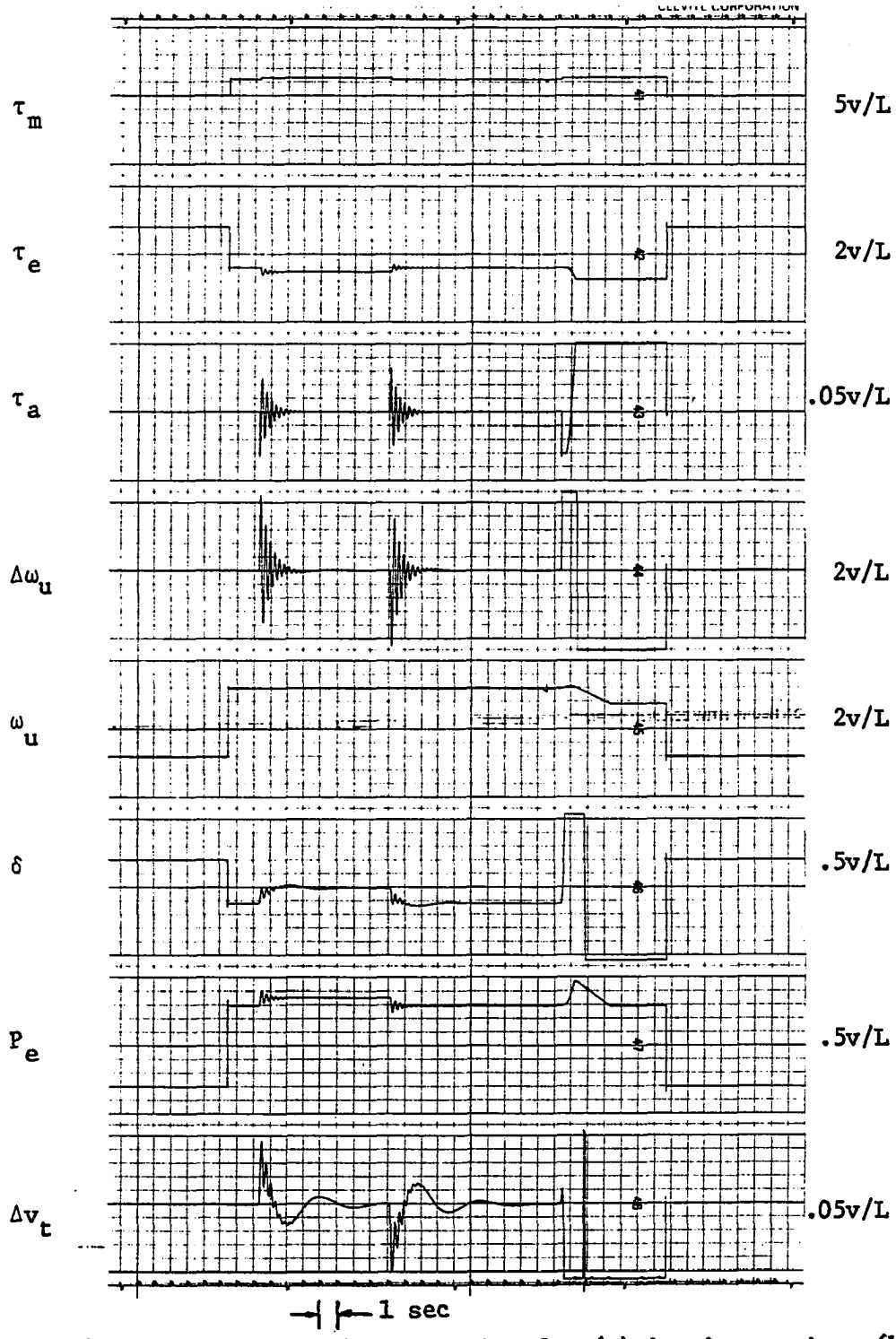

Figure 34. Response of model IV to $\Delta\tau_m$ for (a) λ_d, λ_q varying, (b) λ_d, λ_q held constant at steady state values - slow exciter

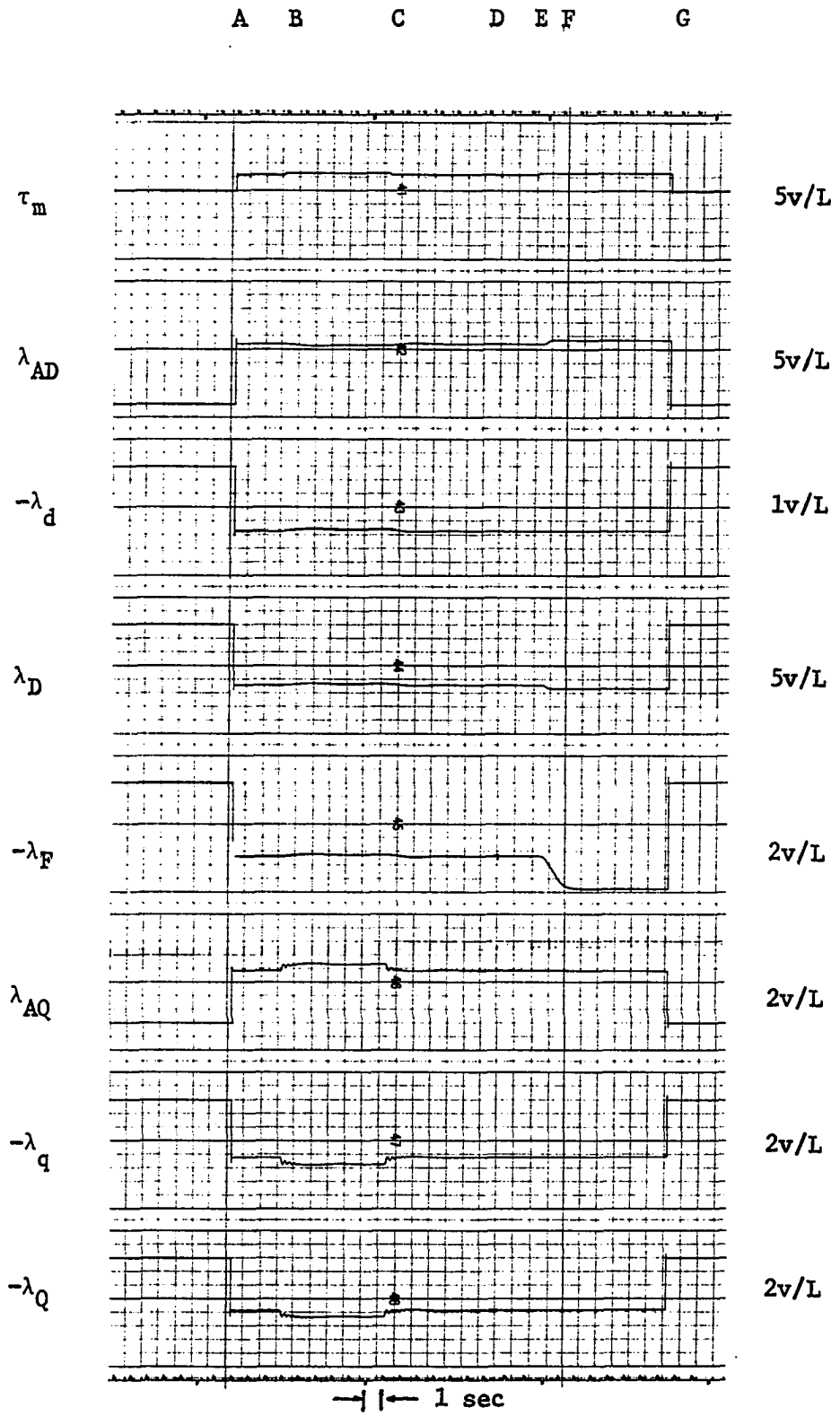

Figure 35. Response of model IV to $\Delta\tau_m$ for (a) λ_d, λ_q varying, (b) λ_d, λ_q held constant at steady state values - slow exciter

the recorder was switched on and $\Delta\tau_m$ was applied at E. Analog computer components started saturating at F. The increase in λ_d during the first second of operation after applying $\Delta\tau_m$ at B is less than 1 volt, which is 0.02 per unit, and which is very small compared to the steady state value of λ_d. Thus in terms of relay operation or automatic system control, λ_d may be assumed constant.

In each of the foregoing runs a corresponding run for v_f constant was made by turning switch 011 to R position (see Appendix C) and setting the potentiometer to a constant voltage observed at the steady state operation.

5. Summary of damping required

The measurement of damping as described in section 3 was performed for the two excitation systems and also for v_f held constant at the steady state values. The results are summarized in Table 9 where the damping represents commonly used units for D (see Appendix C). The values of D are higher than normal. This is due to the presence of local load (see Appendix D).

Table 9. Summary of damping required for the assumption of negligible armature resistance and no amortisseur effects

		Setting of Pot 812	D_u=237(P.S.) (Per unit torque-sec^{-1})	(D_u/ω_e)=.628(P.S.) (Per unit torque-sec/rad)
Fast exciter	v_f varying	.2080	49.30	.1305
	v_f constant	.2244	53.20	.1410
Slow exciter	v_f varying	.2268	53.75	.1425
	v_f constant	.2700	64.00	.1695

There is obviously a cross-coupling to the voltage controller via the exciter but this is relatively unimportant.

C. Simulation of Model III with Damping Included

Using the damping determined in section B, the performance of the simplified linear model, model III, is studied in this section. The study is conducted in four parts: first, a comparison of the simulation with and without damping was made; then the response of the model to $\pm\Delta\tau_m$ and $\pm\Delta v_{ref}$ is presented to show some of the nonlinear characteristics of the response; thirdly, the response of the model to $\Delta\tau_m$ using NLNS, LNS, LS and NLS was studied; fourth, a study similar to that performed on model I, that is holding τ_m constant and applying Δv_{ref}, is presented.

1. Performance of model III with and without damping

Figure 36 shows the response of model III with damping included. The figure was obtained under conditions similar to those used in obtaining Figure 28. The system response shown in Figure 37 is the same as that in Figure 36 except that the fast exciter was used.

The effect of damping on the simulation of the model is shown in Figures 38 and 39, where the system response without damping and then with damping is shown for the two types of exciters.

Figures 40 and 41 show the response of the model to Δv_{ref} without damping and with damping. In this case, the damping has no noticeable effect on the terminal voltage.

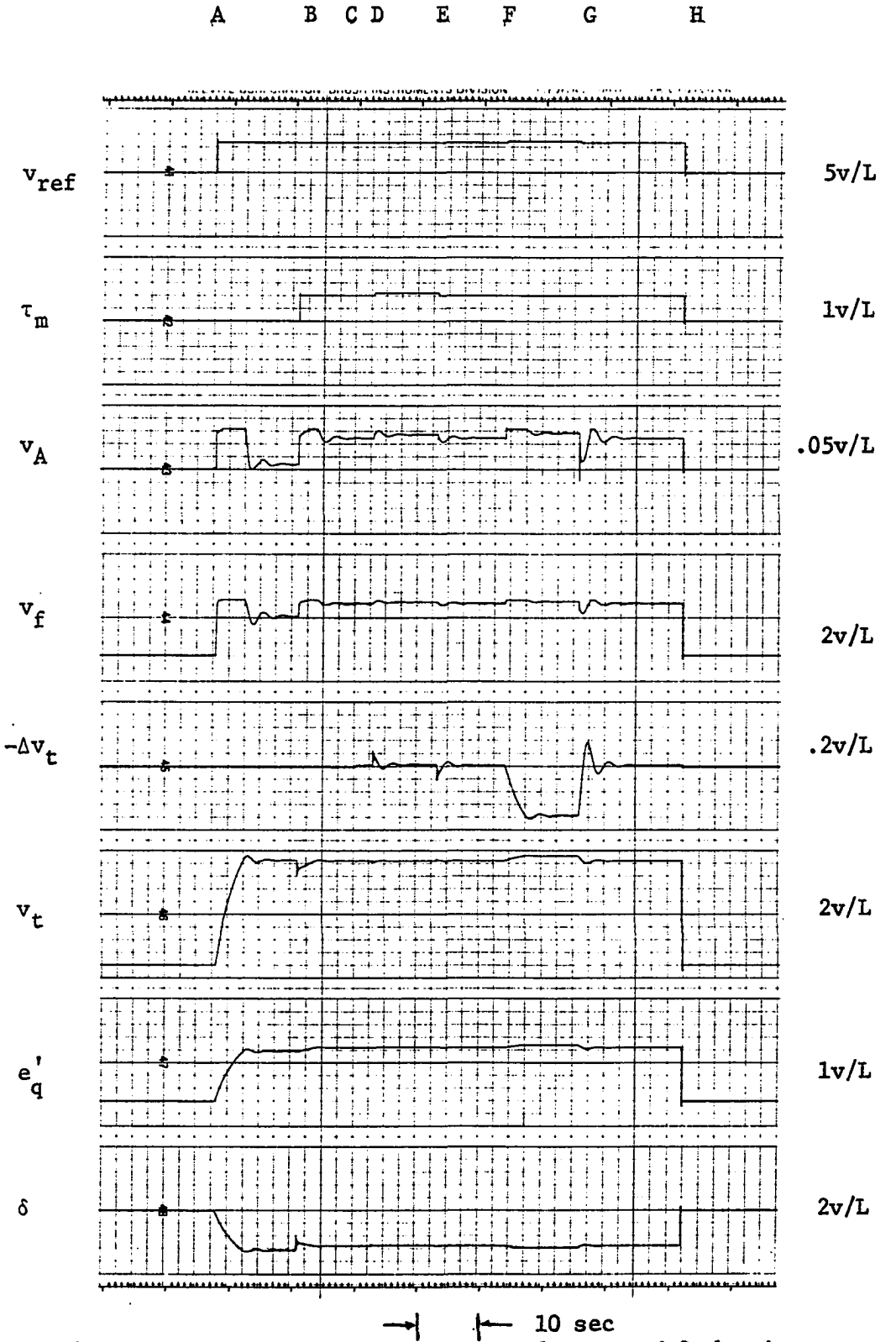

Figure 36. Response of model III to $\Delta\tau_m$ and Δv_{ref} with damping - slow exciter

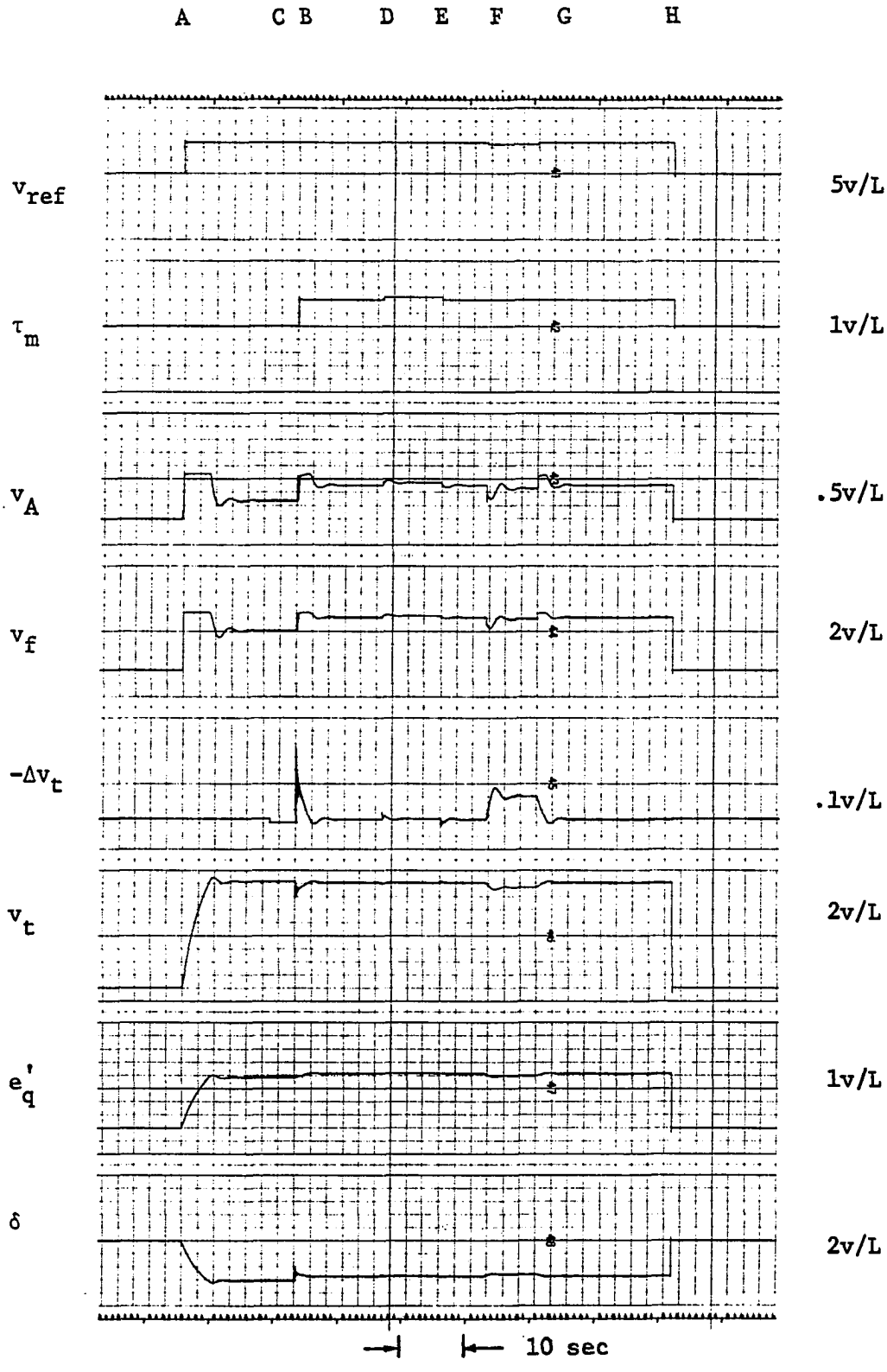

Figure 37. Response of model III to $\Delta\tau_m$ and Δv_{ref} with damping - fast exciter

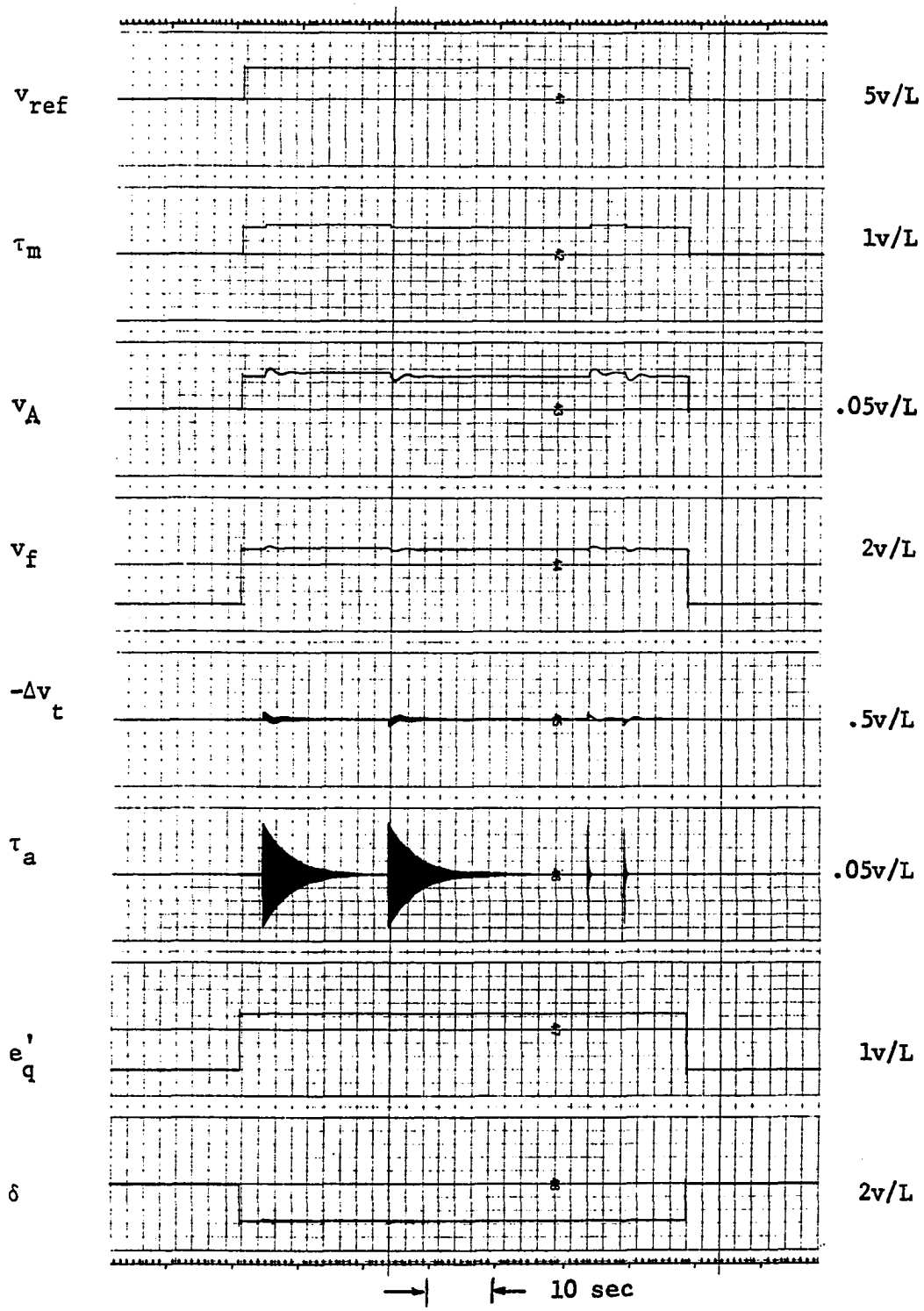

Figure 38. Response of model III to $\Delta\tau_m$ without and then with damping - slow exciter

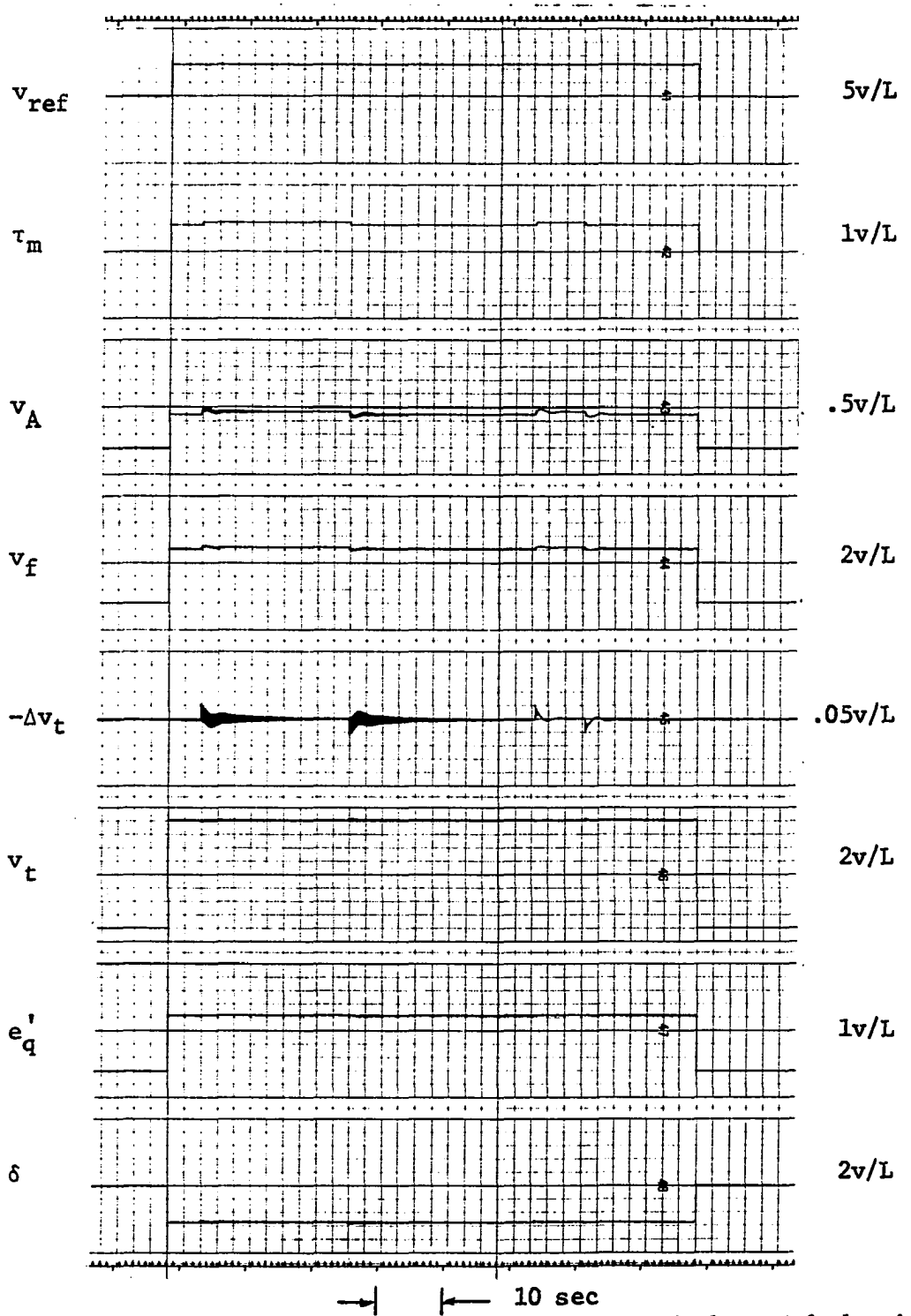

Figure 39. Response of model III to $\Delta\tau_m$ without and then with damping - fast exciter

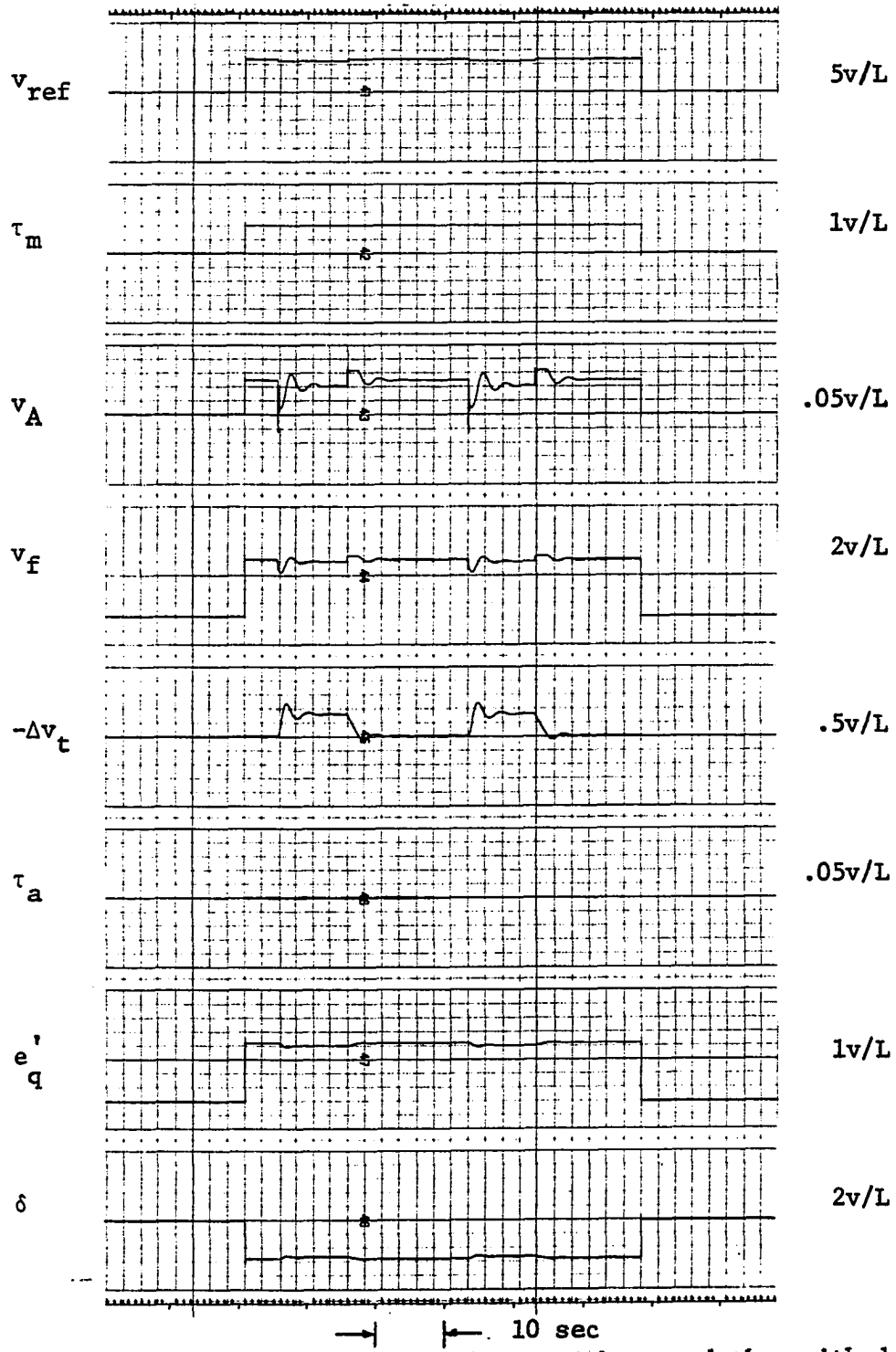

Figure 40. Response of model III to Δv_{ref} without and then with damping - slow exciter

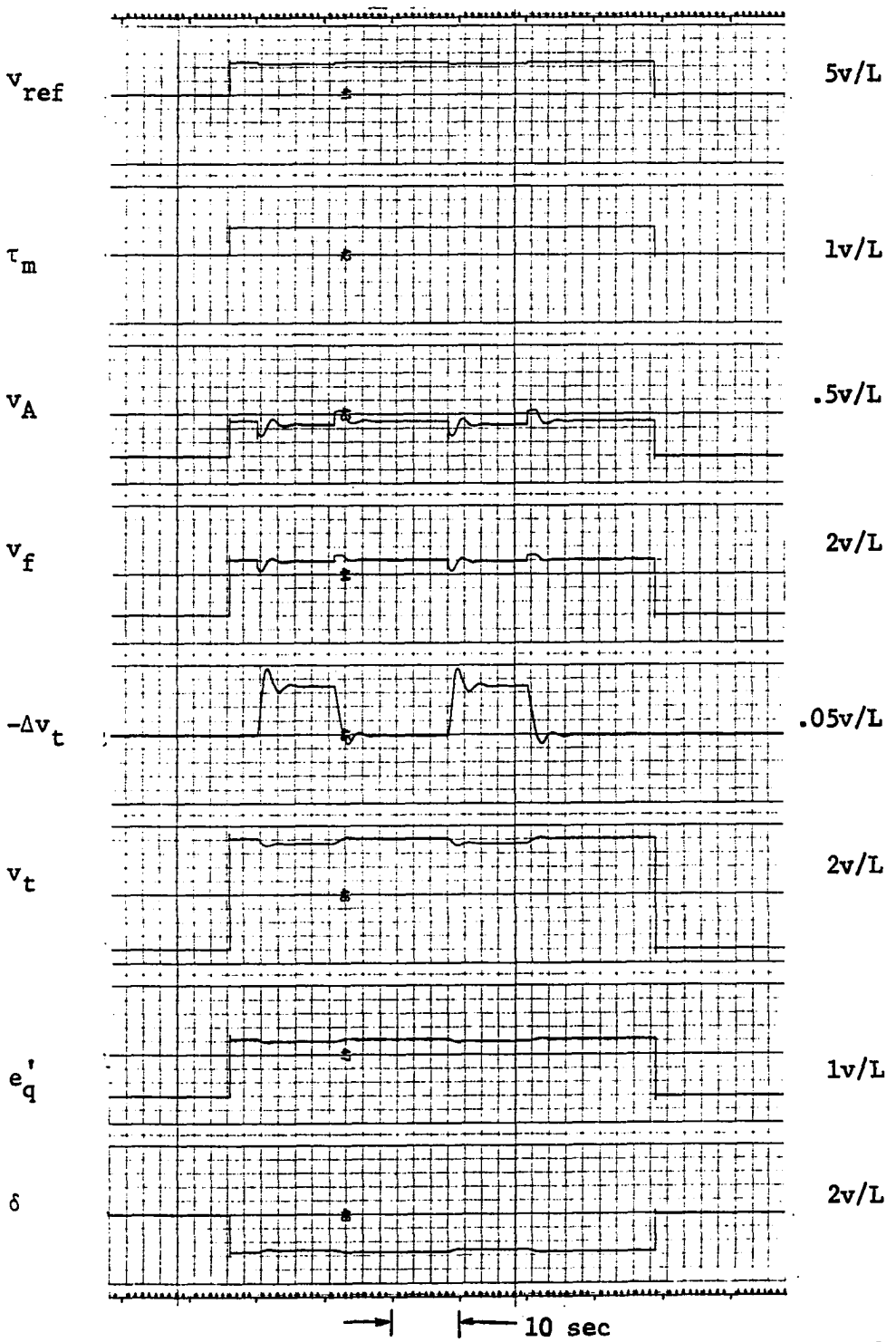

Figure 41. Response of model III to Δv_{ref} without and then with damping - fast exciter

2. Response of model III to $+\Delta\tau_m$, $-\Delta\tau_m$, $+\Delta v_{ref}$ and $-\Delta v_{ref}$ with LS

Some of the nonlinear aspects of the system response may be observed by recording the effects of $+\Delta\tau_m$, $-\Delta\tau_m$, $+\Delta v_{ref}$ and $-\Delta v_{ref}$ on the same chart as shown in Figures 42 and 43 for the slow and fast response exciters, respectively. The time response of the variables recorded is similar for both $+\Delta\tau_m$ and $-\Delta\tau_m$. However, this is not the case with the step change in reference voltage, Δv_{ref}. Each of the four responses of Δv_t to the change in reference voltage is somewhat different from the others. The differences can be observed in terms of the percent overshoot, the rise time and settling time of the responses shown.

3. Response of model III to $\Delta\tau_m$ with NLNS, LNS, LS and NLS

Figures 44 and 45 show the response of model III to $\Delta\tau_m$ with no limiting no saturation (NLNS), limiting but no saturation (LNS), both limiting and saturation (LS) and with no limiting but with saturation (NLS). For NLNS and LNS the time response Δv_t returned to its original steady state value of zero. However, for LS and NLS, Δv_{tss} is about 0.05 volts, indicating that including exciter saturation leads to a small change in the steady state value of the terminal voltage and thereby indicating that the analog simulation exhibits a small error due to the use of DFG.

The fact that the steady state value of Δv_t is negligibly small presents some problem in applying the performance indices used for Δv_t in Chapter IV and defined in Appendix A. A strict adherence to the definition would mean division by zero. Thus in order to compare the response of model III to $\Delta\tau_m$ we would have to define a new set of performance indices.

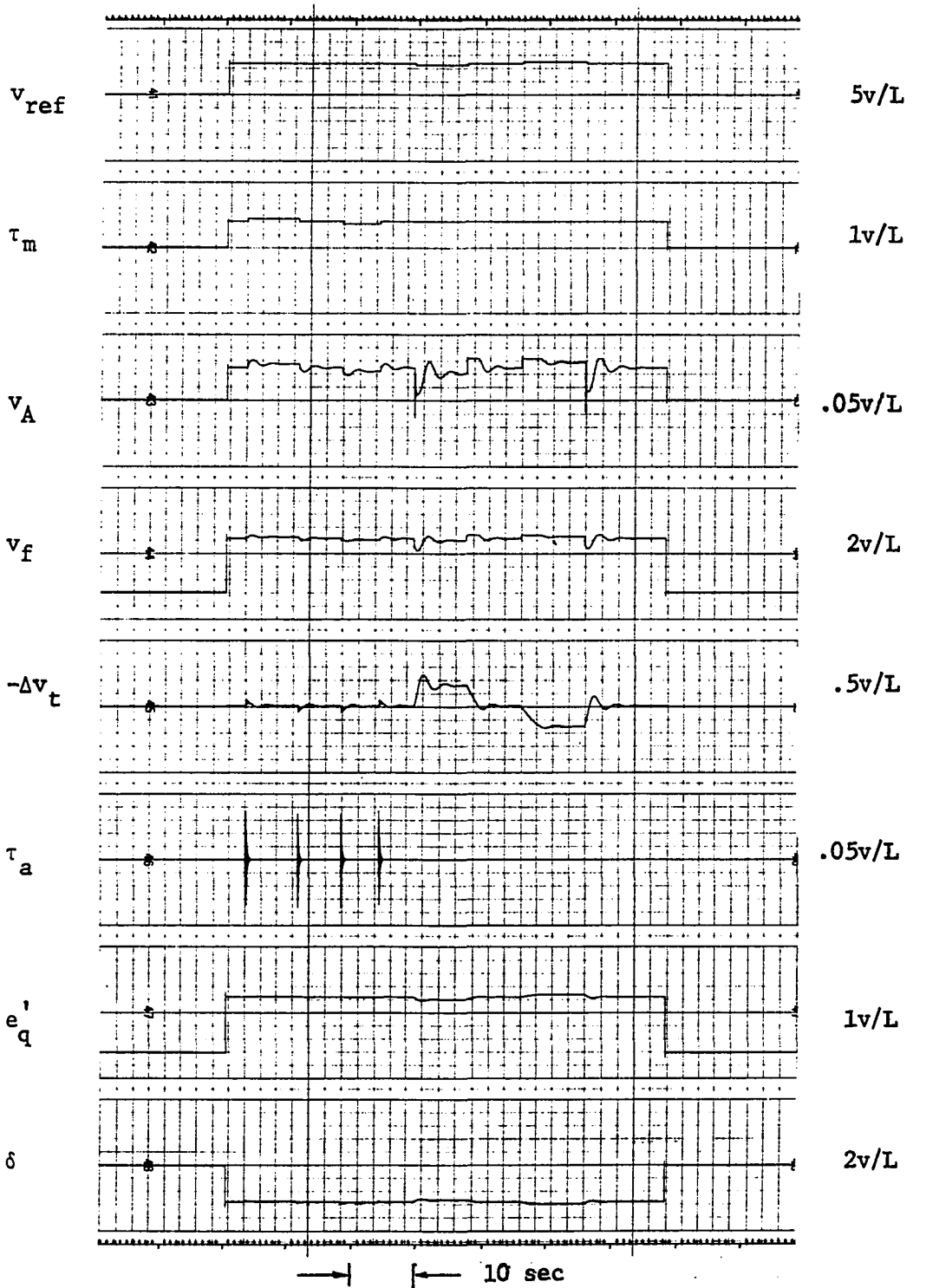

Figure 42. Response of model III, with damping, to $\Delta\tau_m$, $-\Delta\tau_m$, Δv_{ref}, $-\Delta v_{ref}$ - slow exciter

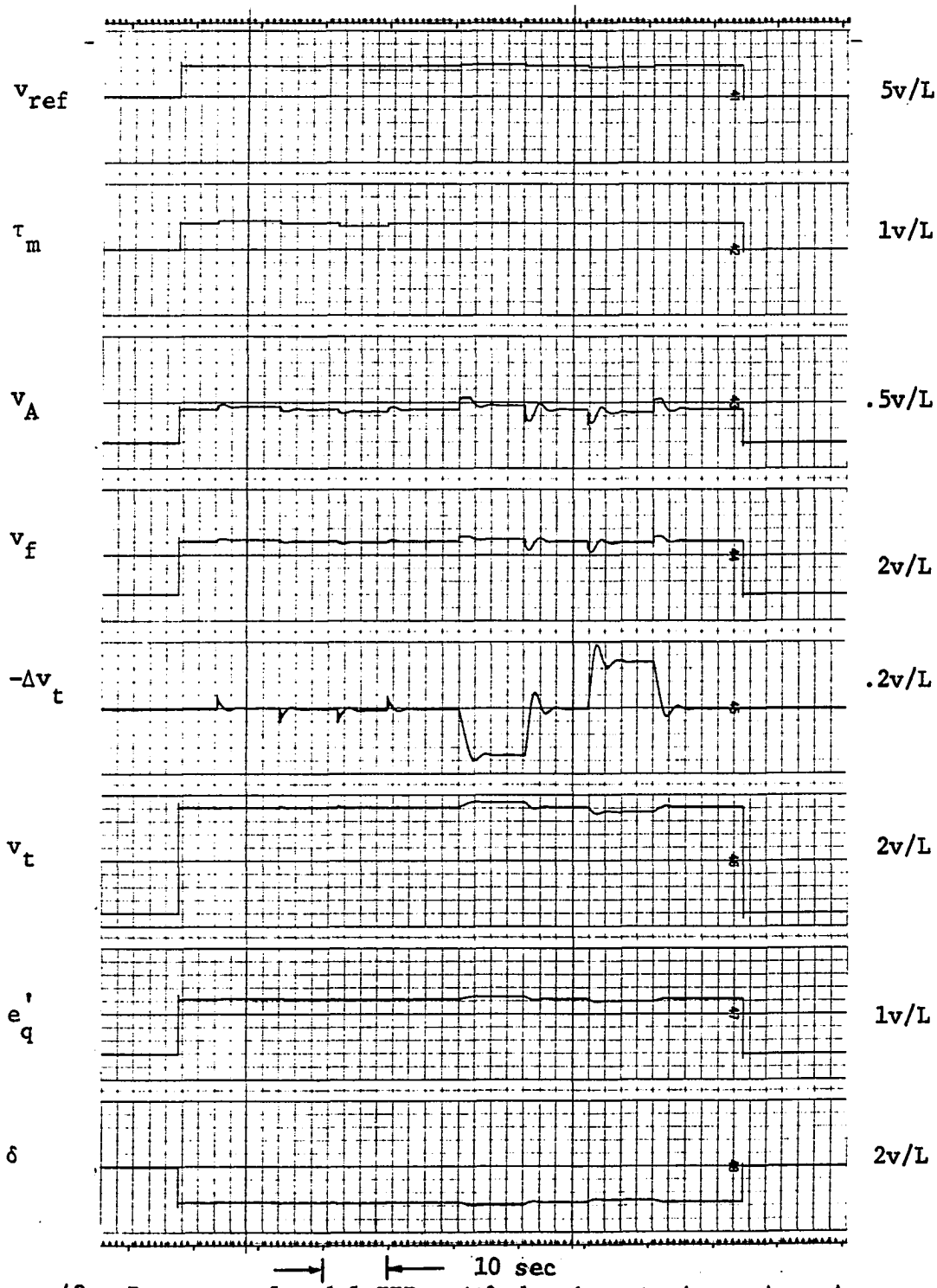

Figure 43. Response of model III, with damping, to $\Delta\tau_m$, $-\Delta\tau_m$, Δv_{ref}, $-\Delta v_{ref}$ - fast exciter

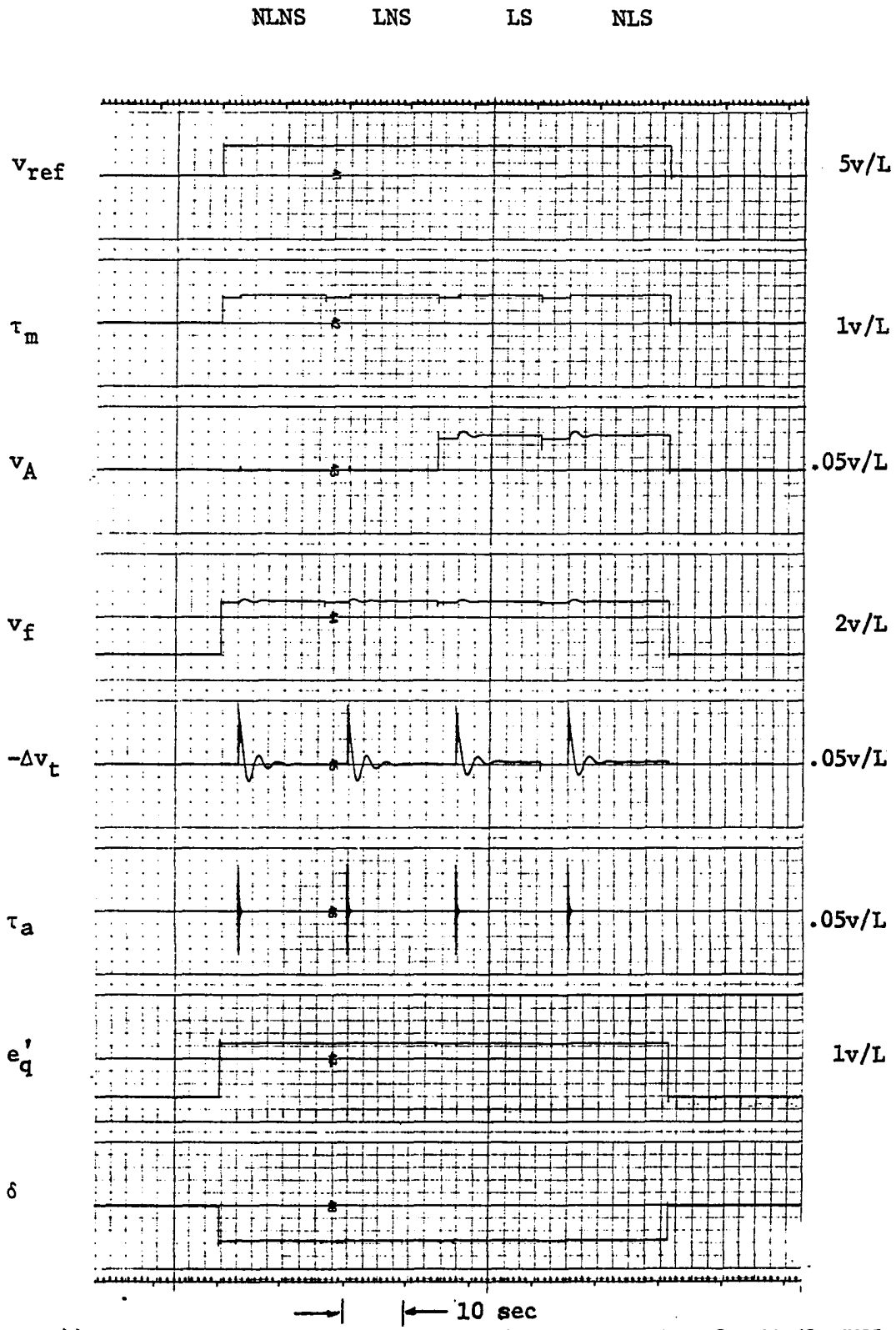

Figure 44. Response of model III, with damping, to $\Delta\tau_m$ for NLNS, LNS, LS, NLS - slow exciter

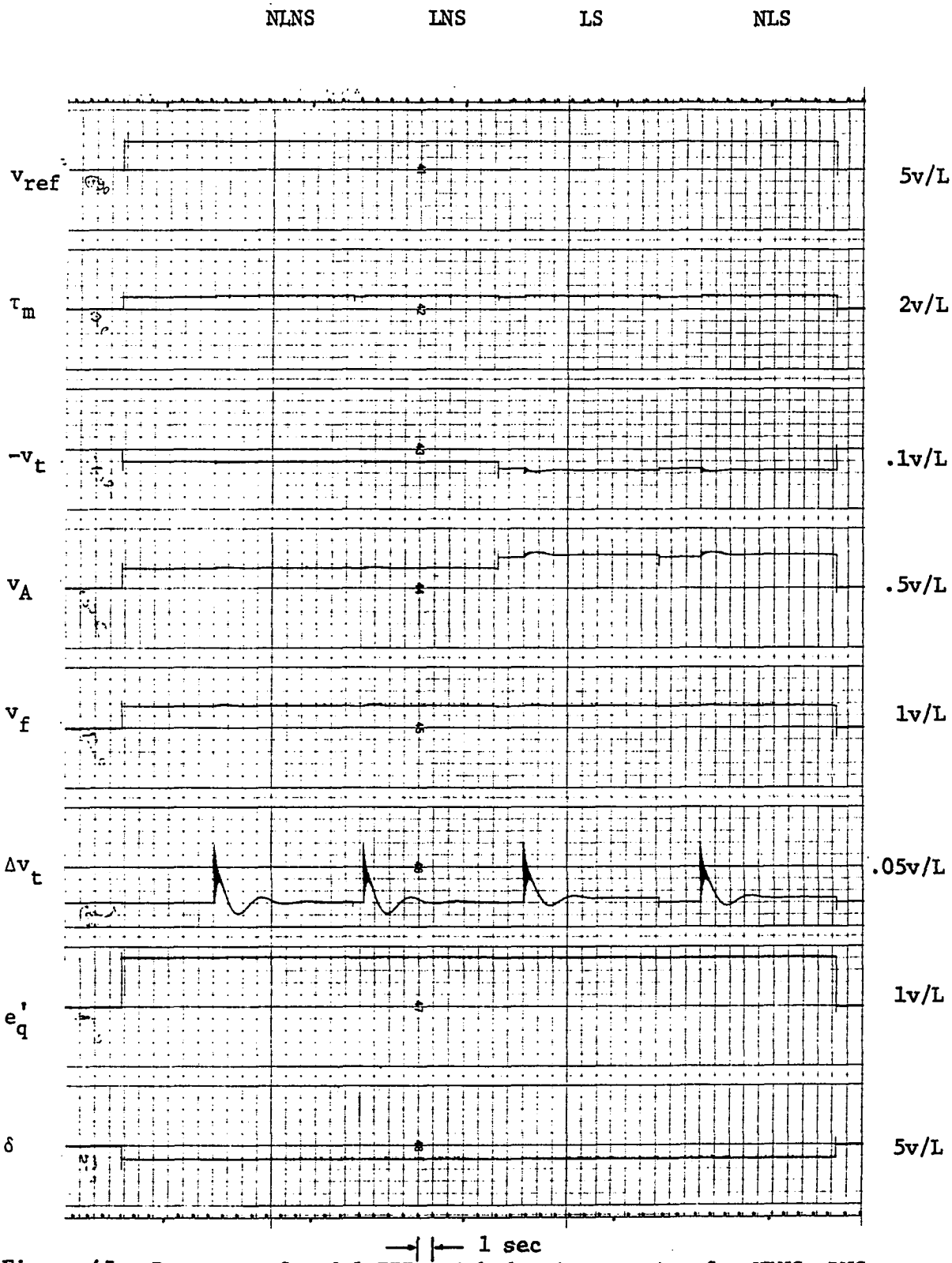

Figure 45. Response of model III, with damping, to $\Delta\tau_m$ for NLNS, LNS, LS, NLS - fast exciter

Since the response of Δv_t to Δv_{ref} lends itself well for the performance indices used thus far this definition is adhered to and no attempt is made to compare the response to $\Delta \tau_m$ in terms of the performance indices.

4. Response of model III to Δv_{ref} with NLNS, LNS, LS and NLS

Figures 46a and 46b show the response of model III to Δv_{ref} with NLNS, LNS, LS and NLS for the slow and fast exciters, respectively. The machine was operated at its full load rating and the step change of 5% in v_{ref} was not enough to force the amplifier into limiting. Thus for this loading condition and the 5% step change the response to NLNS and LNS appear to be the same. Likewise LS and NLS are very similar.

The next step in the study is to perform a series of analog computer runs similar to those outlined for model I in Chapter IV. Four sets of readings were recorded for each of the excitation systems. Set one is the operation of the system with NLNS. In the second set the system was operated with limiting but no saturation, LNS. The third set is the operation of the system with both limiting and saturation, LS, while in the fourth set the system was operated with no limiting but with saturation, NLS.

Tables 10 and 11 compare the system response for the two types of excitation systems considered. The settling time and percent overshoot shown in these tables are compared graphically by plotting them against K_F. The graphs shown in Figures 47-54 parallel those of Figures 20-27 discussed in Chapter IV.

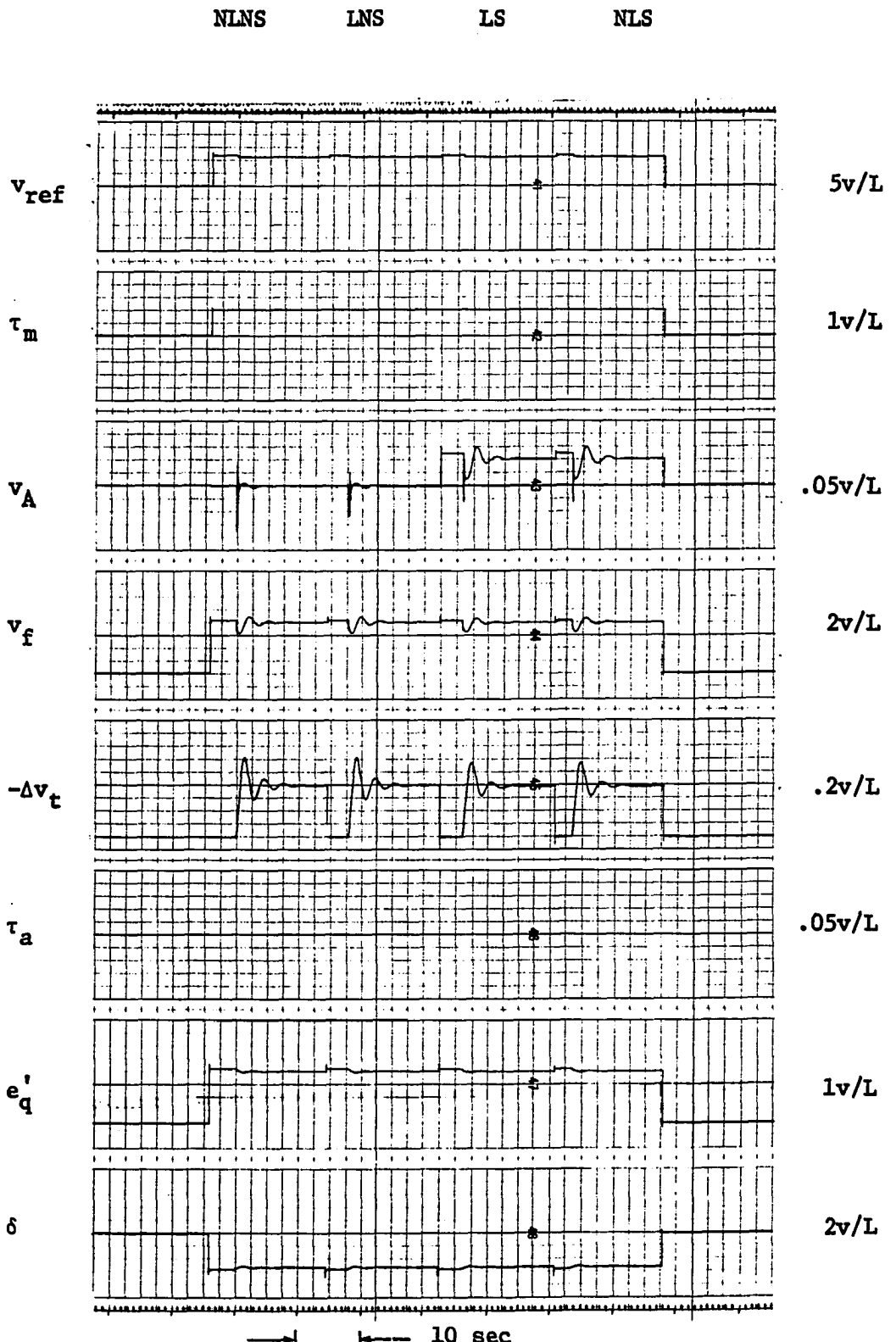

Figure 46a. Response of model III, with damping, to Δv_{ref} for NLNS, LNS, LS, NLS - slow exciter

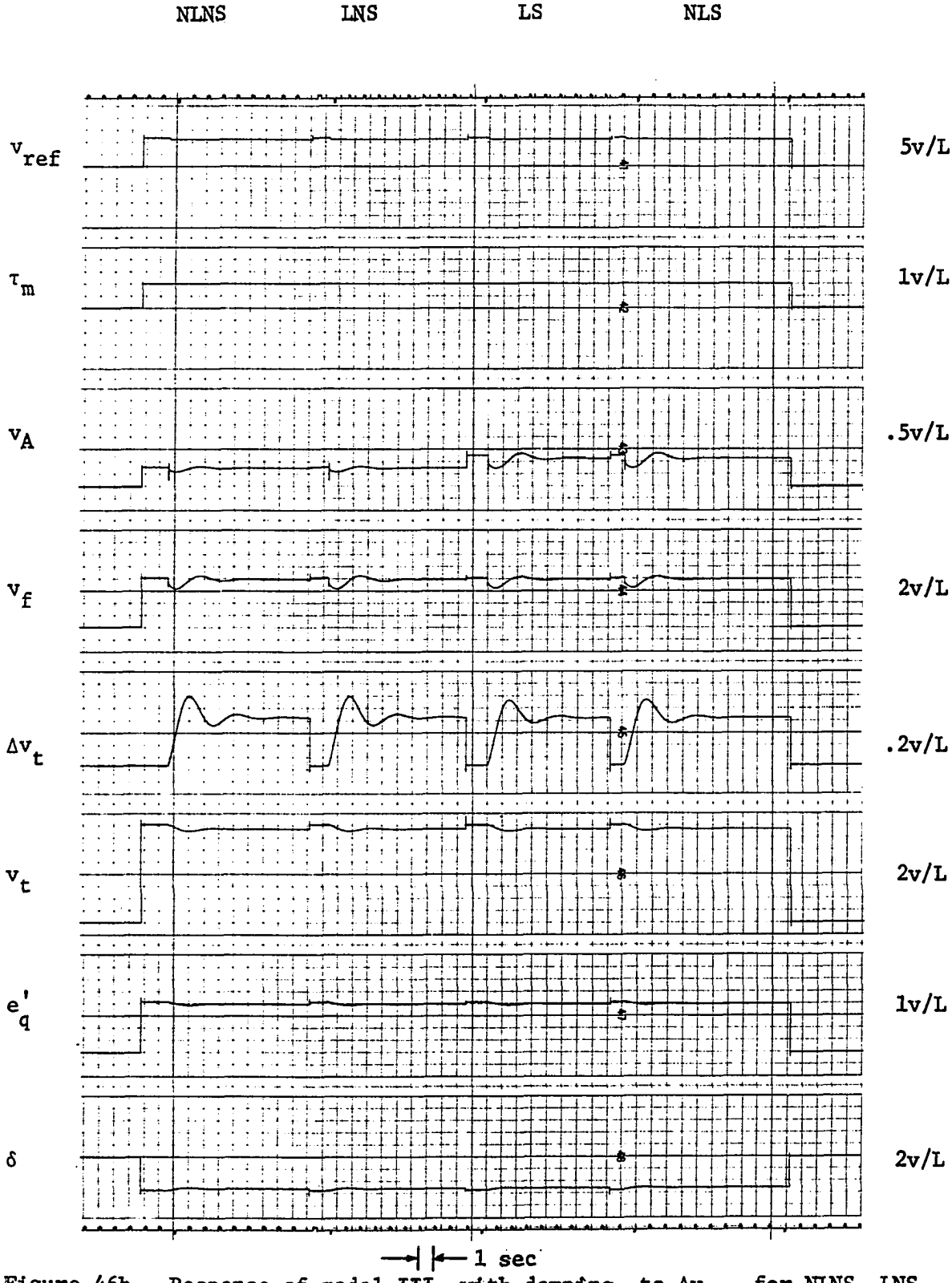

Figure 46b. Response of model III, with damping, to Δv_{ref} for NLNS, LNS, LS, NLS - fast exciter

Table 10. Comparison of results for model III and the low response exciter, τ_m constant and a step change in v_{ref}

T_F	K_A	K_F	No limiting, no saturation			With limiting but no saturation			With both limiting and saturation			No limiting but with saturation		
			Run no.	Set-tling time	% over-shoot	Run no.	Set-tling time	% over-shoot	Run no.	Set-tling time	% over-shoot	Run no.	Set-tling time	% over-shoot
				sec			sec			sec			sec	
.2	400	.015	621	5.8	58.0	641	6.0	56.0	661	4.8	45.0	681	3.2	29.0
		.020	622	6.9	57.5	642	6.8	56.0	662	5.5	42.5	682	3.8	30.0
		.025	623	7.7	57.0	643	7.6	55.5	663	6.1	42.0	683	4.0	30.0
		.030	624	8.5	56.0	644	8.4	55.5	664	7.0	42.0	684	4.7	31.5
		.035	625	9.0	55.0	645	9.0	55.0	665	7.8	44.0	685	4.6	33.0
	600	.015	626	5.8	55.0	646	6.0	55.0	666	5.0	45.0	686	3.1	37.0
		.020	627	6.7	55.0	647	6.8	55.0	667	5.8	46.0	687	3.8	38.0
		.025	628	7.5	55.0	648	7.5	55.0	668	6.2	47.5	688	3.9	39.5
		.030	629	8.5	55.0	649	8.5	55.0	669	6.8	47.5	689	5.5	40.0
		.035	630	8.8	55.0	650	9.0	54.0	670	7.5	47.5	690	5.6	42.0
.1	400	.015	631	13.3	75.0	651	13.5	75.0	671	6.2	59.0	691	3.9	39.0
		.020	632	13.8	74.0	652	14.0	73.0	672	7.1	57.5	692	4.6	40.0
		.025	633	15.5	72.5	653	15.7	72.0	673	8.0	57.0	693	5.0	40.0
		.030	634	16.0	71.0	654	16.2	72.0	674	10.0	57.0	694	5.6	41.0
		.035	635	16.5	70.0	655	16.5	70.0	675	11.0	57.0	695	6.0	42.0
	600	.015	636	12.0	75.0	656	12.0	75.0	676	6.5	62.5	696	5.3	50.0
		.020	637	13.9	73.0	657	14.0	74.0	677	8.2	62.0	697	5.8	50.0
		.025	638	15.2	72.5	658	15.5	73.0	678	9.1	60.0	698	6.5	50.0
		.030	639	16.0	71.0	659	15.8	72.0	679	10.0	60.0	699	7.1	51.0
		.035	640	16.5	70.0	660	16.5	70.0	680	11.0	60.0	700	7.5	52.5

Table 11. Comparison of results for model III and the high response exciter, τ_m constant and a step change in v_{ref}

T_F	K_A	K_F	No limiting, no saturation			With limiting but no saturation			With both limiting and saturation			No limiting but with saturation		
			Run no.	Set-tling time	% over-shoot	Run no.	Set-tling time	% over-shoot	Run no.	Set-tling time	% over-shoot	Run no.	Set-tling time	% over-shoot
				sec			sec			sec			sec	
.2	400	.015	421	3.4	37.5	441	3.6	35.0	461	3.7	30.0	481	3.6	30.0
		.020	422	4.3	42.5	442	4.5	40.0	462	4.4	32.5	482	4.2	32.5
		.025	423	5.0	46.0	443	5.2	42.5	463	4.8	35.0	483	4.8	35.0
		.030	424	5.5	47.0	444	5.9	45.0	464	5.0	36.0	484	5.1	36.0
		.035	425	5.8	47.5	445	6.1	45.0	465	5.8	37.5	485	6.0	37.5
	600	.015	426	3.5	40.0	446	3.5	40.0	466	3.8	35.0	486	3.5	35.0
		.020	427	4.4	43.5	447	4.6	42.5	467	4.3	37.0	487	4.2	36.0
		.025	428	5.0	46.0	448	5.1	42.5	468	5.5	39.0	488	5.1	37.5
		.030	429	5.3	47.5	449	5.5	45.0	469	6.4	40.5	489	5.5	40.0
		.035	430	5.5	50.0	450	6.0	45.0	470	6.5	41.5	490	7.0	40.5
.1	400	.015	431	5.8	55.0	451	6.0	52.5	471	5.0	43.5	491	5.2	42.5
		.020	432	6.8	56.0	452	8.1	55.0	472	5.8	45.0	492	6.0	46.0
		.025	433	8.0	60.0	453	9.1	56.0	473	6.7	46.0	493	6.6	46.0
		.030	434	8.8	61.0	454	9.8	56.5	474	7.4	47.0	494	7.2	46.5
		.035	435	9.1	61.0	455	10.5	56.5	475	8.0	49.0	495	8.0	47.5
	600	.015	436	5.8	56.0	456	6.0	55.0	476	5.2	48.5	496	5.2	48.5
		.020	437	6.9	57.5	457	8.0	56.0	477	6.1	50.0	497	6.2	50.0
		.025	438	7.9	60.0	458	9.2	57.5	478	6.6	51.0	498	6.7	51.0
		.030	439	8.5	62.0	459	10.0	58.5	479	8.5	55.0	499	8.3	53.0
		.035	440	9.6	62.0	460	10.8	59.0	480	8.8	56.0	500	9.0	53.0

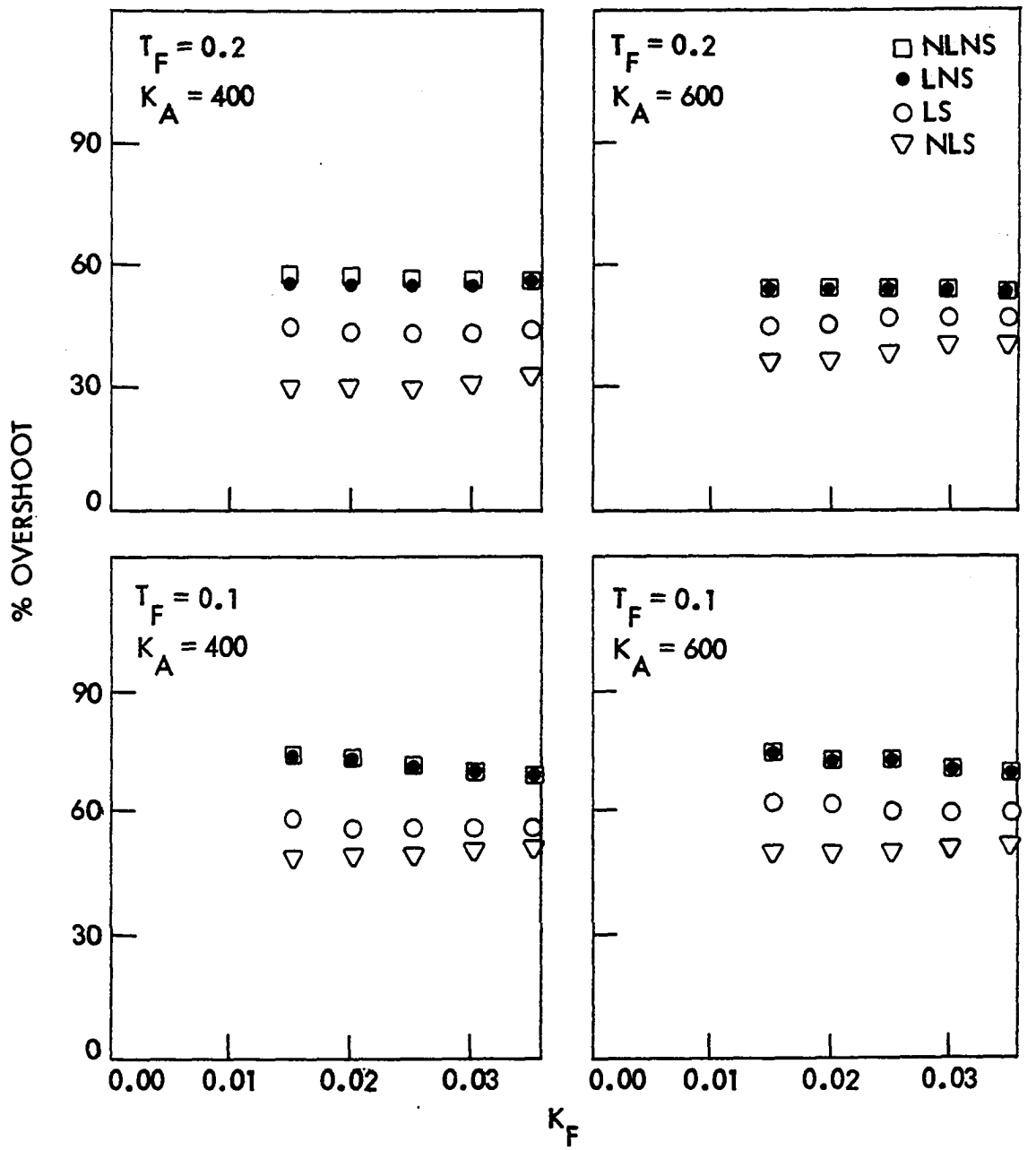

Figure 47. Percent overshoot vs K_F for NLNS, LNS, LS and NLS with low response exciter and model III

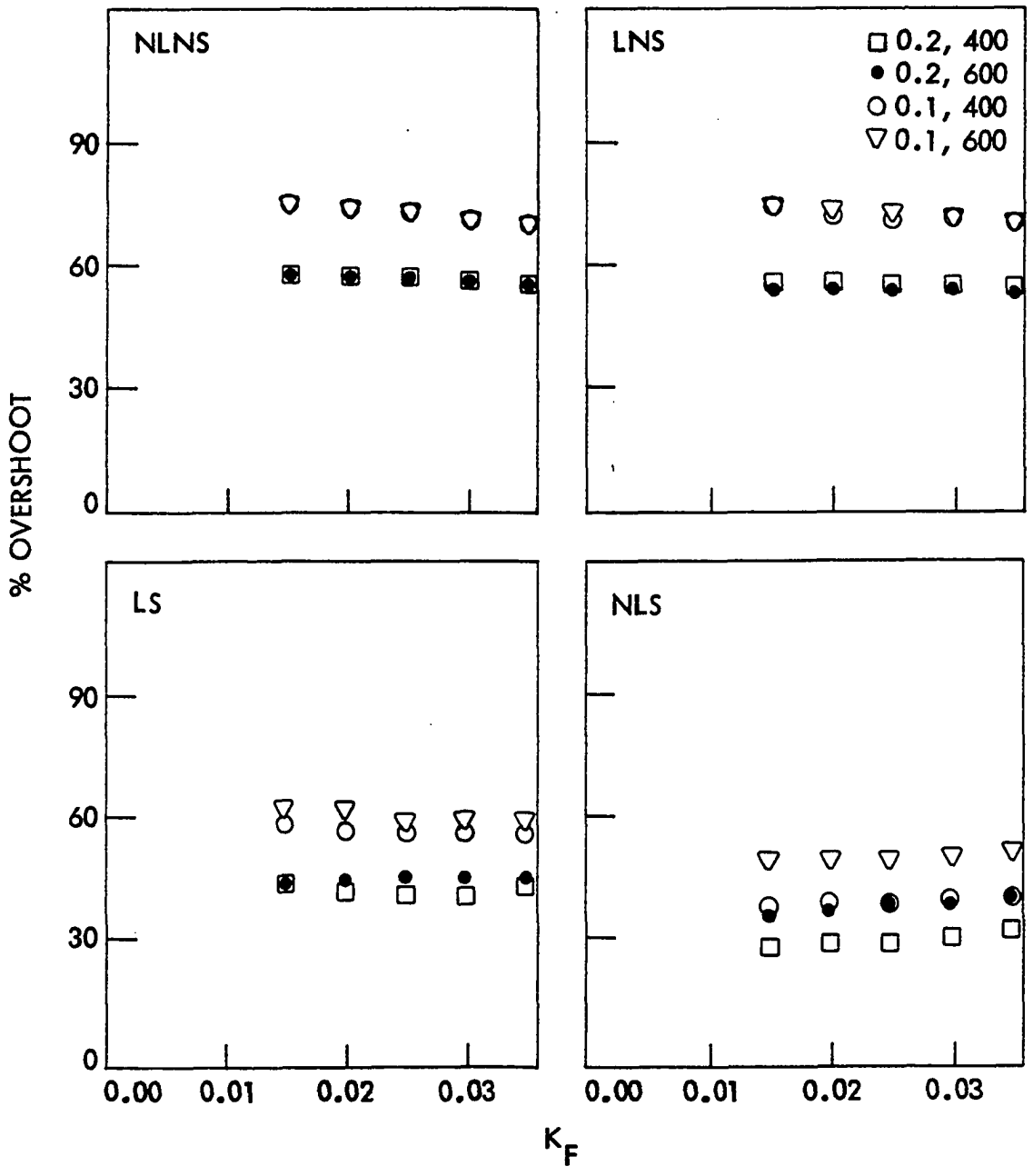

Figure 48. Percent overshoot vs K_F for T_F and K_A of .2/400, .2/600, .1/400 and .1/600 with low response exciter and model III

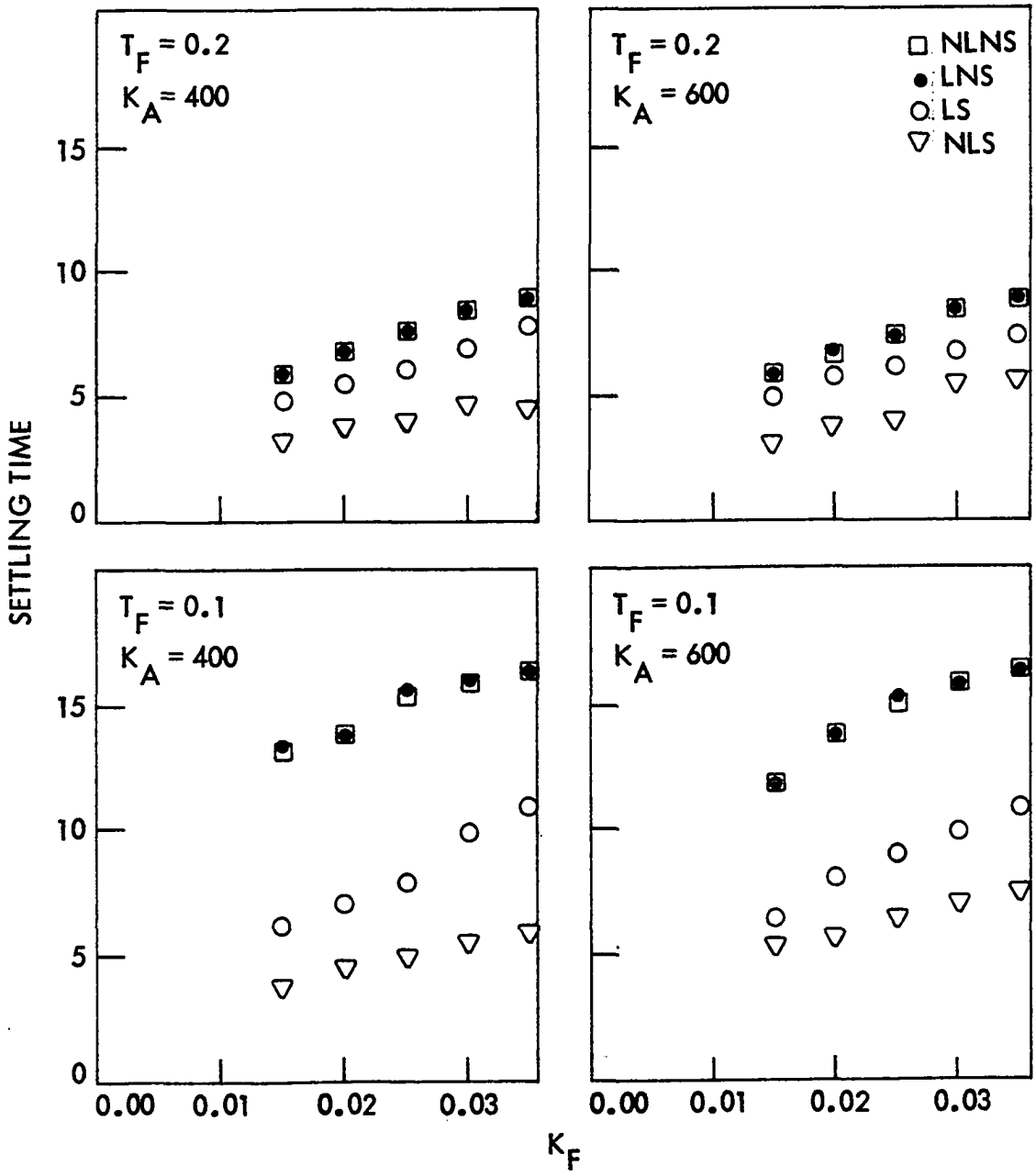

Figure 49. Settling time vs K_F for NLNS, LNS, LS and NLS with low response exciter and model III

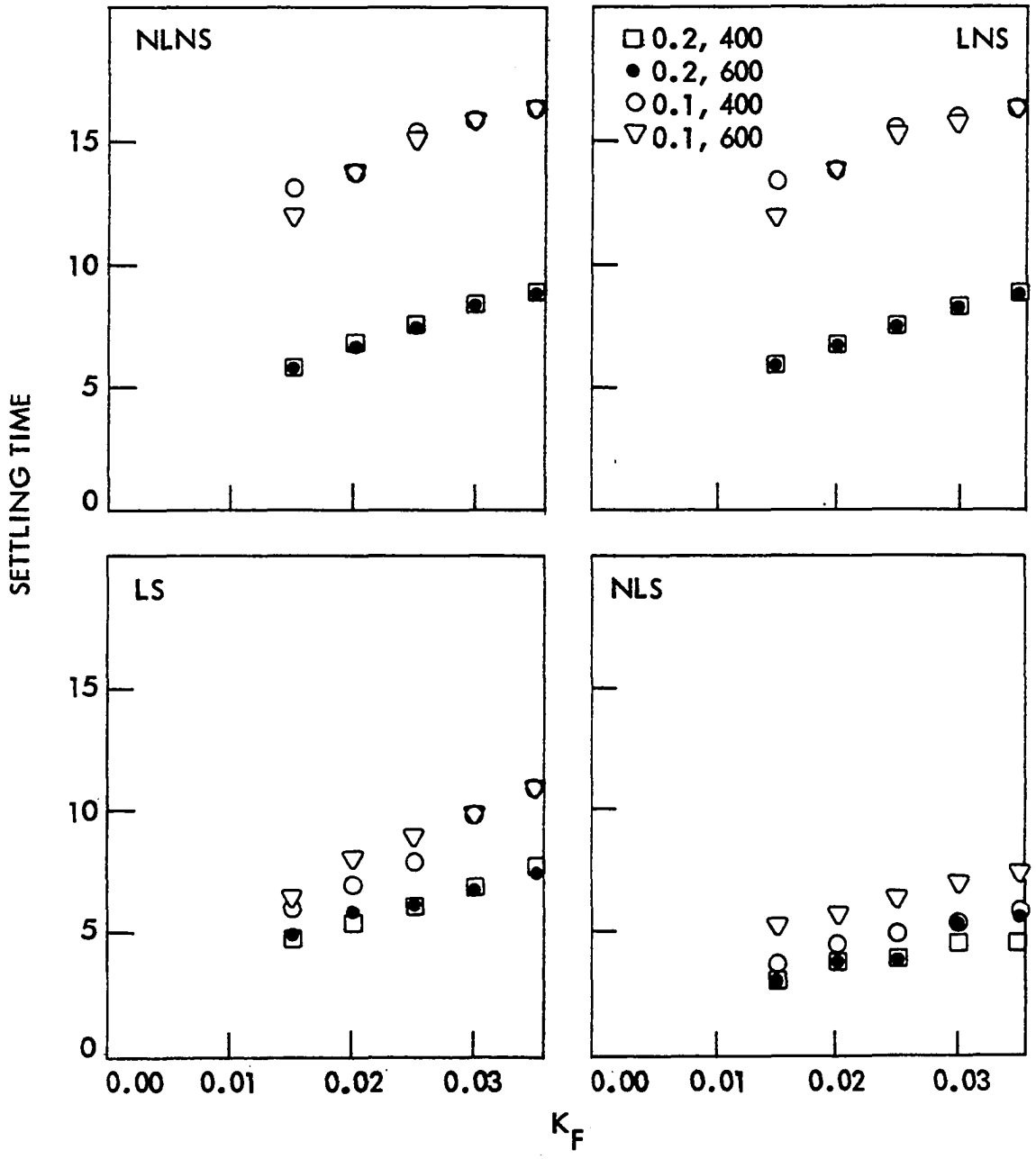

Figure 50. Settling time vs K_F for T_F and K_A of .2/400, .2/600, .1/400 and .1/600 with low response exciter and model III

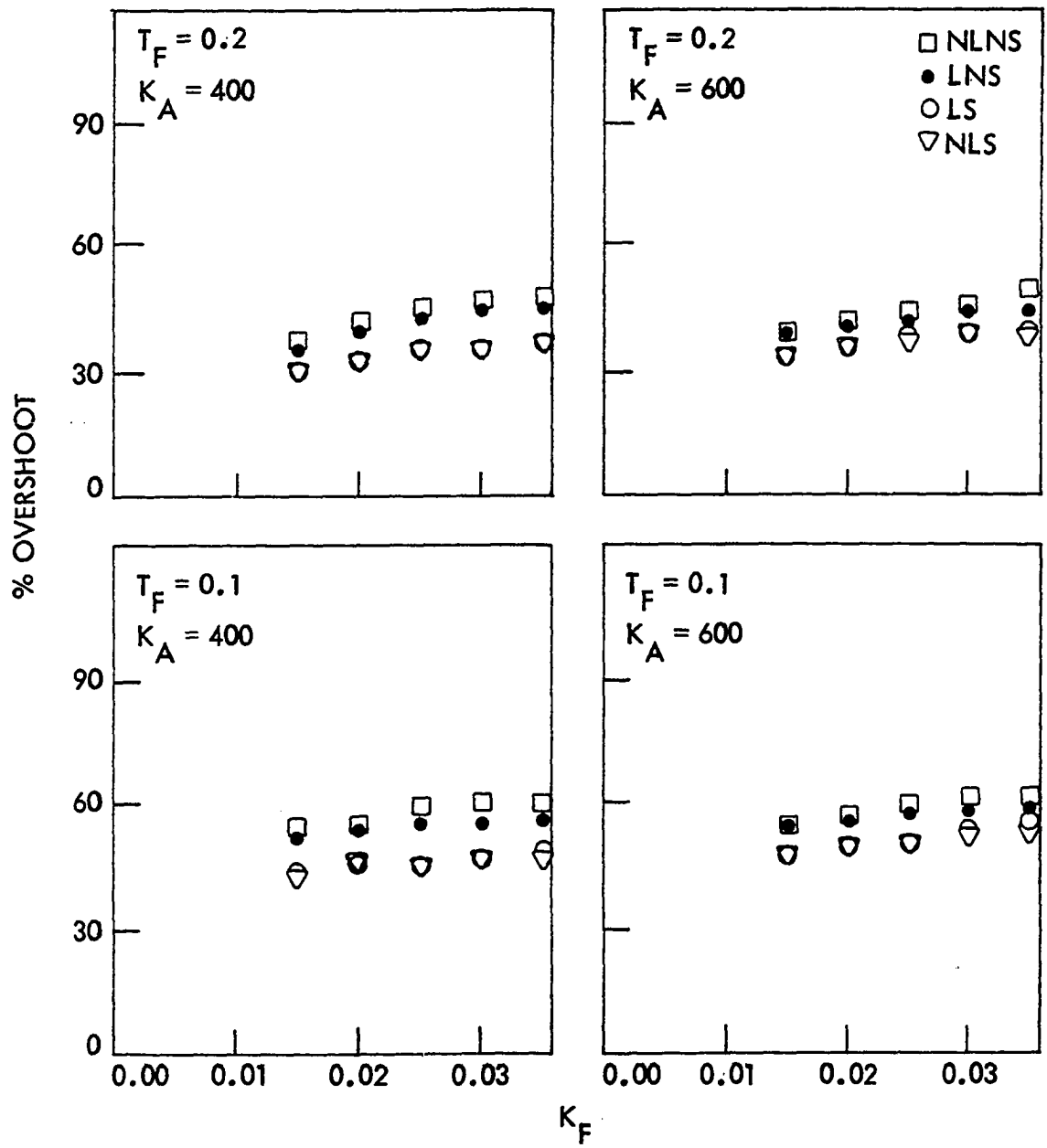

Figure 51. Percent overshoot vs K_F for NLNS, LNS, LS and NLS with high response exciter and model III

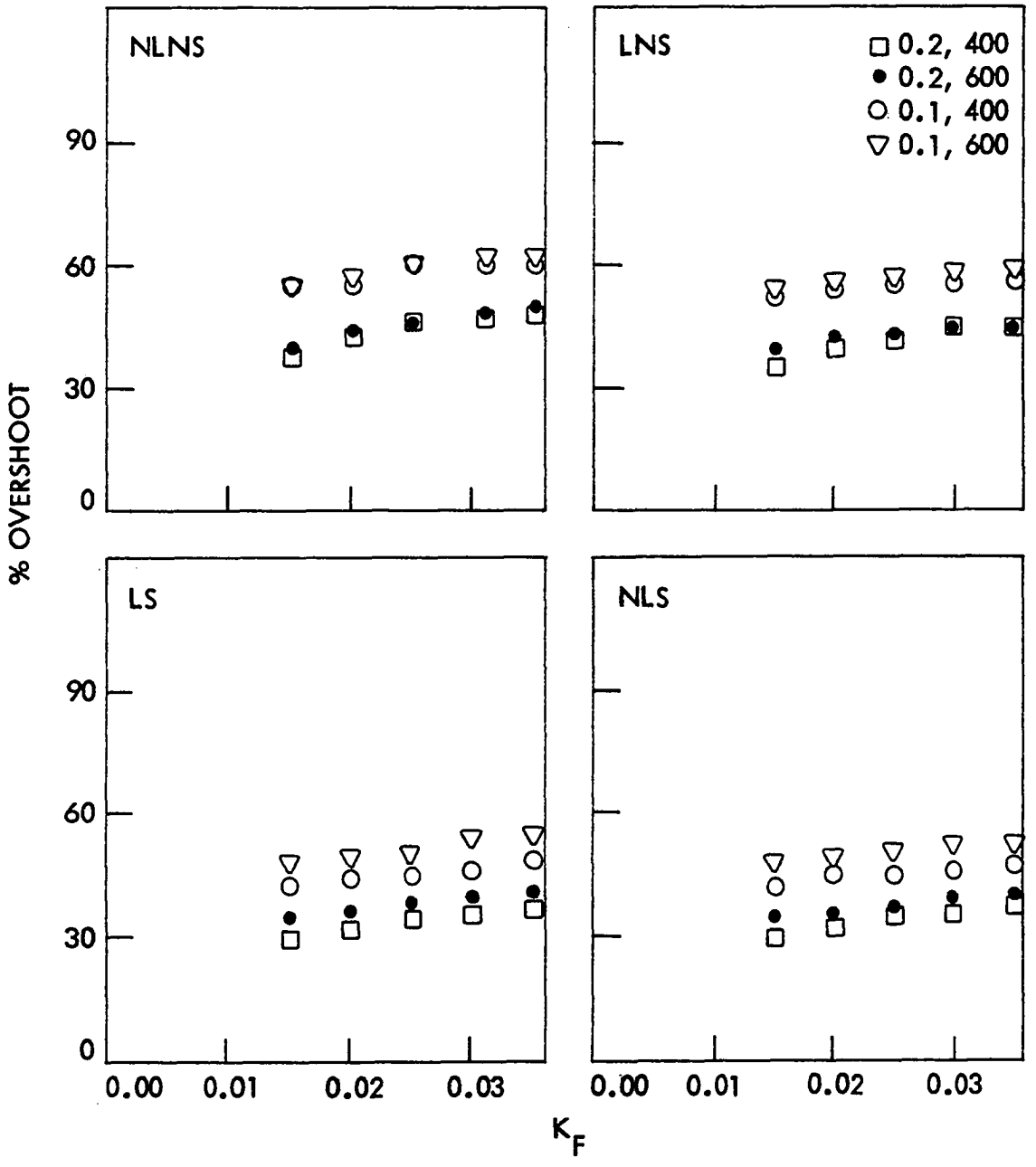

Figure 52. Percent overshoot vs K_F for T_F and K_A of .2/400, .2/600, .1/400 and .1/600 with high response exciter and model III

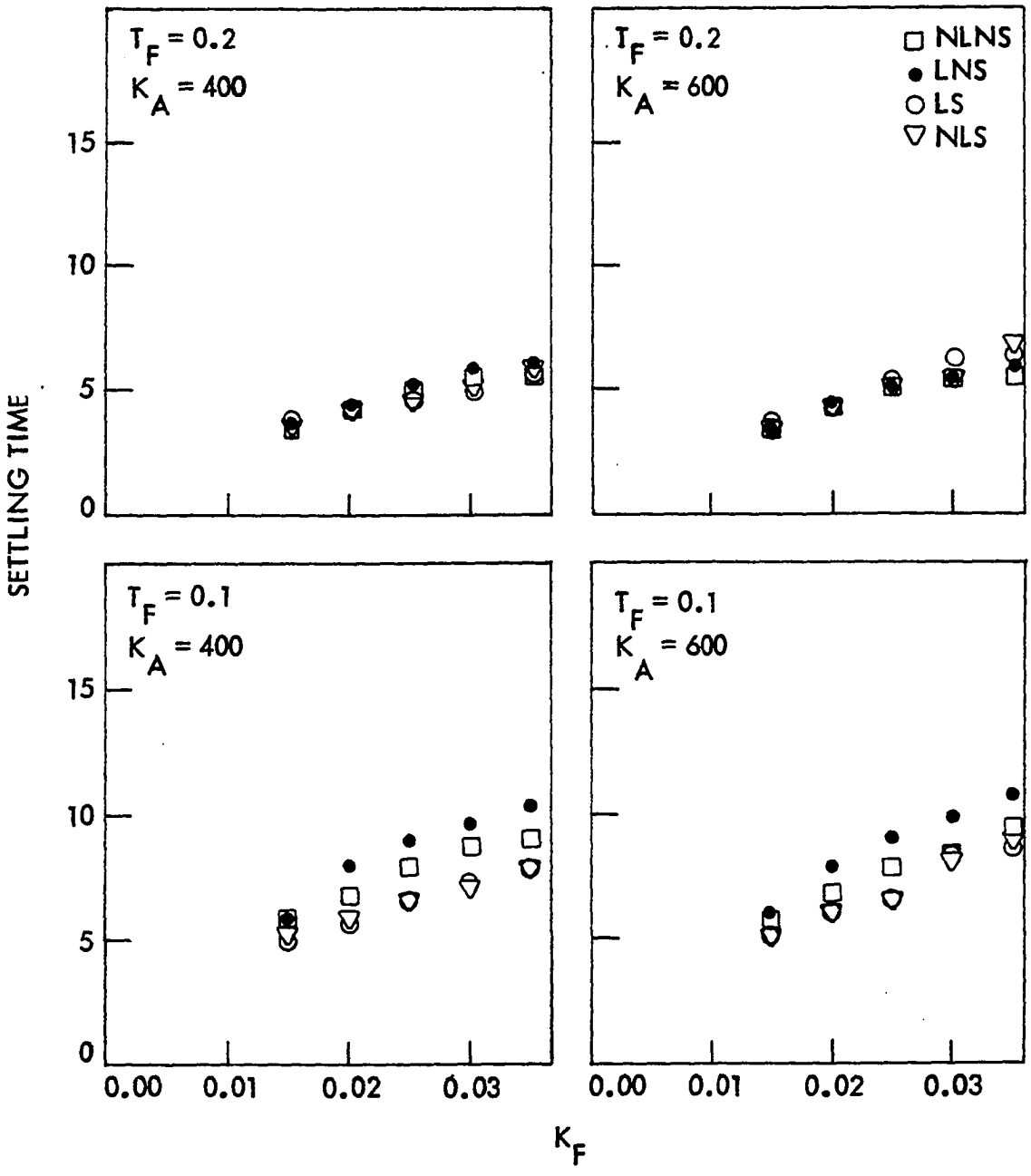

Figure 53. Settling time vs K_F for NLNS, LNS, LS and NLS with high response exciter and model III

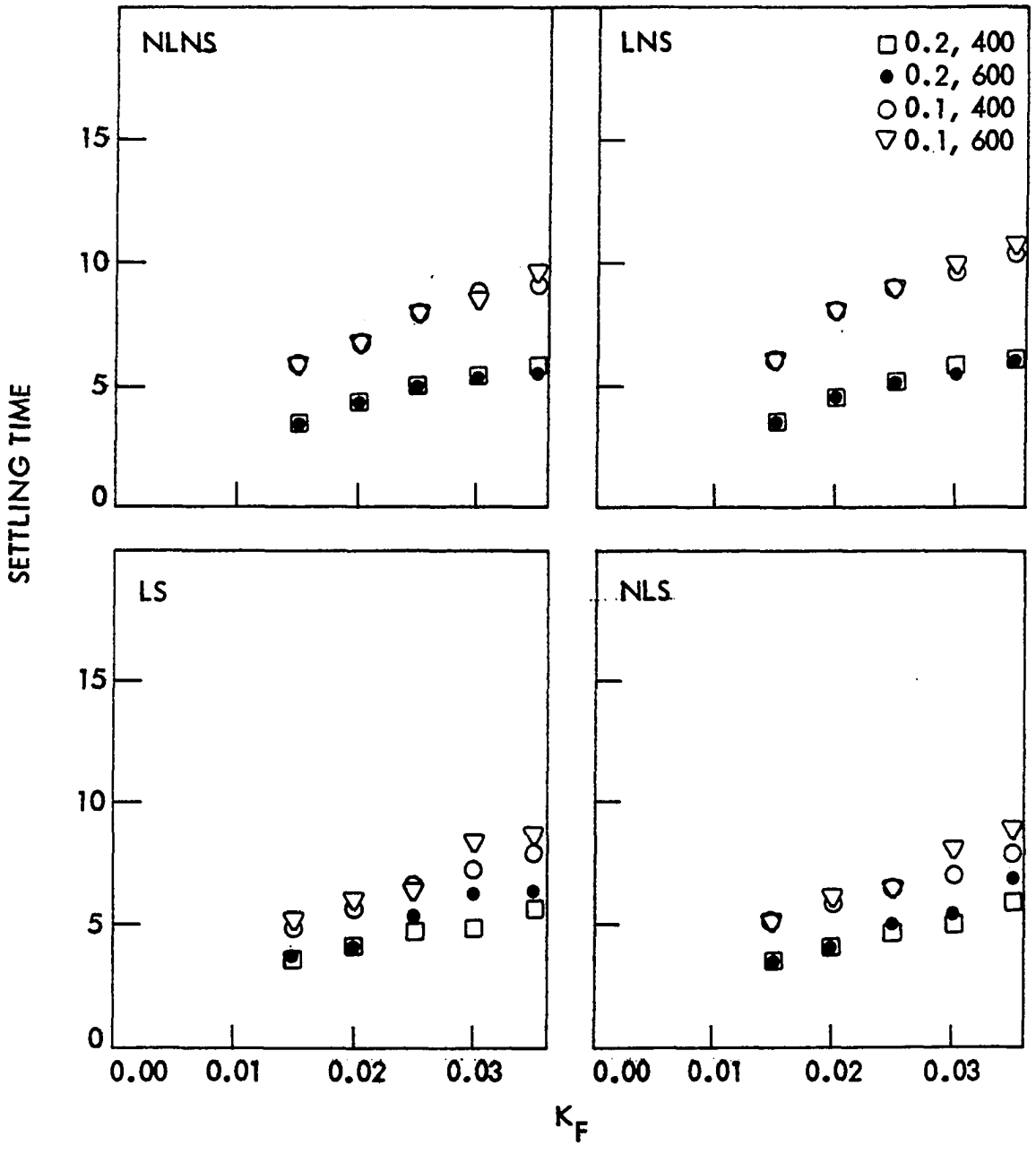

Figure 54. Settling time vs K_F for T_F and K_A of .2/400, .2/600, .1/400 and .1/600 with high response exciter and model III

D. Conclusions on Chapter V

Several conclusions can be made from the studies presented in this chapter. First, a comparison of the graphs shown in Figures 20-27 (see Chapter IV) to the graphs in Figures 47-54 shows that the conclusions 1-8 made in Chapter IV with respect to comparing Figures 20-27 are still valid for comparing Figures 47-54. Some additional conclusions on Chapter V are:

1) Damping improves the performance of model III.
2) The assumption of constant flux linkages is valid only for a period of about one second after a step change in load is applied.
3) The terminal voltage returns to its original steady state value following a step change in load torque with and without amplifier limiting.
4) As discussed in Appendix D, the damping required to improve the performance of model III is a function of the local load, R, connected to the machine terminal.
5) A comparison of Tables 7 and 10 shows that the overshoot observed for model I and the slow exciter is of higher order of magnitude than those of model III and slow exciter. However, the reverse is the case in comparing the settling time.
6) A comparison of Tables 8 and 11 shows that the settling time is longer for model III and fast exciter than model I and fast exciter. However, the overshoot is lower in model I and fast exciter than model III and fast exciter.

7) From conclusions 5 and 6 it would appear that in general the more complicated the machine model, the longer is the settling time for a given excitation system.

8) Inclusion of saturation and limiting lowers overshoot but tends to sustain oscillation longer.

9) The faster response excitation system has better overall performance in the range of K_F, T_F and K_A considered.

In addition to the above it can be said that model I is somewhat optimistic with respect to both overshoot and settling time. The terminal voltage in both models I and III are similar in shape and have the same steady state values. In general the curves in Figures 20-27 for model I are somewhat different from the corresponding ones in Figures 47-54 for model III. Most of the curves for model III can be fitted into straight lines while those in model I cannot. Since τ_m is assumed constant for model I the analog recordings do not display any oscillation for changes in v_{ref}. As shown by τ_a in Figure 38, model III displays high oscillations depending on whether damping is included or not.

VI. MODEL IV - NONLINEAR MODEL

The performance of the nonlinear model, model IV, is discussed in this chapter using the two excitation systems, low and high response exciters. Section A of the chapter analyzes model IV in a way similar to that used for model III in Chapter V, section B examines the effect of saliency on the model and section C considers the effects of machine saturation on the nonlinear model. The conclusions that may be drawn from the studies presented in this chapter are given in section D.

A. General Performance of Model IV

The general performance of the nonlinear model, model IV, discussed in this section parallels section C of Chapter V. Thus model starting, loading and response of the model to step changes in both the load torque and voltage reference are discussed.

1. Loading of model IV

Figures 55 and 56 show the initial response of model IV with the slow and fast exciters, respectively. These figures show how the system is brought to steady state positions before the step changes in τ_m and v_{ref} are applied. In order to establish the initial conditions, integrator 210 (see Appendix C) in which $\Delta\omega$ was determined was held at IC by an electronic switch. The integrator may be released either before or after the load is applied. The extreme left side of the figures represents zero. The system is switched to operate at point A and integrator 210 is released at point B. This release of integrator 210 preceded the application of load in Figure 55 and followed the application of load in

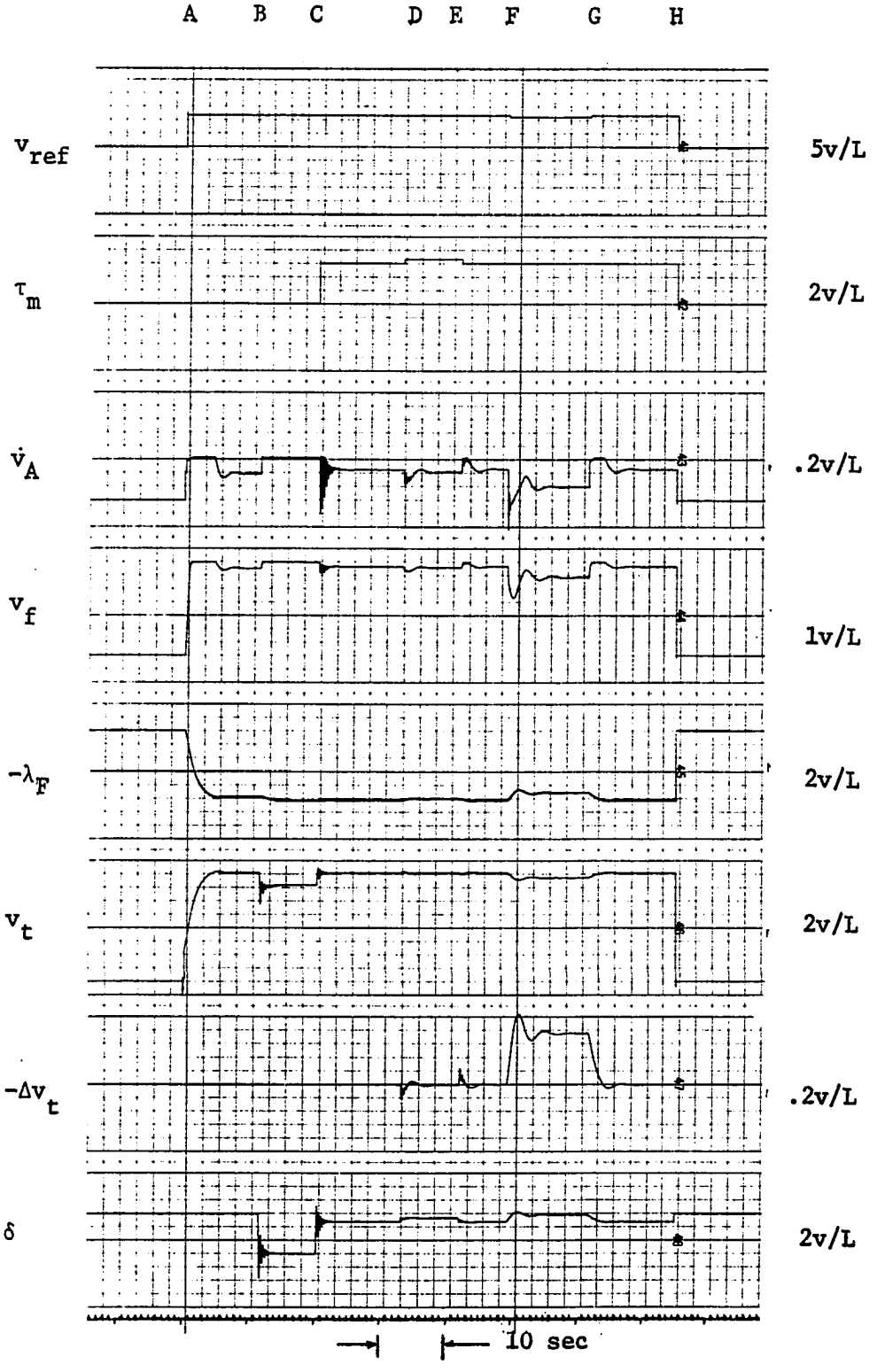

Figure 55. Initial response of model IV with the low response exciter

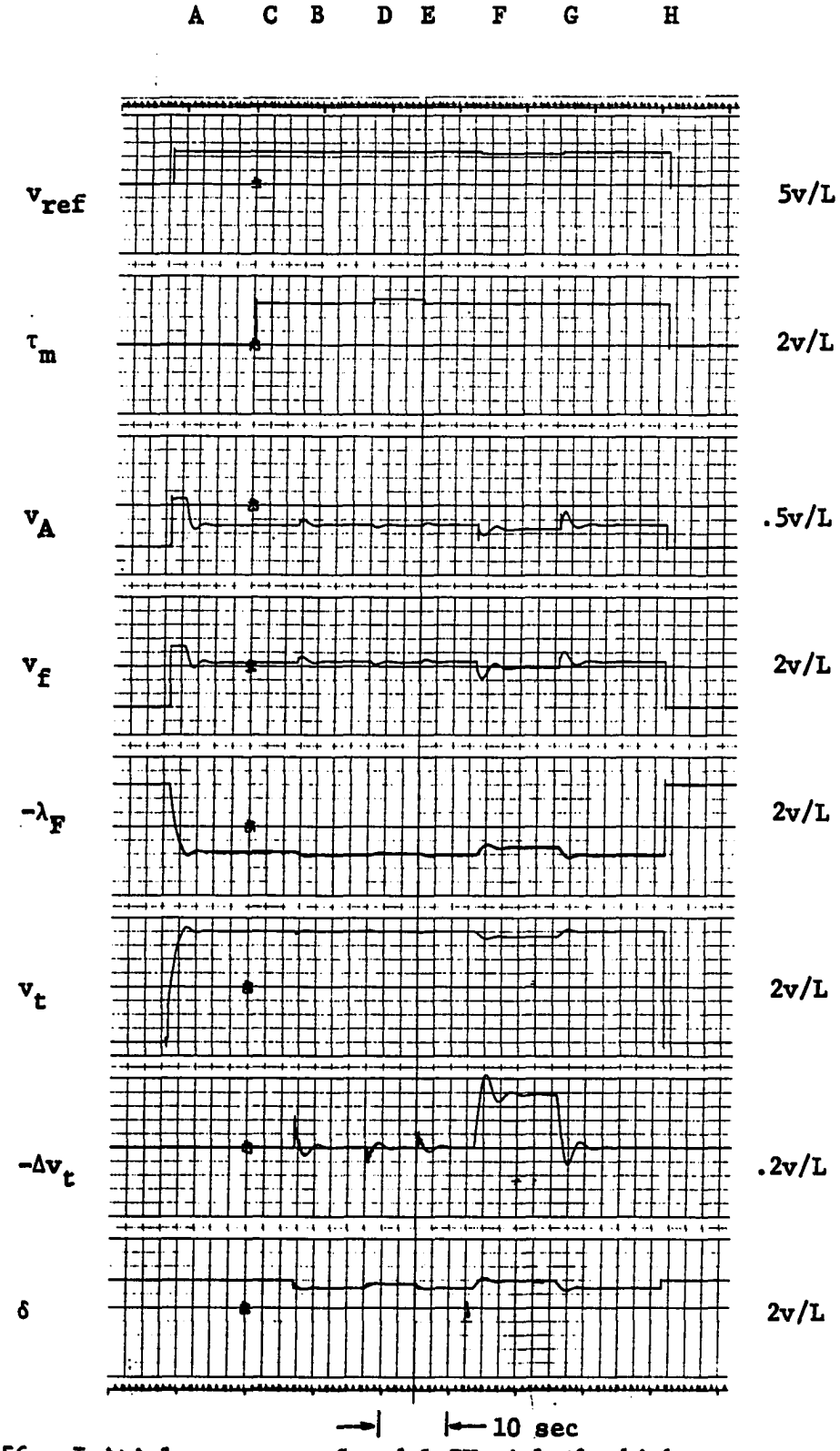

Figure 56. Initial response of model IV with the high response exciter

Figure 56. Step changes in τ_m and v_{ref} are applied and removed at points D, E, F and G. The recorder is returned to zero at point H. Again, as discussed in Chapter V the channel recording Δv_t was not on until the step changes were being applied.

The terminal voltage reaches steady state faster with the fast exciter than with the slow exciter. However, the overshoot is higher in the fast exciter than in the slow exciter.

These figures can also be compared with the similar ones discussed in Chapter V for the linear model, model III. The variables recorded in Figures 55 and 56 were chosen to facilitate such a comparison.

The analog computer was operated in slow millisecond (SMS) analog mode for these and all other chart recordings discussed in this chapter.

2. Response of model IV to $\pm\Delta\tau_m$ and $\pm\Delta v_{ref}$ with LS

Some of the nonlinear characteristics of the system can be observed in the somewhat different responses obtained for the application and removal of $+\Delta\tau_m$, $-\Delta\tau_m$, $+\Delta v_{ref}$ and $-\Delta v_{ref}$ shown in Figure 57 for the slow exciter. Similar responses (not shown) were observed for the fast exciter. Here, as in the case of model III, the response Δv_t to $+\Delta v_{ref}$ is like that of a first order system while the responses to the removal of $+\Delta v_{ref}$ and $-\Delta v_{ref}$ are like those of a second order system but with different overshoot, rise time and settling time.

3. Response of model IV to $\Delta\tau_m$ with NLNS, LNS, LS and NLS

Figures 58 and 59 show the response of model IV to $\Delta\tau_m$ with no limiting no saturation (NLNS), limiting but no saturation (LNS), both limiting

and saturation (LS) and no limiting but with saturation (NLS). The comments made in Chapter V with respect to similar figures, Figures 44 and 45, still apply in this case and no attempt is made to compare the response to $\Delta\tau_m$ in terms of percent overshoot, rise time and settling time. The responses to $\Delta\tau_m$ shown in these figures are very similar.

4. Response of model IV to Δv_{ref} with NLNS, LNS, LS and NLS

Figures 60 and 61 show the response of model IV to Δv_{ref} with NLNS, LNS, LS and NLS for the slow and fast exciters, respectively. As in a parallel discussion in Chapter V, the full load operation being considered and the step change in the reference voltage did not force the amplifier in the regulating system into limiting and, hence, the responses to NLNS and LNS are similar. The difference between both NLNS and LNS and both LS and NLS is due to exciter saturation.

A series of analog computer runs similar to those outlined for models I and III in Chapters IV and V, respectively, were performed. Tables 12 and 13 compare the responses of model IV in terms of the machine terminal voltage for the two types of excitation systems. The settling time and percent overshoot shown in these tables are compared graphically by plotting them against K_F. The graphs shown in Figures 62-69 parallel those of Figures 20-27 and 47-54 discussed in Chapters IV and V, respectively.

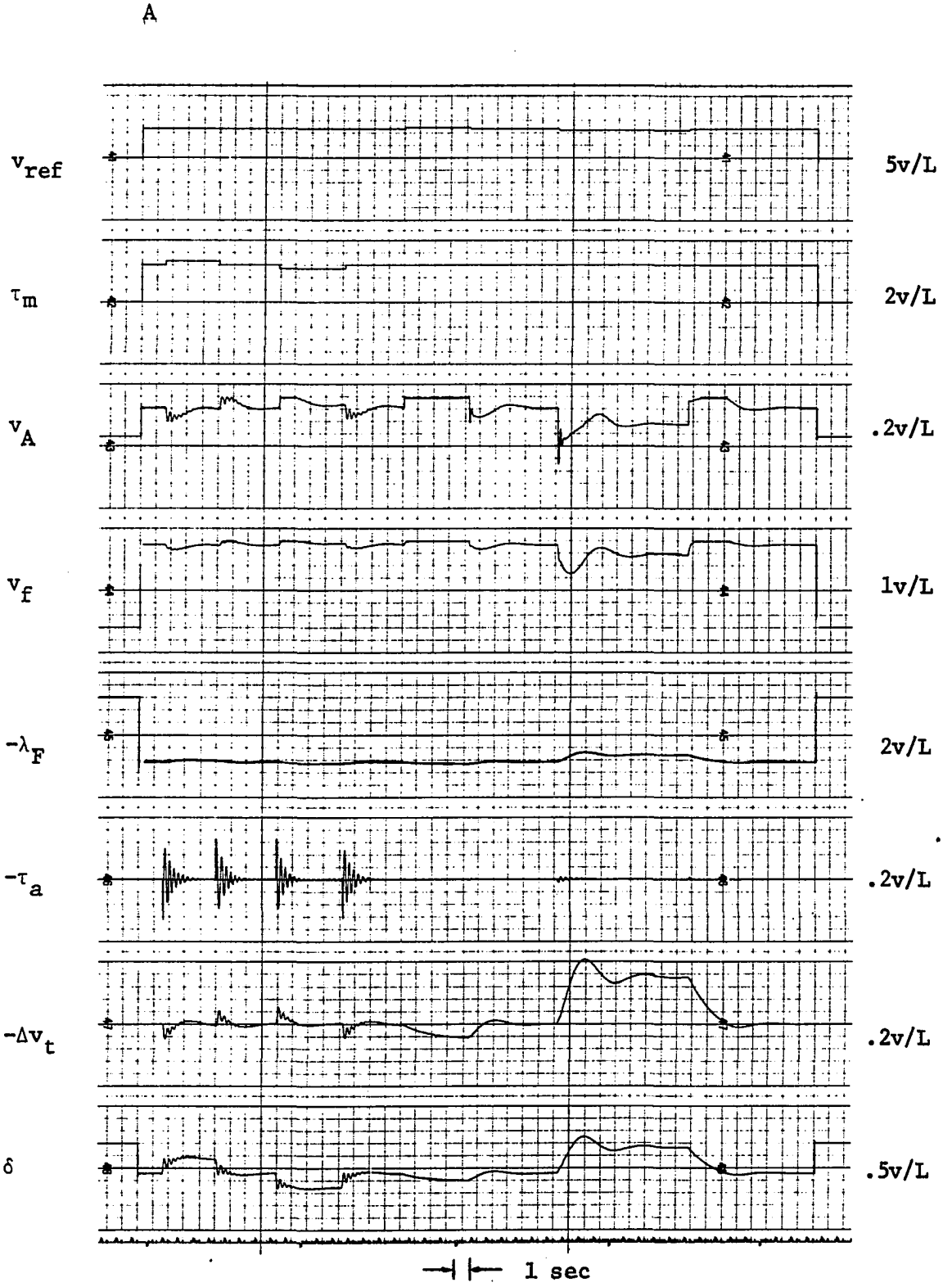

Figure 57. Response of model IV to $\Delta\tau_m$, $-\Delta\tau_m$, Δv_{ref}, $-\Delta v_{ref}$ using the low response exciter

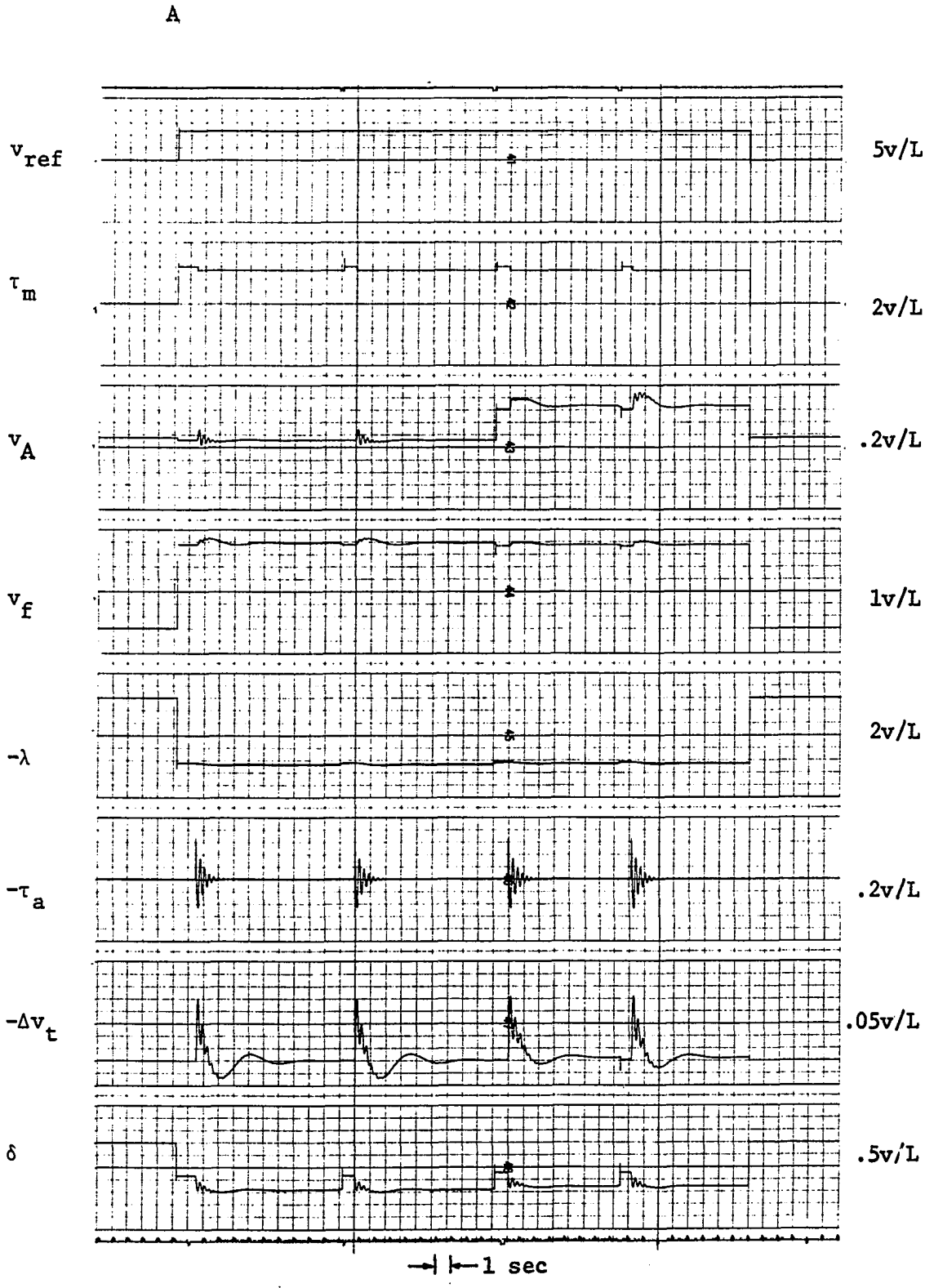

Figure 58. Response of model IV to $\Delta\tau_m$ with NLNS, LNS, LS and NLS using the low response exciter

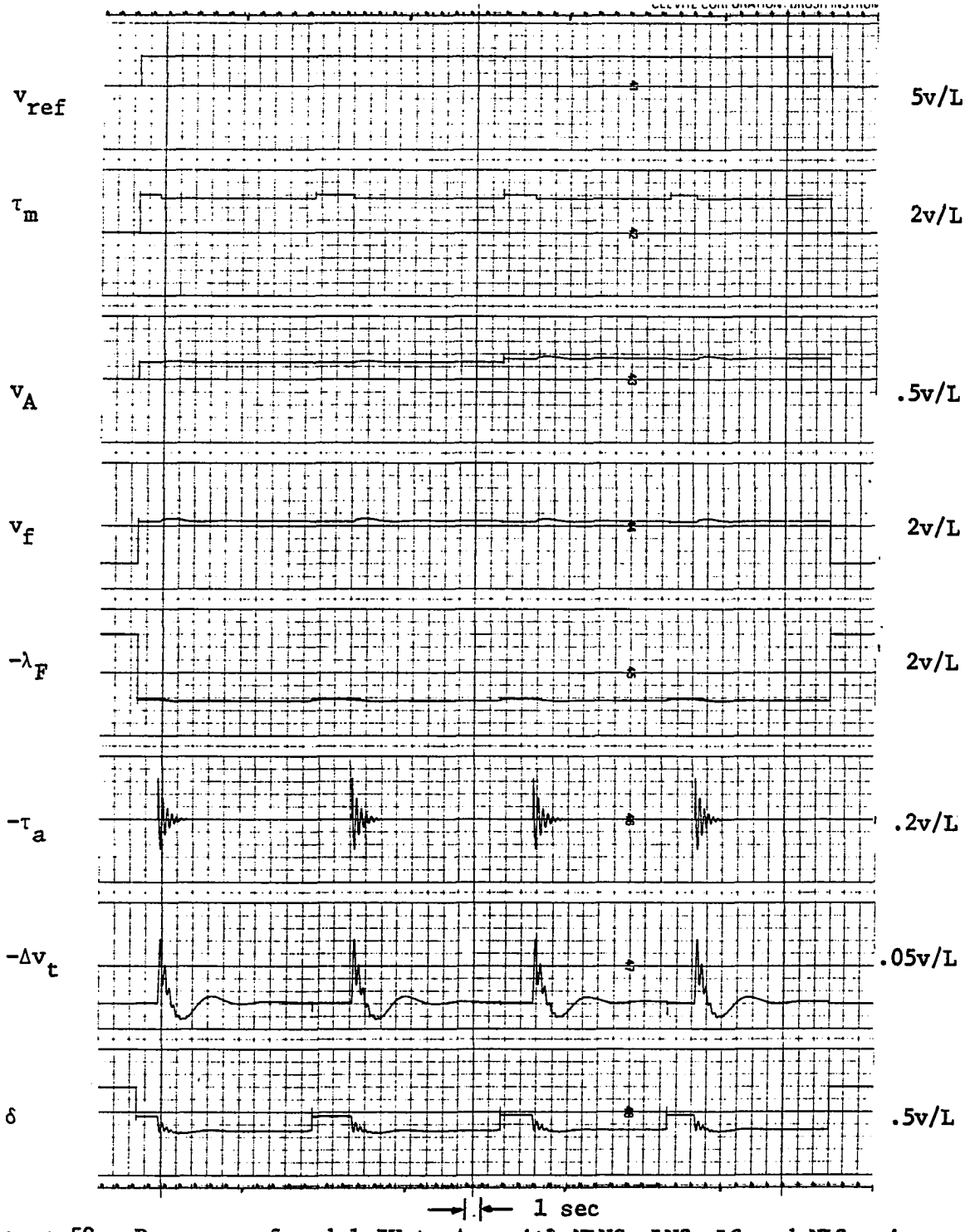

Figure 59. Response of model IV to $\Delta\tau_m$ with NLNS, LNS, LS and NLS using the high response exciter

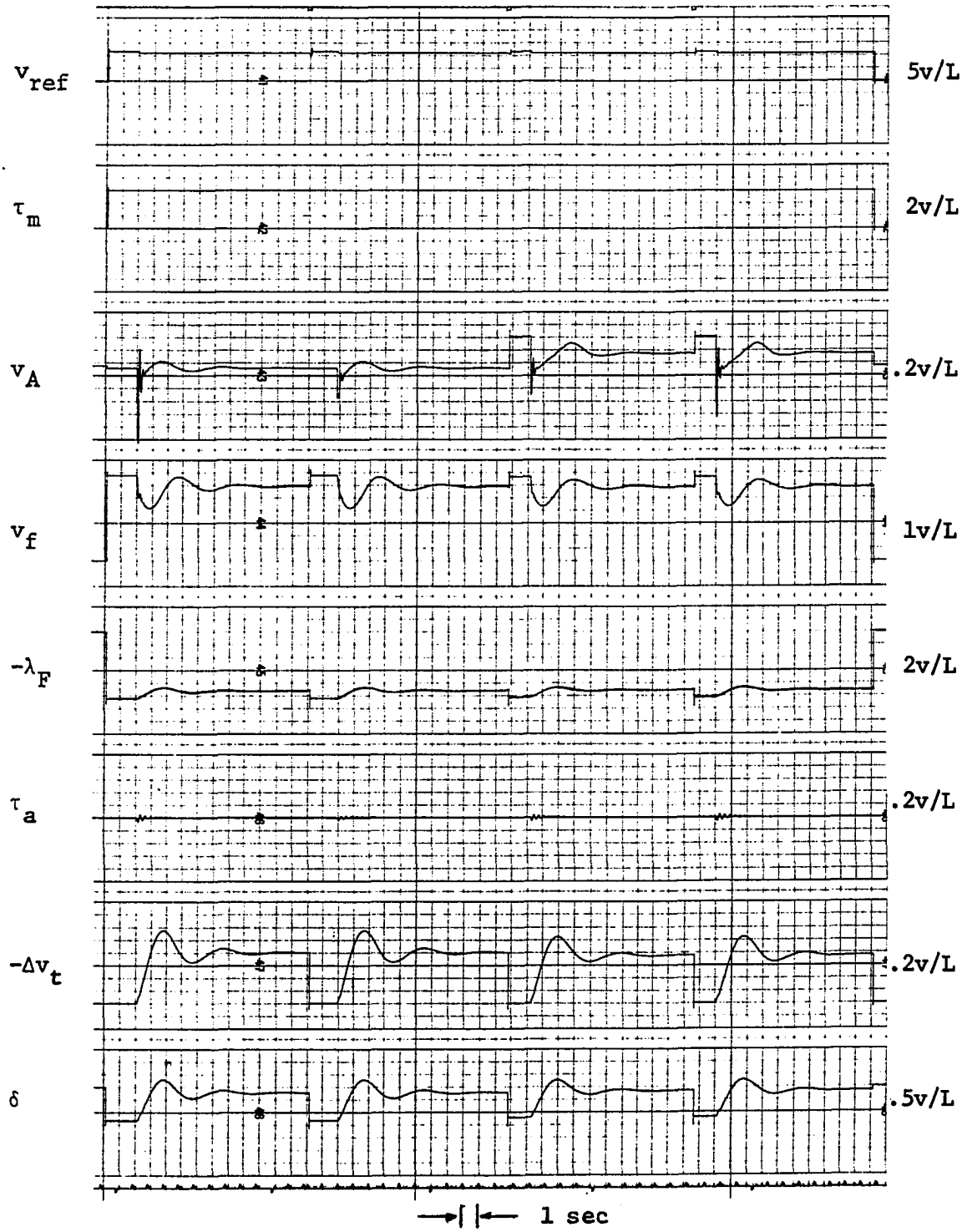

Figure 60. Response of model IV to Δv_{ref} with NLNS, LNS, LS and NLS using the low response exciter

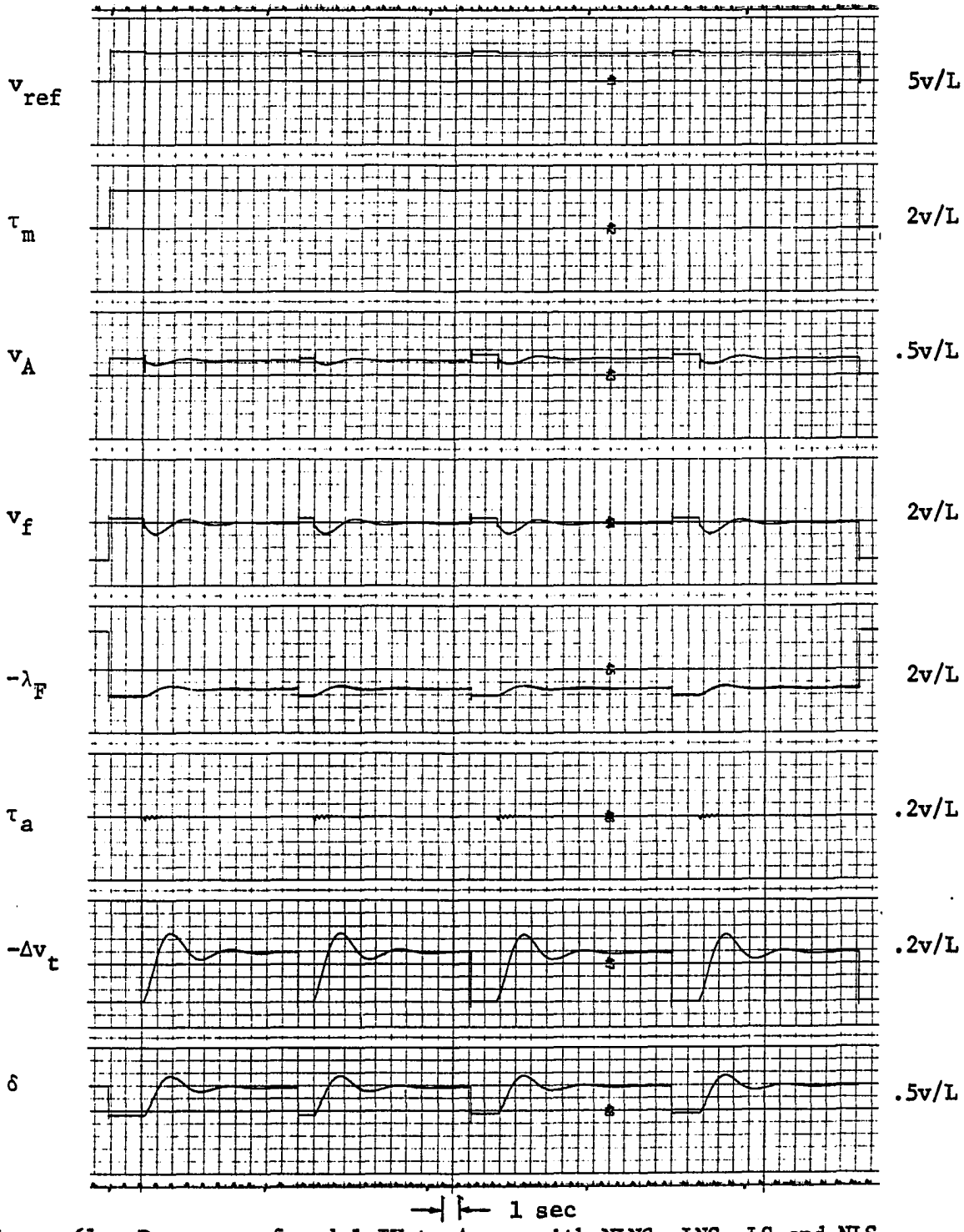

Figure 61. Response of model IV to Δv_{ref} with NLNS, LNS, LS and NLS using the high response exciter

Table 12. Comparison of results for model IV and the slow exciter with τ_m constant and a step change in v_{ref}

T_F	K_A	K_F	No limiting, no saturation			With limiting but no saturation			With both limiting and saturation			No limiting but with saturation		
			Run no.	Settling time	% overshoot	Run no.	Settling time	% overshoot	Run no.	Settling time	% overshoot	Run no.	Settling time	% overshoot
				sec			sec			sec			sec	
.2	400	.015	721	6.0	47.5	741	5.8	47.5	761	5.9	41.0	781	6.0	42.0
		.020	722	6.9	45.0	742	6.9	45.0	762	6.8	39.5	782	7.0	39.5
		.025	723	7.5	42.5	743	7.8	43.0	763	7.5	37.5	783	7.8	38.0
		.030	724	8.3	41.0	744	8.1	41.0	764	8.0	37.0	784	8.1	37.0
		.035	725	9.0	40.0	745	9.0	40.0	765	8.8	36.0	785	9.0	36.5
	600	.015	726	5.7	46.0	746	5.8	45.5	766	5.5	44.0	786	5.8	45.0
		.020	727	6.5	43.5	747	6.9	45.0	767	6.5	42.0	787	6.7	42.0
		.025	728	7.5	43.0	748	7.6	42.5	768	7.2	42.0	788	7.5	42.0
		.030	729	8.2	41.0	749	8.4	41.0	769	8.2	41.0	789	8.0	41.0
		.035	730	8.9	40.0	750	8.9	40.0	770	8.8	40.5	790	9.1	40.0
.1	400	.015	731	10.3	61.0	751	10.2	60.5	771	7.5	53.0	791	7.5	55.0
		.020	732	10.5	57.5	752	10.6	57.5	772	8.7	51.0	792	8.6	50.0
		.025	733	11.0	55.0	753	11.2	55.0	773	9.6	48.0	793	9.5	48.0
		.030	734	12.0	52.5	754	12.3	52.5	774	10.4	47.0	794	10.2	47.0
		.035	735	12.5	50.0	755	12.0	50.0	775	11.0	45.0	795	11.1	44.5
	600	.015	736	10.4	61.0	756	10.1	60.0	776	7.5	58.0	796	7.3	58.0
		.020	737	10.7	57.5	757	10.3	57.5	777	8.2	55.0	797	8.5	55.0
		.025	738	11.1	55.0	758	11.2	55.0	778	9.4	52.5	798	9.5	52.5
		.030	739	12.0	52.5	759	12.2	52.5	779	10.5	50.0	799	10.3	50.0
		.035	740	12.8	50.0	760	11.9	50.0	780	11.0	48.0	800	11.2	47.0

Table 13. Comparison of results for model IV and the fast exciter with τ_m constant and a step change in v_{ref}

T_F	K_A	K_F	No limiting, no saturation			With limiting but no saturation			With both limiting and saturation			No limiting but with saturation		
			Run no.	Set-tling time	% over-shoot	Run no.	Set-tling time	% over-shoot	Run no.	Set-tling time	% over-shoot	Run no.	Set-tling time	% over-shoot
				sec			sec			sec			sec	
.2	400	.015	821	4.2	33.0	841	4.4	33.0	861	4.6	31.5	881	4.7	31.5
		.020	822	5.0	34.0	842	5.0	33.0	862	5.1	32.0	882	5.1	32.0
		.025	823	5.6	34.0	843	5.8	34.0	863	5.7	34.0	883	5.8	32.0
		.030	824	6.2	35.0	844	6.2	34.0	864	6.4	34.0	884	6.2	32.0
		.035	825	6.7	35.0	845	6.5	34.0	865	7.0	34.0	885	6.8	32.0
	600	.015	826	4.4	36.0	846	4.3	36.0	866	4.5	36.5	886	4.4	36.0
		.020	827	5.0	36.0	847	5.1	36.0	867	5.1	36.0	887	5.1	36.0
		.025	828	5.5	36.0	848	5.7	35.0	868	5.7	36.0	888	5.7	36.0
		.030	829	6.2	36.0	849	6.2	35.0	869	6.0	36.0	889	6.2	36.0
		.035	830	6.6	35.5	850	6.8	35.5	870	6.8	36.0	890	6.7	36.0
.1	400	.015	831	7.2	43.5	851	7.1	44.0	871	5.8	43.0	891	5.9	43.0
		.020	832	8.5	43.5	852	8.4	44.0	872	6.7	42.5	892	6.7	43.0
		.025	833	9.1	43.0	853	9.3	44.0	873	7.7	43.0	893	7.5	43.0
		.030	834	10.0	42.5	854	10.2	43.5	874	8.2	42.0	894	8.1	42.5
		.035	835	11.0	41.0	855	11.1	41.0	875	8.8	41.0	895	8.8	42.0
	600	.015	836	7.3	46.0	856	7.2	48.5	876	6.0	47.5	896	5.7	47.5
		.020	837	8.4	46.0	857	8.3	46.5	877	6.8	47.0	897	6.7	47.5
		.025	838	9.3	45.0	858	9.3	46.0	878	7.5	46.5	898	7.5	46.0
		.030	839	10.2	44.0	859	10.2	44.0	879	8.2	45.0	899	8.1	45.0
		.035	840	11.1	43.0	860	11.0	43.5	880	8.9	44.0	900	8.8	44.0

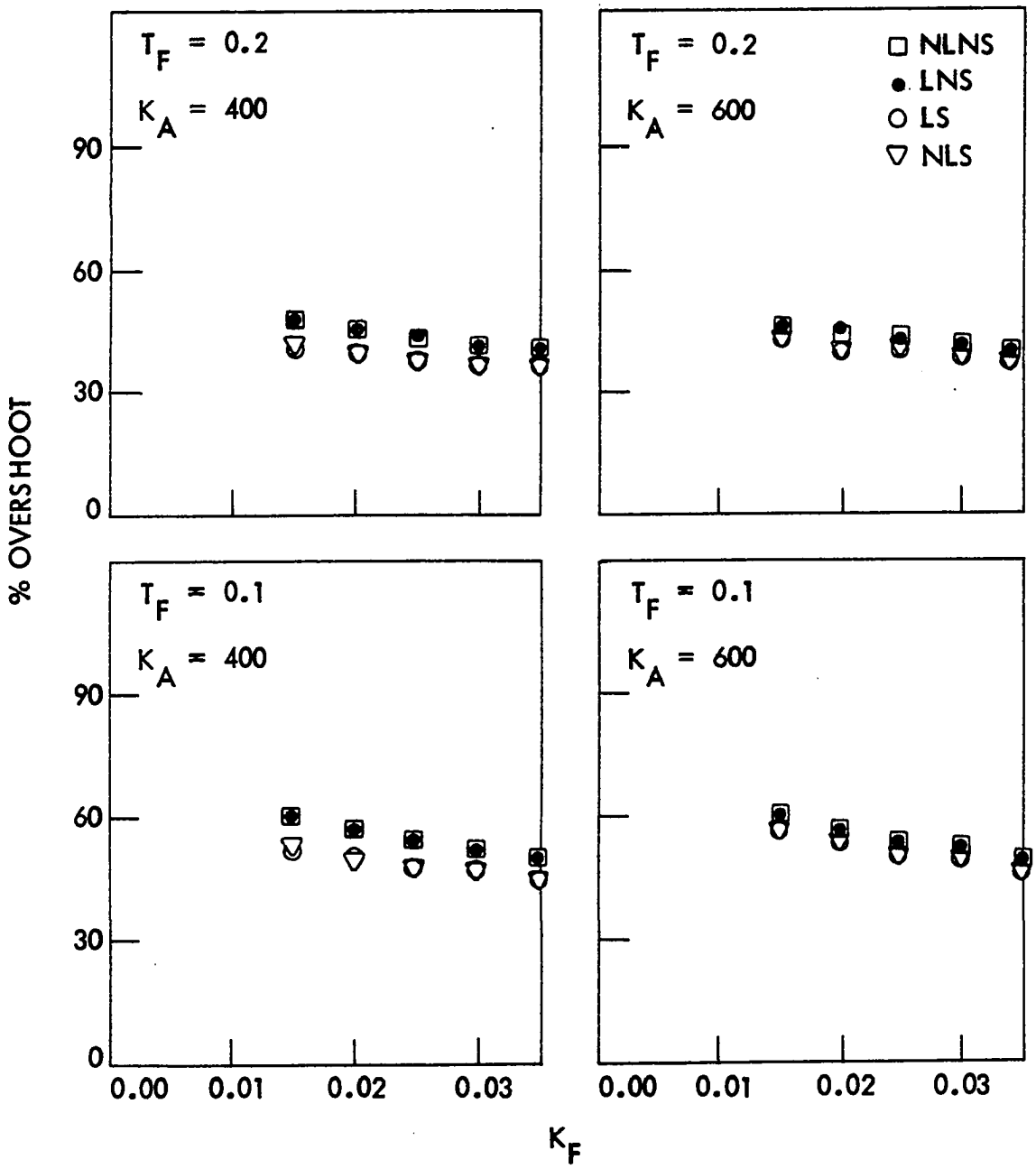

Figure 62. Percent overshoot vs K_F for NLNS, LNS, LS and NLS with low response exciter and model IV

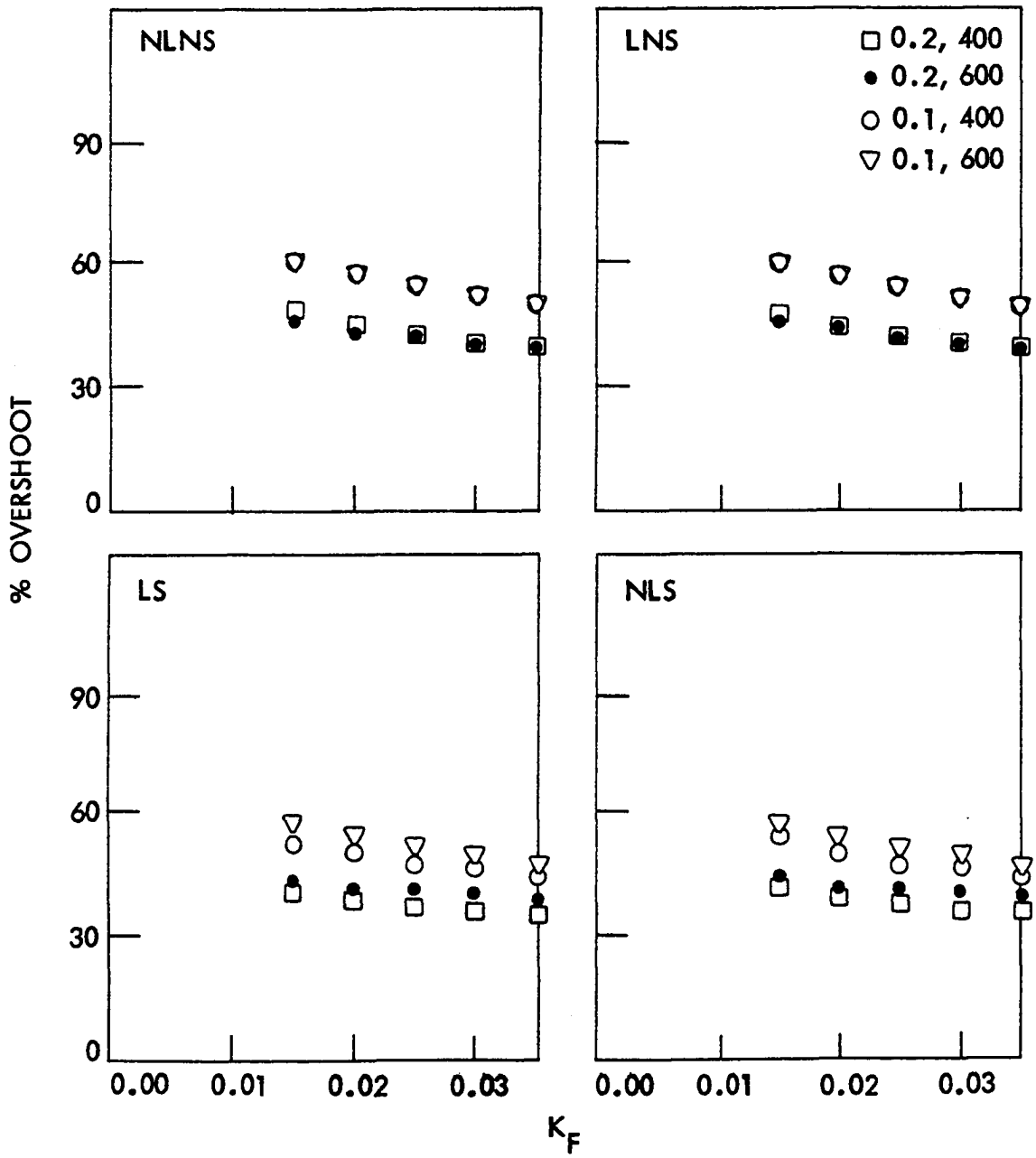

Figure 63. Percent overshoot vs K_F for T_F and K_A of .2/400, .2/600, .1/400 and .1/600 with low response exciter and model IV

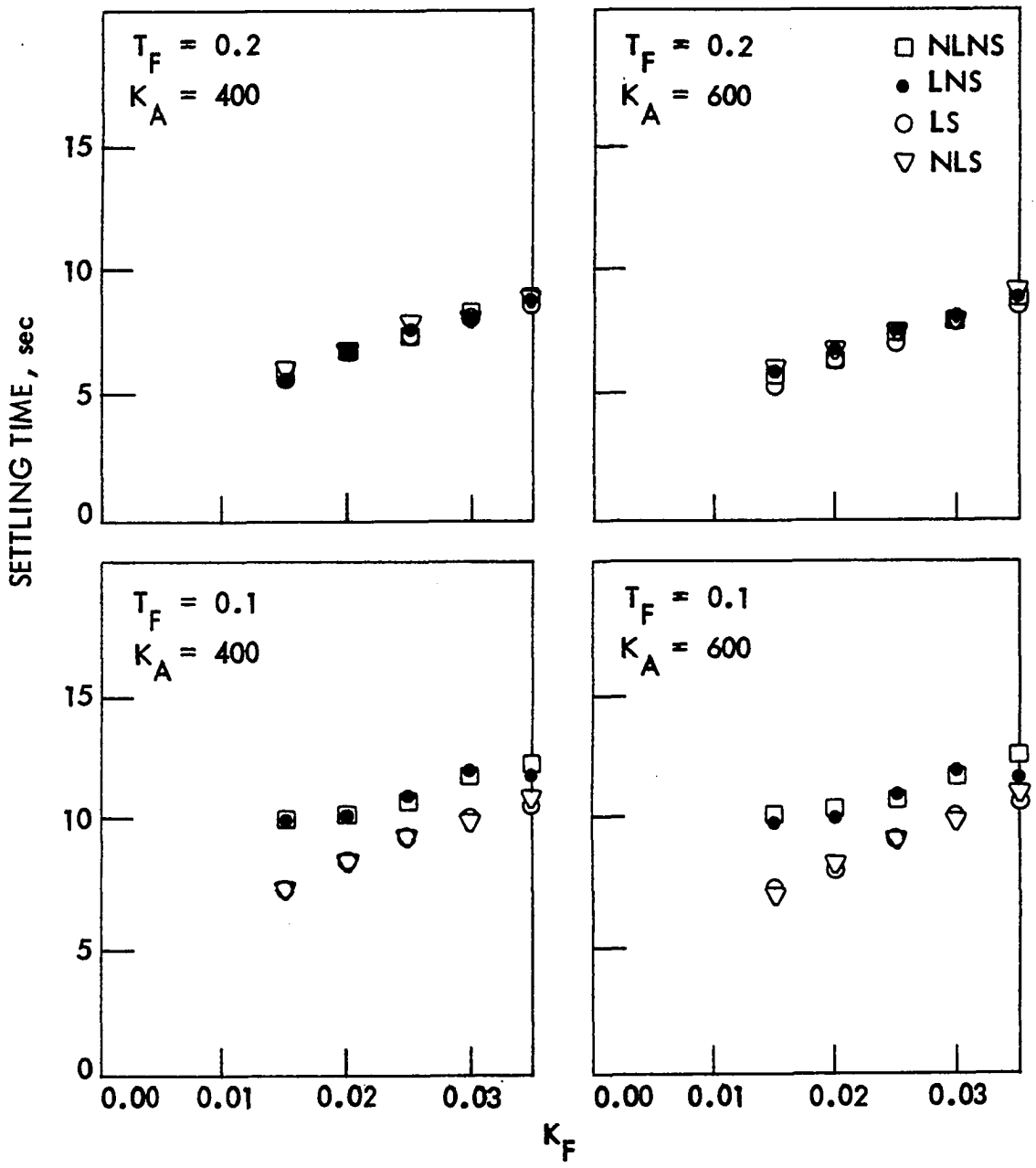

Figure 64. Settling time vs K_F for NLNS, LNS, LS and NLS with low response exciter and model IV

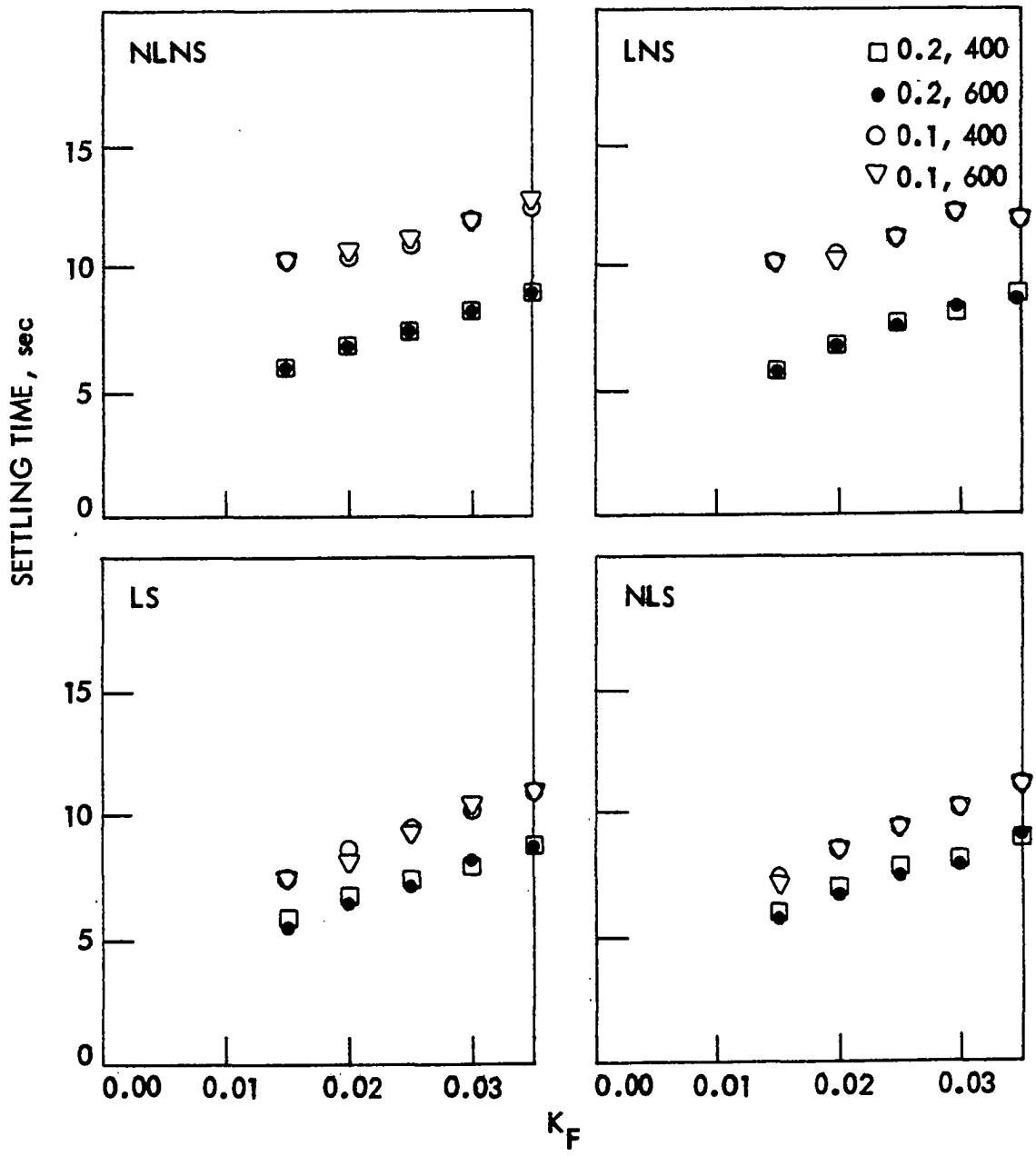

Figure 65. Settling time vs K_F for T_F and K_A of .2/400, .2/600, .1/400 and .1/600 with low response exciter and model IV

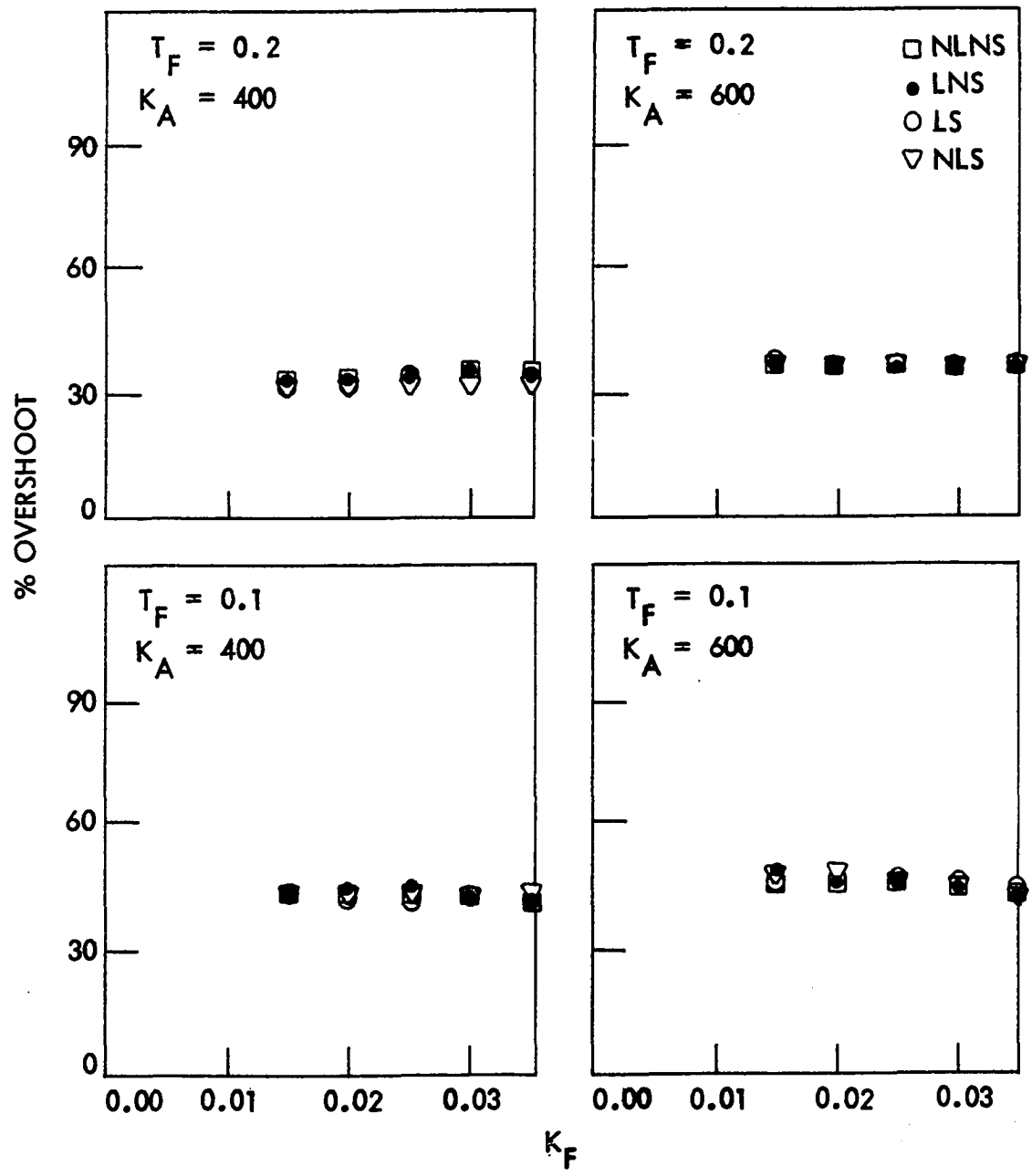

Figure 66. Percent overshoot vs K_F for NLNS, LNS, LS and NLS with high response exciter and model IV

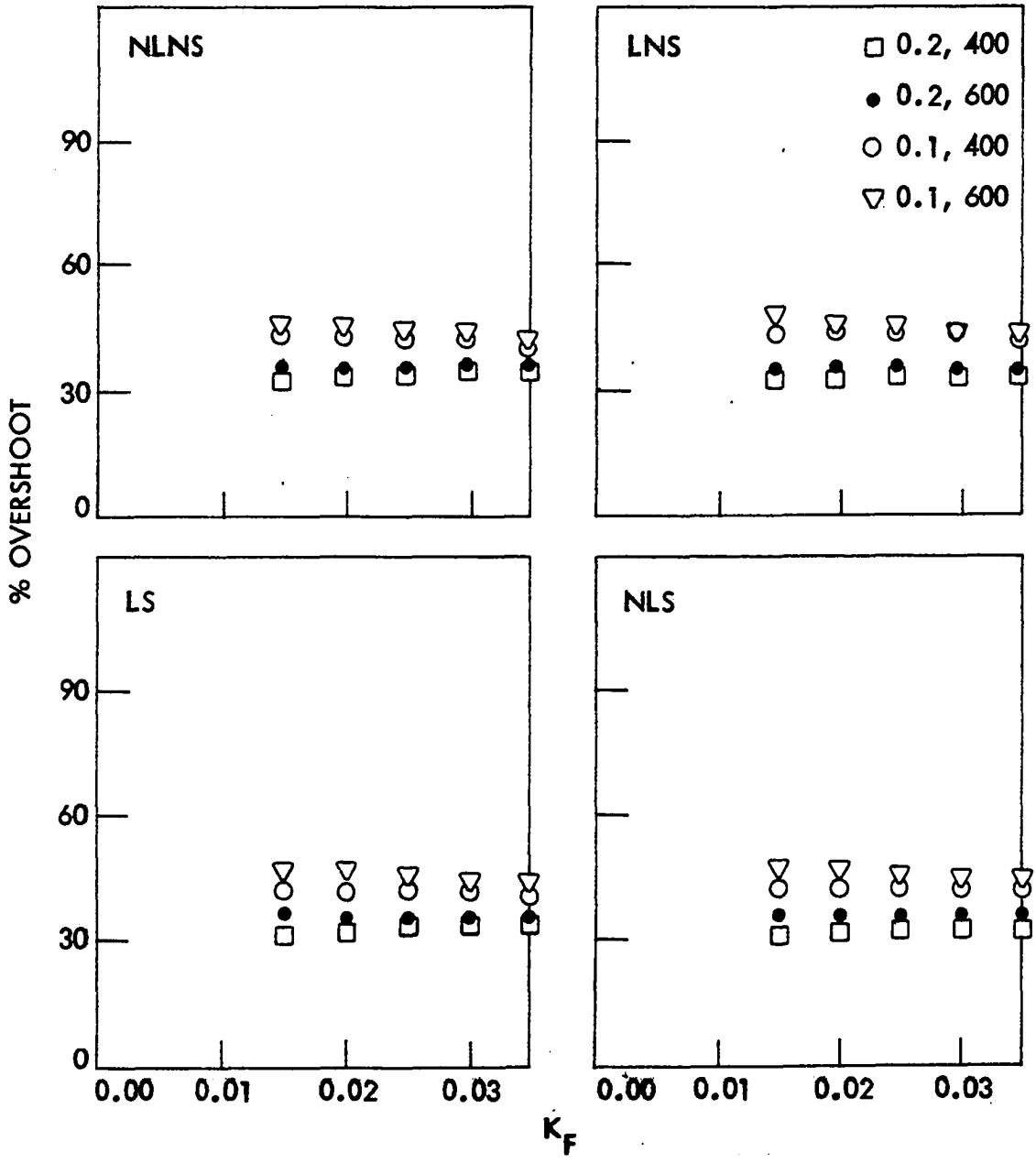

Figure 67. Percent overshoot vs K_F for T_F and K_A of .2/400, .2/600, .1/400 and .1/600 with high response exciter and model IV

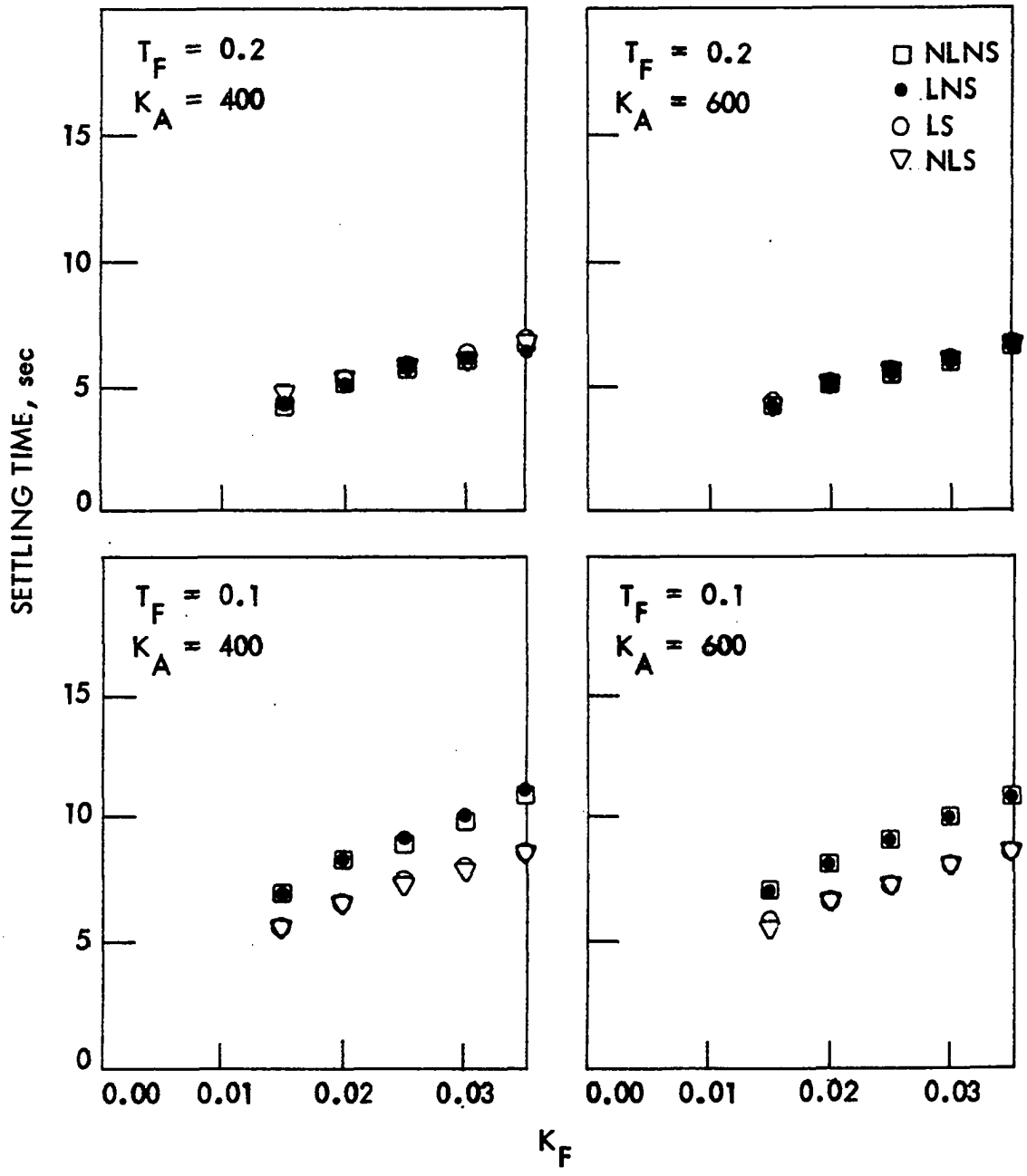

Figure 68. Settling time vs K_F for NLNS, LNS, LS and NLS with high response exciter and model IV

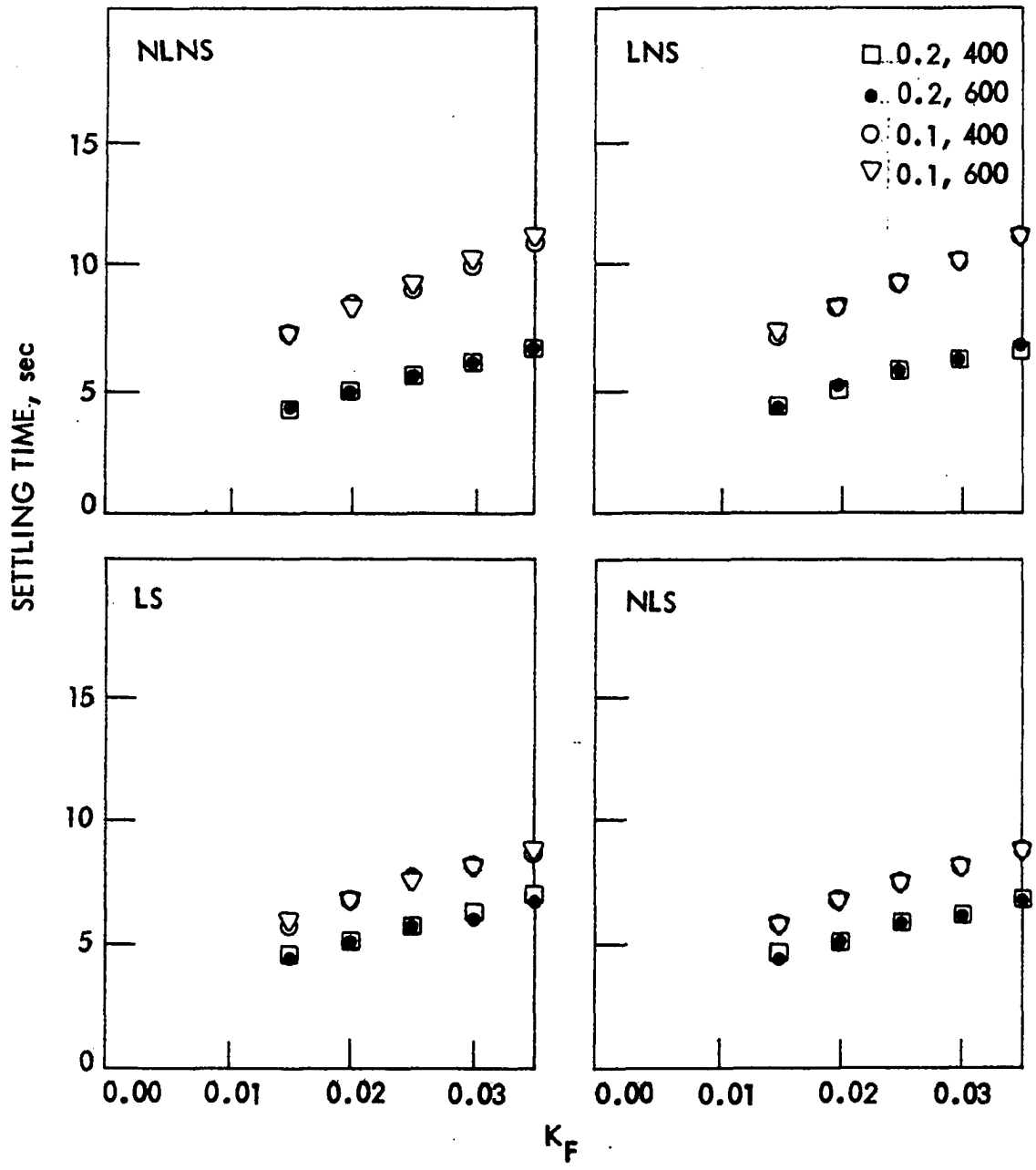

Figure 69. Settling time vs K_F for T_F and K_A of .2/400, .2/600, .1/400 and .1/600 with high response exciter and model IV

B. Effect of Saliency on Model IV

The difference between the direct axis synchronous reactance, X_d, and the quadrature axis synchronous reactance, X_q, may serve as an indicator of the degree of saliency in a synchronous machine.

Table 14. Average values of X_d and X_q in per unit for typical synchronous machines

	Turbo generators (solid rotor)	Water-wheel generators (with dampers)	Synchronous condensers	Synchronous motors (general purpose)	Machine used in this study
X_d	1.100	1.150	1.800	1.200	1.700
X_q	1.080	0.750	1.150	0.900	1.640
X_q/X_d	0.981	0.652	0.638	0.750	0.964
$(X_d-X_q)/X_d$	0.019	0.348	0.362	0.250	0.036
% saliency	1.9	34.8	36.2	25.0	3.6

Consider the average values of X_d and X_q for different types of synchronous machines (4, 62) shown in Table 14. Judging from this table, 30% saliency may be used to study the effect of saliency. The value of 30% saliency is not uncommon in the literature. For example, the machine used in reference 72 has X_d and X_q of 1.2 and 0.8 per unit, respectively, and this corresponds to 33.33% saliency as defined in Table 14. For the machine being used in this study, if we fix X_d at its supplied value of 1.70 per unit then X_q required for 30% saliency is 1.19 per unit. Using this value the potentiometer settings in which X_q appears are changed appropriately (see Appendix C).

Figures 70 and 71 show the response of model IV with and without saliency effects to $\Delta\tau_m$ and Δv_{ref}. First, the system without saliency effects is brought to full load steady state operation. At point A the chart recorder is switched to operate. Thus the values immediately to the right hand side of A are the steady state values without saliency effects. Both $\Delta\tau_m$ and Δv_{ref} are then applied and removed as indicated. At point B, the recorder is stopped. The analog computer is then turned to its pot set condition and the potentiometer changes necessary for the saliency effects are made. The system is restarted and brought to its full load steady state condition before the recorder is turned on again. Thus the values immediately to the right side of point B indicate the steady state conditions which exist when saliency effects are considered.

Figures 70 and 71 have each been presented in three parts in order to show the effects of saliency in as many output variables as possible. Part a shows the effects of saliency on the variables used in the previous figures. Part b shows the variables immediately affected by saliency, at least insofar as potentiometer settings are concerned. Part c shows saliency effects on some other output variables.

From these figures it would appear that the effect of saliency is more noticeable on the steady state quantities than on step changes in τ_m and v_{ref}.

C. Effect of Machine Saturation on Model IV

As mentioned in Chapter II, several studies emphasizing the need to represent machine saturation in stability studies have been presented in the literature. In Chapter II it was also noted that several methods of

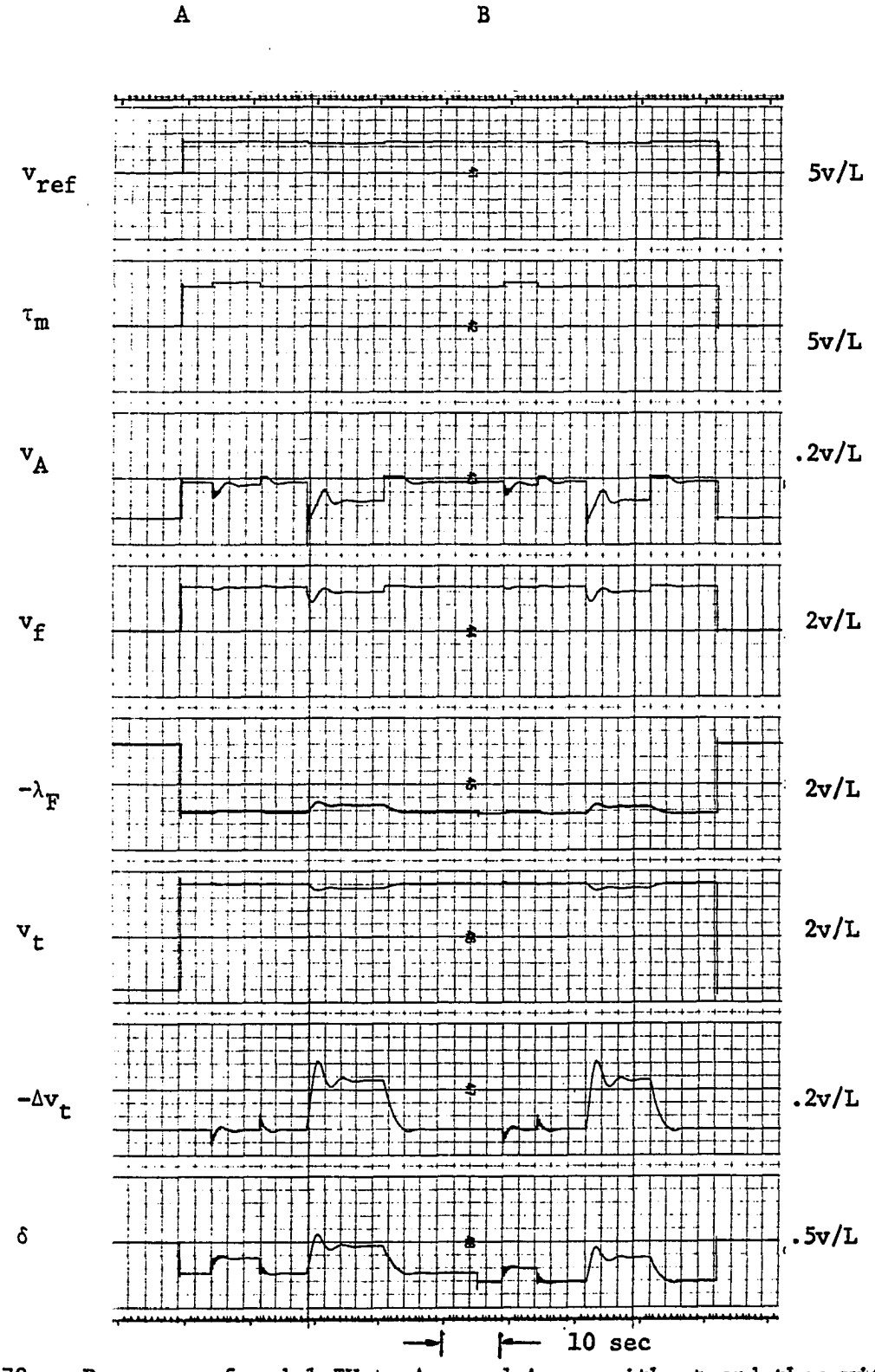

Figure 70a. Response of model IV to $\Delta\tau_m$ and Δv_{ref} without and then with saliency effects using slow exciter

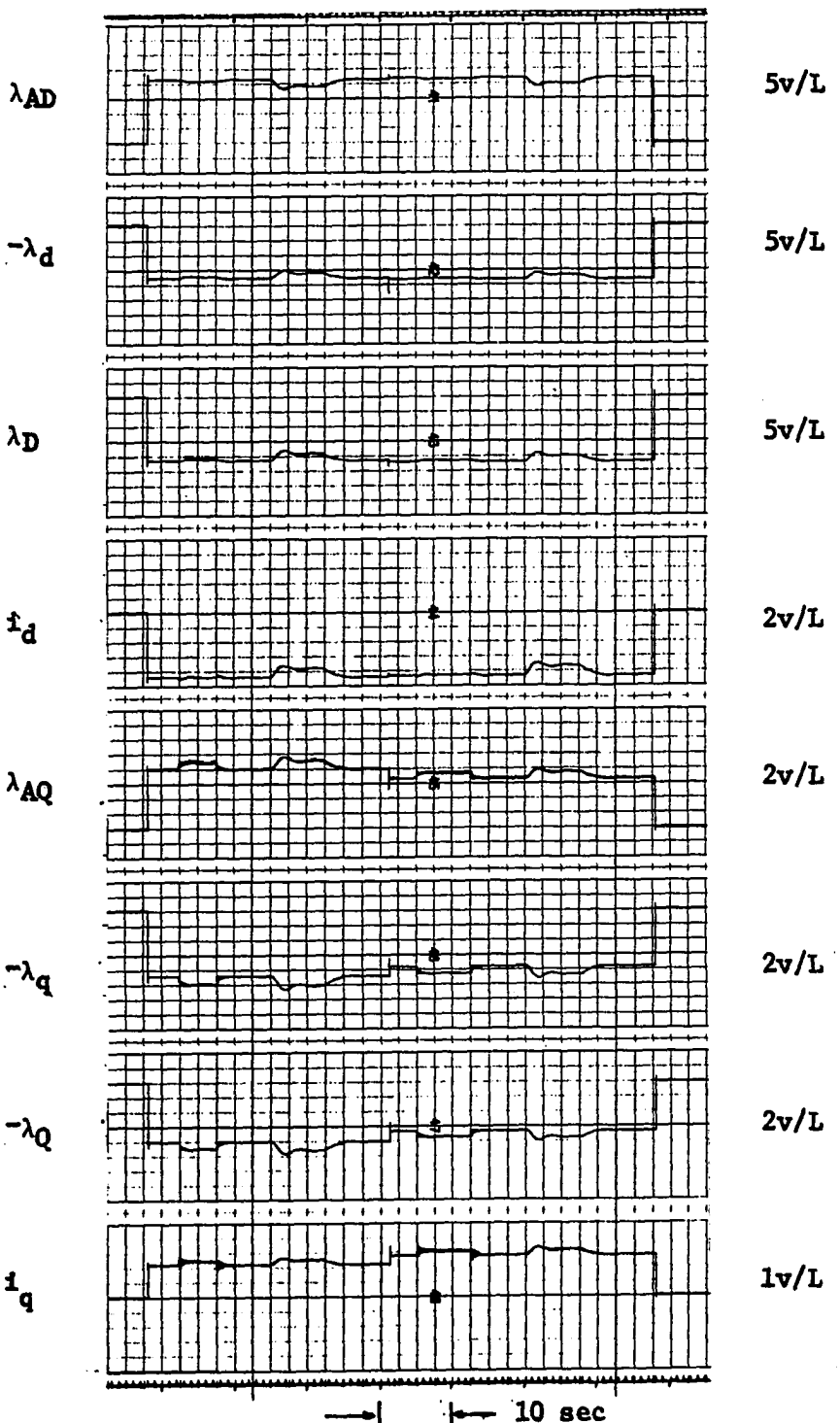

Figure 70b. Response of model IV to $\Delta\tau_m$ and Δv_{ref} without and then with saliency effects using slow exciter

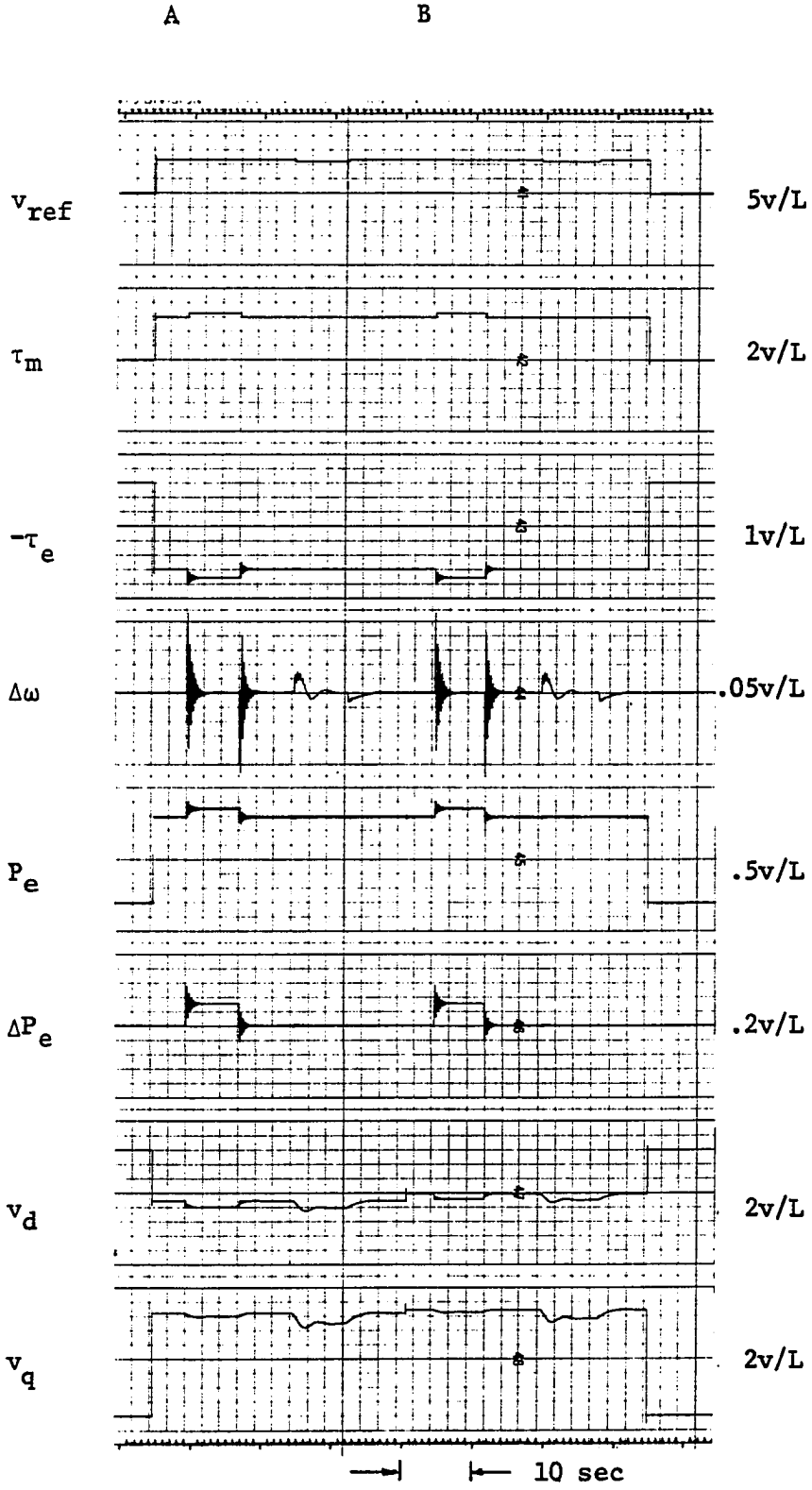

Figure 70c. Response of model IV to $\Delta\tau_m$ and Δv_{ref} without and then with saliency effects using slow exciter

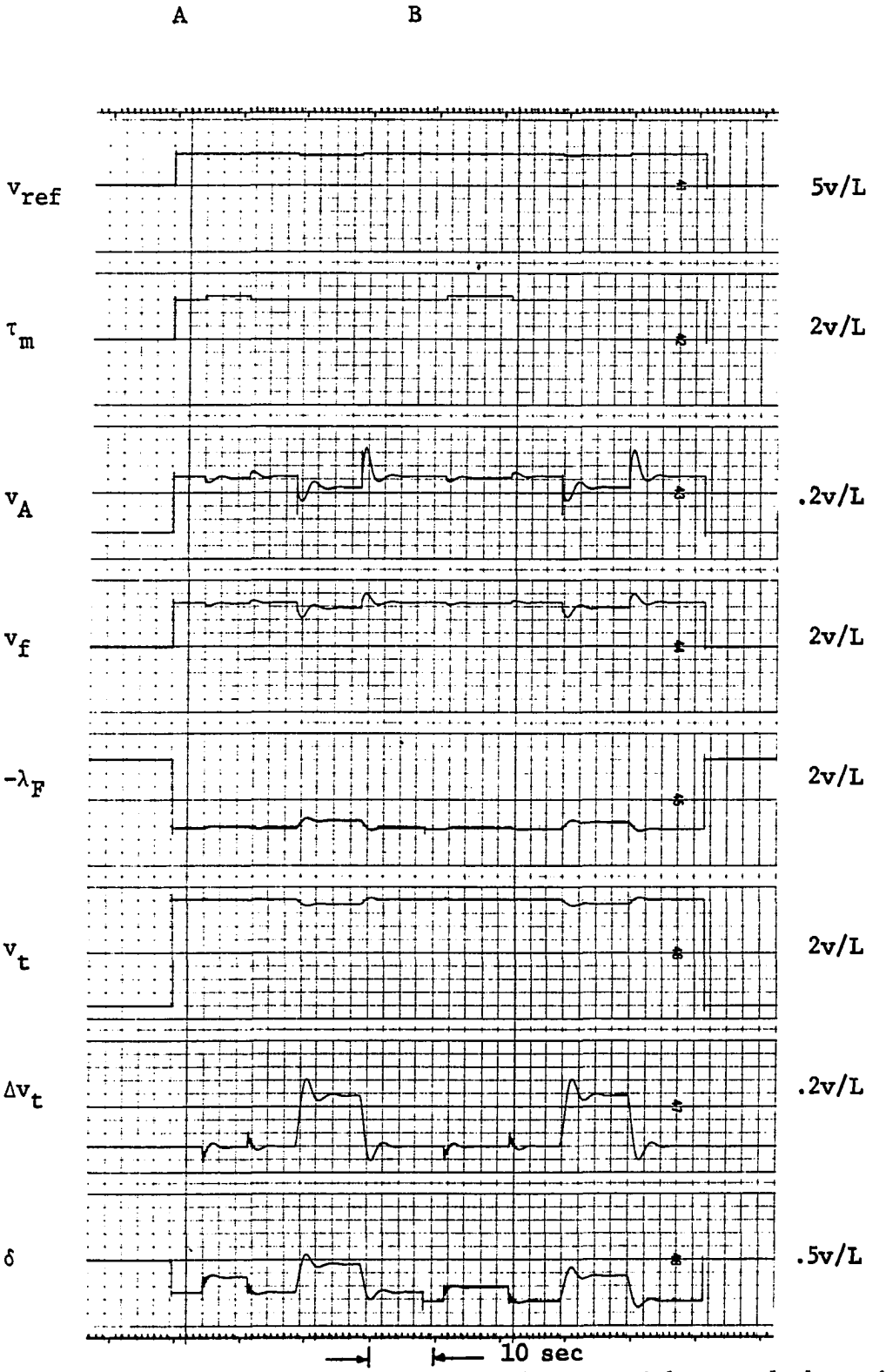

Figure 71a. Response of model IV to $\Delta\tau_m$ and Δv_{ref} without and then with saliency effects using fast exciter

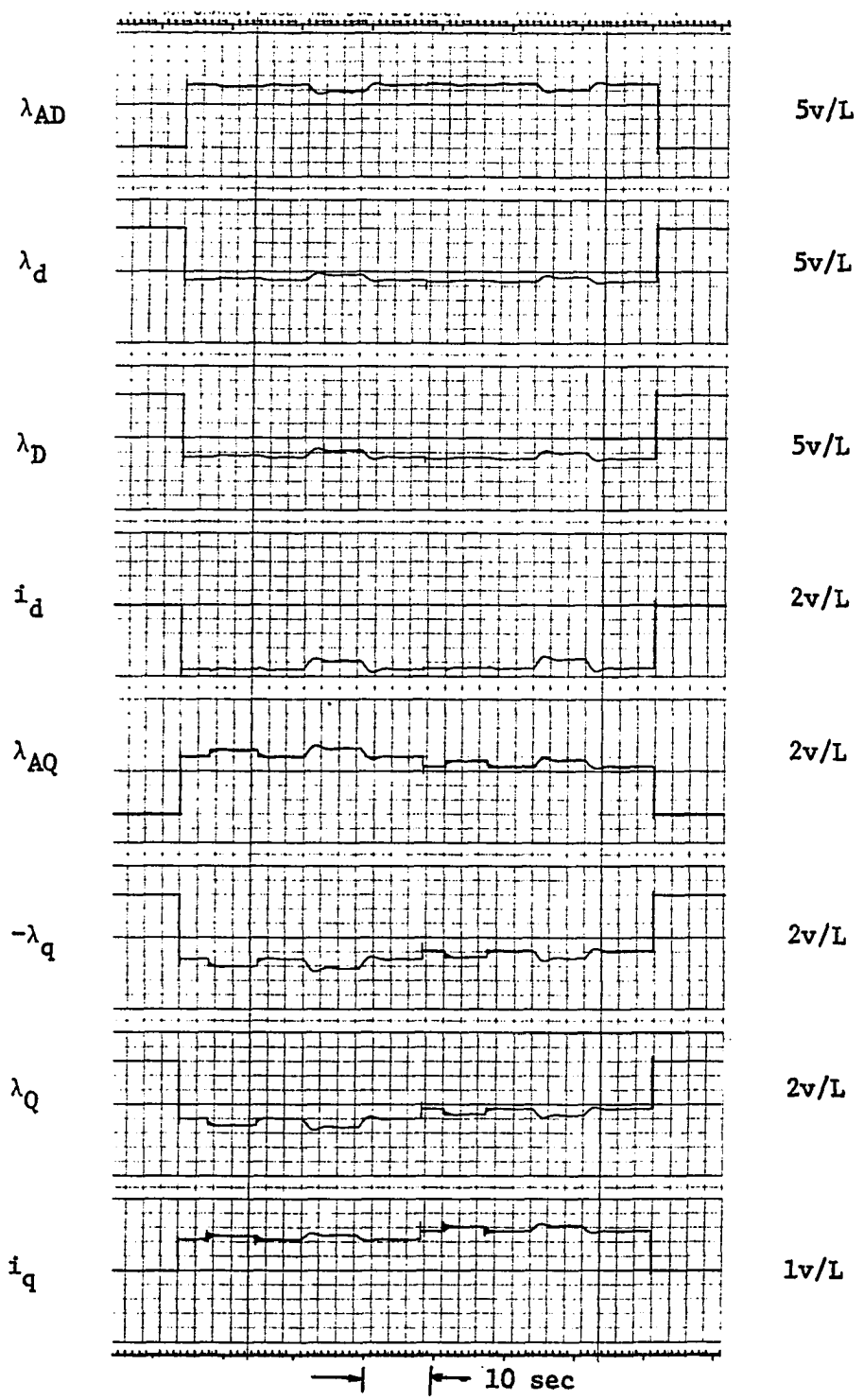

Figure 71b. Response of model IV to $\Delta\tau_m$ and Δv_{ref} without and then with saliency effects using fast exciter

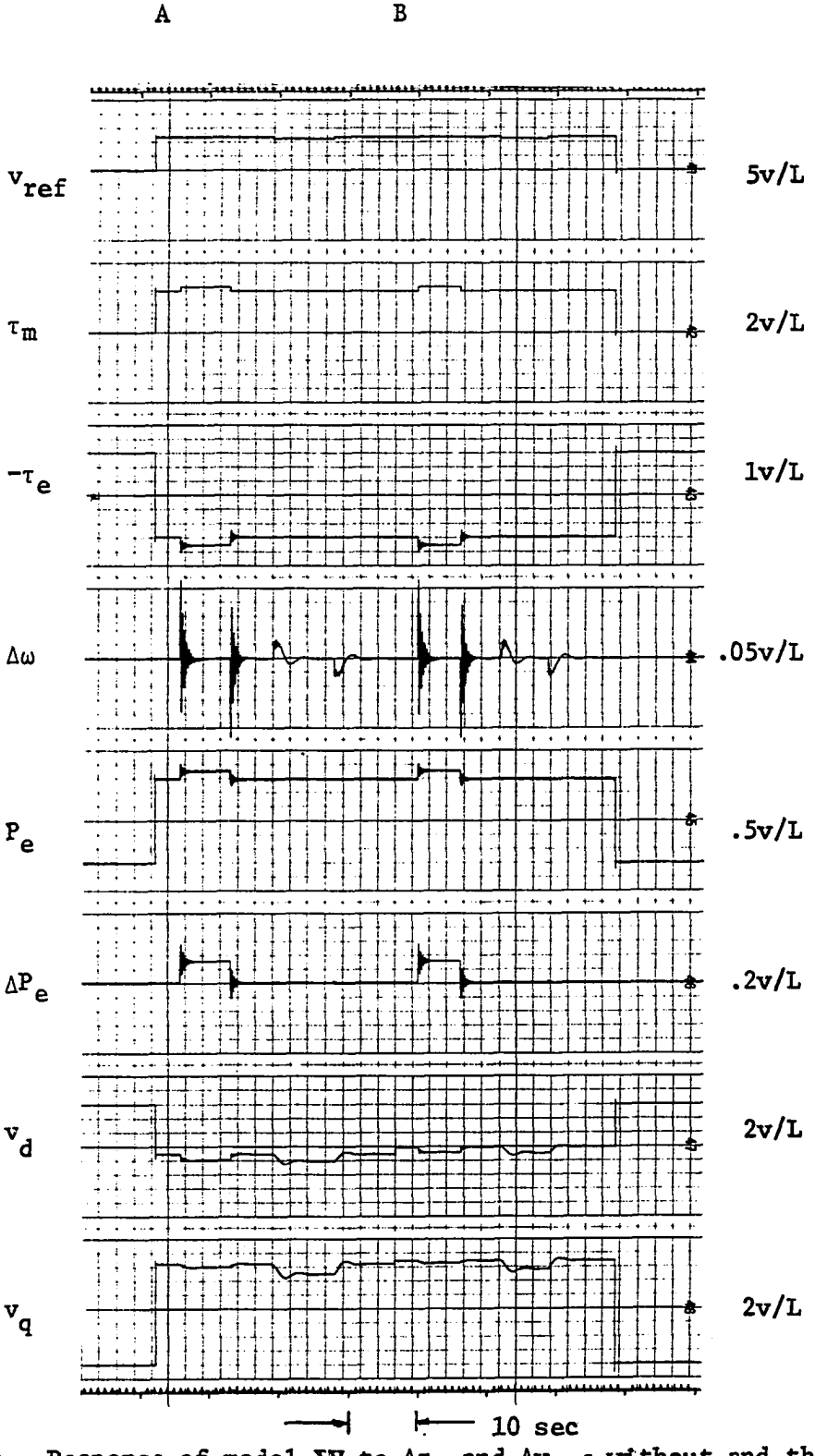

Figure 71c. Response of model IV to $\Delta\tau_m$ and Δv_{ref} without and then with saliency effects using fast exciter

representing machine saturation have been proposed. The lumped-parameter equivalent circuit being used does not permit precise representation of the saturation phenomena. However, a reasonable model can be obtained by treating the direct axis mutual flux linkages, λ_{AD}, and its quadrature axis counterpart, λ_{AQ}, as being saturable. These two quantities appear in the direct and quadrature axis equivalent circuits as shown in Figure 72.

The method used in obtaining d-q-axes saturation is similar to those used in references 10, 14 and 40, and it is a modified form of that recommended for the exciter saturation function (53). As indicated in Table 14 under the discussion on saliency effects, the degree of saliency for the machine being studied is 3.6%. Thus the q-axis saturation curve will be 3.6% less than the d-axis saturation curve which is supplied by the machine manufacturer. Hence for all practical purposes we can assume that the two saturation curves are the same. See Appendix C for the saturation curves used and for simulation considerations.

It is to be noted that the value of δ measured is negative. As shown in Appendix D, this is due to the fact that an R of 0.5 per unit has been used which places a large load on the machine terminal. The system voltage response to both $\Delta\tau_m$ and Δv_{ref} are in the proper direction for this value of load.

The response of model IV to $\Delta\tau_m$ and Δv_{ref} with and without saturation is recorded in three ways: model IV with d-axis saturation, model IV with q-axis saturation and model IV with both d- and q-axes saturation. The results are shown in Figures 73-77 for the two types of exciters. The left half of each figure represents response without saturation effect while the right half is the response with the saturation effect. Part a

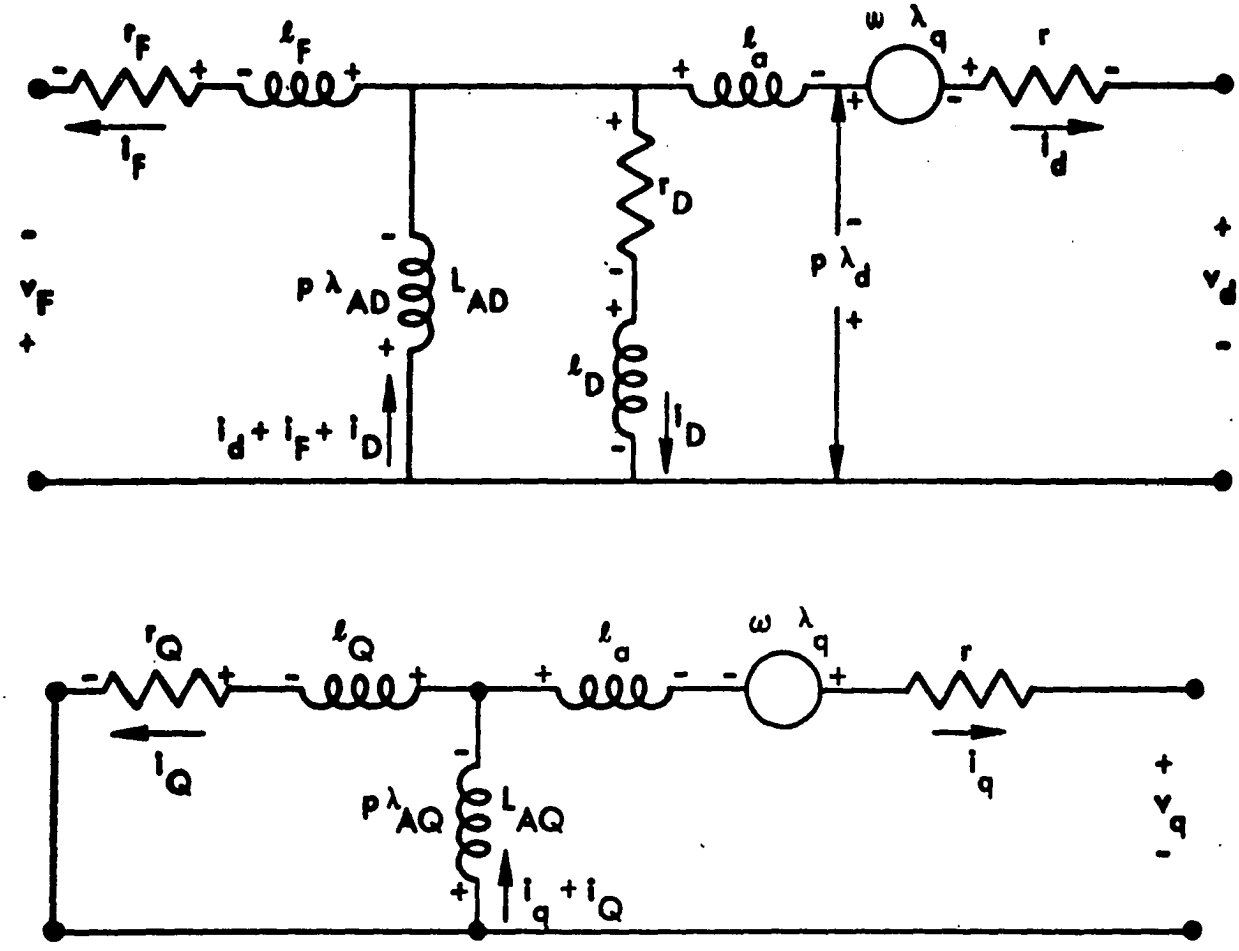

Figure 72. The d-q-axes equivalent circuits of a synchronous machine

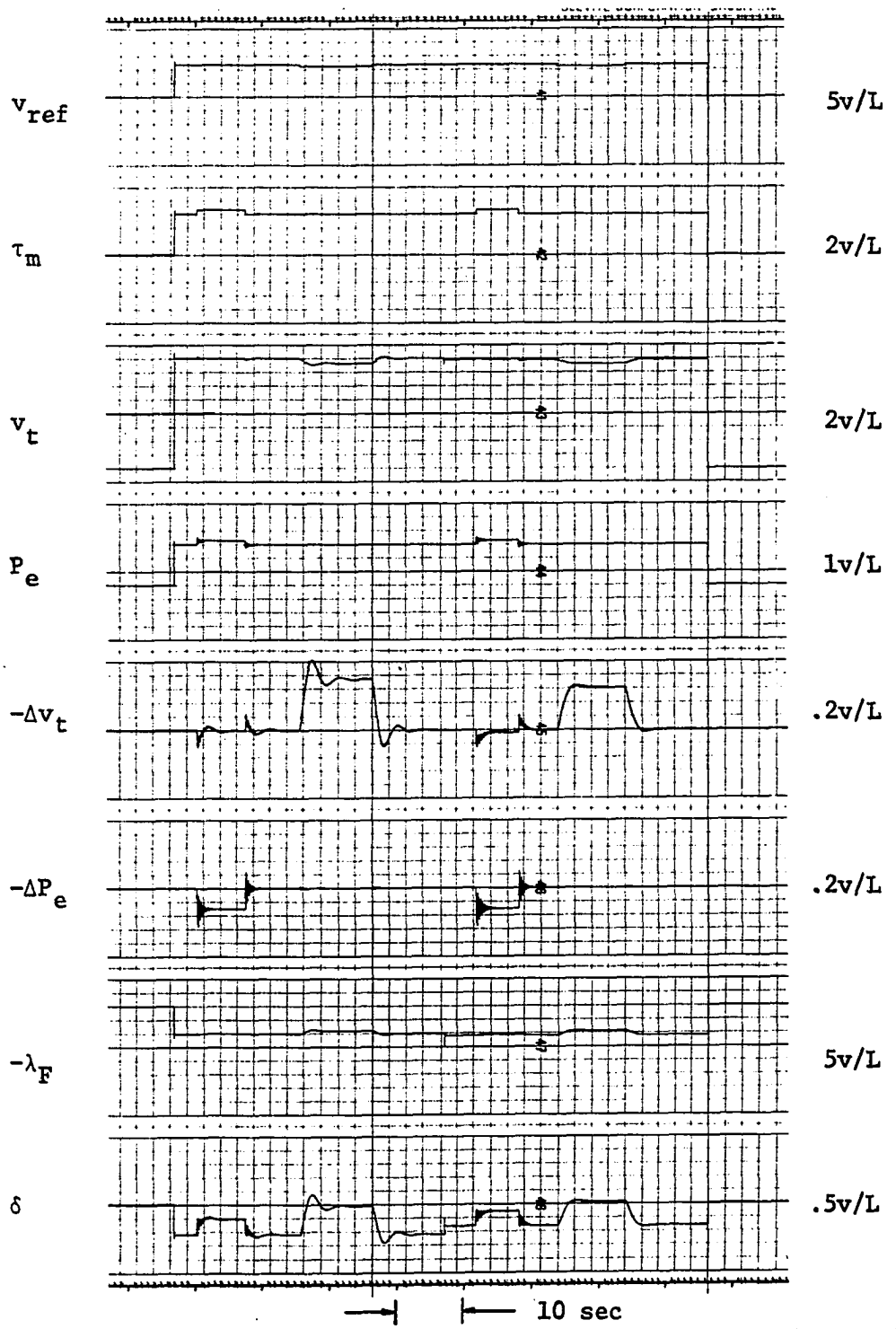

Figure 73a. Effects of $\Delta\tau_m$ and Δv_{ref} on model IV without and then with d-axis saturation using the slow exciter

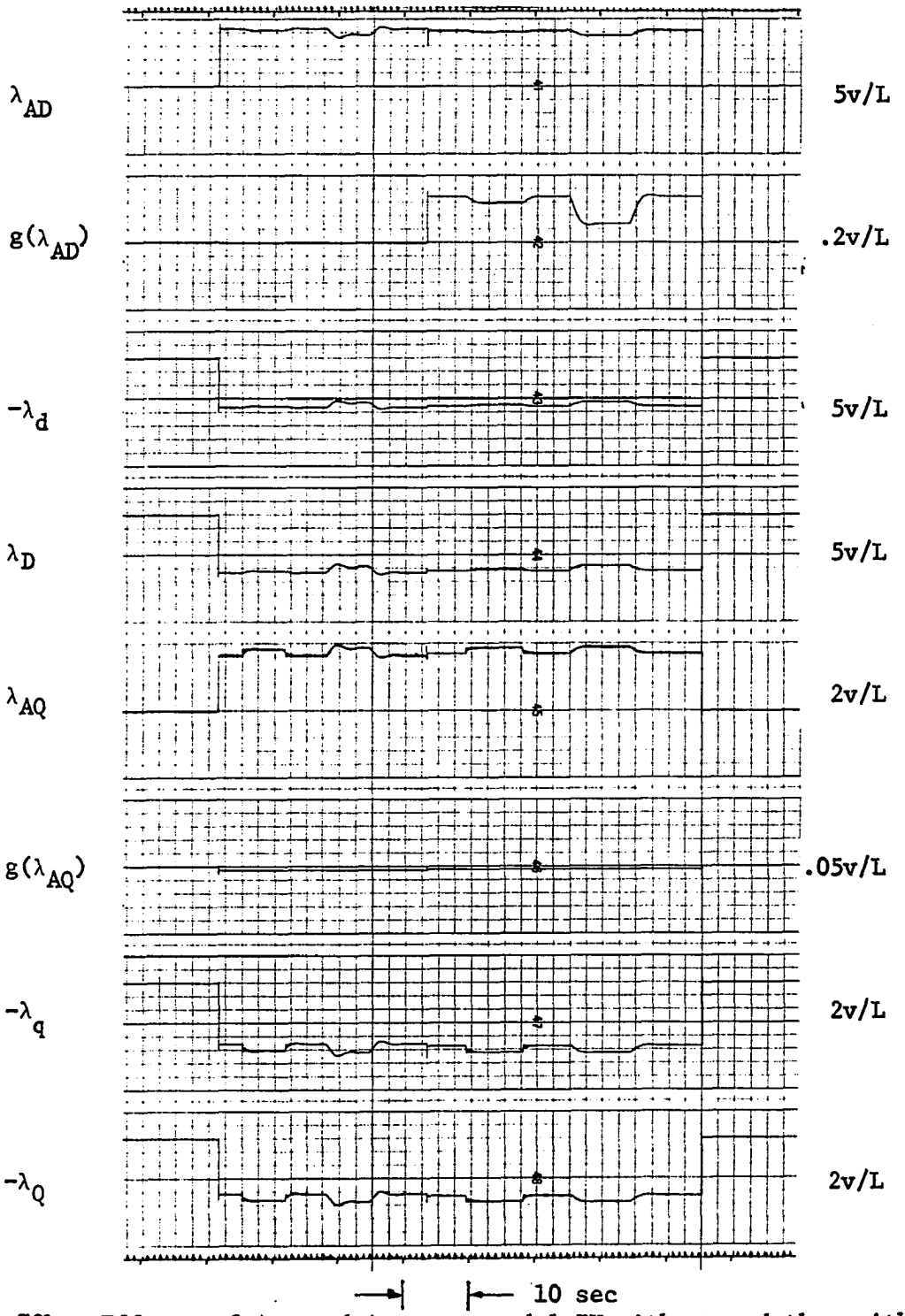

Figure 73b. Effects of $\Delta\tau_m$ and Δv_{ref} on model IV without and then with d-axis saturation using the slow exciter

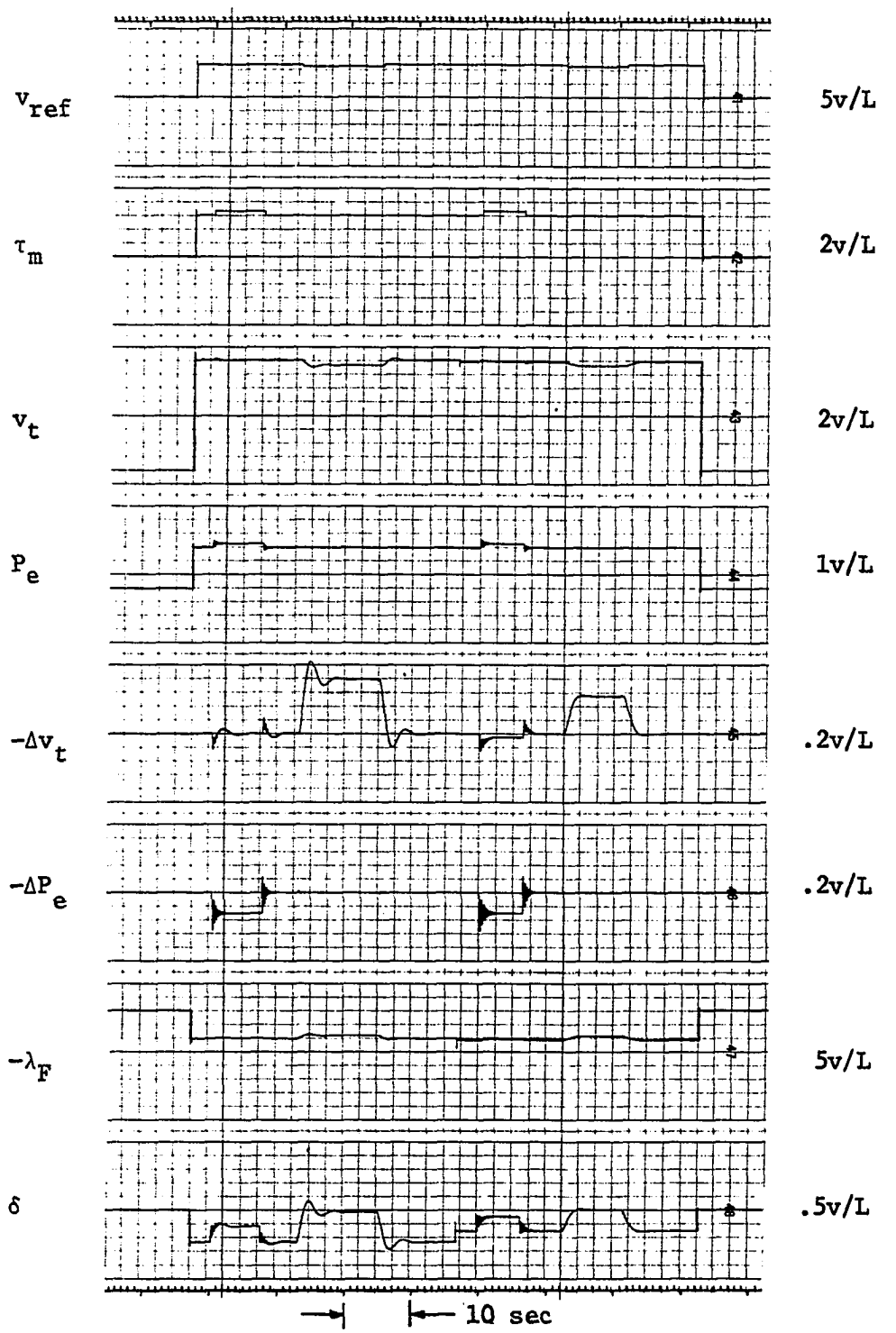

Figure 74a. Effects of $\Delta\tau_m$ and Δv_{ref} on model IV without and then with d-axis saturation using the fast exciter

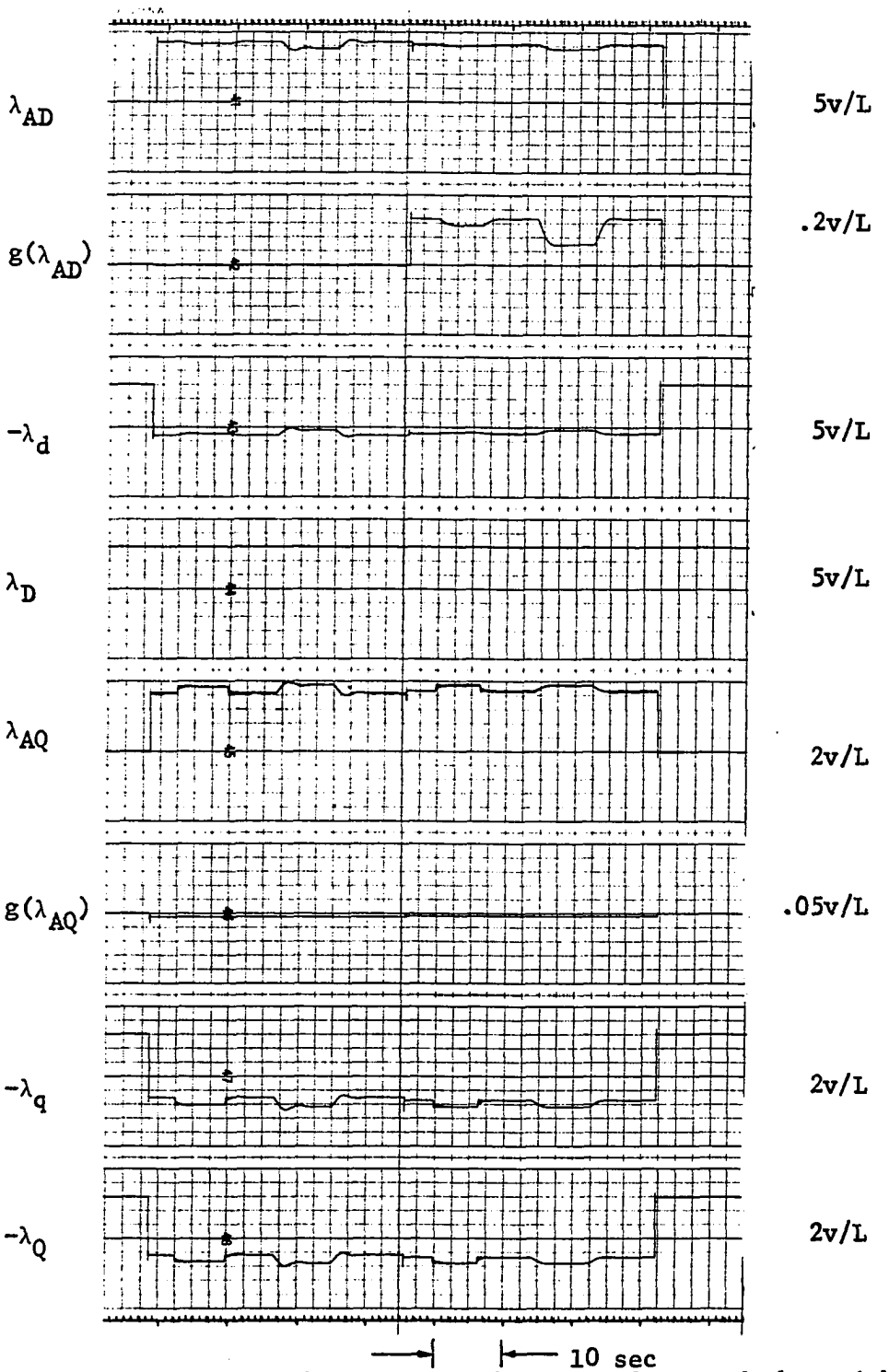

Figure 74b. Effects of $\Delta\tau_m$ and Δv_{ref} on model IV without and then with d-axis saturation using the fast exciter

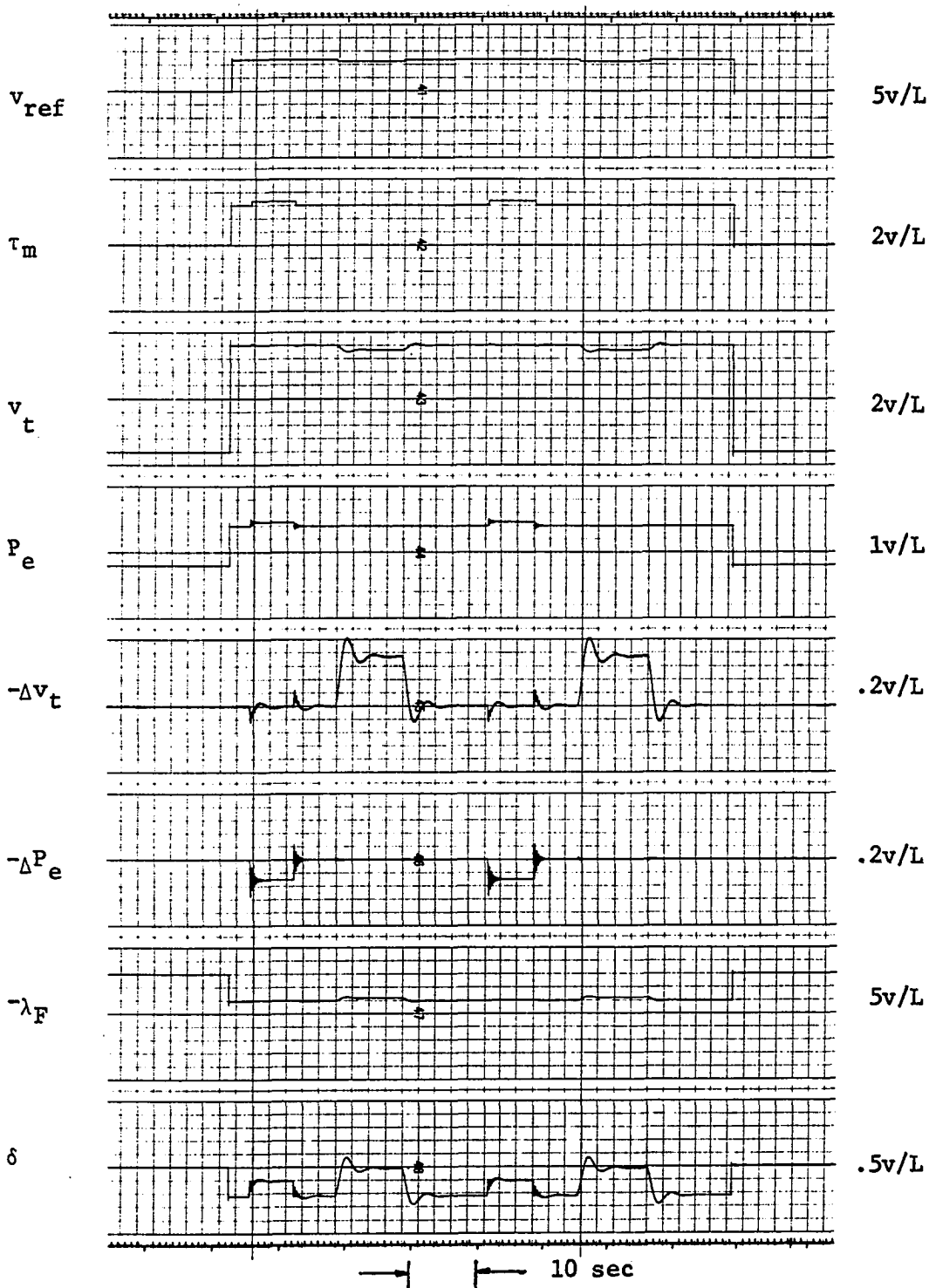

Figure 75a. Effects of $\Delta\tau_m$ and Δv_{ref} on model IV without and then with q-axis saturation using slow exciter

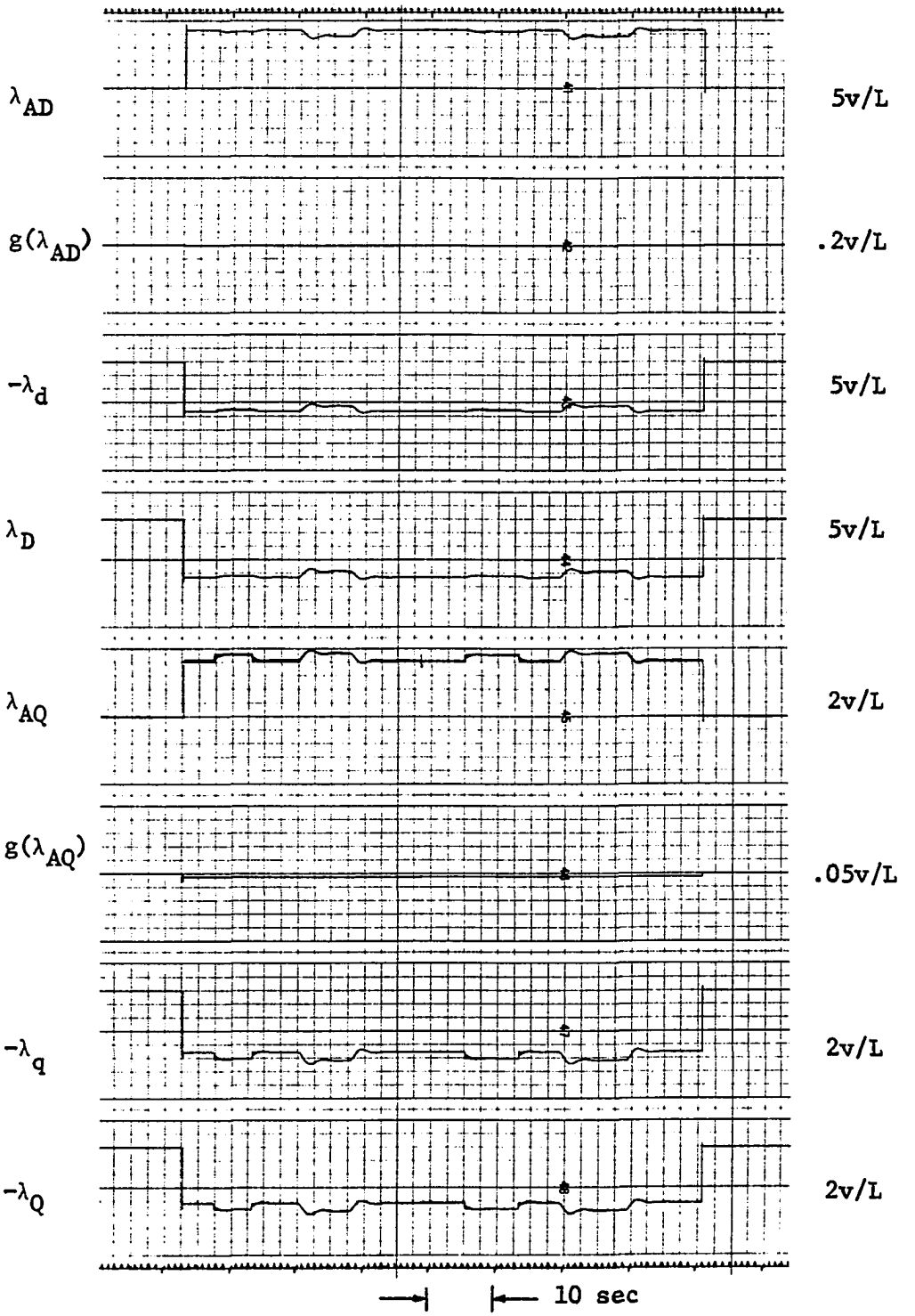

Figure 75b. Effects of $\Delta\tau_m$ and Δv_{ref} on model IV without and then with q-axis saturation using slow exciter

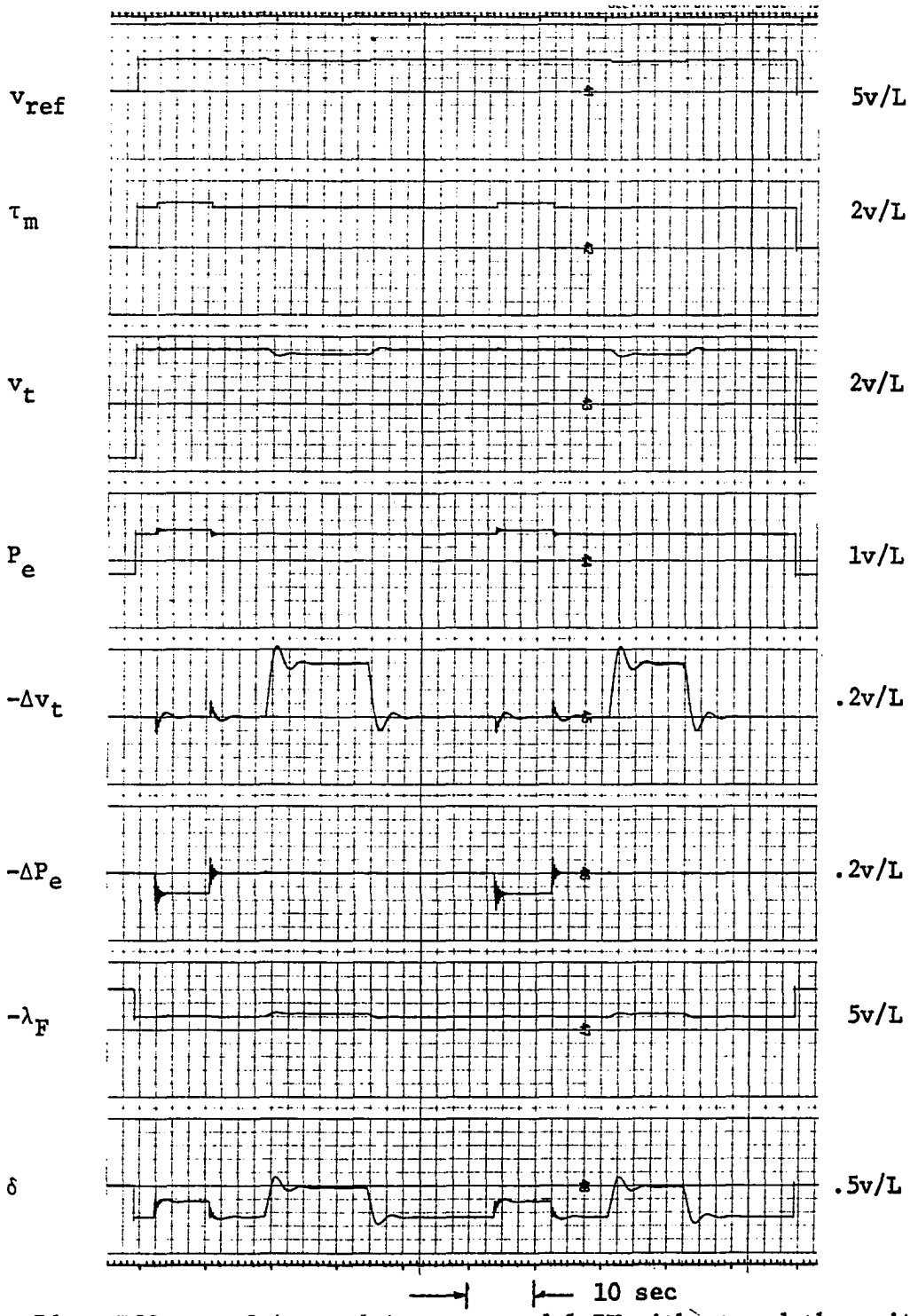

Figure 76a. Effects of $\Delta\tau_m$ and Δv_{ref} on model IV without and then with q-axis saturation using the fast exciter

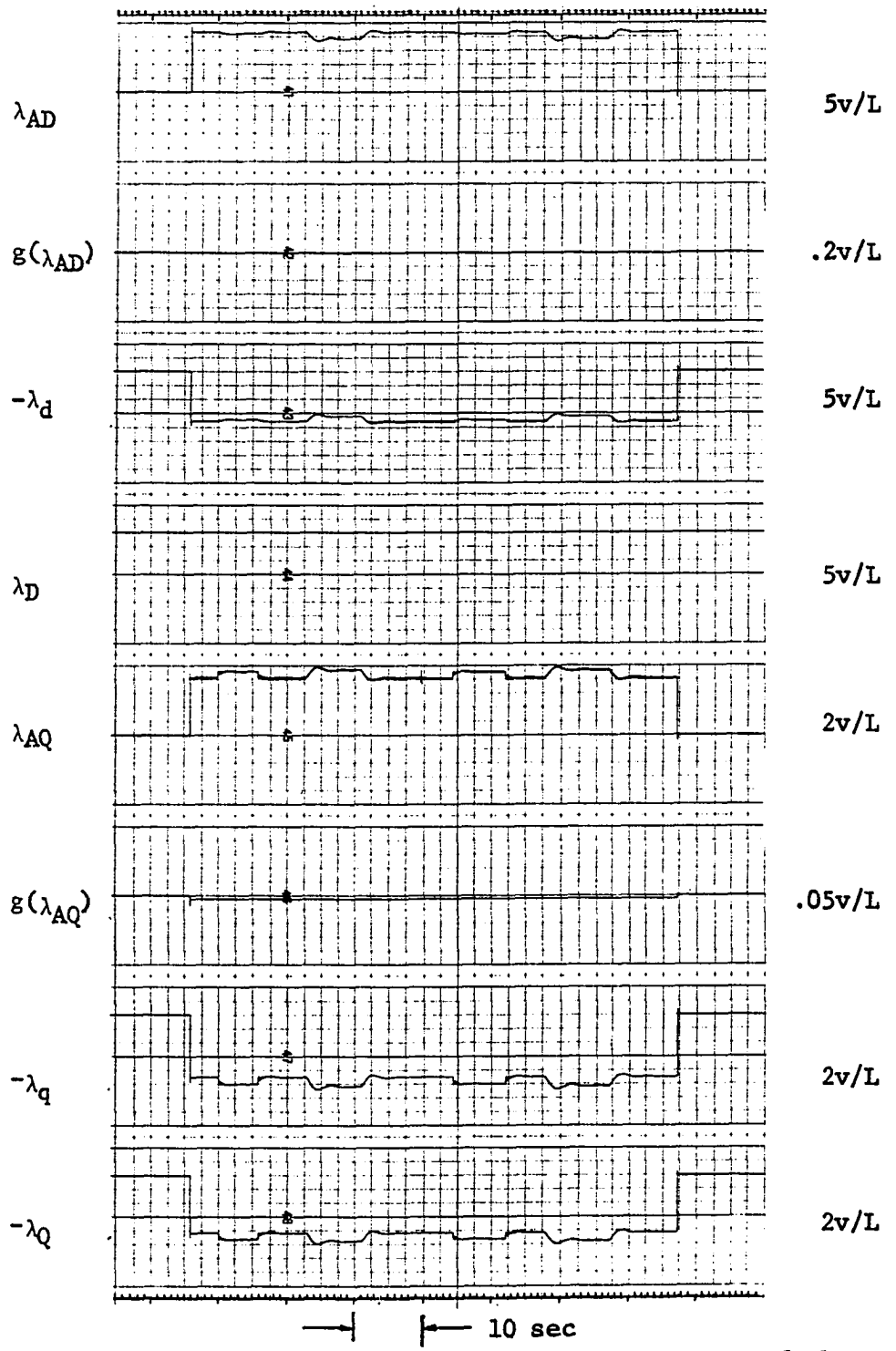

Figure 76b. Effects of $\Delta\tau_m$ and Δv_{ref} on model IV without and then with q-axis saturation using the fast exciter

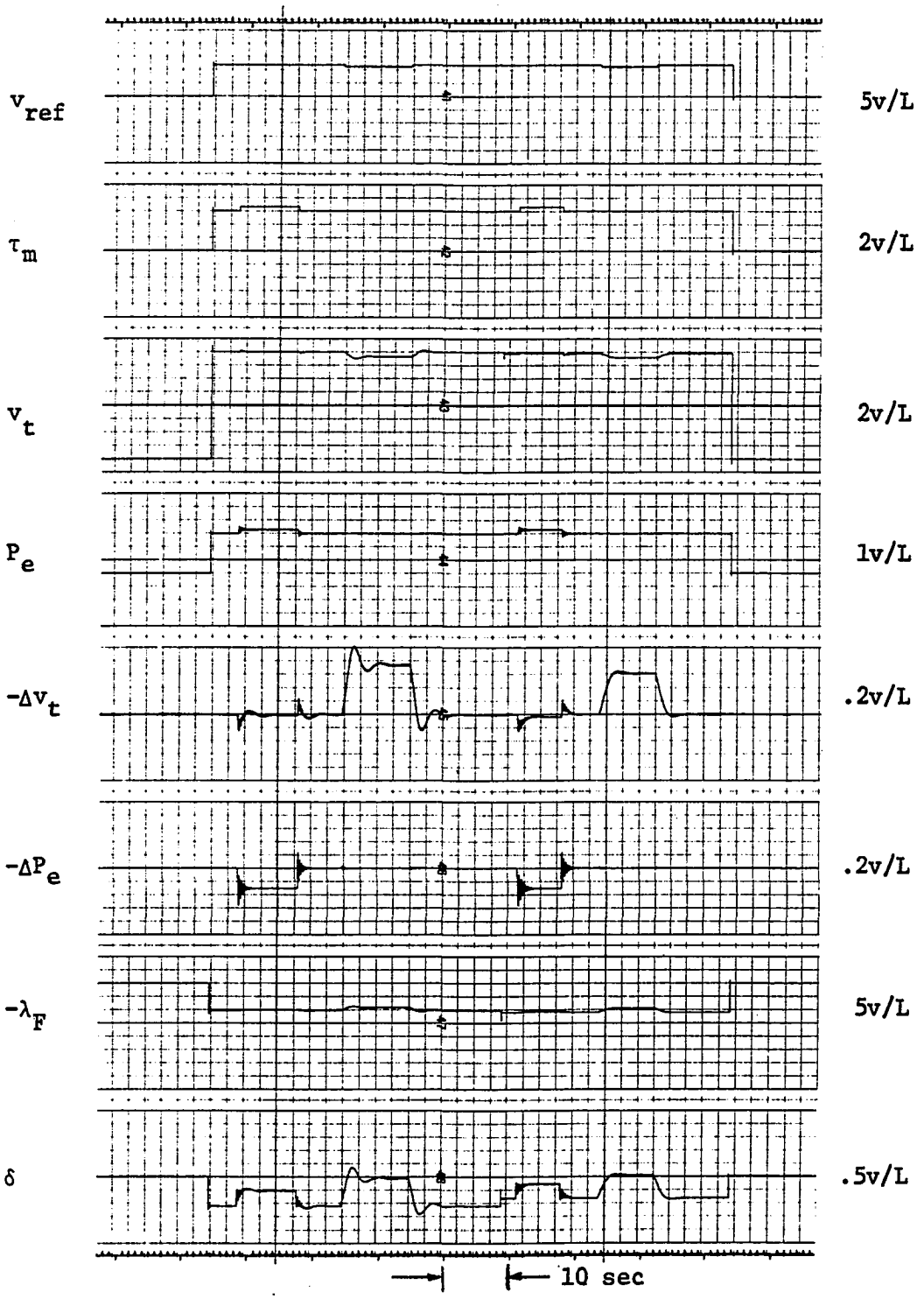

Figure 77a. Effect of $\Delta\tau_m$ and Δv_{ref} on model IV without and then with both d-q-axes saturation using the slow exciter

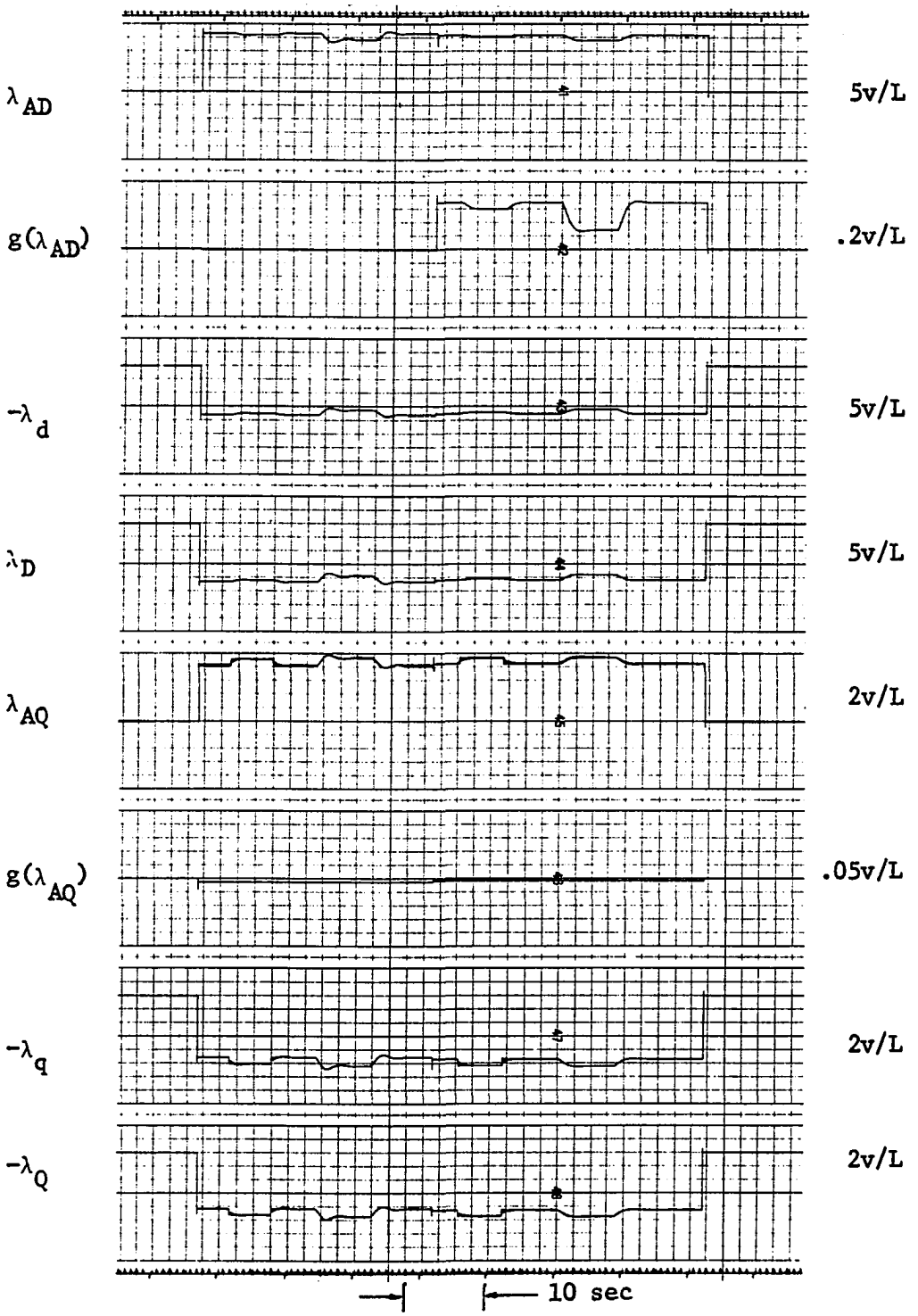

Figure 77b. Effect of $\Delta\tau_m$ and Δv_{ref} on model IV without and then with both d-q-axes saturation using the slow exciter

of the figures records the variables that would permit comparison of the response with those in the previous discussion while part b records the flux linkages in the region where saturation is represented.

As shown in Figures 73 and 74 saturation in the d-axis lowers the overshoot in the terminal voltage considerably. The steady state values of λ_{AQ} are in the linear region of the saturation curve where the saturation function $g(\lambda_{AQ})$ is zero. Hence, as shown in Figures 75 and 76, there is no difference in the response of the system with and without q-axis saturation for the loading used. The combined effect of both d-q-axes saturation which is shown only for the slow exciter is therefore the same as that given by the d-axis saturation alone.

D. Conclusions to Chapter VI

Several conclusions can be drawn from the studies described in this chapter. Such conclusions can be obtained by comparing the studies made in this chapter with those in Chapters IV and V in addition to specific conclusions resulting from this chapter alone.

A comparison of Figures 20-27, 47-54 and 62-69 shows that the conclusions 1-8 made in Chapter IV are still valid for model IV.

Conclusions 3-9 stated in section D of Chapter V still apply for model IV.

Two additional conclusions on Chapter VI are:

1) Machine saliency changes some of the steady state output variables of model IV.
2) Machine saturation lowers the overshoot of the terminal voltage for step changes in $\Delta\tau_m$ and Δv_{ref}.

E. A Comparison of the Models

The analyses presented in Chapters IV, V and VI not only show the effects of the system nonlinearities considered but can also be used to compare the three models, models I, II and III discussed in the analyses. Below are some of the possible qualitative comparisons of the models.

Model I, the first order approximation of a synchronous machine, is the simplest to analyze and the least accurate model but it cannot be used to study the effects of load. Model II describes only the dynamics of the rotor and ignores the machine electrical characteristics. Model IV is the most complicated but also the most accurate of the three approximate models.

The general observations and conclusions on the comparison of the percent overshoot and settling time are the same in the three models. However, the relative magnitudes of these performance indices vary from one model to the other for similar analog computer runs.

The rise time in the three models appears to be too short for any meaningful comparison.

Model I is a one input system while model III is a two input system. This fact explains the relative usefulness of the models and why response of model III more closely approximates that of model IV than model I.

Model IV can be used to investigate the validity of the various simplifying assumptions used in developing simpler models.

In addition to these qualitative comparisons, one can record the response of the variables that are observable in the three models, like the change in the terminal voltage for example, in the same figure to allow a visual comparison.

VII. CONCLUSIONS AND SUGGESTIONS FOR FUTURE WORK

A. Conclusions

The results of the study described in this thesis show that for a synchronous machine connected to an infinite bus through a transmission line the inclusion of exciter saturation and amplifier limiting lowers overshoot but tends to sustain oscillations longer.

In the range of K_F, T_F and K_A considered, the faster response excitation system has better overall performance than the slower response excitation system.

Depending on the simplifying assumptions made, several models of the synchronous machine can be constructed. In this respect it was found that the assumption of constant flux linkages is valid only for a period of about one second after the occurrence of a disturbance.

The inclusion of damping terms in linear models improves the performance of the model and makes the response more closely resemble the performance of the actual machine as represented by a full nonlinear model.

It was observed that the settling time tends to become longer as the models become more complex. This may be accounted for by the fact that the effect of a step input passes through more circuit elements. The more complex representations have eigenvalues close to the origin which are almost impossible to change by the usual compensation techniques.

The effect of saliency is negligible in the transient response to a step change in load torque or voltage reference, but saliency does make a noticeable difference in steady state values of certain variables.

Machine saturation lowers the overshoot of the terminal voltage for step changes in the load torque and voltage reference.

B. Suggestions for Future Work

The analyses presented in this study show, among other things, the importance of using different machine models in system studies in the area of power system stability and control. This approach can be pursued further and several other models can be developed such that, depending on the nature of a particular study and the degree of accuracy desired, a particular model can be used.

The limitations or the extent of validity of the several assumptions usually made in developing machine models can be further investigated.

This study also shows the importance of representing amplifier limiting and saturation on both the exciter and the machine. More accurate representation of saturation can be developed and the effect on the system can then be studied. For example, one can consider separately each of the saturations existing in the alternator (see section D of Chapter II). Also, since limiting and saturation are by no means the only nonlinearities in the system, several types of system nonlinearities can be considered (see section B of Chapter II).

The results of the study presented in this thesis indicate that stability limits obtained without including the effect of nonlinearity may be on the pessimistic side. Therefore, studies can be made to evaluate the degree of discrepancy existing between stability studies neglecting nonlinearities and those which include them. As mentioned in Chapter II, most of the present day stability studies neglect many of the

nonlinearities. The effects of including the regulating system and machine saturation on Lyapunov's methods, Popov's method and Zubov's method, all of which have been applied to power system studies, may be interesting areas to pursue.

The study presented in this thesis considered a regulated machine connected to an infinite bus through a transmission line. Similar studies can be made for multimachine systems. This may, however, necessitate the use of the digital computer rather than the analog computer depending on the complexity of the machine model being used.

VIII. BIBLIOGRAPHY

1. Akutsu, K. Transient stability of electrical system considering load characteristics. Elect. Eng. in Japan (English Translation of Denki Gakkai Zasshi), vol. 86, No. 11, pp. 1-13. November 1966.

2. Aldred, A. S. Electronic analog computer simulation of multimachine power system networks. IEE Proceedings 109A: 195-202. 1962.

3. Aldred, A. S. and Doyle, P. A. Electronic-analysis computer study of synchronous machine transient stability. IEE Proceedings 104A: 152-160. 1957.

4. Anderson, P. M. Analysis of faulted power systems. Unpublished notes. Electrical Engineering Dept., Iowa State University, Ames, Iowa. 1969.

5. Anderson, P. M. and Fouad, A. A. Power system control and stability. Unpublished notes. Electrical Engineering Dept., Iowa State University, Ames, Iowa. 1968.

6. Anderson, P. M. and Musil, J. D. Digital stability analysis of a power generating unit. Proceedings PICA Conference, pp. 502-511. 1969.

7. Baldwin, C. J. and Byerley, R. T. Recent advances in the digital simulation of power system disturbances. Proceedings Third Power Systems Computation Conference, paper D & C4, Rome, July 1969.

8. Bauman, H. A., Manz, O. W., Jr., McCormack, J. E. and Seeley, H. B. System load swings. AIEE Transactions 60: 541-547 and 735-737. 1941.

9. Bobo, P. O., Skooglung, J. W. and Wagner, C. L. Performance of excitation systems under abnormal conditions. IEEE Transactions (PAS) 87: 547-553. 1968.

10. Boffi, L. V. and Haas, V. B., Jr. Analog computer representation of alternators for parallel operations. AIEE Transactions (C&E) 76: 153-158. 1957.

11. Brereton, D. S., Lewis, D. G. and Young, C. C. Representation of induction-motor loads during power-system stability studies. AIEE Transactions (PAS) 76: 451-460. 1957.

12. Brown, P. G., deMello, F. P., Lenfest, E. H. and Mills, R. J. Effects of excitation, turbine energy control, and transmission on transient stability. IEEE Transactions (PAS) 89: 1247-1252. 1970.

13. Buckley, D. F. Analog computer representation of a synchronous machine. Unpublished M.S. thesis. Library, Iowa State University, Ames, Iowa. 1968.

14. Byerly, R. T., Keay, F. W. and Skooglund, J. W. Damping of power oscillations in salient-pole machines with static exciters. IEEE Transactions (PAS) 89: 1009-1021. 1970.

15. Chari, M. V. K. and Silvester, P. Analysis of turboalternator magnetic fields by finite elements. IEEE Transactions (PAS) 90: 454-464. 1971.

16. Cohn, N. Control of generation and power flow on interconnection systems. John Wiley and Sons, Inc., New York. 1967.

17. Concordia, C. Effect of prime-mover speed control characteristics on electric power system performance. IEEE Transactions (PAS) 88: 752-756. 1969.

18. Concordia, C. Equipment modeling-loads. General Electric Company Electric Utility Engineering Seminar on Power System Stability. General Electric Company, Schenectady, New York. 1969.

19. Concordia, C. Steady-state stability of synchronous machines as affected by voltage regulator characteristics. AIEE Transactions 63: 215-220. 1944.

20. Concordia, C. Synchronous machine damping and synchronizing torques. AIEE Transactions 70: 731-737. 1951.

21. Dandeno, P. L., Karas, A. N., McClymont, K. R. and Watson, W. Effect of high-speed rectifier excitation systems on generator stability limits. IEEE Transactions (PAS) 87: 190-201. 1968.

22. Dave, M. P. and Mukhopadhyay, P. Response of single machine connected to bus-bar for variation in load and bus-bar voltage both in magnitude and phase - II - stochastic variation. IEEE Conference paper No. 71CP214-PWR, Winter 1971.

23. deMello, F. P. The effects of control. Power System Dynamics, IEEE Tutorial Course Text 70M62-PWR, pp. 25-40. 1970.

24. deMello, F. P. and Concordia, C. Concepts of synchronous machine stability as affected by excitation control. IEEE Transactions (PAS) 88: 316-330. 1969.

25. deMello, F. P. and Walsh, G. W. Reclosing transients on induction motors with terminal capacitors. AIEE Transactions (PAS) 79: 1206-1213. 1960.

26. deMello, F. P., Dolbec, A. C., Swann, D. A. and Temoshok, M. Analog computer studies of system overvoltages following load rejections. IEEE Transactions (PAS) 82(65): 42-49. April 1963.

27. DeRusso, P. M., Roy, R. J. and Clase, C. M. State variables for engineers. John Wiley and Sons, Inc., New York. 1967.

28. Dinely, J. L., Morris, A. J. and Preece, C. Optimized transient stability from excitation control of synchronous generators. IEEE Transactions (PAS) 87: 1696-1705. 1968.

29. Dorf, R. C. Modern control systems. Addison-Wesley Publishing Company, Reading, Massachusetts. 1967.

30. Dunfield, J. C. and Barton, T. H. Effect of MMF and permeance harmonics in electrical machines. IEE Proceedings (GB) 14: 1443-1450. 1967.

31. El-Abiad, A. H. and Nagappan, K. Transient stability region of multimachine power system. IEEE Transactions (PAS) 85: 169-179. 1966.

32. Electronic Associates, Inc. 8800 System reference handbook. Publication No. 00800.1155-2. Electronic Associates, Inc., West Long Branch, New Jersey. 1967.

33. Elgerd, O. I. Electric energy systems theory: an introduction. McGraw-Hill Book Company, New York. 1971.

34. Ellis, H. M., Hardy, J. E., Blythe, A. L. and Skooglund, J. W. Dynamic stability of the Peace River transmission system. IEEE Transactions (PAS) 85: 586-601. 1966.

35. El-Sherbiny, M, K. and Fouad, A. A. Digital analysis of excitation control for interconnected power systems. IEEE Transactions (PAS) 90: 441-447. 1971.

36. Ewart, D. N. and deMello, F. P. A digital computer program for the automatic determination of dynamic stability limits. IEEE Transactions (PAS) 86: 867-875. 1967.

37. Gelb, A. and Van der Velde, W. E. Multiple-input describing functions and nonlinear system design. McGraw-Hill Book Company, New York. 1968.

38. Gless, G. E. Direct method of Liapunov applied to transient power system stability. IEEE Transactions (PAS) 85: 159-168. 1966.

39. Goldstein, M. and Frank, H. Stability criteria for nonlinear RLC networks. J. Franklin Inst., vol. 288, No. 5, p. 351. 1969.

40. Grainger, J. J. and Ahmari, R. The effect of nondynamic parameters of excitation system on stability performance. IEEE Conference paper No. 71CP185-PWR. Winter 1971.

41. Gran, R. and Rimer, M. Stability analysis of systems with multiple nonlinearities. IEEE Transactions (AC) 10: 94-97. 1965.

42. Gurevich, Y. E. How load parameters influence dynamic stability of power system generators. Electric Tech. USSR, vol. 1969, No. 1. 1969.

43. Hahn, W. Stability of motion. Springer-Verlag Inc., New York. 1967.

44. Hanson, O. W., Goodwin, C. J. and Dandeno, P. L. Influence of excitation and speed control parameters in stabilizing intersystem oscillations. IEEE Transactions (PAS) 87: 1306-1314. 1968.

45. Hauf, A. W. Analysis of the nonlinear nature of synchronous machine parameters and sources of power system oscillations. IEEE Conference paper No. 71CP620-PWR. Summer 1971.

46. Hayashi, C. Nonlinear oscillations in physical systems. McGraw-Hill Book Company, New York. 1964.

47. Humpage, W. D. and Scott, B. Predictor-corrector methods of numerical integration in digital-computer analysis of power system stability. IEEE Proceedings 112: 1557-1565. 1965.

48. Hsu, J. C. and Meyer, A. U. Modern control principles and applications. McGraw-Hill Book Company, New York. 1968.

49. Huelsman, L. P. Circuits, matrices, and linear vector spaces. McGraw-Hill Book Company, New York. 1963.

50. Hwang, H. H. and Tripathi, P. C. Stability analysis and synthesis of generator excitation control. IEEE Conference paper No. 71CP621-PWR. Summer 1971.

51. IEEE Committee Report. Bibliography of rotating electric machinery for 1966-1968. IEEE Transactions (PAS) 89: 1293-1307. 1970.

52. IEEE Committee Report. Computer representation of excitation systems. IEEE Transactions (PAS) 87: 1460-1464. 1968.

53. IEEE Committee Report. Proposed excitation system definitions for synchronous machines. IEEE Transactions (PAS) 88: 1248-1258. 1969.

54. IEEE Committee Report. Recommended phasor diagram for synchronous machine. IEEE Transactions (PAS) 88: 1593-1610. 1969.

55. IEEE Committee Report. Rotating electric machinery -- bibliography for 1962-1965. IEEE Transactions paper No. 31 TP 67-477. 1967.

56. Javanovski, S. B. and Hamman, M. S. A. A. Contribution to the theory of a synchronous performance of synchronous machines with salient poles: Part II. Analysis of MMF and magnetic field angular velocity-power and torque equations. IEEE Transactions (PAS) 90: 418-426. 1971.

57. Kapoor, S. C., Kalsi, S. S. and Adkins, B. Improvement of alternator stability by controlled quadrature excitation. IEE Proceedings (GB) 116: 771-780. 1969.

58. Kasturi, P. and Doraraju, P. Sensitivity analysis of power systems. IEEE Transactions (PAS) 88: 1521-1528. 1969.

59. Keay, F. W. and South, W. H. Design of a power system stabilizer sensing frequency deviation. IEEE Transactions (PAS) 90: 707-713. 1971.

60. Kent, M. H., Schmus, W. R., McCrackin, F. A. and Wheeler, L. M. Dynamical modelling of loads in stability studies. IEEE Transactions (PAS) 88: 756-763. 1969.

61. Kimbark, E. W. Introduction to problems of power system stability. Power System Dynamics, IEEE Tutorial Course Text 70M62-PWR, pp. 5-10. 1970.

62. Kimbark, E. W. Power system stability. Vols. 1 and 3. John Wiley and Sons, Inc., New York. 1948.

63. Kirchmayer, L. K. Economic control of interconnected systems. John Wiley and Sons, Inc., New York. 1959.

64. Krause, P. C. Simulation of a single machine-infinite bus system. Mimeographed. Electrical Engineering Dept., Purdue University, West Lafayette, Indiana. From report submitted to the Bureau of Reclamation. ca. 1965.

65. Krause, P. C. and Towle, J. N. Synchronous machine damping by excitation control with direct and quadrature axis field windings. IEEE Transactions (PAS) 88: 1266-1274. 1969.

66. Ku, Y. H. Transient analysis of rotating machines and stationary networks by means of rotating reference frames. AIEE Transactions 70: 943-954. 1951.

67. Kundu, P. Analysis of torque-speed curves of wound secondary couplings in the nonlinear region of the magnetization curve. IEEE Transactions (PAS) 90: 541-547. 1971.

68. Kundu, P. Analysis of saturation and end-effects in variable speed solid secondary couplings. IEEE Transactions (PAS) 90: 548-555. 1971.

69. LaSalle, J. P. and Lefschetz, S. Stability by Liapunov's direct method with applications. Academic Press, New York. 1961.

70. Laughton, M. A. Matrix analysis of dynamic stability in synchronous multimachine systems. IEE Proceedings (GB) 113: 325-336. 1966.

71. Lefschetz, S. Stability of nonlinear control systems. Academic Press, New York. 1965.

72. Lemay, J. and Barton, T. H. Small perturbation linearization of the saturated synchronous machine equations. IEEE Conference paper No. 71TP515-PWR. Summer 1971.

73. Lewis, W. A. A basic analysis of synchronous machines - Part I. AIEE Transactions (PAS) 77: 436-456. 1958.

74. Lewis, W. A. The principles of synchronous machines. Third lithoprinted edition. Illinois Institute of Technology, Chicago Center, Chicago, Illinois. 1959.

75. Lipo, T. A. and Krause, P. C. Stability analysis for variable frequency operation of synchronous machines. IEEE Transactions (PAS) 87: 227-234. 1968.

76. Lugtu, R. Transient stability analysis of power systems using Liapunov's second method. Unpublished Ph.D. thesis. Library, Iowa State University, Ames, Iowa. 1971.

77. Mane, A. P., Webster, R. H. and Smith, O. J. M. Rotor velocity measurement from power balance analog. IEEE Transactions (PAS) 90: 434-440. 1971.

78. McCrackin, F. G. and Schmus, W. R. The representation of system load in stability studies. Power System Dynamics, IEEE Tutorial Course Text 70M62-PWR, pp. 41-46. 1970.

79. Miles, J. G. Analysis of overall stability of multimachine power systems. IEE Proceedings (GB) 109A: 203-211. 1962.

80. Minorsky, N. Theory of nonlinear control systems. McGraw-Hill Book Company, New York. 1969.

81. Mittelstadt, W. A. Four methods of power system damping. IEEE Transactions (PAS) 87: 1323-1329. 1968.

82. Musil, J. D. Digital stability analysis of power generating units. Unpublished Ph.D. thesis. Library, Iowa State University, Ames, Iowa. 1968.

83. Nagy, I. Analysis of minimum excitation limits of synchronous machines. IEEE Transactions (PAS) 89: 1001-1008. 1970.

84. Nagy, I. Block diagram and torque-angle loop analysis of synchronous machines. IEEE Transactions (PAS) 90: 1528-1536. 1971.

85. Nanda, J. Analysis of steady state stability of a two machine system by the D-decomposition technique. IEEE Transactions (PAS) 90: 1848-1855. 1971.

86. Nanda, J. Some aspects on steady state stability and transient response of a two machine system. IEEE Conference paper No. 71CP14-PWR. Winter 1971.

87. Nandi, Shantanu. Modified simulation of synchronous machine. Unpublished M.S. thesis. Library, Iowa State University, Ames, Iowa. 1971.

88. Neimark, Y. I. On the admissability of linearization in stability investigations (Translated title). Dokl. Akad. Nauk S.S.S.R. 127: 961-964. 1959. Translated by U.S. Department of Commerce, Office of Technical Services, Washington, D.C.

89. Nichelson, H. Integrated control of a nonlinear turboalternator model under fault conditions. IEE Proceedings (GB) 114: 834-844. 1967.

90. Olive, D. W. Digital simulation of synchronous machine transients. IEEE Transactions (PAS) 87: 1669-1675. 1968.

91. Olive, D. W. New techniques for the calculation of dynamic stability. IEEE Transactions (PAS) 85: 767-782. 1966.

92. Oyetunji, A. A. Bibliography on power system stability. Unpublished mimeographed annual report to Affiliate Research Program Sponsors in Power (Annual Report ISU-ERI-AMES-50900). Engineering Research Institute, Iowa State University, Ames, Iowa. 1970.

93. Oyetunji, A. A. Effects of system nonlinearities on system control. Unpublished mimeographed annual report to Affiliate Research Program Sponsors in Power (Annual Report ISU-ERI-AMES 99931). Engineering Research Institute, Iowa State University, Ames, Iowa. 1971.

94. Padiyar, K. R. and Ramshaw, R. S. Dynamic analysis of multimachine power systems. IEEE Conference paper No. 71TP582-PWR. Summer 1971.

95. Pai, M. A., Mohan, M. A. and Gopala, R. J. Power system transient stability regions using Popov's method. IEEE Transactions (PAS) 89: 788-794. 1970.

96. Park, R. H. Two reaction theory of synchronous machines-generalized method of analysis, Part 1. AIEE Transactions 48: 716-730. 1929.

97. Park, R. H. Two reaction theory of synchronous machines, Part 2. AIEE Transactions 52: 352-355. 1933.

98. Perry, H. R., Luini, J. F. and Coulter, J. C. Improved stability with low time constant rotating exciter. IEEE Conference paper No. 71TP16-PWR. Winter 1971.

99. Peterson, H. A. and Krause, P. C. Damping of power swings in a parallel AC and DC system. IEEE Transactions (PAS) 85: 1231. 1966.

100. Peterson, H. A., Krause, P. C., Luini, J. F. and Thomas, C. H. An analog computer study of a parallel AC and DC power system. IEEE Transactions (PAS) 85: 191-209. 1966.

101. Pinnello, J. A. and Van Ness, J. E. Dynamic response of a large power system to a cyclic load produced by a muclear accelerator. IEEE Transactions (PAS) 90: 1856-1862. 1971.

102. Porter, B. Synthesis of dynamical systems. Barnes and Noble, Inc., New York. 1969.

103. Potier, A. Sur la réaction dinduit des alternateurs. Éclairage Élect. (Paris) 24: 133. 1900.

104. Prabhashanker, K. and Janischewsky, W. Digital simulation of multi-machine power systems for stability studies. IEEE Transactions (PAS) 87: 73-80. 1968.

105. Prentice, B. R. Fundamental concepts of synchronous machine reactance. Supplement to 1937 AIEE Transactions 56: 1-21. 1937.

106. Rankin, A. W. Per unit impedances of synchronous machines, Part 1. AIEE Transactions 64: 569-573. 1945.

107. Rankin, A. W. Per unit impedances of synchronous machines, Part 2. AIEE Transactions 64: 839-841. 1945.

108. Ratti, U. Synchronous machine models using feedback control. Consiglio Nationale delle Ricerche, Roma. ca. 1967.

109. Riaz, M. Analogue computer representations of synchronous generators in voltage regulation studies. AIEE Transactions (PAS) 75: 1178-1184. 1956.

110. Robb, D. D. and Krause, P. C. The self excitation of induction machines with application to motor starting. IEEE Transactions (PAS) 90: 579-586. 1971.

111. Schleif, F. R. and Bates, C. G. Governing characteristics for 820,000 horsepower units for Grand Coulee third power plant. IEEE Transactions (PAS) 90: 882-890. 1971.

112. Schleif, F. R., Hunkins, H. D., Hattan, E. E. and Gish, W. B. Control of rotating exciters for power system damping: pilot applications and experience. IEEE Transactions (PAS) 88: 1259-1266. 1969.

113. Schleif, F. R., Hunkins, H. D., Martin, G. E. and Hattan, E. E. Excitation control to improve power line stability. IEEE Transactions (PAS) 87: 1426-1434. 1968.

114. Schleif, F. R., Martin, G. E. and Angell, R. R. Damping of system oscillations with a hydro generating unit. IEEE Transactions (PAS) 86: 438-442. 1967.

115. Schleif, F. R. and White, J. H. Damping for the Northwest-Southwest tieline oscillations -- an analog study. IEEE Transactions (PAS) 85: 1239-1247. 1966.

116. Schroder, D. C. Compensation of synchronous machines for stability. Unpublished Ph.D. thesis. Library, Iowa State University, Ames, Iowa. 1971.

117. Schroder, D. C. Generation of supplementary excitation signals by analog computer for increased power system stability. Unpublished mimeographed Annual Report to Affiliate Research Program Sponsors in Power. Engineering Research Institute, Iowa State University, Ames, Iowa. 1971.

118. Shackshaft, G. Discussion of "Electronic analog computer simulation of multimachine power system networks," by Aldred, A. S. and "Analysis of overall stability of multimachine power systems," by Miles, J. G. IEE Proceedings (GB) 109A: 211. 1962.

119. Shackshaft, G. General-purpose turbo-alternator model. IEE Proceedings (GB) 110: 703-713. 1963.

120. Siddigee, M. W. Direct method of Lyapunov and transient stability analysis. University of Minnesota, thesis. 136 pp. August 1967. (Available from University Microfilms, Ann Arbor, Michigan, USA, order No. 68-1594.)

121. Slemon, G. R. Analytical models for saturated synchronous machines. IEEE Transactions (PAS) 90: 409-417. 1971.

122. Smith, O. J. M. Power system transient control by capacitor switching. IEEE Transactions (PAS) 88: 28-35. 1969.

123. Smith, O. J. M. and Gerez-Greiser, V. Suboptimal control to target of synchronous generators. IEEE Transactions (PAS) 90: 448-453. 1971.

124. Stagg, G. W. Transient stability solution techniques -- examples of transient stability calculation. Power System Dynamics, IEEE Tutorial Course Text 70M62-PWR, pp. 47-52. 1970.

125. Stagg, G. W. and El-Abiad, A. H. Computer methods in power system analysis. McGraw-Hill Book Company, New York. 1968.

126. Swidan, M. A. Study of damping power in interconnected power systems. Unpublished Ph.D. thesis. Library, Iowa State University, Ames, Iowa. 1964.

127. Teichgraeber, R. D., Harris, F. W. and Johnson, G. L. New stability measure for multimachine power systems. IEEE Transactions (PAS) 89: 233-239. 1970.

128. Tinney, W. F. Evaluation of concepts for studying transient stability. Power System Dynamics, IEEE Tutorial Course Text 70M62-PWR, pp. 53-60. 1970.

129. Undrill, J. M. Dynamic stability calculations for an arbitrary number of interconnected machines. IEEE Transactions (PAS) 87: 835-844. 1968.

130. Undrill, J. M. Power system stability studies by the method of Liapunov: Part 1 -- state space approach to synchronous machine modeling. IEEE Transactions (PAS) 86: 791-801. 1967.

131. Undrill, J. M. Power system stability studies by the method of Liapunov: Part 2 -- the interconnection of hydrogenerating sets. IEEE Transactions (PAS) 86: 802-811. 1967.

132. Undrill, J. M. Structure in the computation of power system non-linear dynamic response. IEEE Transactions (PAS) 88: 1-6. 1969.

133. Undrill, J. J. and Woodward, J. L. Nonlinear hydro governing model and improved calculation for determining temporary droop. IEEE Transactions (PAS) 86: 443-453. 1967.

134. Van Ness, J. E. Root loci of load frequency control systems. IEEE Transactions (PAS) 82: 712-726. 1963.

135. Van Ness, J. E. and Goddard, W. F. Formation of the coefficient matrix of a large dynamic system. IEEE Transactions (PAS) 87: 80-83. 1968.

136. Warchol, E. J., Schleif, F. R., Gish, W. B. and Church, J. R. Alinement and modeling of Hanford excitation control for system damping. IEEE Transactions (PAS) 90: 714-724. 1971.

137. Webster, R. H., Mane, A. P. and Smith, O. J. M. Series capacitor switching to quench electromechanical transients in power systems. IEEE Transactions (PAS) 90: 427-433. 1971.

138. Westinghouse Electric Corporation. Electrical transmission and distribution reference book. 4th ed. Westinghouse Electric Corporation, Pittsburgh, Pennsylvania. 1964.

139. Willems, J. L. and Willems, J. C. The application of Liapunov methods to the computation of transient stability regions for multimachine power systems. IEEE Transactions (PAS) 89: 795-801. 1970.

140. Wright, I. A. and Morsztyn, K. Subharmonic oscillations in power systems -- theory and practice. IEEE Transactions (PAS) 89: 1805-1815. 1970.

141. Young, C. C. The art and science of dynamic stability analyses. IEEE Conference paper No. 68CP702-PWR. ASME/IEEE Joint Power Conference. September 1968.

142. Young, C. C. The synchronous machine. Power System Dynamics, IEEE Tutorial Course Text 70M62-PWR, pp. 11-24. 1970.

143. Yu, Y. N. and Vongsuriya, K. Nonlinear power system stability study by Liapunov function and Zubov's method. IEEE Transactions (PAS) 86: 1480-1484. 1967.

144. Yu, Y. N. and Vongsuriya, K. Steady-state stability limits of a regulated synchronous machine connected to an infinite system. IEEE Transactions (PAS) 85: 759-767. 1966.

IX. ACKNOWLEDGMENTS

The author would like to express his gratitude to all the people and institutions who contributed in some way to make this dissertation possible.

My deepest appreciation goes to my major professor and chairman of the committee Dr. P. M. Anderson for his suggestions, encouragement and valuable guidance throughout the entire investigation.

Sincere thanks are also due Dr. D. D. Robb for his helpful discussions on various aspects of machine theory, applications and simulation.

Many thanks to Dr. R. J. Lambert, Dr. A. N. Michel and Dr. R. M. Stewart whose guidance as committee members is greatly appreciated.

The author also wishes to thank Dr. A. A. Fouad for his helpful discussions.

Thanks are also due Dr. D. C. Schroder, whose work precedes this, for his help at the initial stages of the simulation setup; Dr. R. M. Willett for his help with the analog computer simulations; Mr. Jerry Kern of the Engineering Editorial Office for preparing the figures and the Affiliate Research Program in Electric Power, Engineering Research Institute, for their financial support.

Finally the author would like to thank his parents for their patience and understanding during the many years of studies leading to this dissertation.

X. APPENDIX A. THE EXCITATION SYSTEMS

A. Derivation of Model I

The rotor or field winding voltage of a synchronous machine without damper windings can be written as (5, 33):

$$v_f = r_f i_f + L_f \frac{di_f}{dt} - \sqrt{\frac{3}{2}} M_f \frac{di_d}{dt} \qquad [A-1]$$

where

subscript f denotes field winding,

subscript d denotes direct axis,

and letters v, i, r, L, and M, respectively, have their usual meaning of voltage, current, resistance, self-inductance and mutual inductance.

The stator currents can be neglected if we assume that the machine is lightly loaded or that the generator is operating open-circuited. Then the magnitude of the direct-axis current component i_d will be negligible and the last term of Equation A-1 can be neglected:

$$v_f = r_f i_f + L_f \frac{di_f}{dt} \qquad [A-2]$$

Also under the no load condition, the stator voltage in phase "a" of the machine can be written as (33):

$$e_a = -\omega M_f i_{fo} \text{ Sin } \omega t = \sqrt{2}\, \mathfrak{J}_m[E_a e^{j\omega t}] \qquad [A-3]$$

where

$$E_a \triangleq \frac{-\omega M_f i_{fo}}{\sqrt{2}} \qquad [A-4]$$

ω = rotor speed

and subscript o refers to the no load operation.

Both the terminal voltage and the generator emf are equal under no load condition and hence:

$$|V| = |E| = \frac{\omega M_f i_{fo}}{\sqrt{2}} \qquad [A-5]$$

Take Laplace transform of Equations A-2 and A-5 and solve for the transfer function:

$$|V|(S) = \frac{\omega M_f i_f(S)}{\sqrt{2}} \qquad [A-6]$$

$$v_f(S) = (r_f + SL_f) i_f(S) \qquad [A-7]$$

$$\frac{|V|(S)}{v_f(S)} = \frac{\omega M_f}{\sqrt{2}[r_f + SL_f]} = \frac{\omega M_f}{\sqrt{2}} \frac{1}{1 + S(\frac{L_f}{r_f})} \triangleq \frac{K_G}{1 + ST_G} \qquad [A-8]$$

where

$$K_G \triangleq \frac{\omega M_f}{\sqrt{2}}$$

$$T_G = T'_{do} \triangleq \frac{L_f}{r_f} \qquad [A-9]$$

Equation A-8 is the desired transfer function for machine model I.

B. Excitation System Transfer Functions

The main components of the excitation system are potential transformer and rectifier, voltage comparator, amplifier, exciter and compensator which in this case is a rate feedback compensator. The following is a brief presentation of the mathematical representation of the various components (5, 33, 116).

1. Potential transformer and rectifier

This component of the excitation system can be represented by a first order system whose transfer function is:

$$\frac{v_{dc}}{v_t} = \frac{K_R}{1 + ST_R} \qquad [A-10]$$

where

K_R is the regulator input filter gain,

T_R is the regulator input filter time constant,

v_t is the generator terminal voltage,

v_{dc} is the rectified output voltage of the component.

2. Voltage comparator

The voltage comparator compares the terminal voltage with a reference voltage. If the excitation system had a feedback compensator or any other auxiliary signal the compensating voltage v_{st} is also fed into the comparator. The error voltage v_e can therefore be expressed as:

$$v_e = v_{ref} - v_{dc} - v_{st} \qquad [A-11]$$

3. Amplifier

This device which may be a rotating, magnetic or electronic amplifier can be characterized by a gain factor K_A, a time constant T_A and a transfer function of the form:

$$\frac{v_R}{v_e} = \frac{K_A}{1 + ST_A} \qquad [A-12]$$

If amplifier saturation is taken into consideration, it can be represented by limiting:

$$v_{Rmin} < v_R < v_{Rmax} \qquad [A-13]$$

4. Exciter

This is basically an amplifier and has a transfer function similar to that in Equation A-10 or A-12. However, if exciter saturation is taken into consideration, the saturation factor S_E enters into the transfer function and the exciter equation becomes:

$$v_f = \frac{v_R - S_E v_f}{K_E + ST_E} \qquad [A-14]$$

5. Rate feedback compensator

This device can be a stabilizing transformer (33). A stabilizing current i_{st} flows in the primary winding to give the relation:

$$v_R = Ri_{st} + L\frac{di_{st}}{dt}$$

The transformer output can be expressed as:

$$v_{st} = M \frac{di_{st}}{dt}$$

Hence the transfer function is:

$$\frac{v_{st}}{v_R} = \frac{SM}{R + SL} = \frac{M}{R} \frac{S}{1 + S\frac{L}{R}} \triangleq \frac{SK_F}{1 + ST_F} \qquad [A-15]$$

Combining Equations A-10 to A-15 leads to Figure 16 presented in Chapter IV.

C. Excitation System Parameters and Saturation Function

The parameters used in simulating the excitation systems are shown in Table 15. The slow excitation system contains an amplidyne voltage regulator having a response ratio of 0.5 and the fast excitation system is a rotating rectifier exciter with static voltage regulator having a response ratio of 2.23. The two excitation systems are from references 5 and 98, respectively. Some of the parameters, saturation and regulator limiting, shown in Table 15 were not given by the references. The values of S_E used for the two excitation systems are:

$$S_{Emax} = 0.95 \qquad [A-16]$$

$$S_{E\ 0.75max} = 0.22 \qquad [A-17]$$

Using a method suggested in IEEE Committee Report (52), the corresponding regulator limiting is computed.

$$v_{Rmax} = (K_E + S_{Emax})\ E_{FDmax} \qquad [A-18]$$

v_{Rmax} = 3.18 per unit for the slow excitation system

= 8.68 per unit for the fast excitation system.

Table 15. Excitation system parameters

Symbol	Slow exciter	Fast exciter
K_A	Variable	Variable
T_A	0.1	0.02
T_E	0.5	0.015
K_E	-0.05	1.0
K_F	Variable	Variable
T_F	Variable	Variable
v_{Rmax}	3.18 per unit	8.68 per unit
v_{Rmin}	-3.18 per unit	-8.68 per unit
T_R	0.05	0.005
K_R	1.0	1.0
S_{Emax}	0.95	0.95
$S_{E\ 0.75max}$	0.22	0.22
E_{FDmax}	3.50 per unit	4.45 per unit
K_G	1.0[a]	1.0[a]
T_G	1.0[a]	1.0[a]
T'_{do}	5.9	5.9

[a]Values used for convenience.

1. Saturation curve for the slow exciter

The S_E given in Equations A-16 and A-17 and the no load saturation curve given for the machine (see Appendix C) are used to sketch an exciter saturation similar to that in Figure 78. For values of E_{FD} greater than that at point C on the no load curve, the corresponding field current has two components: a linear portion determined by the distance from the E_{FD} axis to the air gap line, and a nonlinear portion determined by the distance from the air gap line to the no load saturation curve. This nonlinear portion can be expressed as (82):

$$S_E = A_E e^{B_E(v_f - 0.8)} \qquad [A-19]$$

An alternative method of calculating S_E suggested by the IEEE Committee Report (52) is shown in Figure 78. The S_E obtained with Equation A-19 compares very well with that obtained with the alternative method (116).

Substituting the values chosen for S_{Emax} and $S_{E\ 0.75max}$ and E_{FDmax} of 3.50 per unit into Equation A-19 and solving the resulting simultaneous equations give 0.0102 and 1.68 for A_E and B_E, respectively. Hence the applicable equation for S_E is:

$$S_E = 0.0102e^{1.68(v_f - 0.8)}$$

$$= 0.00267e^{1.68v_f} \qquad [A-20]$$

The calculation of S_E using Equation A-20 and the required $S_E v_f$ are shown in Table 16. The curve of $S_E v_f$ versus v_f used in setting the Diode Function Generator on the analog computer is given in Figure 79.

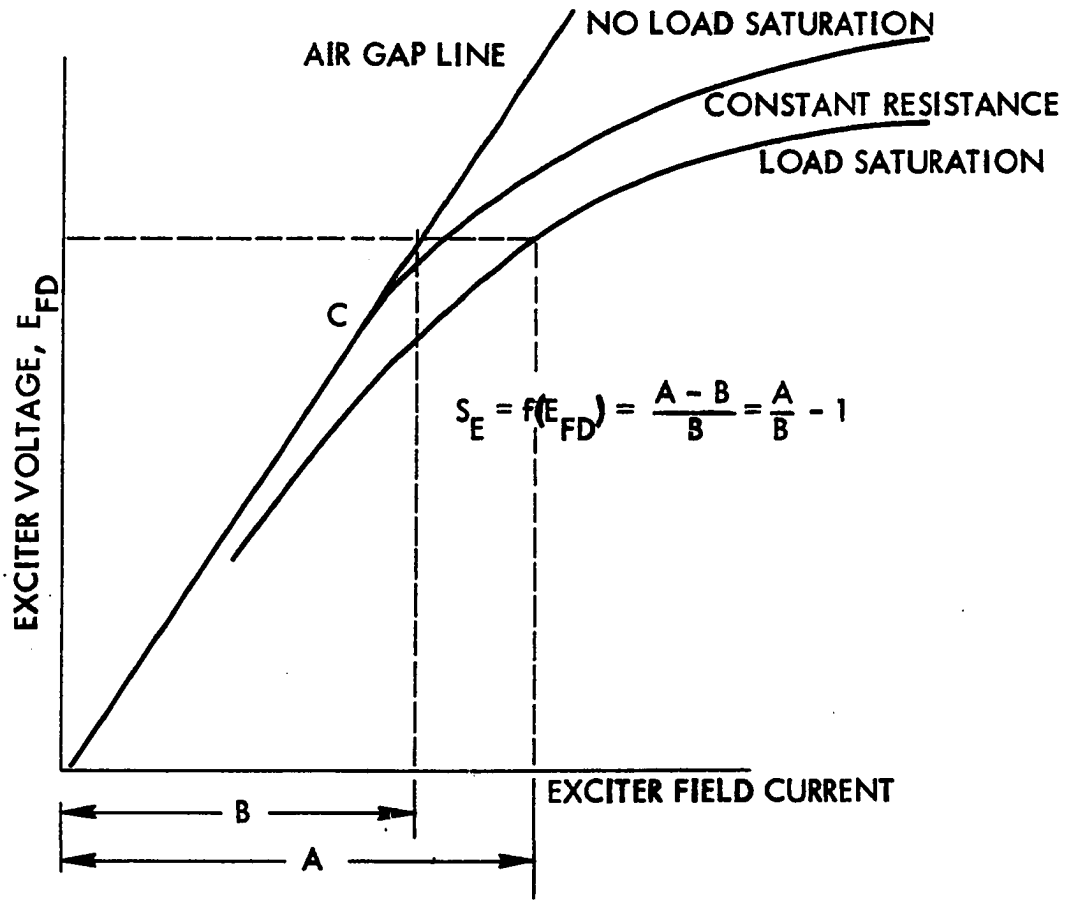

Figure 78. Calculation of exciter saturation

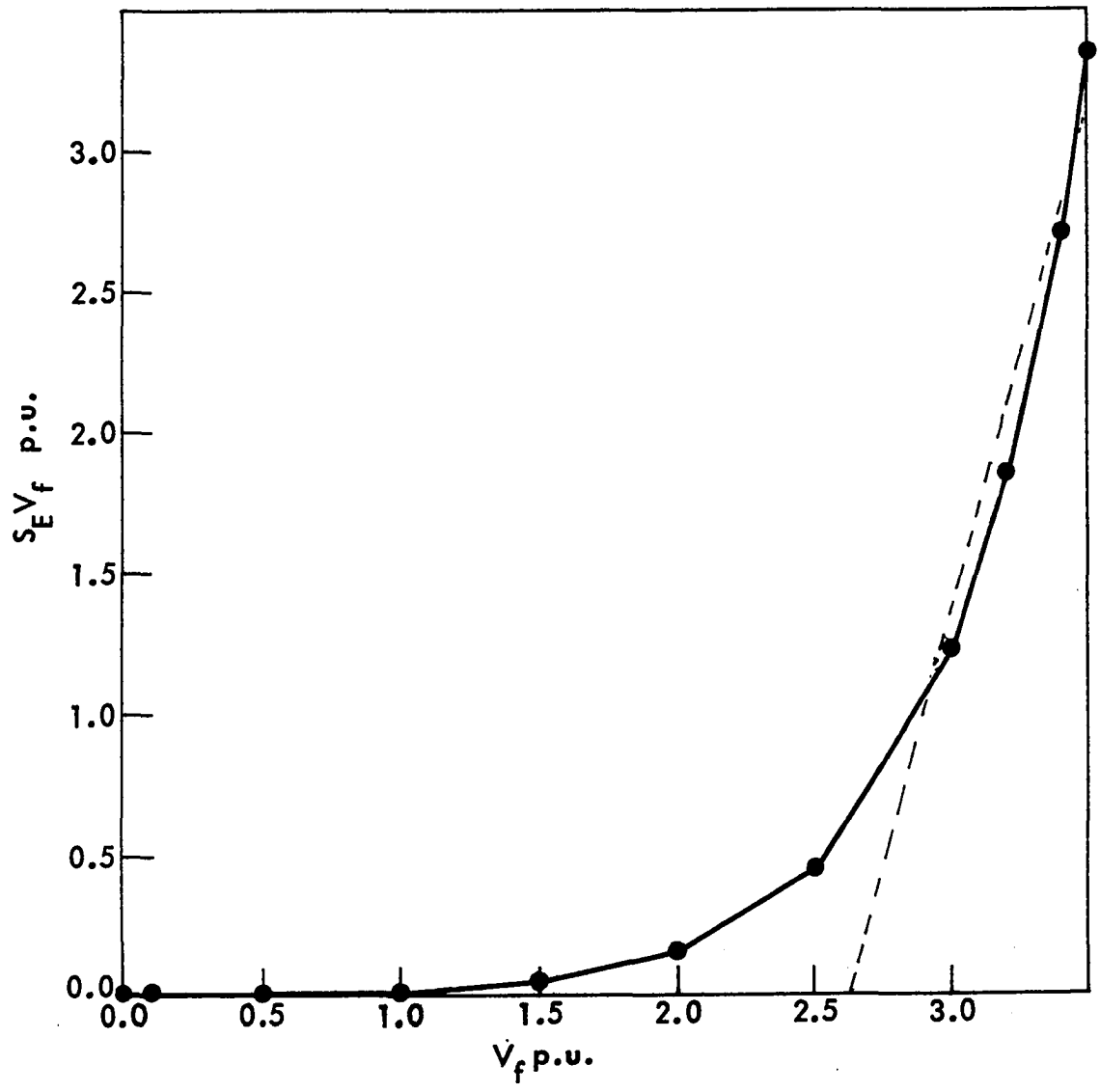

Figure 79. Curve used to set DFG for the slow exciter

Table 16. Calculation of $S_E v_f$ for the low response exciter

v_f per unit	$1.68v_f$	$e^{1.68v_f}$	S_E	$S_E v_f$ per unit
0.0	0.000	1.000	0.00267	0.000000
0.1	0.168	1.183	0.00316	0.000316
0.5	0.840	2.320	0.00620	0.003100
1.0	1.680	5.350	0.01430	0.014300
1.5	2.520	12.400	0.03310	0.049650
2.0	3.360	28.800	0.07700	0.154000
2.5	4.200	67.000	0.17900	0.447500
3.0	5.040	154.000	0.41100	1.233000
3.5	5.880	360.000	0.96000	3.360000

2. Saturation curve for the fast exciter

Substituting the values chosen for S_{Emax} and $S_{E\ 0.75max}$ and E_{FDmax} of 4.45 per unit into Equation A-19 and solving the resulting simultaneous equations give 0.00785 and 1.318 for A_E and B_E, respectively. Hence the applicable equation for S_E is:

$$S_E = 0.00785e^{1.318(v_f - 0.8)}$$

$$= 0.00272e^{1.318v_f} \qquad [A-21]$$

The calculations of S_E using Equation A-21 and the required $S_E v_f$ are shown in Table 17. The curve of $S_E v_f$ versus v_f used in setting the Diode Function Generator on the analog computer is shown in Figure 80.

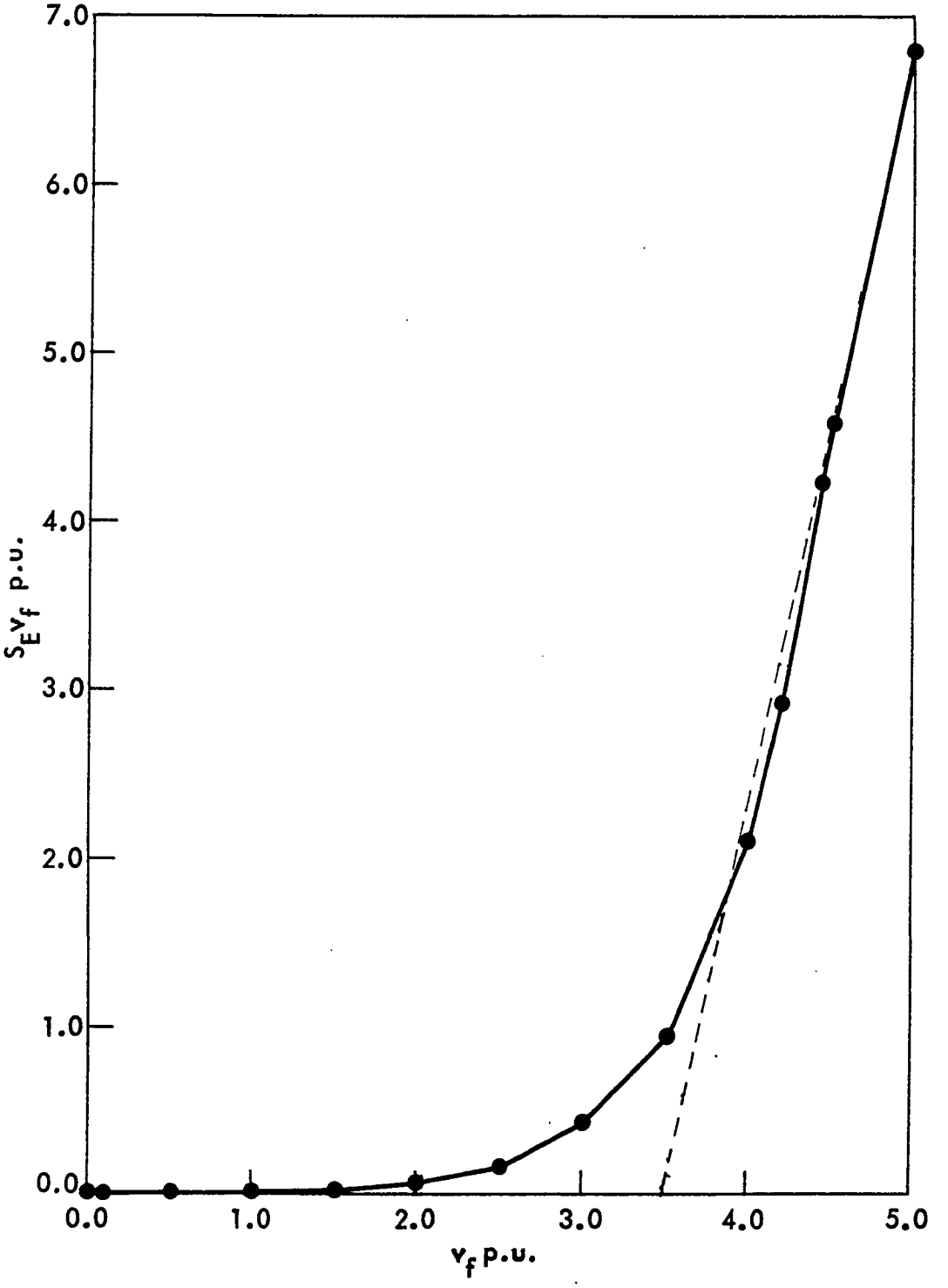

Figure 80. Curve used to set DFG for the fast exciter

Table 17. Calculation of $S_E v_f$ for the high response exciter

v_f per unit	$1.318v_f$	$e^{1.318v_f}$	S_E	$S_E v_f$ per unit
0.0	0.000	1.00	0.00272	0.0000
1.5	1.975	7.15	0.01945	0.0292
2.0	2.640	14.00	0.03810	0.0762
2.5	3.300	27.20	0.07400	0.1850
3.0	3.954	52.00	0.14150	0.4240
3.5	4.610	100.00	0.27200	0.9520
4.0	5.270	194.00	0.52700	2.1100
4.2	5.540	255.00	0.69400	2.9200
4.5	5.930	375.00	1.02000	4.5800
5.0	6.600	730.00	1.36000	6.8000

D. Simulation of the Excitation Systems with Model I

The analog computer setup and the potentiometer settings required for the simulation of the two excitation systems with model I are given in this section.

It is considered appropriate at this point to give a general outline of the simulation setup used on the EAI 8812 analog computer. The three models simulated are all patched on the board at the same time and with a minimum of changes in the patching each of them can be simulated without disrupting the patching of the other models.

The general patching diagram can be summarized with a modified form of Figure 16 shown in Figure 81.

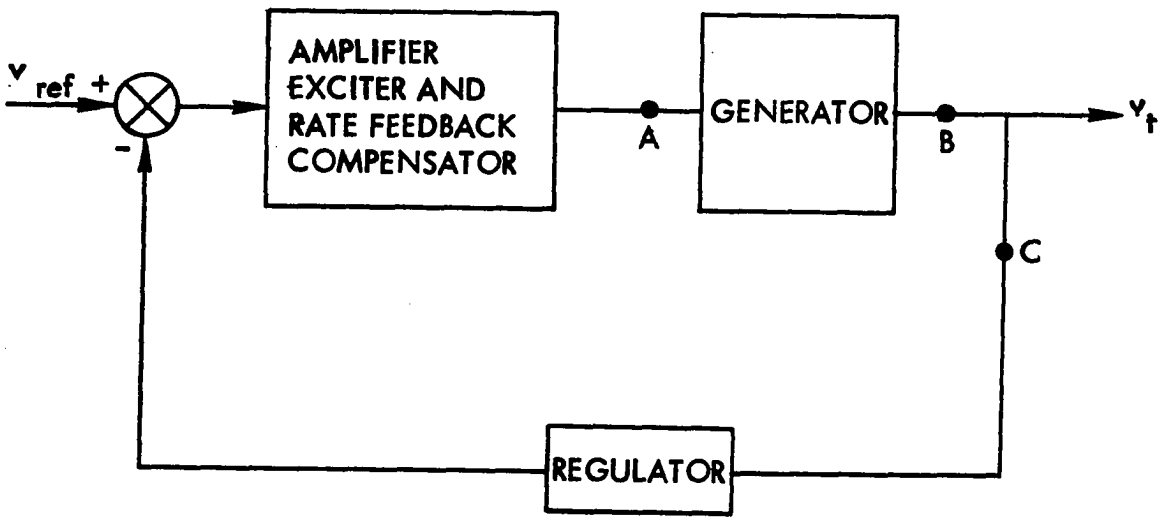

Figure 81. A block diagram of the simulation setup

Point A indicates where the signal $-v_f$ is connected to the machine, in this case the input to a particular machine model. Point B is where the machine or model output is connected to the patching setup to record the voltage response and point C indicates where the regulator is connected to the machine output. Thus by changing these three connections, any model can be readily simulated. In the case of model I, which is presently under consideration, the patching diagram is shown in Figure 82a. Note that inverter 613 is required only for the slow exciter.

The settings required for simulating Figure 82a for the two excitation systems are given in Tables 18a and 18b and 19a and 19b. Table 20 shows the typical settings for the various run numbers indicated in Tables 7 and 8 of Chapter IV. The table shown is that used for simulating model I with no amplifier limiting and no exciter saturation (NLNS).

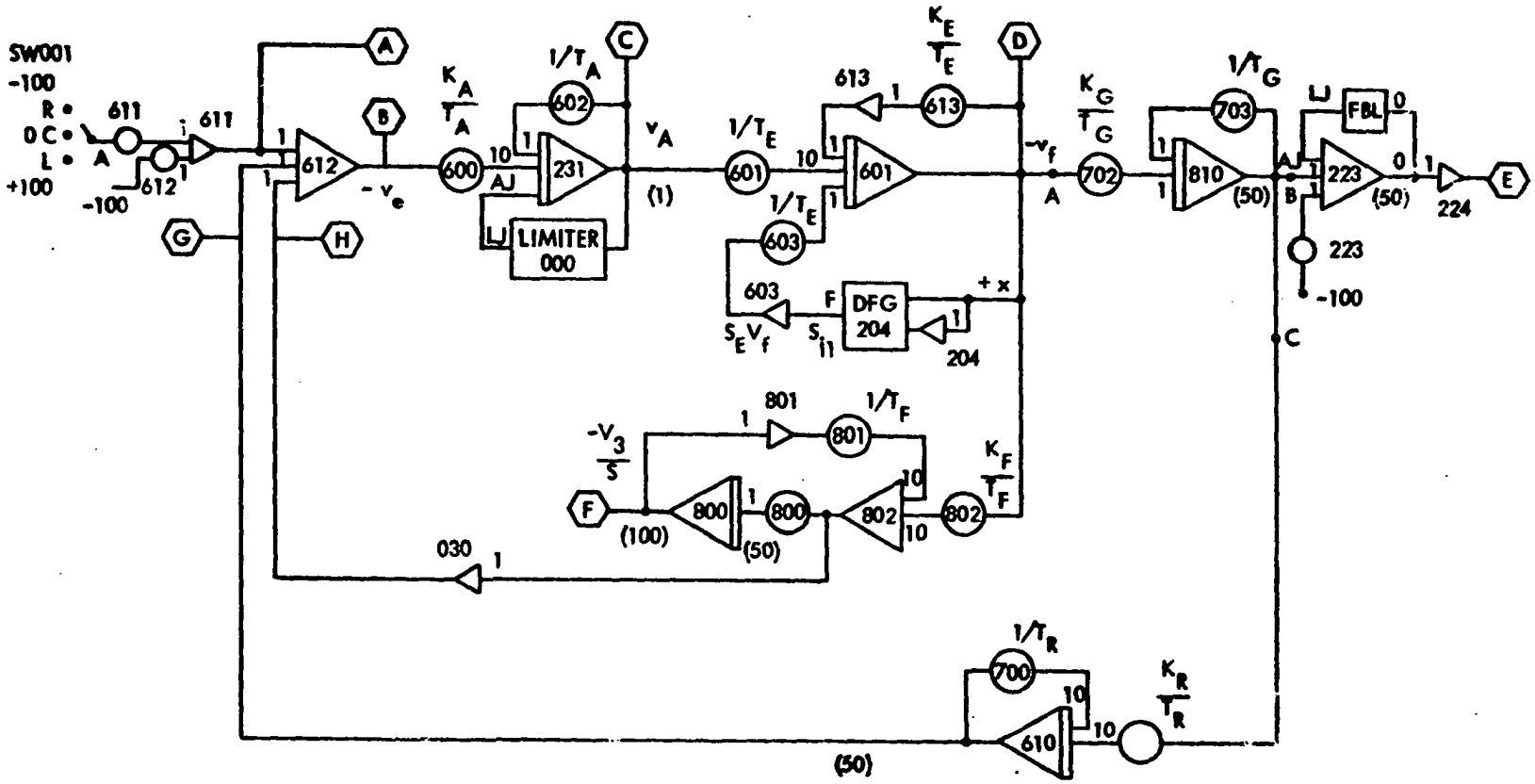

Figure 82a. Simulation diagram showing slow exciter with rate feedback and model I

Table 18a. Pot. settings for the simulation of model I with the slow exciter

Pots.	Pot. setting	Amp. gain	Variable	Value	Scaling	Value x scaling
600	$K_A/5000$	10	K_A/T_A	$10K_A$	1/100 1/50	$K_A/500$
601	.02	10	$1/T_E$	2	10/100	20/100
602	.1	1	$1/T_A$	10	1/100	1/10
603	.02	1	$1/T_E$	2	1/100	2/100
611	.0290	1	Δv_{ref}	5% full load		
612	.5900	1	v_{ref}	Full load		
613	.001	1	$\lvert K_E \rvert / T_E$	.1	1/100	.1/100
700	.02	10	$1/T_R$	20	1/100	1/5
701	.01445	10	$K_R/\sqrt{3}\ T_R$	$20/\sqrt{3}$	50/100x40	$1/4\sqrt{3}$
702	.04	1	K_G/T_G	1	40/1000	4/100
703	.01	1	$1/T_G$	1	1/100	1/100
800	.02	1	K_{31}	1	100/100x50	1/50
801	$1/20T_F$	10	$1/T_F$		50/100	$1/2T_F$
802	$K_F/2T_F$	10	K_F/T_F		50/10	$5K_F/T_F$

Table 18b. Settings for the 10-segment DFG #204

	1	2	3	4	5	6	7	8	9	10
v_f = X	0	10	15	20	25	30	32	34	35	37
$S_E v_f$ = Y	0	0	0.49	1.54	4.475	12.33	18.55	27.2	33.6	50

Table 19a. Pot. settings for the simulation of model I with the fast exciter

Pots.	Pot. setting	Amp. gain	Variable	Value	Scaling	Value x scaling
600	$K_A/1000$	10	K_A/T_A	$50K_A$	1/100x1/50	$K_A/100$
601	.667	10	$1/T_E$	66.7	10/100	6.67
602	.5	1	$1/T_A$	50	1/100	1/2
603	.667	1	$1/T_E$	66.7	1/100	2/3
611	.0290	1	Δv_{ref}	5% full load		
612	.5900	1	v_{ref}	Full load		
613	.667	1	K_E/T_E	66.7	1/100	.667
700	.2	10	$1/T_R$	200	1/100	2.0
701	.1445	10	$K_R/\sqrt{3}\,T_R$	$200/\sqrt{3}$	50/100x40	1.445
702	.04	1	K_G/T_G	1	40/1000	.04
703	.01	1	$1/T_G$	1	1/100	.01
800	.02	1	K_{31}	1	100/100x50	1/50
801	$1/20T_F$	10	$1/T_F$		50/100	$1/2T_F$
802	$K_F/2T_F$	10	K_F/T_F		50/10	$5K_F/T_F$

Table 19b. Settings for the 10-segment DFG #204

	1	2	3	4	5	6	7	8	9	10
v_f = X	0	15	20	25	30	35	40	42	45	50
$S_E v_f$ = Y	0	.292	.762	1.85	4.24	9.52	21.1	29.2	45.8	68

Table 20. A sample table of pot. settings with run numbers 11-30

Run no.	T_F	Pot. 801 $1/20T_F$	K_A	Pot. 600 $K_A/5000$	K_F	Pot. 802 $K_F/2T_F$
11	.2	.2500	400	.0800	.015	.0375
12	"	"	"	"	.020	.0500
13	"	"	"	"	.025	.0625
14	"	"	"	"	.030	.0750
15	"	"	"	"	.035	.0875
16	"	"	600	.1200	.015	.0375
17	"	"	"	"	.020	.0500
18	"	"	"	"	.025	.0625
19	"	"	"	"	.030	.0750
20	"	"	"	"	.035	.0875
21	.1	.5000	400	.0800	.015	.0375
22	"	"	"	"	.020	.0500
23	"	"	"	"	.025	.0625
24	"	"	"	"	.030	.0750
25	"	"	"	"	.035	.0875
26	"	"	600	.1200	.015	.0375
27	"	"	"	"	.020	.0500
28	"	"	"	"	.025	.0625
29	"	"	"	"	.030	.0750
30	"	"	"	"	.035	.0875

E. Definition of Performance Indices

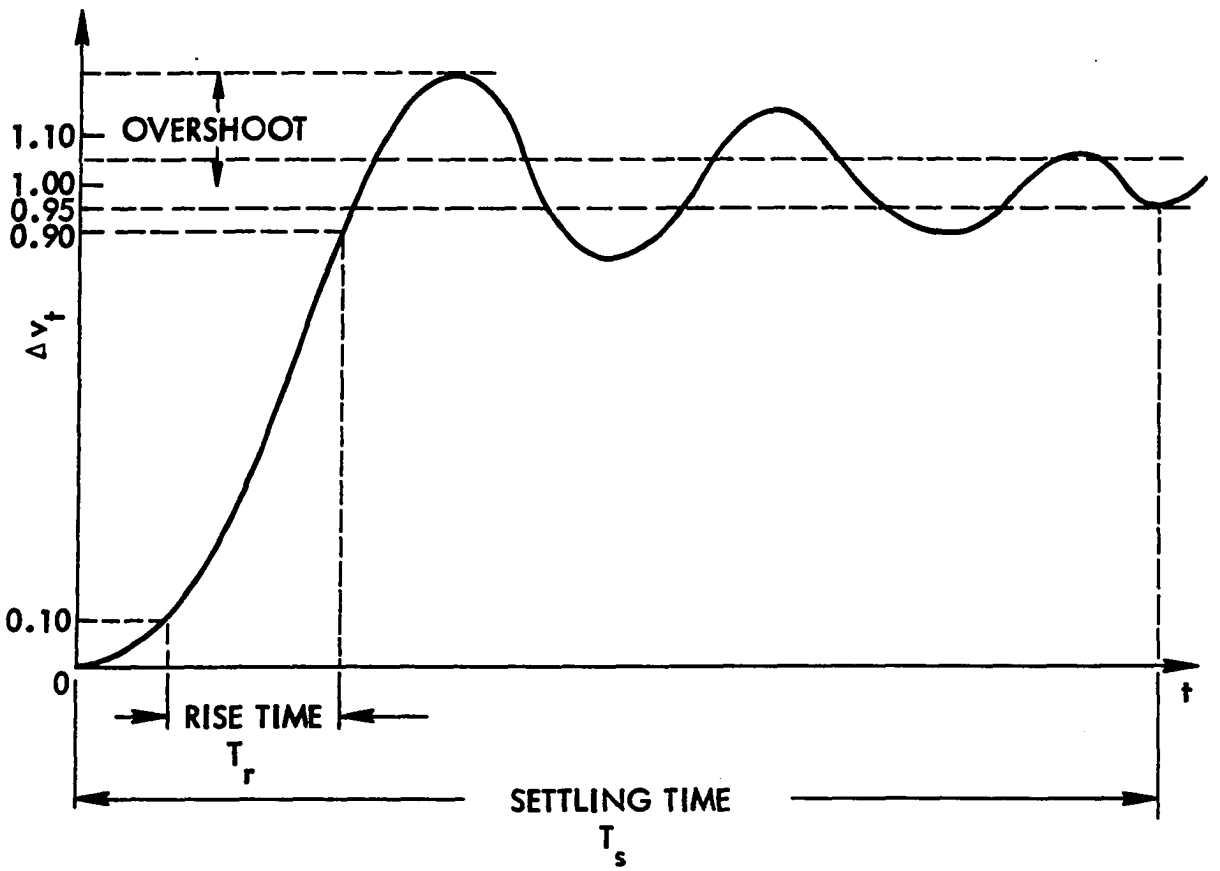

Figure 82b. Sketch showing the definition of performance indices used

Figure 82b shows how the performance indices used in Chapters IV, V and VI are defined.

XI. APPENDIX B. LINEAR MODEL

A. Mathematical Derivation of Model III

The assumptions made in developing model III have been discussed in section D of Chapter III. This section of Chapter XI deals with the mathematical manipulations performed on Equations 2-11 given below, to obtain the linearized equations used in model III.

By eliminating the terms due to the assumptions from the machine equations (see Appendix C), the system equations for this model as given in Chapter III are found. These equations, listed here for convenience, are:

$$v_t^2 = v_d^2 + v_q^2 \qquad [2]$$

$$-v_d = \lambda_q = -X_q i_q \qquad [3]$$

$$v_q = \lambda_d = e_q' - X_d' i_d \qquad [4]$$

$$e_q = e_q' + (X_q - X_d') i_d \qquad [5]$$

$$\tau_e = e_q i_q \qquad [6]$$

$$i_d = [e_q - V_B \cos \delta]\{[X_E + X_q]/[R_E^2 + (X_E + X_q)^2]\} - V_B \sin \delta \{R_E/[R_E^2 + (X_E + X_q)^2]\} \qquad [7]$$

$$i_q = [e_q - V_B \cos \delta]\{R_E/[R_E^2 + (X_E + X_q)^2]\} + V_B \sin \delta \{[X_E + X_q]/[R_E^2 + (X_E + X_q)^2]\} \qquad [8]$$

$$e'_q = X_{ad} i_{fd} - (X_d - X'_d) i_d \quad [9]$$

$$T'_{do} \left(\frac{de'_q}{dt}\right) = e_{fd} - X_{ad} i_{fd} \quad [10]$$

$$\tau_m - \tau_e = M \frac{d^2\delta}{dt^2} \quad [11]$$

Using subscript "o" for the operation at the quiescent point and "Δ" for a small increment the above equations can be linearized as follows.

Linearize Equation 2:

$$(v_{to} + v_{t\Delta})^2 = (v_{do} + v_{d\Delta})^2 + (v_{qo} + v_{q\Delta})^2$$

$$v_{to}^2 + v_{t\Delta}^2 + 2v_{to}v_{t\Delta} = v_{do}^2 + v_{d\Delta}^2 + 2v_{do}v_{d\Delta} + v_{qo}^2 + 2v_{qo}v_{q\Delta} + v_{q\Delta}^2$$

$$v_{to}^2 = v_{do}^2 + v_{qo}^2 \quad [B-1]$$

$$v_{t\Delta} = \frac{v_{do}}{v_{to}} v_{d\Delta} + \frac{v_{qo}}{v_{to}} v_{q\Delta} \quad [B-2]$$

Linearize Equation 3:

$$-v_{do} - v_{d\Delta} = -X_q i_{qo} - X_q i_{q\Delta}$$

$$-v_{do} = -X_q i_{qo} \quad [B-3]$$

$$-v_{d\Delta} = -X_q i_{q\Delta} \quad [B-4]$$

Linearize Equation 4:

$$v_{qo} + v_{q\Delta} = e'_{qo} + e'_{q\Delta} - X'_d i_{do} - X'_d i_{d\Delta}$$

$$v_{qo} = e'_{qo} - X'_d i_{do} \quad [B-5]$$

$$v_{q\Delta} = e'_{q\Delta} - X'_d i_{d\Delta} \qquad [B-6]$$

Linearize Equation 5:

$$e_{qo} + e_{q\Delta} = e'_{qo} + e'_{q\Delta} + (X_q - X'_d)i_{do} + (X_q - X'_d)i_{d\Delta}$$

$$e_{qo} = e'_{qo} + (X_q - X'_d)i_{do} \qquad [B-7]$$

$$e_{q\Delta} = e'_{q\Delta} + (X_q - X'_d)i_{d\Delta} \qquad [B-8]$$

Linearize Equation 6:

$$\tau_{eo} + \tau_{e\Delta} = (e_{qo} + e_{q\Delta})(i_{qo} + i_{q\Delta})$$

$$= e_{qo}i_{qo} + e_{qo}i_{q\Delta} + e_{q\Delta}i_{qo} + e_{q\Delta}i_{q\Delta}$$

$$\tau_{eo} = e_{qo}i_{qo} \qquad [B-9]$$

$$\tau_{e\Delta} = e_{qo}i_{q\Delta} + e_{q\Delta}i_{qo} \qquad [B-10]$$

Linearize Equation 7:

Define $D \triangleq R_E^2 + (X_E + X_q)^2$

$$(i_{do} + i_{d\Delta}) = [e_{qo} + e_{q\Delta} - V_B(\cos\delta_o \cos\delta_\Delta - \sin\delta_o \sin\delta_\Delta)]\frac{X_E+X_q}{D}$$

$$- V_B(\sin\delta_o \cos\delta_\Delta + \cos\delta_o \sin\delta_\Delta)\frac{R_E}{D}$$

$$= (e_{qo} - V_B \cos\delta_o)\frac{X_E+X_q}{D} + (e_{q\Delta} + V_B\,\delta_\Delta \sin\delta_o)\frac{X_E+X_q}{D}$$

$$- V_B \sin\delta_o(\frac{R_E}{D}) - V_B\,\delta_\Delta \cos\delta_o(\frac{R_E}{D})$$

$$i_{do} = (e_{qo} - V_B \cos \delta_o)\frac{X_E+X_q}{D} - V_B \sin \delta_o(\frac{R_E}{D}) \quad [B-11]$$

$$i_{d\Delta} = (e_q + V_B \delta_\Delta \sin \delta_o)\frac{X_E+X_q}{D} - V_B \delta_\Delta \cos \delta_o(\frac{R_E}{D}) \quad [B-12]$$

Similarly the linearized forms of Equation 8 are:

$$i_{qo} = (e_{qo} - V_B \cos \delta_o)\frac{R_E}{D} + V_B \sin \delta_o(\frac{X_E+X_q}{D}) \quad [B-13]$$

$$i_{q\Delta} = (e_{q\Delta} + V_B \delta_\Delta \sin \delta_o)\frac{R_E}{D} + V_B \delta_\Delta \cos \delta_o(\frac{X_E+X_q}{D}) \quad [B-14]$$

Linearize Equation 9:

$$e'_{qo} + e'_{q\Delta} = X_{ad}(i_{fdo} + i_{fd\Delta}) - (X_d - X'_d)(i_{do} + i_{d\Delta})$$

$$e'_{qo} = X_{ad} i_{fdo} - (X_d - X'_d) i_{do} \quad [B-15]$$

$$e'_{q\Delta} = X_{ad} i_{fd\Delta} - (X_d - X'_d) i_{d\Delta} \quad [B-16]$$

Linearize Equation 10:

$$T'_{do}[\frac{d}{dt}(e'_{qo} + e'_{q\Delta})] = e_{fdo} + v_{fd\Delta} - X_{ad}(i_{fdo} + i_{fd\Delta})$$

$$T'_{do}\frac{de'_{qo}}{dt} = e_{fdo} - X_{ad} i_{fdo} \quad [B-17]$$

$$T'_{do}\frac{de'_{q\Delta}}{dt} = e_{fd\Delta} - X_{ad} i_{fd\Delta} \quad [B-18]$$

Linearize Equation 11:

$$(\tau_{mo} + \tau_{m\Delta}) - (\tau_{eo} + \tau_{e\Delta}) = M\frac{d^2}{dt^2}(\delta_o + \delta_\Delta)$$

$$\tau_{mo} - \tau_{eo} = M\frac{d^2\delta_o}{dt^2} \quad [B-19]$$

$$\tau_{m\Delta} - \tau_{e\Delta} = M\frac{d^2\delta_\Delta}{dt^2} \quad [B-20]$$

Starting with Equations B-2, B-10 and B-16 the other linearized equations are repeatedly substituted to obtain simplified equations for $v_{t\Delta}$, $e'_{q\Delta}$ and $\tau_{e\Delta}$ as follows.

Substitute B-4 and B-6 for $v_{d\Delta}$ and $v_{q\Delta}$, respectively, into Equation B-2 and simplify the result.

$$v_{t\Delta} = \frac{v_{do}}{v_{to}} v_{d\Delta} + \frac{v_{qo}}{v_{to}} v_{q\Delta} \qquad [B-2]$$

$$v_{t\Delta} = \frac{v_{do}}{v_{to}} X_q i_{q\Delta} + \frac{v_{qo}}{v_{to}} [e'_{q\Delta} - X'_d i_{d\Delta}]$$

$$v_{t\Delta} = \frac{v_{qo}}{v_{to}} e'_{q\Delta} + [\frac{v_{do}}{v_{to}} X_q \frac{R_E}{D} - \frac{v_{qo}}{v_{to}} X'_d (\frac{X_E+X_q}{D})] e_{q\Delta}$$

$$+ \frac{v_{do}}{v_{to}} X_q V_B (\frac{R_E}{D} \sin \delta_o + \frac{X_E+X_q}{D} \cos \delta_o)\delta_\Delta$$

$$+ \frac{v_{qo}}{v_{to}} X'_d V_B (\frac{R_E}{D} \cos \delta_o - \frac{X_E+X_q}{D} \sin \delta_o)\delta_\Delta \qquad [B-21]$$

Substitute Equation B-12 for $i_{d\Delta}$ in Equation B-8 and simplify the result.

$$e_{q\Delta} = e'_{q\Delta} + (X_q - X'_d) i_{d\Delta} \qquad [B-8]$$

$$= e'_{q\Delta} + (X_q - X'_d)[(e_{q\Delta} + V_B \sin \delta_o \delta_\Delta)\frac{X_E+X_q}{D} - V_B \frac{R_E}{D} \cos \delta_o \delta_\Delta]$$

$$= e'_{q\Delta} + (X_q - X'_d)(\frac{X_E+X_q}{D}) e_{q\Delta}$$

$$+ V_B (X_q - X'_d)[(\frac{X_E+X_q}{D}) \sin \delta_o - \frac{R_E}{D} \cos \delta_o]\delta_\Delta$$

Rearranging the above to solve for $e_{q\Delta}$:

$$\frac{1}{D}[D - (X_q - X_d')(X_E + X_q)]e_{q\Delta} = e'_{q\Delta} + V_B(X_q - X_d')[\frac{(X_E+X_q)}{D} \sin \delta_o - \frac{R_E}{D} \cos \delta_o]\delta_\Delta$$

Define $A \triangleq D - (X_q - X_d')(X_E + X_q)$

$$= R_E^2 + (X_E + X_q)^2 - (X_q - X_d')(X_E + X_q)$$

$$= R_E^2 + (X_E + X_q)(X_E + X_d') \qquad [B-22]$$

Then

$$e_{q\Delta} = \frac{D}{A} e'_{q\Delta} + (\frac{X_q - X_d'}{A}) V_B [(X_E+X_q) \sin \delta_o - R_E \cos \delta_o]\delta_\Delta \qquad [B-23]$$

Substitute Equation B-23 for $e_{q\Delta}$ in Equation B-21 and simplify the result.

$$v_{t\Delta} = \frac{v_{qo}}{v_{to}} e'_{q\Delta} + \frac{v_{do}}{v_{to}} X_q V_B (\frac{R_E}{D} \sin \delta_o + \frac{X_E+X_q}{D} \cos \delta_o)\delta_\Delta$$

$$+ \frac{v_{qo}}{v_{to}} X_d' V_B (\frac{R_E}{D} \cos \delta_o - \frac{X_E+X_q}{D} \sin \delta_o)\delta_\Delta$$

$$+ [\frac{v_{do}}{v_{to}} X_q \frac{R_E}{D} - \frac{v_{qo}}{v_{to}} X_d' \frac{(X_E+X_q)}{D}]$$

$$\{\frac{D}{A} e'_{q\Delta} + \frac{(X_q - X_d')}{A} V_B [(X_E+X_q) \sin \delta_o - R_E \cos \delta_o]\delta_\Delta\}$$

$$v_{t\Delta} = \{\frac{v_{do}}{v_{to}} (\frac{X_q R_E}{A}) + \frac{v_{qo}}{v_{to}} [1 - X_d' \frac{(X_E+X_q)}{A}]\} e'_{q\Delta}$$

$$+ \frac{v_{do}}{v_{to}} X_q \frac{R_E}{D} \frac{(X_q - X_d')}{A} V_B [(X_E+X_q) \sin \delta_o - R_E \cos \delta_o]\delta_\Delta$$

(Equation continued on next page)

$$- \frac{v_{qo}}{v_{to}} X_d' \left(\frac{X_E+X_q}{D}\right)\frac{(X_q-X_d')}{A} V_B \left[(X_E+X_q) \sin \delta_o - R_E \cos \delta_o\right]\delta_\Delta$$

$$+ \frac{v_{do}}{v_{to}} X_q V_B \left[\frac{R_E}{D} \sin \delta_o + \frac{X_E+X_q}{D} \cos \delta_o\right]\delta_\Delta$$

$$+ \frac{v_{qo}}{v_{to}} X_d' V_B \left[\frac{R_E}{D} \cos \delta_o - \frac{X_E+X_q}{D} \sin \delta_o\right]\delta_\Delta \qquad \text{[B-24]}$$

In Equation B-24, consider the terms containing both $\frac{v_{do}}{v_{to}}$ and δ_Δ, define it as K_{51} and simplify.

$$K_{51} \triangleq \frac{v_{do}}{v_{to}} X_q \frac{R_E}{D} \frac{(X_q-X_d')}{A} V_B \left[(X_E+X_q) \sin \delta_o - R_E \cos \delta_o\right]\delta_\Delta$$

$$+ \frac{v_{do}}{v_{to}} X_q V_B \left[\frac{R_E}{D} \sin \delta_o + \frac{X_E+X_q}{D} \cos \delta_o\right]\delta_\Delta$$

$$= \frac{v_{do}}{v_{to}} X_q V_B \left[\frac{R_E(X_q-X_d')(X_E+X_q)}{DA} \sin \delta_o - \frac{R_E^2(X_q-X_d')}{DA} \cos \delta_o\right.$$

$$\left. + \frac{R_E}{D} \sin \delta_o + \frac{X_E+X_q}{D} \cos \delta_o\right]\delta_\Delta$$

$$K_{51} = \frac{v_{do}}{v_{to}} X_q \frac{V_B}{A} \left[R_E \sin \delta_o + (X_E+X_d') \cos \delta_o\right]\delta_\Delta \qquad \text{[B-25]}$$

Similarly, in Equation B-24, consider the terms containing both $\frac{v_{qo}}{v_{to}}$ and δ_Δ, define it as K_{52} and simplify.

$$K_{52} \triangleq \frac{v_{qo}}{v_{to}} X_d' V_B \left[\frac{R_E}{D} \cos \delta_o - \frac{(X_E+X_q)}{D} \sin \delta_o\right]\delta_\Delta$$

$$- \frac{v_{qo}}{v_{to}} X_d' \frac{(X_E+X_q)}{D}\frac{(X_q-X_d')}{A} V_B \left[(X_E-X_q) \sin \delta_o - R_E \cos \delta_o\right]\delta_\Delta$$

$$K_{52} = \frac{v_{qo}}{v_{to}} X_d' \frac{V_B}{A} [R_E \cos \delta_o - (X_E+X_q) \sin \delta_o]\delta_\Delta$$

Define $K_5 \triangleq \frac{1}{\delta_\Delta} (K_{51} + K_{52})$

$$= \frac{v_{do}}{v_{to}} X_q \frac{V_B}{A} [R_E \sin \delta_o + (X_E + X_d') \cos \delta_o]\delta_\Delta$$

$$+ \frac{v_{qo}}{v_{to}} X_d' \frac{V_B}{A} [R_E \cos \delta_o - (X_E + X_q) \sin \delta_o]\delta_\Delta \quad [B-26]$$

Referring to Equation B-24 we observe that K_5 includes all the coefficients of δ_Δ and thus to complete the simplification we can define the coefficient of $e'_{q\Delta}$ as:

$$K_6 \triangleq \frac{v_{do}}{v_{to}} \frac{X_q R_E}{A} + \frac{v_{qo}}{v_{to}} [1 - X_d' \frac{(X_E+X_q)}{A}] \quad [B-27]$$

Therefore, Equation B-24 becomes:

$$v_{t\Delta} = K_5\delta_\Delta + K_6 e'_{q\Delta} \quad [B-28]$$

Solve Equation B-16 for $i_{fd\Delta}$.

$$e'_{q\Delta} = X_{ad} i_{fd\Delta} - (X_d - X_d') i_{d\Delta} \quad [B-16]$$

$$i_{fd\Delta} = \frac{1}{X_{ad}} [e'_{q\Delta} + (X_d - X_d') i_{d\Delta}] \quad [B-29]$$

Substitute Equation B-29 for $i_{fd\Delta}$ in Equation B-18 and then substitute for $i_{d\Delta}$ in the resulting equation:

$$T_{do}' \frac{de_q'}{dt} = e_{fd\Delta} - X_{ad} i_{fd\Delta} \quad [B-18]$$

$$T'_{do}\frac{de'_{q\Delta}}{dt} = e_{fd\Delta} - e'_{q\Delta} - (X_d - X'_d)i_{d\Delta}$$

$$= e_{fd\Delta} - e'_{q\Delta} - (X_d - X'_d)\{[e_{q\Delta} + V_B\,\delta_\Delta \sin\delta_o]\frac{X_E+X_q}{D}$$

$$- \frac{V_B R_E}{D}\cos\delta_o\delta_\Delta\}$$

Substitute B-23 for $e_{q\Delta}$ in the above equation and simplify the result.

$$T'_{do}\frac{de'_{q\Delta}}{dt} = e_{fd\Delta} - e'_{q\Delta} - V_B \sin\delta_o\,(X_d - X'_d)\frac{(X_E + X_q)}{D}\,\delta_\Delta$$

$$+ (X_d - X'_d)\,\frac{V_B R_E}{D}\cos\delta_o\delta_\Delta - (X_d - X'_d)\frac{(X_E + X_q)}{D}$$

$$\{\frac{D}{A}\,e'_{q\Delta} + \frac{V_B}{A}\,(X_q - X'_d)[(X_E+X_q)\sin\delta_o - R_E\cos\delta_o]\delta_\Delta\}$$

$$T'_{do}\frac{de'_{q\Delta}}{dt} = e_{fd\Delta} - [1 + (X_d - X'_d)(\frac{X_E+X_q}{A})]e'_{q\Delta}$$

$$- \frac{V_B}{A}\,(X_d - X'_d)(X_E + X_q)\sin\delta_o\delta_\Delta$$

$$+ \frac{V_B R_E}{A}\,(X_d - X'_d)\cos\delta_o\delta_\Delta$$

Rearranging the above:

$$T'_{do}\frac{de_{q\Delta}}{dt} + [1 + \frac{(X_d - X'_d)(X_E + X_q)}{A}]e'_{q\Delta} = e_{fd\Delta}$$

$$+ \frac{V_B}{A}\,(X_d - X'_d)[R_E\cos\delta_o - (X_E + X_q)\sin\delta_o]\delta_\Delta \qquad [B\text{-}30]$$

Take Laplace transform of Equation B-30 and simplify the result.

$$[ST'_{do} + 1 + \frac{(X_d - X'_d)(X_E + X_q)}{A}]e'_{q\Delta} = e_{fd\Delta}$$

$$+ \frac{V_B}{A}(X_d - X'_d)[R_E \cos \delta_o - (X_E + X_q) \sin \delta_o]\delta_\Delta$$

Multiply the above by K_3, where K_3 is defined as:

$$K_3 \triangleq [1 + (X_d - X'_d)(X_E + X_q)]^{-1}$$

Define $K_4 \triangleq \frac{V_B}{A}(X_d - X'_d)[-R_E \cos \delta_o + (X_E + X_q) \sin \delta_o]$

Then,

$$[1 + K_3 ST'_{do}]e'_{q\Delta} = K_3 e_{fd\Delta} - K_3 K_4 \delta_\Delta$$

or

$$e'_{q\Delta} = \frac{K_3 e_{fd\Delta}}{1 + ST'_{do} K_3} - \frac{K_3 K_4}{1 + ST'_{do} K_3}\delta_\Delta \qquad [B-31]$$

Substitute Equations B-14 and B-23 for $i_{q\Delta}$ and $e_{q\Delta}$, respectively, in Equation B-10 and simplify the result.

$$\tau_{e\Delta} = e_{qo} i_{q\Delta} + e_{q\Delta} i_{qo} \qquad [B-10]$$

$$\tau_{e\Delta} = e_{qo}[(e_{q\Delta} + V\delta_\Delta \sin \delta_o)\frac{R_E}{D} + V_B \delta_\Delta \cos \delta_o (\frac{X_E + X_q}{D})] + e_{q\Delta} i_{qo}$$

$$\tau_{e\Delta} = [\frac{e_{qo} R_E}{A} + \frac{A + D - A}{A} i_{qo}]e'_{q\Delta}$$

$$+ \frac{V_B}{A} e_{qo} \frac{R_E}{D}[(X_q - X'_d)(X_E + X_q) \sin \delta_o - R_E(X_q - X'_d) \cos \delta_o]\delta_\Delta$$

$$+ \frac{V_B}{A} i_{qo} [(X_q - X_d')(X_E + X_q) \sin \delta_o - R_E(X_q - X_d') \cos \delta_o]\delta_\Delta$$

$$+ \frac{V_B e_{qo}}{DA} \{R_E[R_E^2 + (X_E + X_q)(X_E + X_d')] \sin \delta_o + (X_E + X_q)$$

$$[R_E^2 + (X_E + X_q)(X_E + X_d')] \cos \delta_o]\}\delta_\Delta$$

$$\tau_{e\Delta} = \{\frac{e_{qo} R_E}{A} + [1 + (X_E + X_q)(X_q - X_d')] \frac{i_{qo}}{A}\} e_{q\Delta}'$$

$$+ \frac{V_B i_{qo}}{A} [(X_q - X_d')(X_E + X_q) \sin \delta_o - R_E(X_q - X_d') \cos \delta_o]\delta_\Delta$$

$$+ \frac{V_B e_{qo}}{A} [R_E \sin \delta_o + (X_E + X_d') \cos \delta_o]\delta_\Delta$$

$$\therefore \tau_{e\Delta} = K_1 \delta_\Delta + K_2 e_{q\Delta}' \qquad [B\text{-}32]$$

where

$$K_1 \triangleq \frac{V_B i_{qo}}{A} [(X_q - X_d')(X_E + X_q) \sin \delta_o - R_E(X_q - X_d') \cos \delta_o]$$

$$+ \frac{V_B e_{qo}}{A} [R_E \sin \delta_o + (X_E + X_d') \cos \delta_o] \qquad [B\text{-}33]$$

$$K_2 \triangleq \frac{e_{qo} R_E}{A} + \frac{i_{qo}}{A} (X_E + X_q)(X_q - X_d') \qquad [B\text{-}34]$$

In summary, the simplified equations involving $v_{t\Delta}$, $e_{q\Delta}'$ and δ_Δ are:

$$v_{t\Delta} = K_5 \delta_\Delta + K_6 e_{q\Delta}' \qquad [B\text{-}28]$$

$$e_{q\Delta}' = K_3 \frac{(e_{fd\Delta} - K_4 \delta_\Delta)}{1 + ST_{do}' K_3} \qquad [B\text{-}31]$$

$$\tau_{e\Delta} = K_1\delta_\Delta + K_2 e'_{q\Delta} \qquad [B-32]$$

The torque equations necessary to complete the model are developed in Appendix C and are presented here for convenience.

$$\Delta\omega = \frac{1}{M}\int \tau_a dt \qquad [B-33]$$

$$\delta_\Delta = 377 \int \Delta\omega dt \qquad \text{radians} \qquad [B-34]$$

where

$$\tau_a \triangleq \tau_{m\Delta} - \tau_{e\Delta} \qquad [B-35]$$

Equations B-28, B-31 to B-34 lead to the block diagram shown in Figure 83 with the subscript Δ's deleted.

B. Simulation of Model III

The calculation of the constants K_1 to K_6 defined in section A and potentiometer settings used in simulating model III are discussed in this section.

A complete list of data for the synchronous machine as given in references 5 and 116 is presented in Appendix C. Using the machine data and a computer program developed in reference 116, the constants K_1 to K_6 are determined. Table 21 gives a summary of both the input data and the output of the computer program.

A block diagram of model III with the excitation system is shown in Figure 84. The analog computer simulation diagram of the block diagram is shown in Figure 85. Here the point A discussed in section D of Appendix A corresponds to the output of integrator 601, point B is the

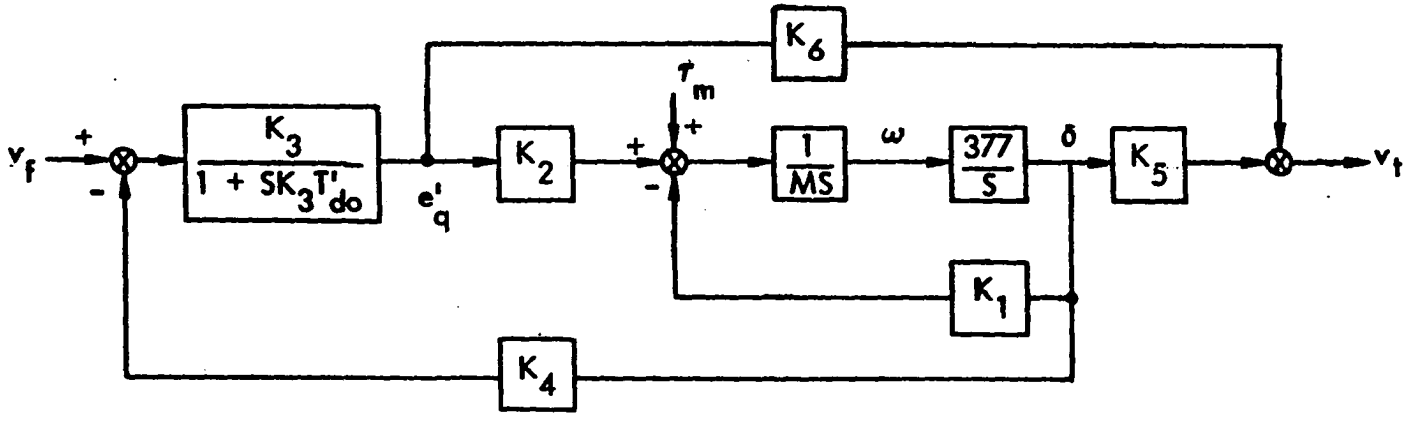

Figure 83. Block diagram for model III without damping

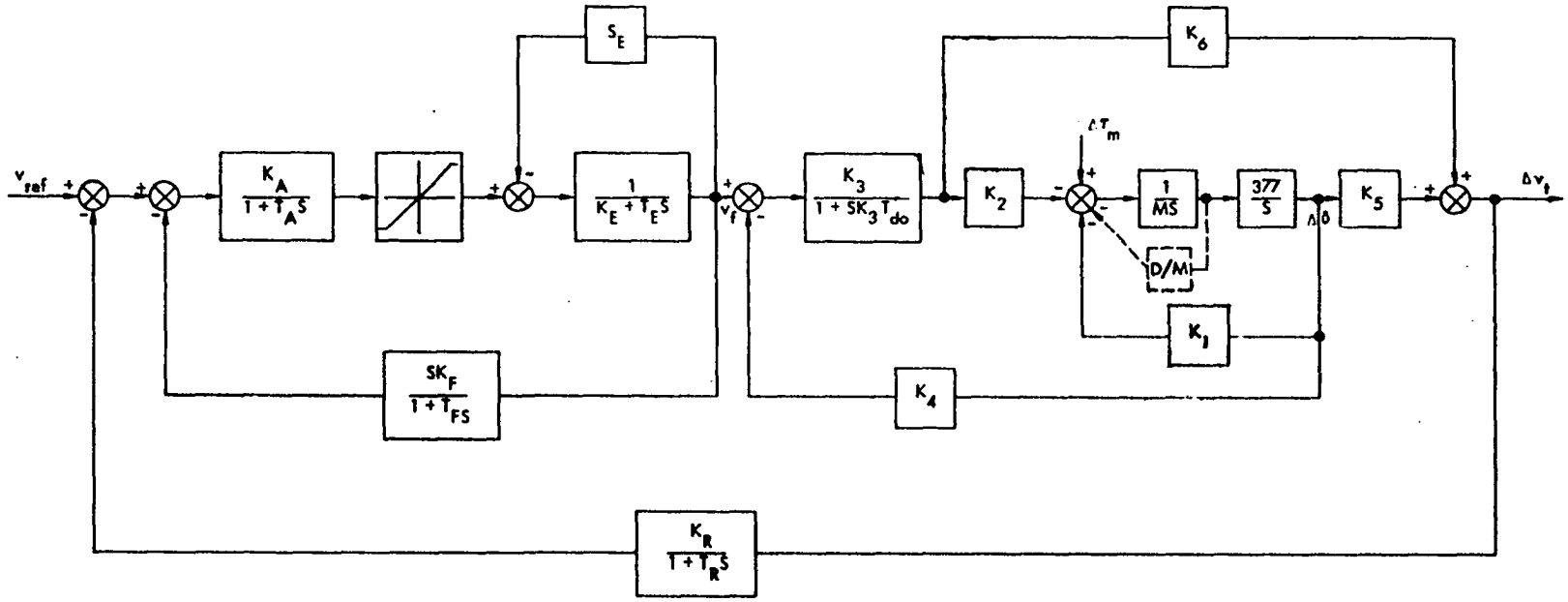

Figure 84. Block diagram for model III with the excitation system

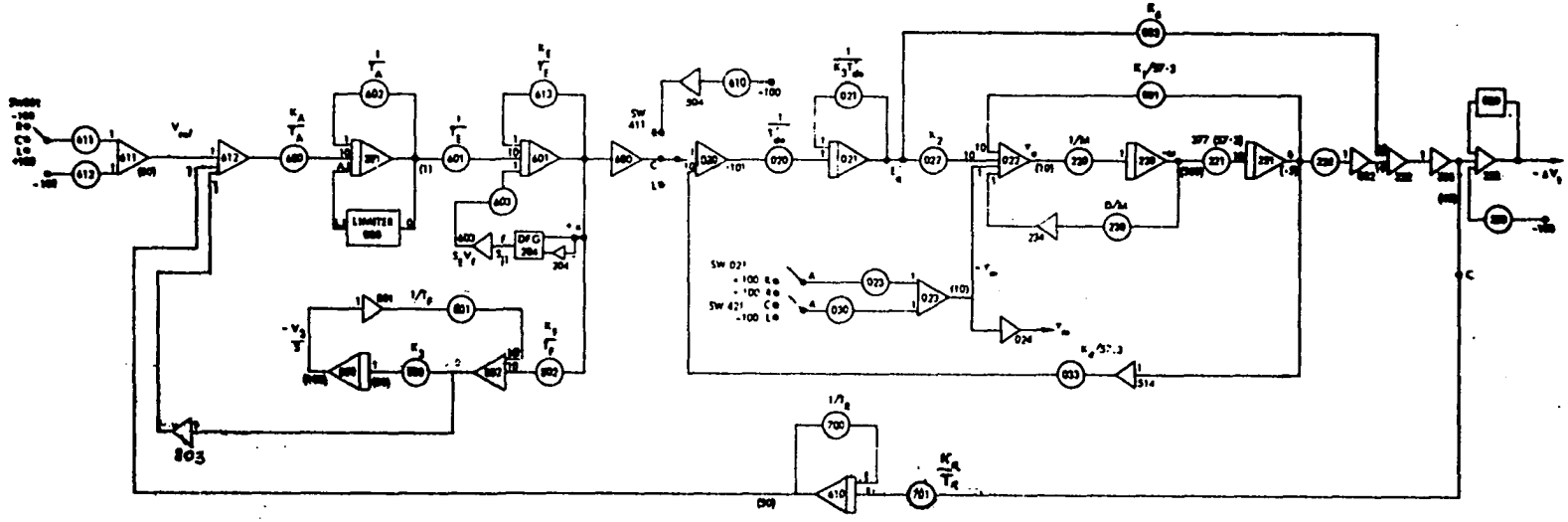

Figure 85. Simulation diagram for model III with the fast exciter

Table 21. Summary of the input data and output of the computer program

Machine data and line parameters	
R_E	0.02
X_E	0.40
X_d	1.70
X'_d	0.15
X_q	1.64

Initial conditions for the machine	
Single-phase power output	1.000
Single phase var output	0.620
Infinite bus voltage (ABC)	1.000
Terminal voltage (odq)	2.031
Direct axis current	-1.591
Quadrature axis current	0.700
Direct axis terminal voltage	-1.148
Quadrature axis terminal voltage	1.675
Delta, angle from infinite bus to q-axis in degrees	53.750

Linearized machine constants	
K_1	4.8866
K_2	2.6731
K_3	0.2620
K_4	3.9067
K_5	-0.8004
K_6	0.5958

output terminal of inverter 230 going into gain 1 input of summing amplifier 223 and point C is the output of the inverter 230 going into the high side of potentiometer 701.

Tables 22 and 23 show the potentiometer settings used in simulating model III with slow and fast exciters, respectively. The lower portion of the two tables is for machine model III while the upper portion corresponds to the two exciters. The settings for the function generator and the amplifier limiting are as discussed in Appendix A.

Figure 86 shows the steady state voltages of a sample run made with the fast exciter and with both limiting and saturation represented.

Table 22. Pot. settings for simulation of model III with the slow exciter

Pots.	Pot. setting	Amp. gain	Variable	Value	Scaling	Value x scaling
600	$K_A/5000$	10	K_A/T_A	$10K_A$	1/100x1/50	$K_A/500$
601	.02	10	$1/T_E$	2	10/100	20/100
602	.1	1	$1/T_A$	10	1/100	1/10
603	.02	1	$1/T_E$	2	1/100	2/100
611	.0290	1	Δv_{ref}	5% full load		
612	.5900	1	v_{ref}	Full load		
613	.001	1	$\lvert K_E \rvert / T_E$	.1	1/100	.1/100
700	.02	10	$1/T_R$	20	1/100	1/5
701	.0145	10	$K_R/\sqrt{3}\ T_R$	$20/\sqrt{3}$	50/100x40	$1/4\sqrt{3}$
800	.02	1	K_{31}	1	100/100x50	1/50
801	$1/20T_F$	10	$1/T_F$		50/100	$1/2T_F$
802	$K_F/2T_F$	10	K_F/T_F		50/10	$5K_F/T_F$
020	.0017	1	$1/T'_{do}$	.1693	1/100	.001693
021	.0065	1	$1/K_3T'_{do}$	.647	1/100	.00647
022	.2673	10	K_2	2.6731	1	2.6731
023	.1	1	τ_m	1.0	10/100	.1
030	.01	1	$0.1\tau_m$	.1	10/100	.01
031	.1704	10	$K_1/57.3$	.0852	10/.5	1.704
032	.2383	10	K_6	.5959	40/10	2.3832
033	.1362	10	$K_4/57.3$	.0681	10/.5	1.362
220	.5275	1	1/M	.211	50/100x10	.5275
221	.216	10	377(57.3)	21600	.5/100x500	.216
222	-.1116	10	K_5	-.01395	40/.5	-1.116
230	.2268	1	D/M	11.34	10/500	.2268

Table 23. Pot. settings for simulation of model III with the fast exciter

Pots.	Pot. setting	Amp. gain	Variable	Value	Scaling	Value x scaling
600	$K_A/1000$	10	K_A/T_A	$50K_A$	1/100x1/50	$K_A/100$
601	.6667	10	$1/T_E$	66.67	10/100	6.667
602	.5	1	$1/T_A$	50	1/100	1/2
603	.6667	1	$1/T_E$	66.67	1/100	2/3
611	.0290	1	Δv_{ref}	5% full load		
612	.5900	1	v_{ref}	Full load		
613	.6667	1	K_E/T_E	66.67	1/100	.6667
700	.2	10	$1/T_R$	200	1/100	2.0
701	.1445	10	$K_R/\sqrt{3}\ T_R$	$200/\sqrt{3}$	50/100x1/40	$1/4\sqrt{3}$
800	.02	1	K_{31}	1	100/100x50	1/50
801	$1/20T_F$	10	$1/T_F$		50/100	$1/2T_F$
802	$K_F/2T_F$	10	K_F/T_F		50/10	$5K_F/T_F$
020	.0017	1	$1/T'_{do}$	.1693	1/100	.001693
021	.0065	1	$1/K_3T'_{do}$	.647	1/100	.00647
022	.2673	10	K_2	2.6731	1	2.6731
023	.1	1	τ_m	1.0	10/100	.1
030	.01	1	$.1\tau_m$	.1	10/100	.01
031	.1704	10	$K_1/57.3$	.0852	10/.5	1.704
032	.2383	10	K_6	.5959	40/10	2.3832
033	.1362	10	$K_4/57.3$	.0681	10/.5	1.362
220	.5275	1	1/M	.211	500/100x10	.5275
221	.216	10	377(57.3)	21600	.5/100x500	.216
222	-.1116	10	K_5	-.01395	40/.5	-1.116
230	.2268	1	D/M	11.34	10/500	.2268

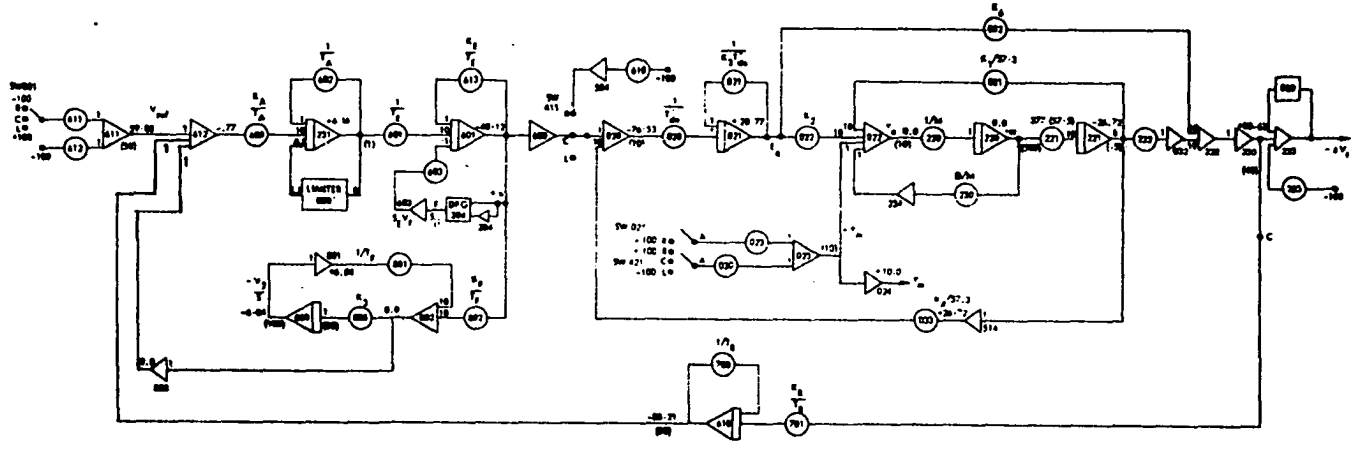

Figure 86. Steady state voltages at full load with limiting and saturation for fast exciter

XII. APPENDIX C. THE NONLINEAR MODEL

This chapter covers the mathematical development of the nonlinear model, model IV, the simulation of model IV under the assumptions made in developing model III, the changes necessary for saliency considerations and the development of the d-q-axes saturation functions.

A. Development of the Nonlinear Model

The assumptions made in developing model IV, the pictorial representation of the synchronous machine and the resulting circuit diagram have been presented in section E of Chapter III. This section outlines the results of the mathematical manipulations necessary on the equations presented in Chapter III. A more complete description of the development can be found in references 4, 5, 33 and 116. The required analog computer diagrams and simulation considerations are also discussed.

1. Basic equations

The flux linkage equations for the six circuits of the synchronous machine are given by Equation 20 in Chapter IV and are restated below for convenience.

$$\begin{bmatrix} \lambda_a \\ \lambda_b \\ \lambda_c \\ \lambda_F \\ \lambda_D \\ \lambda_Q \end{bmatrix} = \begin{bmatrix} L_{aa} & L_{ab} & L_{ac} & L_{aF} & L_{aD} & L_{aQ} \\ L_{ba} & L_{bb} & L_{bc} & L_{bF} & L_{bD} & L_{bQ} \\ L_{ca} & L_{cb} & L_{cc} & L_{cF} & L_{cD} & L_{cQ} \\ L_{Fa} & L_{Fb} & L_{Fc} & L_{FF} & L_{FD} & L_{FQ} \\ L_{Da} & L_{Db} & L_{Dc} & L_{DF} & L_{DD} & L_{DQ} \\ L_{Qa} & L_{Qb} & L_{Qc} & L_{QF} & L_{QD} & L_{QQ} \end{bmatrix} \begin{bmatrix} i_a \\ i_b \\ i_c \\ i_F \\ i_D \\ i_Q \end{bmatrix} \quad \text{weber-turns} \qquad [20]$$

where

$$L_{jk} = \begin{matrix}\text{(self-inductance when } j = k \\ \text{(mutual inductance when } j \neq k\end{matrix}$$

The inductances in Equation 20 are defined as follows.

The stator self-inductances are:

$$\begin{aligned} L_{aa} &= L_s + L_m \cos 2\theta \\ L_{bb} &= L_s + L_m \cos 2(\theta-120) \qquad \text{henrys} \qquad L_s > L_m \\ L_{cc} &= L_s + L_m \cos 2(\theta+120) \end{aligned} \qquad \text{[C-1]}$$

If slot effects and saturation are neglected the rotor self-inductances are constants and may be defined as:

$$\begin{aligned} L_{FF} &= L_F \\ L_{DD} &= L_D \qquad \text{henrys} \\ L_{QQ} &= L_Q \end{aligned} \qquad \text{[C-2]}$$

The stator mutual inductances are:

$$\begin{aligned} L_{ab} = L_{ba} &= -[M_s + L_m \cos 2(\theta+30)] \\ L_{bc} = L_{cb} &= -[M_s + L_m \cos 2(\theta-90)] \qquad \text{henrys} \qquad M_s > L_m \\ L_{ca} = L_{ac} &= -[M_s + L_m \cos 2(\theta+150)] \end{aligned} \qquad \text{[C-3]}$$

The rotor mutual inductances are:

$$\begin{aligned} L_{FD} = L_{DF} &= M_R \\ L_{FQ} = L_{QF} &= 0 \qquad \text{henrys} \\ L_{DQ} = L_{QD} &= 0 \end{aligned} \qquad \text{[C-4]}$$

The stator-to-field mutual inductances are:

$$\begin{aligned} L_{aF} &= L_{Fa} = + M_F \cos\theta \\ L_{bF} &= L_{Fb} = + M_F \cos(\theta-120) \qquad \text{henrys} \\ L_{cF} &= L_{Fc} = + M_F \cos(\theta+120) \end{aligned} \qquad \text{[C-5]}$$

The stator-to-d-axis damper winding mutual inductances are:

$$\begin{aligned} L_{aD} &= L_{Da} = + M_D \cos\theta \\ L_{bD} &= L_{Db} = + M_D \cos(\theta-120) \qquad \text{henrys} \\ L_{cD} &= L_{Dc} = + M_D \cos(\theta+120) \end{aligned} \qquad \text{[C-6]}$$

The stator-to-q-axis damper winding mutual inductances are:

$$\begin{aligned} L_{aQ} &= L_{Qa} = + M_Q \sin\theta \\ L_{bQ} &= L_{Qb} = + M_Q \sin(\theta-120) \qquad \text{henrys} \\ L_{cQ} &= L_{Qc} = + M_Q \sin(\theta+120) \end{aligned} \qquad \text{[C-7]}$$

The above definitions of inductances show that most of the inductances are time varying. By applying an appropriate Park-type transformation, also referred to by some authors as Blondel transformation, the time varying characteristic of Equation 20 can be removed. An orthogonal transformation is applied in this case and it is defined as:

$$\underline{P} \overset{\Delta}{=} \sqrt{2/3} \begin{bmatrix} \sqrt{1/2} & \sqrt{1/2} & \sqrt{1/2} \\ \cos\theta & \cos(\theta-120) & \cos(\theta+120) \\ \sin\theta & \sin(\theta-120) & \sin(\theta+120) \end{bmatrix} \qquad \text{[C-8]}$$

Applying the above transformation to Equation 20 leads to:

$$\begin{bmatrix} \lambda_o \\ \lambda_d \\ \lambda_q \\ \lambda_F \\ \lambda_D \\ \lambda_Q \end{bmatrix} = \begin{bmatrix} L_o & 0 & 0 & 0 & 0 & 0 \\ 0 & L_d & 0 & +\sqrt{3/2}M_F & +\sqrt{3/2}M_D & 0 \\ 0 & 0 & L_q & 0 & 0 & +\sqrt{3/2}M_Q \\ 0 & +\sqrt{3/2}M_F & 0 & L_F & M_R & 0 \\ 0 & +\sqrt{3/2}M_D & 0 & M_R & L_D & 0 \\ 0 & 0 & +\sqrt{3/2}M_Q & 0 & 0 & L_Q \end{bmatrix} \begin{bmatrix} i_o \\ i_d \\ i_q \\ i_F \\ i_D \\ i_Q \end{bmatrix} \text{ weber-turns} \qquad [C\text{-}9a]$$

where

$$L_d = L_s + M_s + 3/2\ L_m$$
$$L_q = L_s + M_s - 3/2\ L_m \quad \text{henrys} \qquad [C\text{-}9b]$$
$$L_o = L_s - 2M_s$$

Using ℓ for a leakage inductance, Equation C-9a can be modified to separate the mutual and leakage inductance terms.

$$\begin{bmatrix} \lambda_o \\ \lambda_d \\ \lambda_q \\ \lambda_F \\ \lambda_D \\ \lambda_Q \end{bmatrix} = \begin{bmatrix} (L_o-\ell_o)+\ell_o & 0 & 0 & 0 & 0 & 0 \\ 0 & (L_d-\ell_d)+\ell_d & 0 & +\sqrt{3/2}M_F & +\sqrt{3/2}M_D & 0 \\ 0 & 0 & (L_q-\ell_q)+\ell_q & 0 & 0 & +\sqrt{3/2}M_Q \\ 0 & +\sqrt{3/2}M_F & 0 & (L_F-\ell_F)+\ell_F & M_R & 0 \\ 0 & +\sqrt{3/2}M_D & 0 & M_R & (L_D-\ell_D)+\ell_D & 0 \\ 0 & 0 & +\sqrt{3/2}M_Q & 0 & 0 & (L_Q-\ell_Q)+\ell_Q \end{bmatrix} \begin{bmatrix} i_o \\ i_d \\ i_q \\ i_F \\ i_D \\ i_Q \end{bmatrix} \text{ weber-turns} \qquad [C\text{-}10]$$

The voltage equations for the machine are given in Chapter III as Equation 18 and is restated below for convenience.

$$\begin{bmatrix} v_a \\ v_b \\ v_c \\ -v_F \\ 0 \\ 0 \end{bmatrix} = -\begin{bmatrix} r_a & 0 & 0 & 0 & 0 & 0 \\ 0 & r_b & 0 & 0 & 0 & 0 \\ 0 & 0 & r_c & 0 & 0 & 0 \\ 0 & 0 & 0 & r_F & 0 & 0 \\ 0 & 0 & 0 & 0 & r_D & 0 \\ 0 & 0 & 0 & 0 & 0 & r_Q \end{bmatrix} \begin{bmatrix} i_a \\ i_b \\ i_c \\ i_F \\ i_D \\ i_Q \end{bmatrix} - \begin{bmatrix} \dot{\lambda}_a \\ \dot{\lambda}_b \\ \dot{\lambda}_c \\ \dot{\lambda}_F \\ \dot{\lambda}_D \\ \dot{\lambda}_Q \end{bmatrix} + \begin{bmatrix} \underline{v}_n \\ \underline{0} \end{bmatrix} \quad \text{volts} \qquad [18]$$

where

$$\underline{v}_n = -r_n \begin{bmatrix} 1 & 1 & 1 \\ 1 & 1 & 1 \\ 1 & 1 & 1 \end{bmatrix} \begin{bmatrix} i_a \\ i_b \\ i_c \end{bmatrix} - L_n \begin{bmatrix} 1 & 1 & 1 \\ 1 & 1 & 1 \\ 1 & 1 & 1 \end{bmatrix} \begin{bmatrix} \dot{i}_a \\ \dot{i}_b \\ \dot{i}_c \end{bmatrix} \quad \text{volts} \qquad [19]$$

$$= -\underline{R}_n \, \underline{i}_{abc} - \underline{L}_n \, \dot{\underline{i}}_{abc} \text{ volts}$$

Applying the Park-type transformation, Equation C-8, to the voltage equations leads to:

$$\begin{bmatrix} v_o \\ v_d \\ v_q \\ -v_F \\ 0 \\ 0 \end{bmatrix} = -\begin{bmatrix} r+3r_n & 0 & 0 & 0 & 0 & 0 \\ 0 & r & +\omega L_q & 0 & 0 & +\omega\sqrt{3/2}M_Q \\ 0 & -\omega L_d & r & -\omega\sqrt{3/2}M_F & -\omega\sqrt{3/2}M_D & 0 \\ 0 & 0 & 0 & r_F & 0 & 0 \\ 0 & 0 & 0 & 0 & r_D & 0 \\ 0 & 0 & 0 & 0 & 0 & r_Q \end{bmatrix} \begin{bmatrix} i_o \\ i_d \\ i_q \\ i_F \\ i_D \\ i_Q \end{bmatrix}$$

(Equation continued on next page)

$$-\begin{bmatrix} L_o+3L_n & 0 & 0 & 0 & 0 & 0 \\ 0 & L_d & 0 & +\sqrt{3/2}M_F & +\sqrt{3/2}M_D & 0 \\ 0 & 0 & L_q & 0 & 0 & +\sqrt{3/2}M_Q \\ 0 & +\sqrt{3/2}M_F & 0 & L_F & M_R & 0 \\ 0 & +\sqrt{3/2}M_D & 0 & M_R & L_D & 0 \\ 0 & 0 & +\sqrt{3/2}M_Q & 0 & 0 & L_Q \end{bmatrix} \begin{bmatrix} \dot{i}_o \\ \dot{i}_d \\ \dot{i}_q \\ \dot{i}_F \\ \dot{i}_D \\ \dot{i}_Q \end{bmatrix} \quad \text{volts} \qquad [C\text{-}11]$$

Using Equations C-9 and C-11 and defining p as d/dt the machine voltage equations can be written as:

$$\begin{bmatrix} v_o \\ v_d \\ v_q \\ -v_F \\ 0 \\ 0 \end{bmatrix} = -\begin{bmatrix} r+3r_n+3L_np & 0 & 0 & 0 & 0 & 0 \\ 0 & r & 0 & 0 & 0 & 0 \\ 0 & 0 & r & 0 & 0 & 0 \\ 0 & 0 & 0 & r_F & 0 & 0 \\ 0 & 0 & 0 & 0 & r_D & 0 \\ 0 & 0 & 0 & 0 & 0 & r_Q \end{bmatrix} \begin{bmatrix} i_o \\ i_d \\ i_q \\ i_F \\ i_D \\ i_Q \end{bmatrix}$$

$$-\begin{bmatrix} p & 0 & 0 & 0 & 0 & 0 \\ 0 & p & \omega & 0 & 0 & 0 \\ 0 & -\omega & p & 0 & 0 & 0 \\ 0 & 0 & 0 & p & 0 & 0 \\ 0 & 0 & 0 & 0 & p & 0 \\ 0 & 0 & 0 & 0 & 0 & p \end{bmatrix} \begin{bmatrix} \lambda_o \\ \lambda_d \\ \lambda_q \\ \lambda_F \\ \lambda_D \\ \lambda_Q \end{bmatrix} \quad \text{volts} \qquad [C\text{-}12]$$

If we now select an appropriate set of base quantities and then normalize the above equations the same form of equations results except that we may now use subscript "u" to indicate per unit quantities (4, 5,

116). In the remaining part of the development of the nonlinear model we will assume the equations have been appropriately normalized and that we are now dealing with per unit quantities without necessarily using the subscript u.

2. Equivalent circuits

The equivalent circuits of the synchronous machine can be developed from the per unit form of Equations C-10 and C-11. Consider the per unit form of Equation C-10 with λ_o now referred to as λ_o^*.

$$\begin{bmatrix} \lambda_o^* \\ \lambda_d \\ \lambda_q \\ \lambda_F \\ \lambda_D \\ \lambda_Q \end{bmatrix} = \begin{bmatrix} (L_o-\ell_o)+\ell_o & 0 & 0 & 0 & 0 & 0 \\ 0 & (L_d-\ell_d)+\ell_d & 0 & +\sqrt{3/2}M_F & +\sqrt{3/2}M_D & 0 \\ 0 & 0 & (L_q-\ell_q)+\ell_q & 0 & 0 & +\sqrt{3/2}M_Q \\ 0 & +\sqrt{3/2}M_F & 0 & (L_F-\ell_F)+\ell_F & M_R & 0 \\ 0 & +\sqrt{3/2}M_D & 0 & M_R & (L_D-\ell_D)+\ell_D & 0 \\ 0 & 0 & +\sqrt{3/2}M_Q & 0 & 0 & (L_Q-\ell_Q)+\ell_Q \end{bmatrix} \begin{bmatrix} i_o \\ i_d \\ i_q \\ i_F \\ i_D \\ i_Q \end{bmatrix} \quad \text{per unit} \qquad [C\text{-}13]$$

The inductance terms in one equation can be expressed in terms of the other inductances in the same equation by setting the current corresponding to that row of equation to 1.0 and setting all other currents to zero. It is found that the per unit mutual inductances in the d-axis are all equal so that one can define the magnetizing inductance in the d-axis as:

$$L_{AD} = (L_d-\ell_a) = \sqrt{3/2}M_F = \sqrt{3/2}M_D = (L_F-\ell_F) = M_R = (L_D-\ell_D) \qquad [C\text{-}14]$$

Similarly it is found that the per unit mutual inductances in the q-axis are also the same and the magnetizing inductance in the q-axis

may be defined as:

$$L_{AQ} = (L_q - \ell_a) = \sqrt{3/2}M_Q = (L_Q - \ell_Q) \qquad [C\text{-}15]$$

where ℓ_a denotes the armature leakage inductance in per unit and is the same in both axes, that is:

$$\ell_a = \ell_d = \ell_q$$

The flux linkage equation C-11 may be rewritten as:

$$\begin{aligned}
\lambda_o^* &= L_o i_o \\
\lambda_d &= \lambda_{AD} + \ell_a i_d \\
\lambda_q &= \lambda_{AQ} + \ell_a i_q \\
\lambda_F &= \lambda_{AD} + \ell_F i_F \qquad \text{per unit} \\
\lambda_D &= \lambda_{AD} + \ell_D i_D \\
\lambda_Q &= \lambda_{AQ} + \ell_Q i_Q
\end{aligned} \qquad [C\text{-}16]$$

where

$$\lambda_{AD} = L_{AD}(i_d + i_F + i_D) \qquad [C\text{-}17]$$

$$\lambda_{AQ} = L_{AQ}(i_q + i_Q) \qquad \text{per unit} \qquad [C\text{-}18]$$

Similarly the per unit form of the voltage Equation C-11 may be rewritten in terms of the mutual and leakage flux linkages as:

$$\begin{aligned}
v_o &= -(r+3r_n)i_o - p\lambda_o \quad \text{where } \lambda_o = i_o(L_o+3L_n) \\
v_d &= -ri_d - \omega\lambda_q - p\lambda_{AD} - \ell_a p i_d \\
v_q &= -ri_q + \omega\lambda_d - p\lambda_{AQ} - \ell_a p i_q \qquad \text{per unit} \\
-v_F &= -r_F i_F - p\lambda_F = -r_F i_F - p\lambda_{AD} - \ell_F p i_F \\
0 &= -r_D i_D - p\lambda_{AD} - \ell_D p i_D \\
0 &= -r_Q i_Q - p\lambda_{AQ} - \ell_Q p i_Q
\end{aligned} \qquad [C\text{-}19]$$

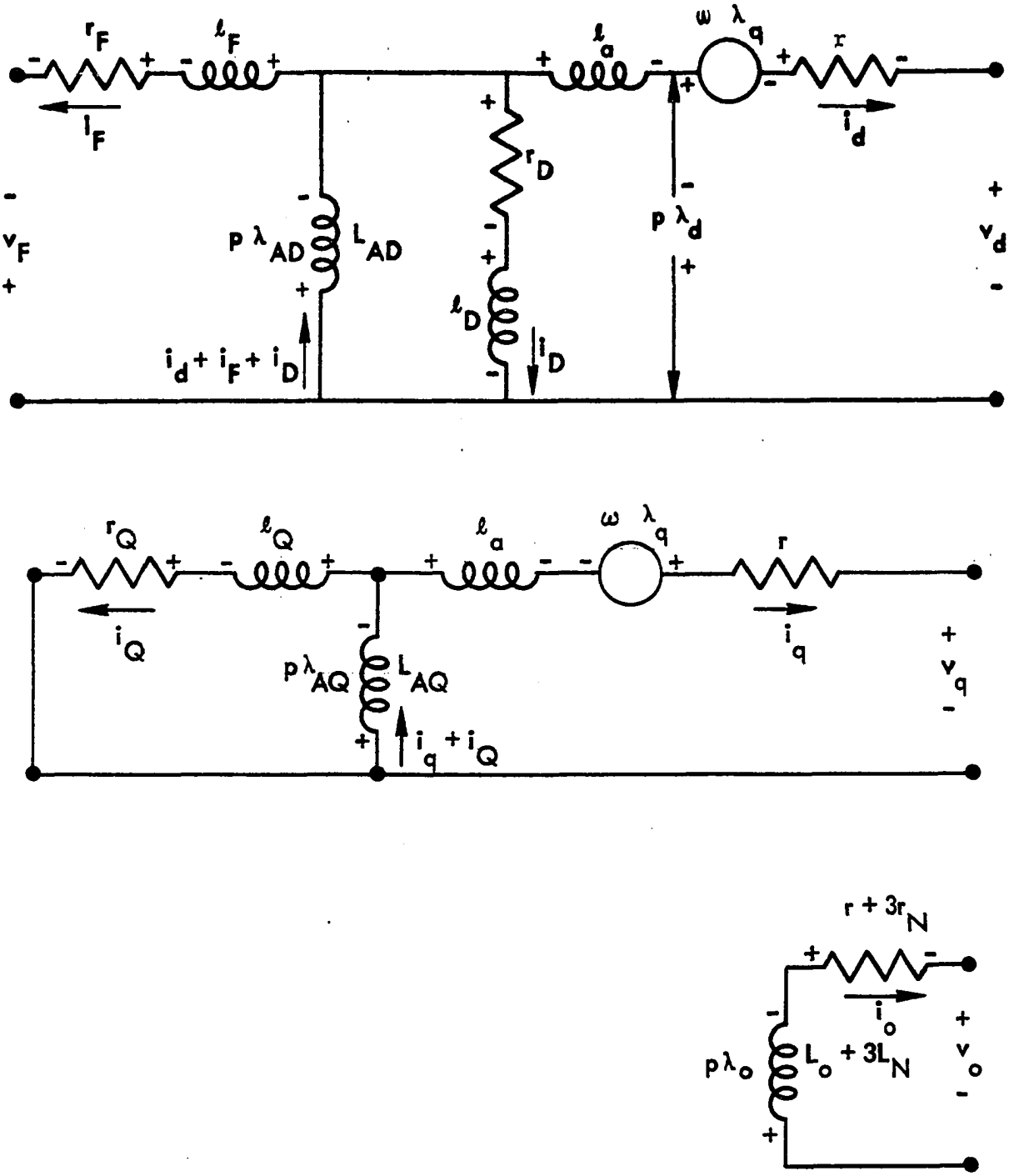

Figure 87. Equivalent circuits for synchronous machine

Equation C-19 describes the equivalent circuits shown in Figure 87.

3. Analog computer equations and diagrams

Solving Equation C-16 for the currents we have:

$$i_o = \frac{\lambda_o}{L_o + 3L_n}$$

$$i_d = \frac{\lambda_d - \lambda_{AD}}{\ell_a}$$

$$i_q = \frac{\lambda_q - \lambda_{AQ}}{\ell_a}$$

$$i_F = \frac{\lambda_F - \lambda_{AD}}{\ell_F} \qquad \text{per unit} \qquad [C\text{-}20]$$

$$i_D = \frac{\lambda_D - \lambda_{AD}}{\ell_D}$$

$$i_Q = \frac{\lambda_Q - \lambda_{AQ}}{\ell_Q}$$

From Equation C-17:

$$\lambda_{AD} = L_{AD}[i_d + i_F + i_D] \qquad [C\text{-}17]$$

$$= L_{AD}\left[\frac{\lambda_d - \lambda_{AD}}{\ell_a} + \frac{\lambda_F - \lambda_{AD}}{\ell_F} + \frac{\lambda_D - \lambda_{AD}}{\ell_D}\right]$$

$$= L_{AD}\left[\frac{\lambda_d}{\ell_a} + \frac{\lambda_F}{\ell_F} + \frac{\lambda_D}{\ell_D} - \lambda_{AD}\left[\frac{1}{\ell_a} + \frac{1}{\ell_F} + \frac{1}{\ell_D}\right]\right]$$

$$\lambda_{AD}\left[\frac{1}{L_{AD}}+\frac{1}{\ell_a}+\frac{1}{\ell_F}+\frac{1}{\ell_D}\right]L_{AD}=\left[\frac{\lambda_d}{\ell_a}\quad\frac{\lambda_F}{\ell_F}\quad\frac{\lambda_D}{\ell_D}\right]L_{AD}$$

$$\lambda_{AD} = L_{MD}\left[\frac{\lambda_d}{\ell_a}+\frac{\lambda_F}{\ell_F}+\frac{\lambda_D}{\ell_D}\right] \qquad [C-21]$$

where

$$L_{MD} \triangleq \frac{1}{\frac{1}{L_{AD}}+\frac{1}{\ell_a}+\frac{1}{\ell_F}+\frac{1}{\ell_D}} \qquad [C-22]$$

Similarly from Equation C-18:

$$\lambda_{AQ} = L_{AQ}[i_q + i_Q] \qquad [C-18]$$

$$\lambda_{AQ} = L_{AQ}\left[\frac{\lambda_q - \lambda_{AQ}}{\ell_a}+\frac{\lambda_Q - \lambda_{AQ}}{\ell_Q}\right]$$

$$= L_{AQ}\left(\frac{\lambda_q}{\ell_a}+\frac{\lambda_Q}{\ell_Q}-\lambda_{AQ}\left(\frac{1}{\ell_a}+\frac{1}{\ell_Q}\right)\right)$$

$$\lambda_{AQ}\left[\frac{1}{L_{AQ}}+\frac{1}{\ell_a}+\frac{1}{\ell_a}\right]L_{AQ} = L_{AQ}\left(\frac{\lambda_q}{\ell_a}+\frac{\lambda_Q}{\ell_a}\right)$$

$$\lambda_{AQ} = L_{MQ}\left[\frac{\lambda_q}{\ell_a}+\frac{\lambda_Q}{\ell_Q}\right] \qquad [C-22]$$

where

$$L_{MQ} \triangleq \frac{1}{\frac{1}{L_{AQ}}+\frac{1}{\ell_a}+\frac{1}{\ell_Q}} \qquad [C-23]$$

Equation C-19 can now be solved for the flux linkages using the above quantities and the fact that

$$p_u = \frac{d}{dt_u} = \frac{1}{\omega_B}\frac{d}{dt} \qquad [C-24]$$

where

u indicates per unit

ω_B is the base speed or synchronous speed of the machine.

The results of these manipulations are:

$$\lambda_o = -\omega_B \int (v_o + \frac{r + 3r_n}{L_o + 3L_n}\lambda_o)dt \qquad [C-25]$$

$$\lambda_d = \omega_B \int [-v_d + \frac{r}{\ell_a}(\lambda_{AD} - \lambda_d) - \frac{\omega}{\omega_B}\lambda_q] dt \qquad [C-26]$$

$$\lambda_q = \omega_B \int [-v_q - \frac{r(\lambda_q - \lambda_{AQ})}{\ell_a} + \frac{\omega}{\omega_B}\lambda_d] dt \qquad [C-27]$$

$$\lambda_F = \omega_B \int [v_F + \frac{r_F}{\ell_F}(\lambda_{AD} - \lambda_F)] dt \qquad [C-28]$$

$$\lambda_D = \omega_B \int + \frac{r_D(\lambda_{AD} - \lambda_D)}{\ell_D} dt \qquad [C-29]$$

$$\lambda_Q = \omega_B \int \frac{r_Q}{\ell_Q}(\lambda_{AQ} - \lambda_Q)\, dt \qquad [C-30]$$

The next step in the development of the analog computer equations is to write the mechanical torque equations and express them in a form suitable for the analog computer simulation. The motion of the machine rotor may be expressed as:

$$J \frac{2}{p} \frac{d\omega}{dt} = \tau_m - \tau_e \quad \text{newton meters} \qquad [C-31]$$

where

J = rotor inertia kilogram meter^2

p = the number of poles of the machine

ω = speed of rotor in radians/sec

τ_m, τ_e = mechanical and electrical torque, respectively, newton meters

The form of Equation C-31 remains the same when expressed in per unit. Assuming base quantities compatible to those used for the flux linkages and voltage equations have been determined, the form of Equation C-31 that can be used on the analog computer is:

$$\Delta\omega \triangleq \frac{p}{2}\left[\frac{1}{2H}\right]\int \tau_a dt \qquad [C-32]$$

where

$$\tau_a = \tau_m - \tau_e \qquad [C-33]$$

$$H = \frac{\text{inertially stored energy at synchronous speed}}{\text{rated KVA of machine}} \quad \text{sec} \qquad [C-34]$$

$\Delta\omega$ = speed deviation from the synchronous speed

From the above definition of $\Delta\omega$ we note that the machine speed ω at any instant can be expressed as:

$$\omega = \omega_o + \Delta\omega \qquad [C-35]$$

where

ω_o is the initial value and equals 1.

The angle θ appearing in Figure 8, the pictorial representation of a synchronous machine, can be expressed as

$$\theta = \omega_B t + \delta + 90° \quad \text{electrical radians} \qquad [C-36]$$

where

δ is the angle between the infinite bus voltage and the q-axis of the machine.

$$\text{Define } \omega \triangleq \dot{\theta} = \omega_B + \dot{\delta} \qquad [C-37]$$

Thus from Equations C-35 and C-37 we have that:

$$\Delta\omega = \dot{\delta} \quad \text{radians/sec} \qquad [C-38]$$

$$\delta = \int \Delta\omega dt + \delta_o \quad \text{radians} \qquad [C-39]$$

$$\delta = (57.3 \frac{\text{degrees}}{\text{radian}}) [\omega_B \int \Delta\omega dt + \delta_o] \quad \text{mechanical degrees} \qquad [C-40]$$

The electrical torque for the machine and the terminal voltage may, respectively, be expressed as (73, 116):

$$\tau_e = \frac{p}{2} [\lambda_d i_q - \lambda_q i_d] \qquad [C-41]$$

$$v_{todq} = \sqrt{3}\, v_{tabc} = \sqrt{v_d^2 + v_q^2} \qquad [C-42]$$

Figure 88 shows phase a of a synchronous machine connected to an infinite bus through a transmission line. If V_B is defined as the rms value of the infinite bus line-to-neutral voltage, the infinite bus voltages in the three phases may be expressed as:

$$\begin{aligned} V_{a\infty} &= \sqrt{2}\, V_B \cos \omega_B t \\ V_{b\infty} &= \sqrt{2}\, V_B \cos(\omega_B t - 120) \\ V_{c\infty} &= \sqrt{2}\, V_B \cos(\omega_B t + 120) \end{aligned} \qquad \text{volts} \qquad [C\text{-}43]$$

or

$$\underline{V}_{abc\infty} = \sqrt{2}\, V_B \begin{bmatrix} \cos \omega_B t \\ \cos(\omega_B t - 120) \\ \cos(\omega_B t + 120) \end{bmatrix} \text{ volts} \qquad [C\text{-}44]$$

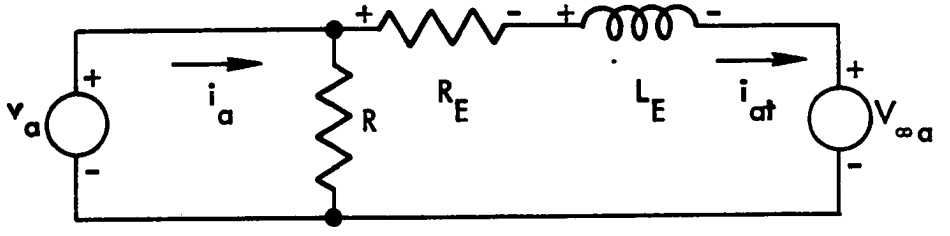

Figure 88. Synchronous machine connected to an infinite bus through a transmission line

Figures similar to Figure 88 can be drawn for phases b and c. The voltages for the three circuits can be expressed as:

$$\underline{v}_{abc} = \underline{V}_{abc\infty} + R_E \underline{i}_{abc} + L_E \dot{\underline{i}}_{abc} \qquad \text{volts} \qquad [C\text{-}45]$$

Applying the Park-type transformation, Equation C-8 to Equation C-45, and simplifying the results lead to:

$$\begin{bmatrix} v_o \\ v_d \\ v_q \end{bmatrix} = \sqrt{3}\, V_B \begin{bmatrix} 0 \\ -\sin\delta \\ +\cos\delta \end{bmatrix} + R_E \begin{bmatrix} i_o \\ i_d \\ i_q \end{bmatrix} + L_E \begin{bmatrix} \dot{i}_o \\ \dot{i}_d \\ \dot{i}_q \end{bmatrix} - \omega L_E \begin{bmatrix} 0 & 0 & 0 \\ 0 & 0 & -1 \\ 0 & 1 & 0 \end{bmatrix} \begin{bmatrix} i_o \\ i_d \\ i_q \end{bmatrix} \quad [C\text{-}46]$$

The d- and q-axes voltage equations are solved for $\dot{i}_{dt}$ and $\dot{i}_{qt}$ where the subscript t indicates currents flowing from the generator terminals to the infinite bus. The results are:

$$\dot{i}_{dt} = \frac{1}{L_E P}\left[v_d + \sqrt{3}\, V_B \sin\delta - R_E i_{dt} - \omega L_E i_{qt}\right] \quad [C\text{-}47]$$

$$\dot{i}_{qt} = \frac{1}{L_E P}\left[v_q - \sqrt{3}\, V_B \cos\delta - R_E i_{qt} + \omega L_E i_{dt}\right] \quad [C\text{-}48]$$

After introducing an appropriate normalization the form of Equations C-47 and C-48 suitable for the analog computer setup are:

$$i_{dt} = \frac{\omega_B}{L_E}\int \left[v_d + \sqrt{3}\sin\delta - R_E i_{dt} - \omega L_E i_{qt}\right]dt \quad [C\text{-}49]$$

$$i_{qt} = \frac{\omega_B}{L_E}\int \left[v_q - \sqrt{3}\cos\delta - R_E i_{qt} + \omega L_E i_{dt}\right]dt \quad [C\text{-}50]$$

If a large resistance R is placed at the machine terminals the voltages v_d and v_q can be expressed in terms of the currents i_q, i_d, i_{qt} and i_{dt} as (116):

$$v_d = R(i_d - i_{dt}) \quad [C\text{-}51]$$

$$v_q = R(i_q - i_{qt}) \quad [C\text{-}52]$$

$$\lambda_{AD} = L_{MD}\left[\frac{\lambda_d}{\ell_a} + \frac{\lambda_F}{\ell_F} + \frac{\lambda_D}{\ell_D}\right] \qquad [C\text{-}21]$$

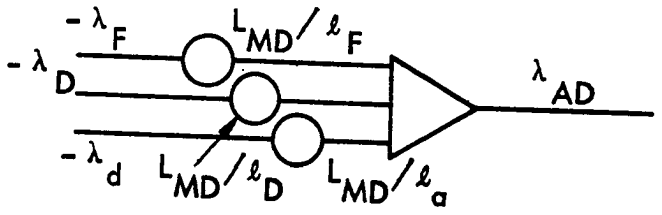

$$\lambda_d = \omega_B \int \left[-v_d + \frac{r}{\ell_a}(\lambda_{AD} - \lambda_d) - \frac{\omega}{\omega_B}\lambda_q\right] dt \qquad [C\text{-}26]$$

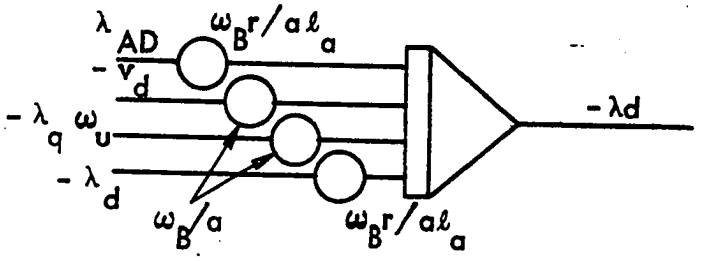

$$\lambda_F = \omega_B \int \left[v_F + \frac{r_F}{\ell_F}(\lambda_{AD} - \lambda_F)\right] dt \qquad [C\text{-}28]$$

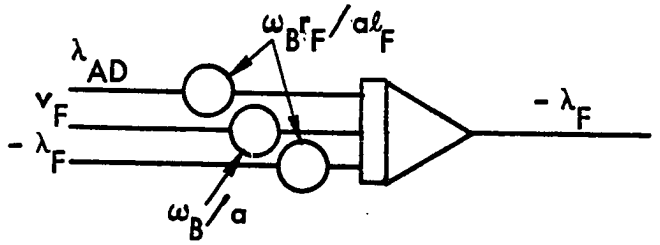

$$\lambda_D = \omega_B \int \frac{r_D(\lambda_{AD} - \lambda_D)}{\ell_D} dt \qquad [C\text{-}29]$$

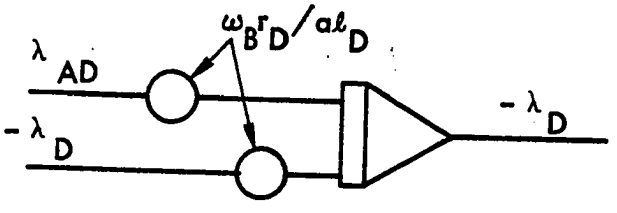

Figure 89. Analog computer diagrams for direct axis equations

$$\lambda_{AQ} = L_{MQ}\left[\frac{\lambda_q}{\ell_a} + \frac{\lambda_Q}{\ell_Q}\right] \qquad [C\text{-}22]$$

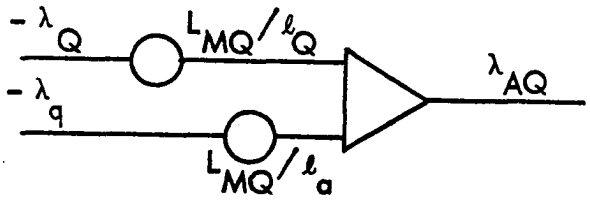

$$\lambda_q = \omega_B \int \left[-v_q - \frac{r(\lambda_q - \lambda_{AQ})}{\ell_a} + \frac{\omega}{\omega_B}\lambda_d\right] dt \qquad [C\text{-}27]$$

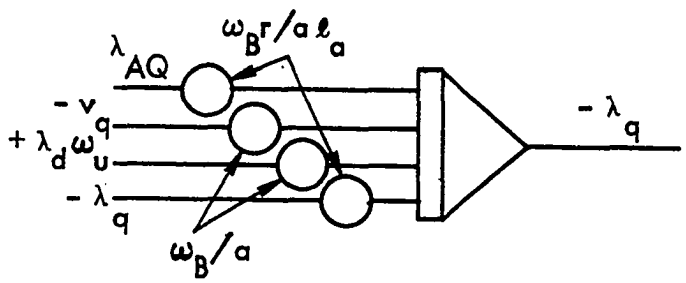

$$\lambda_Q = \omega_B \int \frac{r_Q(\lambda_{AQ} - \lambda_Q)}{\ell_Q}\, dt \qquad [C\text{-}30]$$

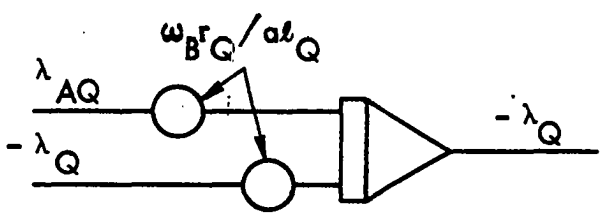

Figure 90. Analog computer diagrams for quadrature axis equations

$$\tau_e = \frac{p}{2} [\lambda_d i_q - \lambda_q i_d] \qquad [C-41]$$

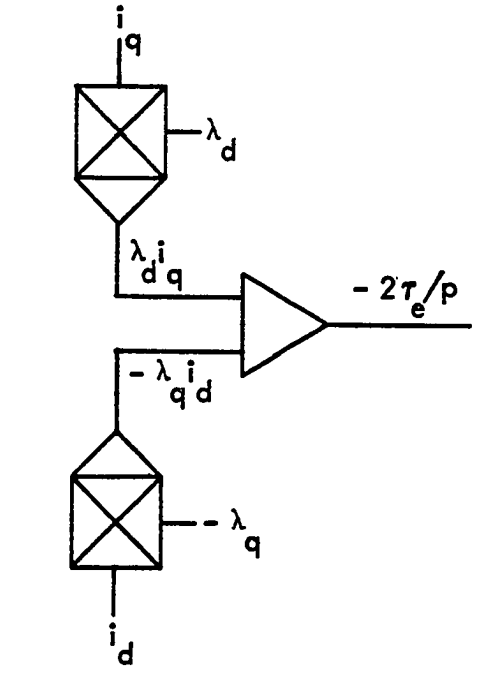

$$\tau_a = \tau_m - \tau_e \qquad [C-33]$$

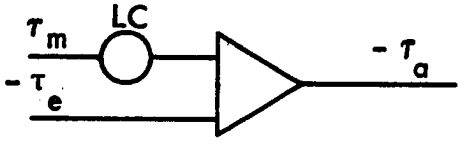

Figure 91. Analog computer diagrams for torque equations

$$\Delta\omega = \frac{p}{2}\frac{1}{2H}\int \tau_a \, dt \qquad [C\text{-}32]$$

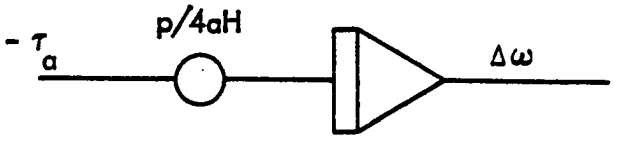

$$\omega = \Delta\omega + 1 \qquad (C\text{-}35]$$

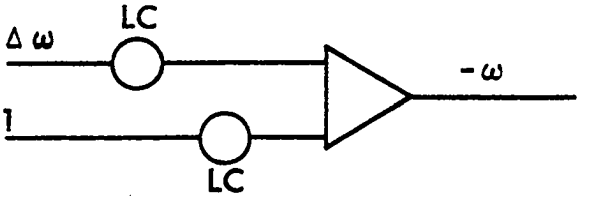

$$\delta = 47.3[\omega_B \int \Delta\omega \, dt + \delta_o] \qquad [C\text{-}40]$$

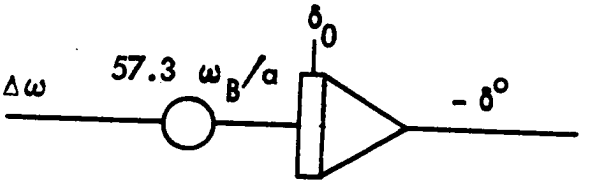

Figure 92. Analog computer diagrams for mechanical equations

$$i_{dt} = \frac{\omega_B}{L_E} \int [v_d + \sqrt{3} \sin \delta - R_E i_{dt} - \omega L_E i_{qt}] \, dt \qquad [C\text{-}49]$$

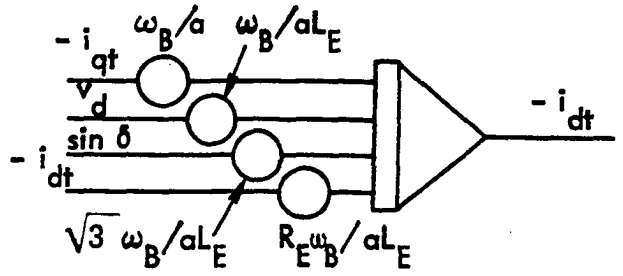

$$i_{qt} = \frac{\omega_B}{L_E} \int [v_q - \sqrt{3} \cos \delta - R_E i_{qt} + \omega L_E i_{dt}] \, dt \qquad [C\text{-}50]$$

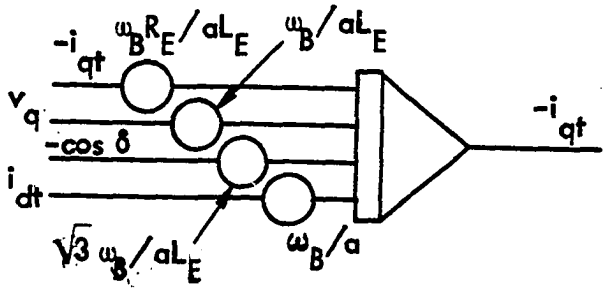

$$v_d = R(i_d - i_{dt}) \qquad [C\text{-}51]$$

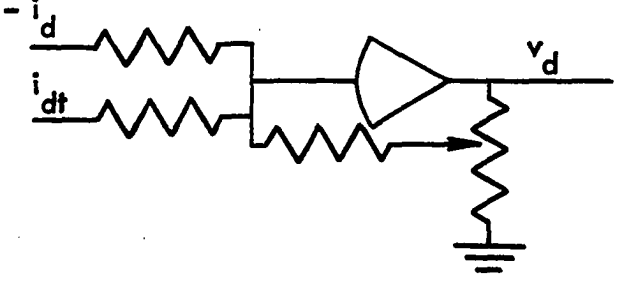

$$v_q = R(i_q - i_{qt}) \qquad [C\text{-}52]$$

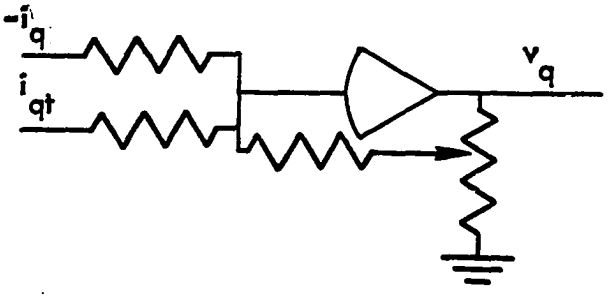

Figure 93. Analog computer diagrams for load equations

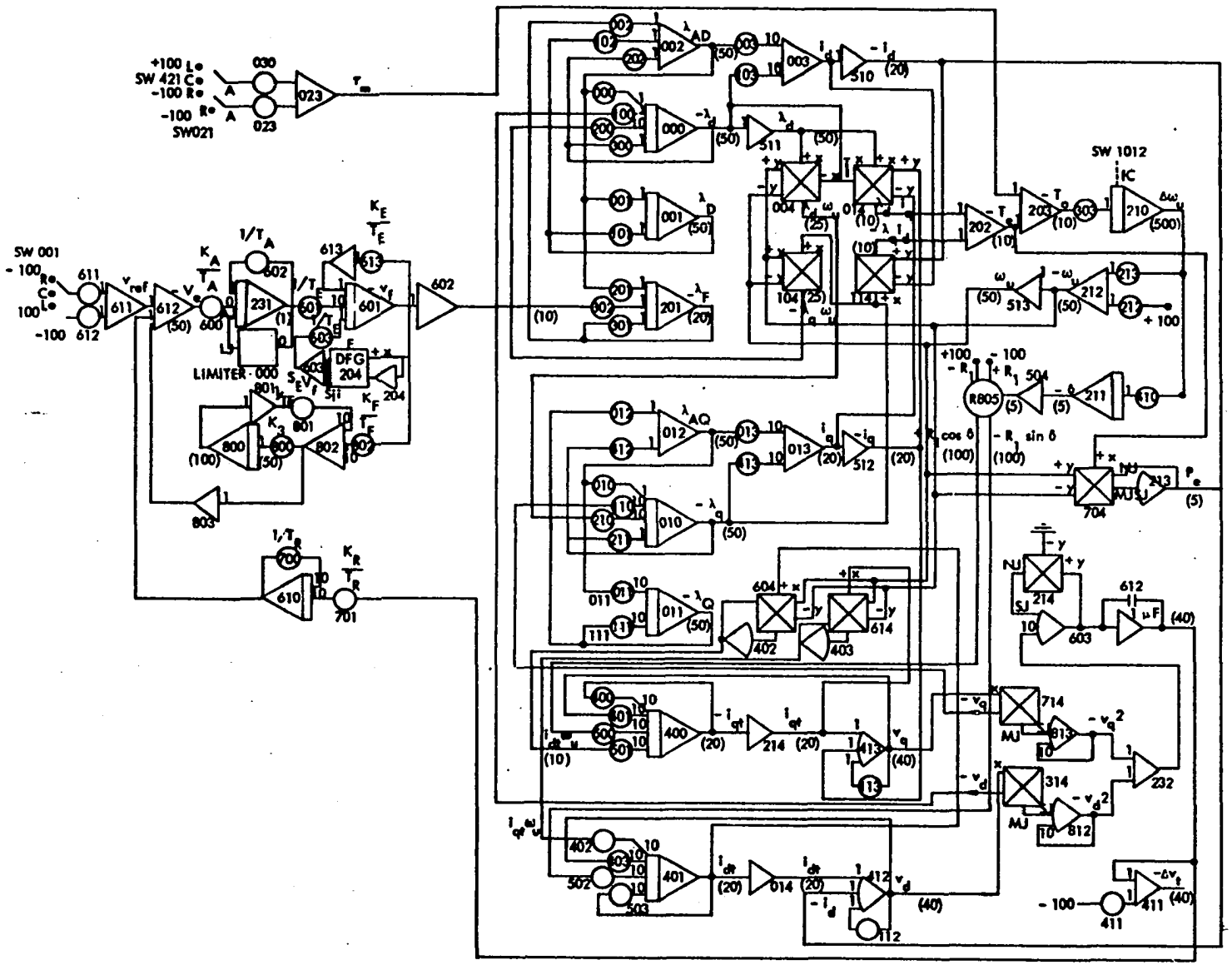

Figure 94. Simulation diagram for model IV with the slow exciter

The governor is considered to be comparatively slow for the period of time considered in this study and, therefore, the governor is not represented. This is an example of how duration of effects of a particular section of the system can serve as a means of simplifying a model (see first part of Chapter III).

The analog computer diagrams of the equations presented in this section and which are used in the simulation diagram for the synchronous machine are shown in Figures 89-93. The complete simulation diagram with the slow exciter is shown in Figure 94.

4. Machine data and potentiometer settings for model IV

Table 24 shows the machine data (5). Unless otherwise stated all the values in the table are in per unit. The potentiometer settings for the machine are given in Table 25. The data and the settings for the excitation system have been presented in Appendix A.

Table 24. Machine data

$L_d = 1.70$	$\ell_D = 0.055$	$r_q = 0.0198$
$L_q = 1.64$	$L_D = 1.605$	$R = 100$
$\ell_a = 0.15$	$\ell_Q = 0.036$	$L_{MD} = 0.02818$
$L_{AD} = 1.55$	$L_Q = 1.526$	$L_{MQ} = 0.02846$
$L_{AQ} = 1.49$	$r = 0.001126$	
$\ell_f = 0.101$	$r_F = 0.00805$	
$L_F = 1.65$	$r_D = 0.0132$	
$H = 2.37$ sec		
$T'_{do} = 5.90$ sec		

Table 25. Potentiometer settings for synchronous machine

Potentiometer number	Potentiometer settings	Amplifier gain	Constant	Numerical substitutions	Value	Scaling	Value x scaling
000	0.0283	1	$r\omega_B/\ell_a$	.001126(377)/.15	2.8300	0.010	0.0283
001	0.9040	1	$r_D\omega_B/\ell_D$	.0132(377)/.055	90.400	0.010	0.9040
002	0.6960	1	L_{MD}/ℓ_F	.02818/.101	0.2785	2.500	0.6960
003	0.2665	10	$1/\ell_a$	1/.15	6.6660	0.400	2.6650
010	0.0283	1	$r\omega_B/\ell_a$	.001126(377)/.15	2.8300	0.010	0.0283
011	0.2070	10	$r_Q\omega_B/\ell_Q$	.0198(377)/.036	207.00	1.000	2.0700
012	0.7906	1	L_{MQ}/ℓ_Q	.02846/.036	0.7906	1.000	0.7906
013	0.2665	10	$1/\ell_a$		6.6660	0.400	2.6650
100	0.4710	10	ω_B		377.00	0.0125	4.7100
101	0.9040	1	$r_D\omega_B/\ell_D$		90.400	0.010	0.9040
102	0.5120	1	L_{MD}/ℓ_D	.02818/.055	0.5120	1.000	0.5120
103	0.2665	10	$1/\ell_a$		6.6660	0.400	2.6650
110	0.4710	10	ω_B		377.00	0.0125	4.7100
111	0.2070	10	$r_Q\omega_B/\ell_Q$		207.00	0.010	2.0700
112	0.0050	1	R	100.	100.00	2.000	200.00
113	0.0050	1	R	100.	100.00	2.000	200.00
200	0.7540	10	ω_B		377.00	0.020	7.5400
201	0.1212	.1	$r_F\omega_B/\ell_F$	.000805(377)/.101	3.0300	0.004	.01212
202	0.1879	1	L_{MD}/ℓ_a	.02818/.15	0.1879	1.000	0.1879
210	0.7540	10	ω_B		377.00	0.020	7.5400
211	0.0283	1	$r\omega_B/\ell_a$	.001126(377)/.15	2.8300	0.010	0.0283
212	0.5000	1	ω_B/ω_B		1.0000	0.500	0.5000

Table 25 (Continued)

Potentiometer number	Potentiometer settings	Amplifier gain	Constant	Numerical substitutions	Value	Scaling	Value x scaling
213	0.1000	1	L.C.	1	1.0000	0.100	0.1000
300	0.0283	1	$r\omega_B/\ell_a$	.001126(377)/.15	2.8300	0.010	0.0283
301	0.3030	.1	$r_F\omega_B/\ell_F$		3.0300	0.010	0.0303
302	0.0778	.1	$\omega_B$xbase change	377(162v/157KV)	0.3890	0.020	0.00778
303	0.1055	1	p/2 1/2H	1/2(2.37)	0.2110	0.500	0.1055
400	0.0188	10	$R_E\omega_B/L_E$	.02(377)/.4	18.850	0.010	0.1885
401	0.4710	10	ω_B/L_E	377/.4	944.00	0.005	4.7100
402	0.7540	10	ω_B		377.00	0.020	7.5400
403	0.4710	10	ω_B/L_E		944.00	0.005	4.7100
410	0.2160	1	$57.3\omega_B$	57.3(377)	21,600	10^{-5}	0.2160
412	0.1897	1	L_{MQ}/ℓ_a	.02846/.15	0.1897	1.000	0.1897
413	0.2665	10	$1/\ell_a$		6.6660	0.400	2.6650
500	0.3264	10	$\sqrt{3}\omega_B/L_E$	3(377)/.4	1632.0	0.002	3.2640
501	0.7540	10	ω_B		377.00	0.020	7.5400
502	0.3264	10	$\sqrt{3}\omega_B/L_E$		1632.0	0.002	3.2640
503	0.0188	10	$R_E\omega_E/L_E$		18.850	0.010	0.1885
612	0.0291	1	5% full load				
613	0.5905	1	full load				
610	0.0300	1	10% full load	.3pu	0.3000	0.100	0.0300
611	0.3000	1	full load τ_m	3pu	3.0000	0.100	0.3000

B. Simulation of Model IV Under the Assumptions of Model III

Figure 95 shows the patching diagram used for the simulation of model IV under the assumptions used in developing model III. The changes made in this diagram as compared to Figure 94 include the connection of a feedback path from the output of integrator 210 to the input of summer 203 through inverter 233, potentiometer 812 and switch 401. Another change made in the analog patching is the connection of a mechanical switch 011 between inverter 602 and potentiometer 302. This connection permits the removal of the regulating system and then supplying a constant field voltage through potentiometer 810 and inverter 030.

The simulation technique used has been summarized in section B of Chapter V.

As mentioned in Chapter V, the value of D computed may be specified in two ways depending upon whether real time or normalized time is being used. The quantity indicated by the setting of potentiometer 812 is D/M and the appropriate scaling factor. However, M equals 2H and we can write:

$$\frac{D}{2H} \cdot \text{scaling} = \text{Pot. setting (P.S.)} \qquad \text{[C-53a]}$$

where scaling factor equals 10/500 in this case.

$$D = (\text{P.S.}) \frac{2H}{\text{scaling}} \qquad \text{[C-53b]}$$

H is defined as given by Equation C-34. The larger values of D given in Table 9 (see Chapter V) result from the use of per unit time. When the real time is used the smaller values of D shown in Table 9 apply.

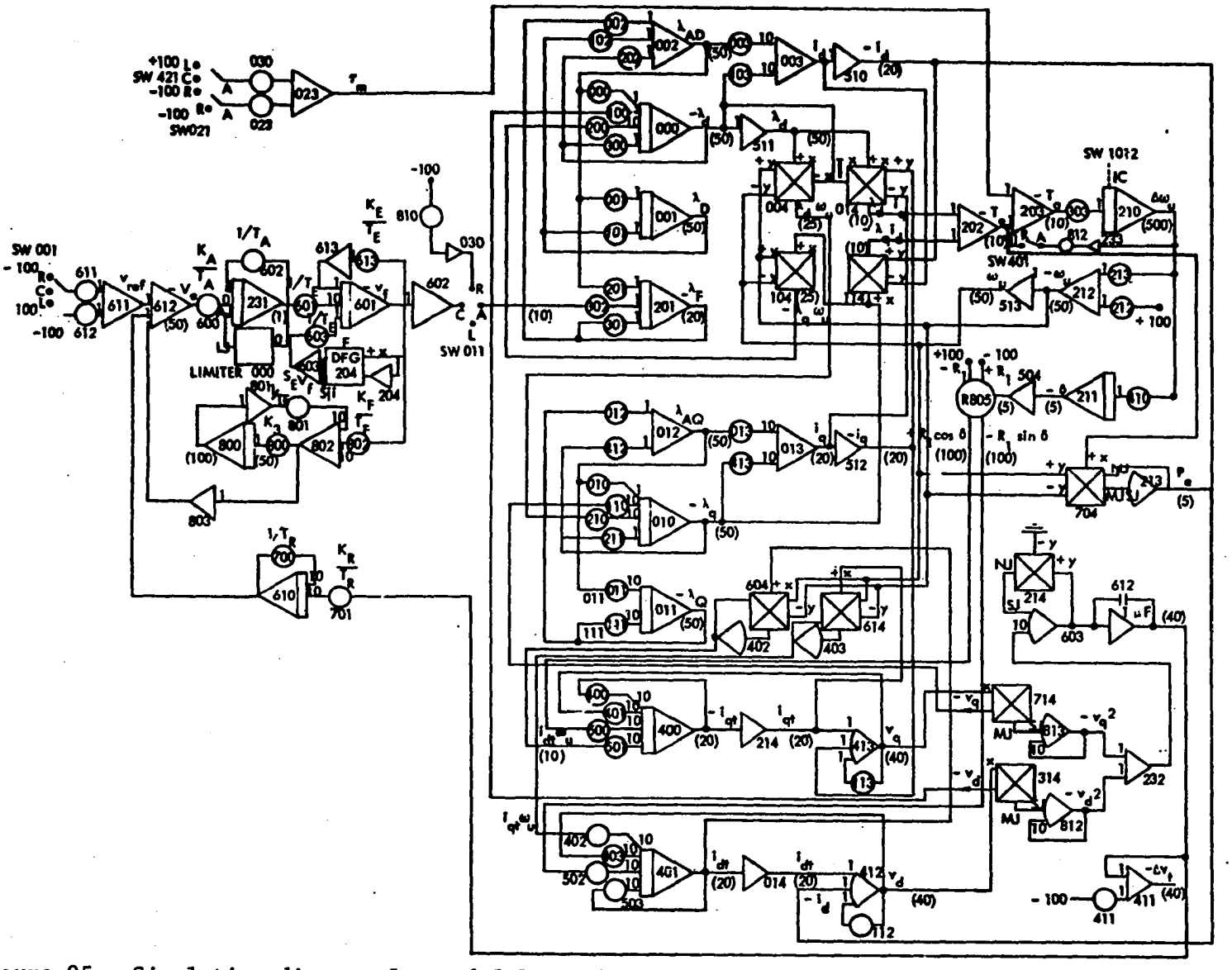

Figure 95. Simulation diagram for model IV with changes needed for assumptions of model III

$$H = \frac{\text{inertially stored energy at synchronous speed}}{\text{rated KVA of machine}} \quad \text{sec} \qquad [C\text{-}34]$$

C. Saliency Considerations

The two equations affected by the saliency considerations are:

$$L_{AQ} = L_Q - \ell_Q \qquad [C\text{-}15]$$

$$L_{MQ} = \frac{1}{\frac{1}{L_{AQ}} + \frac{1}{\ell_a} + \frac{1}{\ell_Q}} \qquad [C\text{-}23]$$

With L_Q equals 1.19 as discussed in Chapter VI and both ℓ_a and ℓ_Q as given in Table 24:

$$L_{AQ} = 1.19 - 0.15 = 1.04 \text{ per unit}$$

$$L_{MQ} = \frac{1}{\frac{1}{1.04} + \frac{1}{0.15} + \frac{1}{0.036}} = 0.0282$$

From the potentiometer settings given in Table 25, L_{MQ} appears in the settings for 012 and 412. Recomputing these settings leads to 0.7825 and 0.1880 for 012 and 412, respectively.

D. Saturation Functions

The no load saturation curve supplied with the machine data is shown in Figure 95. The saturation function g(v) can be defined as:

$$g(v) = \frac{\text{field current to give that voltage on the magnetization curve}}{\text{field current to give that voltage on the air gap line}} - 1$$

$$= \frac{i_{fm}}{i_{fa}} - 1 \qquad [C-54]$$

Using the no load curve and Equation C-54 the saturation function is calculated as shown in Table 26. The resulting saturation curve is shown in Figure 97. Since v is in per unit, this same curve applies for λ_{AD} and λ_{AQ} if we use the same function for d- and q-axes.

Since only two diode function generators are available, the exciter saturation function was approximated by two straight line segments. The segments are line $v_f = 0$ and the broken lines shown in Figures 79 and 80 in Appendix A. The slopes for the two lines are 3.75 and 4.70 for slow and fast exciters, respectively. Saturation considerations alter Equations C-21 and C-22 as shown in Figure 98. Figure 99 shows simulation diagram used for saturation considerations.

Table 26. Computation of the machine saturation function

v_{abc} p.u.	$v_{odq} = \sqrt{3}\, v_{abc}$ p.u.	i_{fm} amps.	i_{fa} amps.	$\frac{i_{fm}}{i_{fa}}$	g(v)	v_{odq} volts	g(v) volts
0.750	1.300	260	260	1.0000	0.0000	65.00	0.000
0.850	1.400	305	292	1.0445	0.0445	70.00	2.225
0.950	1.645	357	327	1.0917	0.0917	82.25	4.585
1.000	1.732	390	342	1.1404	0.1404	86.60	7.020
1.050	1.820	430	360	1.1944	0.1944	91.00	9.720
1.075	1.865	450	370	1.2162	0.2162	93.25	10.810
1.100	1.905	480	378	1.2698	0.2698	95.25	13.490
1.125	1.930	515	385	1.3377	0.3377	96.50	16.885
1.150	1.992	550	395	1.3924	0.3924	99.60	19.620
1.175	2.018	600	400	1.5000	0.5000	100.90	25.000

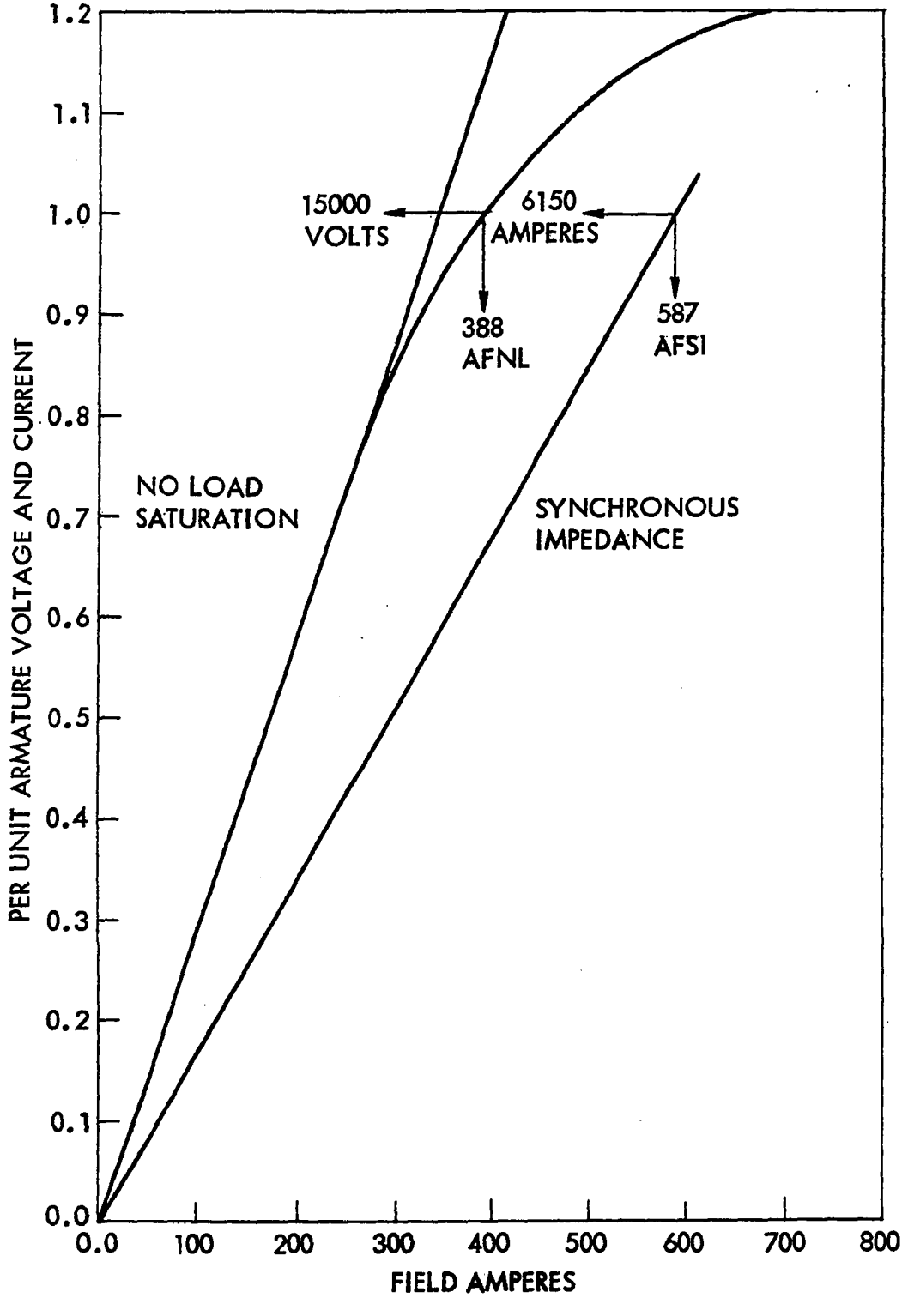

Figure 96. No load saturation curve for the synchronous machine

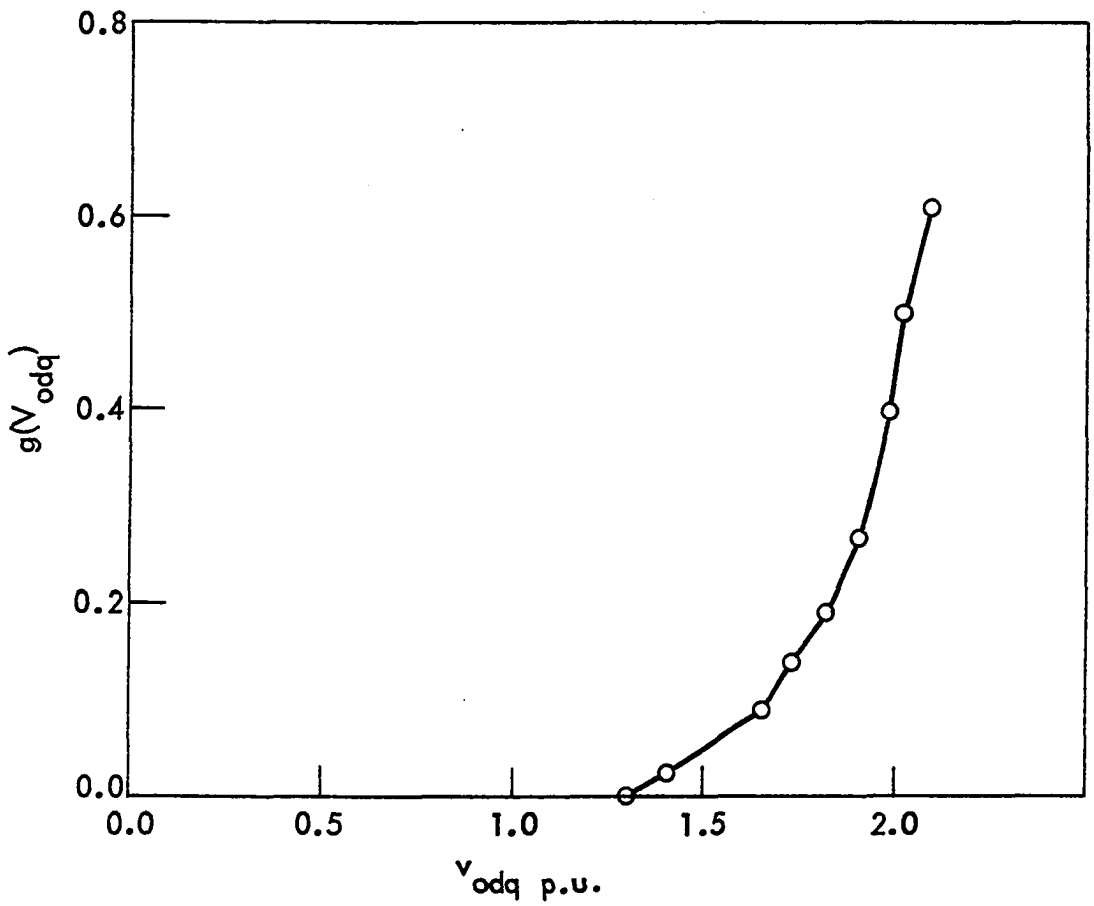

Figure 97. Saturation function for model IV

$$\lambda_{AD} = L_{MD}\left[\frac{\lambda_d}{\ell_a} + \frac{\lambda_F}{\ell_F} + \frac{\lambda_D}{\ell_D}\right] - g(\lambda_{AD}) \qquad \text{[C-21']}$$

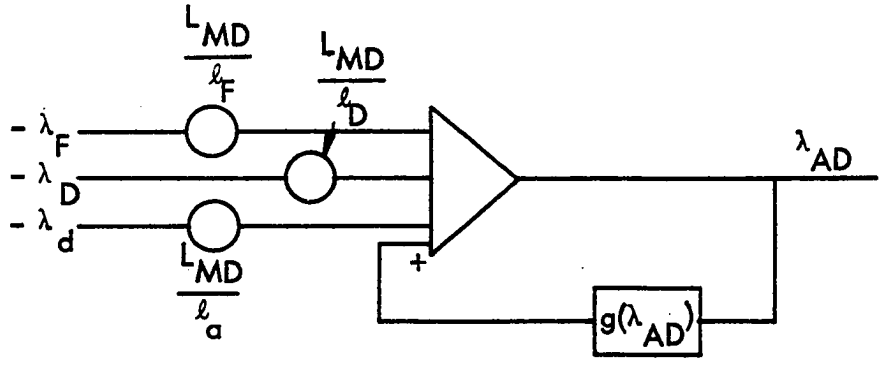

$$\lambda_{AQ} = L_{MQ}\left[\frac{\lambda_q}{\ell_a} + \frac{\lambda_Q}{\ell_Q}\right] - g(\lambda_{AQ}) \qquad \text{[C-22']}$$

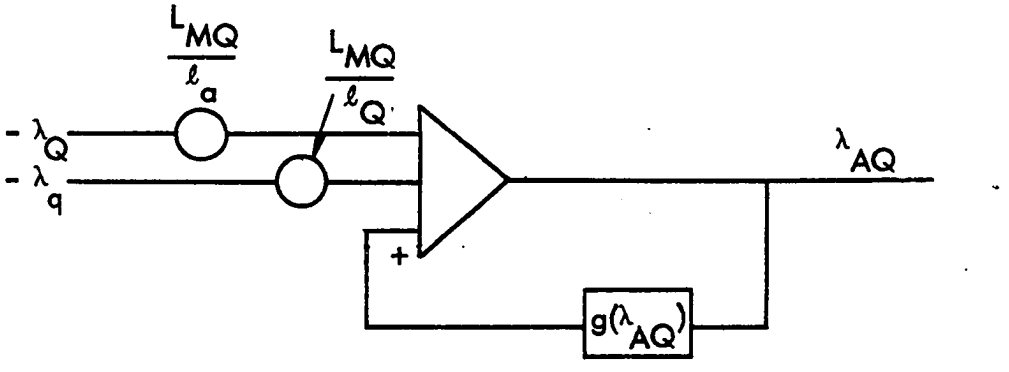

Figure 98. Analog computer diagrams for λ_{AD} and λ_{AQ} with saturation effects

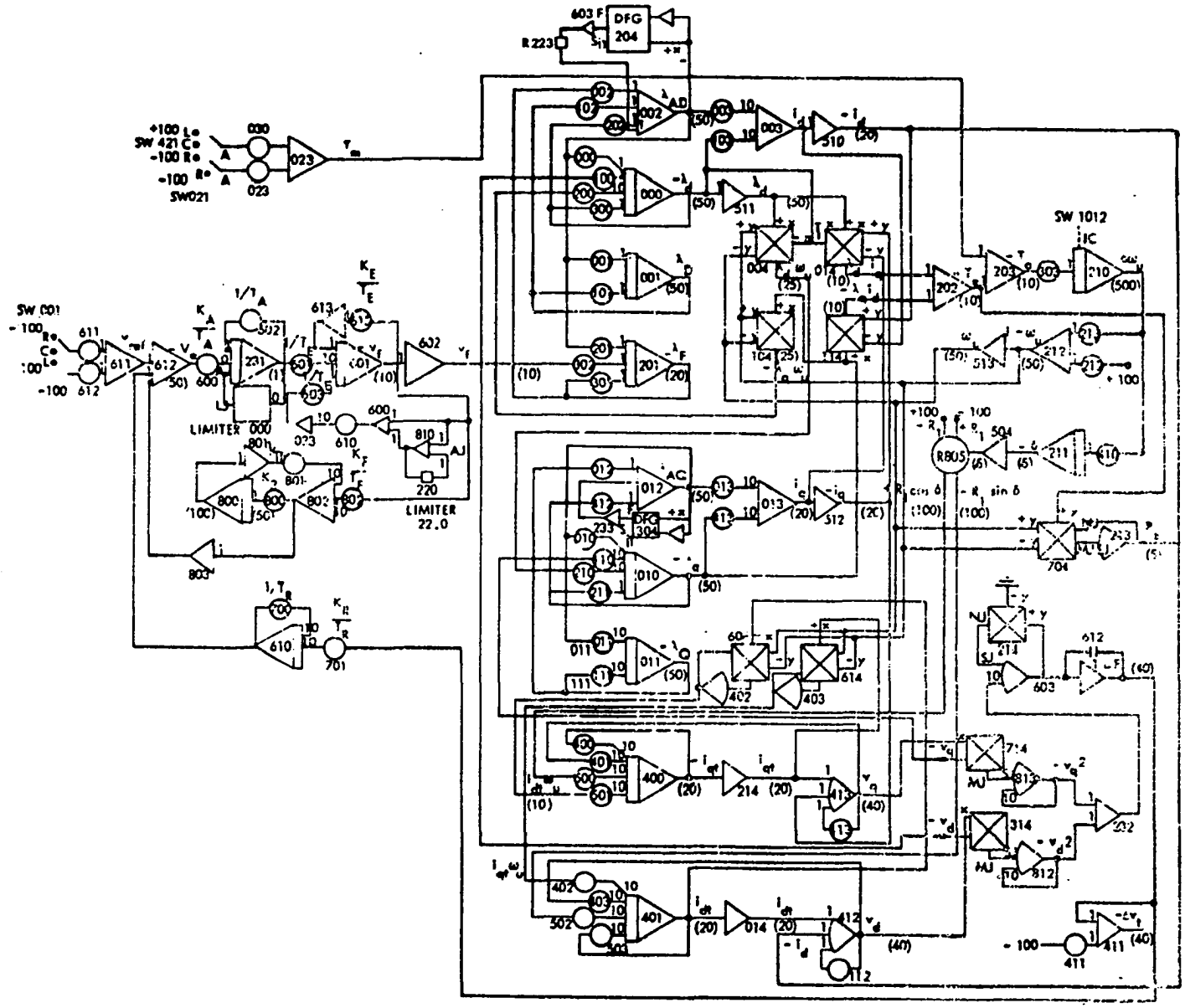

Figure 99. Simulation diagram for model IV with d-q-axes saturation

XIII. APPENDIX D. ON THE EFFECT OF LOCAL LOAD

As noted in section C of Chapter VI, the negative values of δ found there indicate the presence of a large local load on the machine terminals. This appendix describes the effects of local load. The amount of local load is controlled by the resistance R, which also is used for the computation of the machine terminal voltages v_d and v_q.

$$v_d = R(i_d - i_{dt}) \qquad [C-51]$$

$$v_q = R(i_q - i_{qt}) \qquad [C-52]$$

Equations C-51 and C-52, restated above for convenience, show how v_d and v_q are related to the currents if a resistance R is connected to the terminals of the machine. The analog computer implementation of the equations is shown in Figures 93 and 94 where potentiometers 112 and 113 are used for R. As shown in Table 25, the potentiometer setting required for an R of 100 per unit is 0.005 when the summing amplifiers 412 and 413 are used as high gain amplifiers. Disconnecting the one meg-ohm feedback resistor changes 412 and 413 to high gain amplifiers (32). If the feedback resistor is connected as was done in the simulations discussed in Chapter VI and potentiometers 112 and 113 are set at 0.005, then the value of R being used is 0.5 per unit which represents a large local load. The result of this is a δ of about -35 degrees when the generator has zero load. Thus the loading and system changes discussed in Chapter VI always add to or subtract from this fixed value of δ equals -35 degrees.

The equations for model III were developed for the special case of zero local load. Zero local load is approximated by letting R equal 100 per unit. R equals 100 per unit has been accomplished as has been

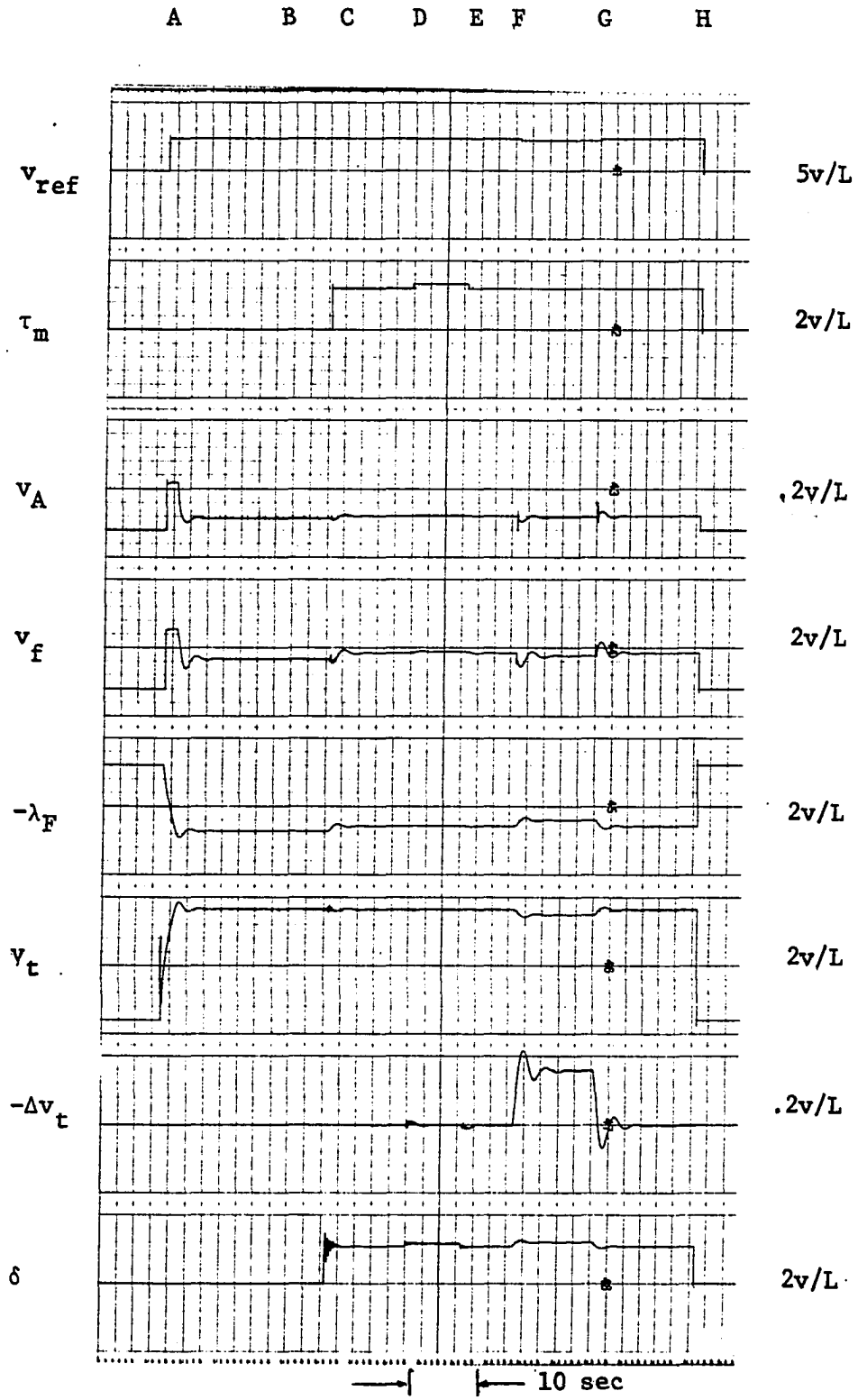

Figure 100. Initial response of model IV with the high response exciter and R = 100 p.u.

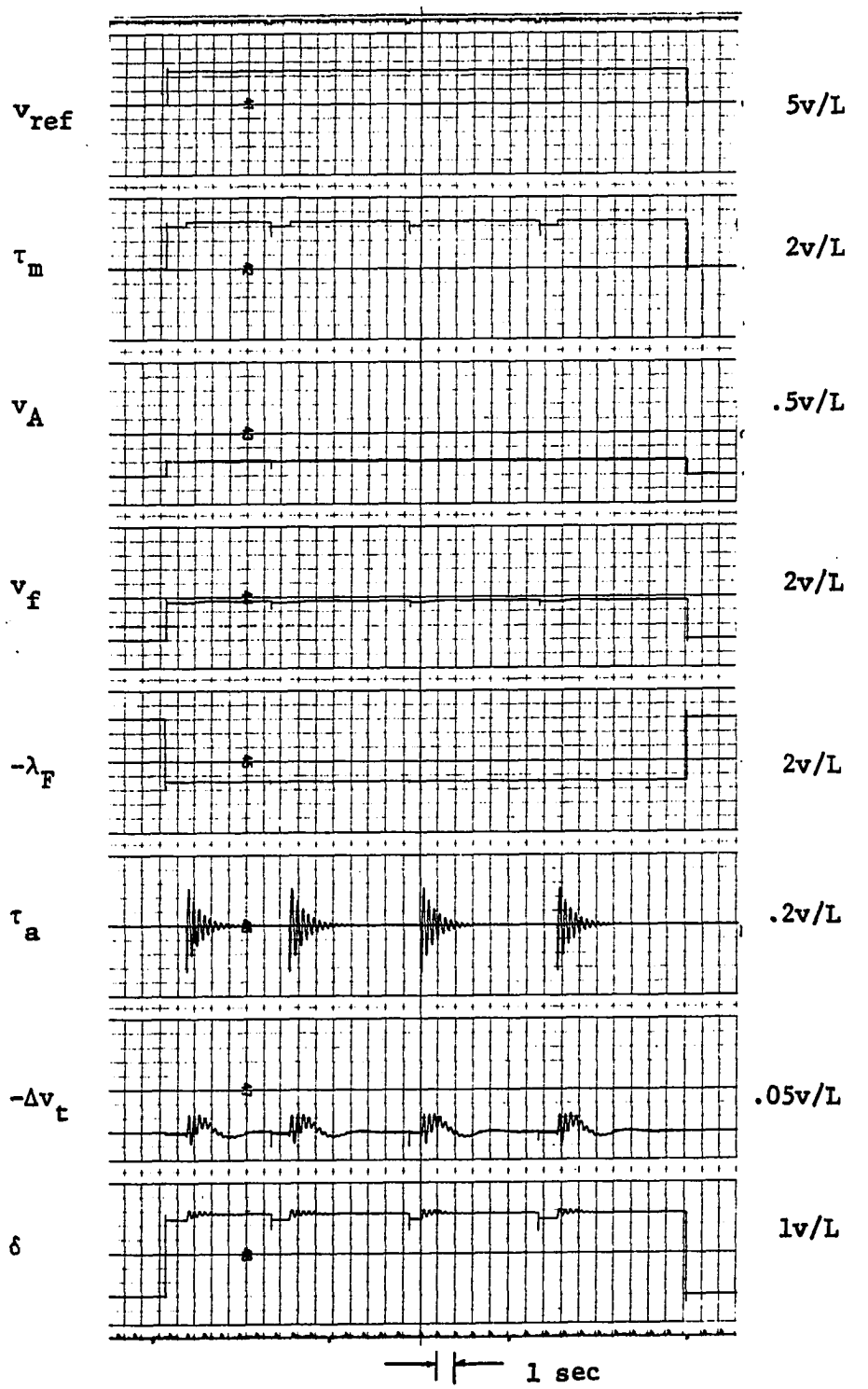

Figure 101. Response of model IV to $\Delta\tau_m$ with NLNS, LNS, LS and NLS using high response exciter and R = 100 p.u.

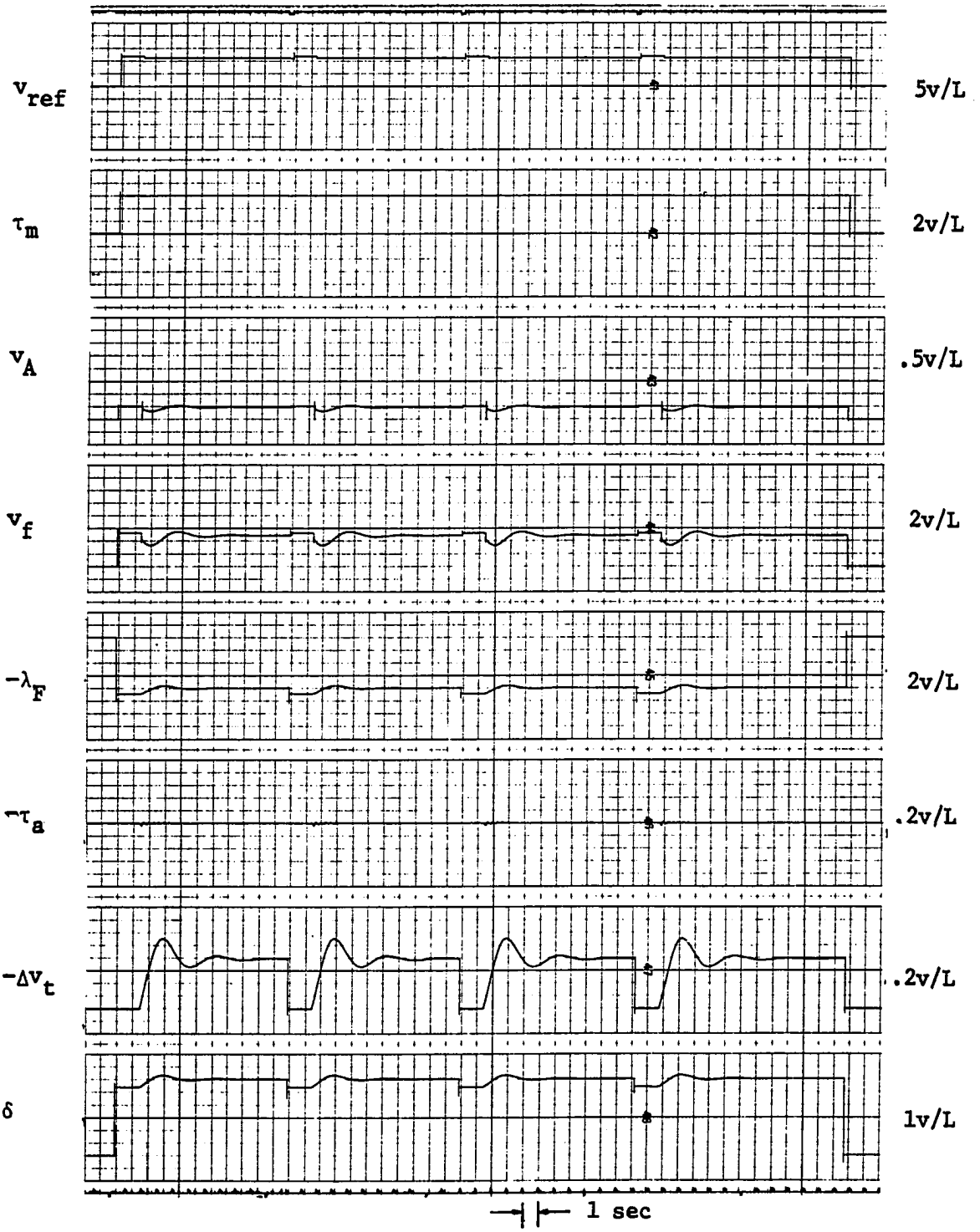

Figure 102. Response of model IV to Δv_{ref} with NLNS, LNS, LS and NLS using high response exciter and R = 100 p.u.

described in the foregoing. The remainder of this appendix is devoted to comparisons of performance with and without local load.

Figures 100, 101 and 102 are a rerun of Figures 56, 59 and 61, respectively, when R equals 100 per unit was used. In this case the exciter saturation is approximated by the two segment straight-line setup shown in Figure 99. A comparison of Figures 100, 101 and 102, respectively, with 56, 59 and 61 shows some differences in the response shown in the corresponding figures.

A comparison of the performance with and without local load indicates that the system is more oscillatory without local load. (Compare the δ and τ_a traces.) Field voltage is lower without local load. This suggests less reactive generation without local load. A subsequent determination of initial operating conditions verifies the result that lower v_f accompanies the zero local load operating condition.

The more oscillatory response without local load implies that an effect of local load is to increase damping.

Model III was developed with no local load and the corresponding linearized machine constants shown in Table 21, page 187, were determined for no local load. Hence the damping corresponding to no local load has also been determined. Table 27 shows the effect of local load on damping coefficient D.

Table 27. Summary of damping required for R = 0.5 p.u. and R = 100 p.u.

	Setting of Pot 812	D_u=237(P.S.) (Per unit torque-sec^{-1})	(D_u/ω_e)=.628(P.S.) (Per unit torque-sec/rad)
R = 0.5 p.u. Fast exciter	.2080	49.30	.1305
Slow exciter	.2268	53.75	.1425
R = 100 p.u. Fast exciter	.1250	29.65	.0785
Slow exciter	.1400	33.20	.0880

It is apparent that the effect of local load increases D significantly.

The following work establishes the initial loading conditions with and without local load.

Table 28. Steady state quantities used in compiling Table 29

Variable	Level volts	R = 0.5 p.u. Value volts	R = 0.5 p.u. Value p.u.	R = 100 p.u. Value volts	R = 100 p.u. Value p.u.
v_d	40	-34.74	-0.86850	-46.53	-1.16325
v_q	40	+73.63	1.84075	+66.49	1.66250
v_t	40	81.47	2.03750	81.20	2.03000
i_d	20	-46.03	-2.30150	-31.75	-1.58750
i_q	20	10.69	0.53450	13.76	0.68800
i_{dt}	20	-11.12	-0.55600	-31.52	-1.57600
i_{qt}	20	-63.31	-3.16550	+13.42	0.67100
δ	0.5	- 6.88	-13.76°	26.97	53.94°
P_e	5	15.00	3.0	14.98	2.996
i_{dR}			-1.7455		-0.0115
i_{qR}			3.700		0.017

The initial or steady state conditions also serve as a means of studying the effect of the local load. Table 28 shows the steady state values both with and without the local load. First the value of R is verified with the initial conditions as shown in Figure 103.

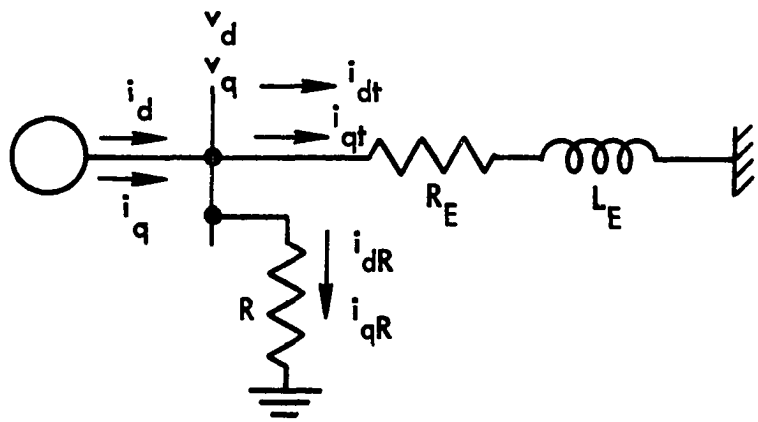

Figure 103. Diagram for computing R

Check for R = 0.5 p.u.

$$R = \frac{v_d}{i_{dR}} = \frac{-0.8685}{-1.7455} = 0.497 \text{ p.u.}$$

$$R = \frac{v_q}{i_{qR}} = \frac{1.8408}{3.70} = 0.498 \text{ p.u.}$$

Check for R = 100 p.u.

$$R = \frac{v_d}{i_{dR}} = \frac{-1.1633}{-0.0115} = 101.5 \text{ p.u.}$$

$$R = \frac{v_q}{i_{qR}} = \frac{1.6625}{0.017} = 98 \text{ p.u.}$$

The phasor diagrams for the steady state conditions are shown in Figure 104.

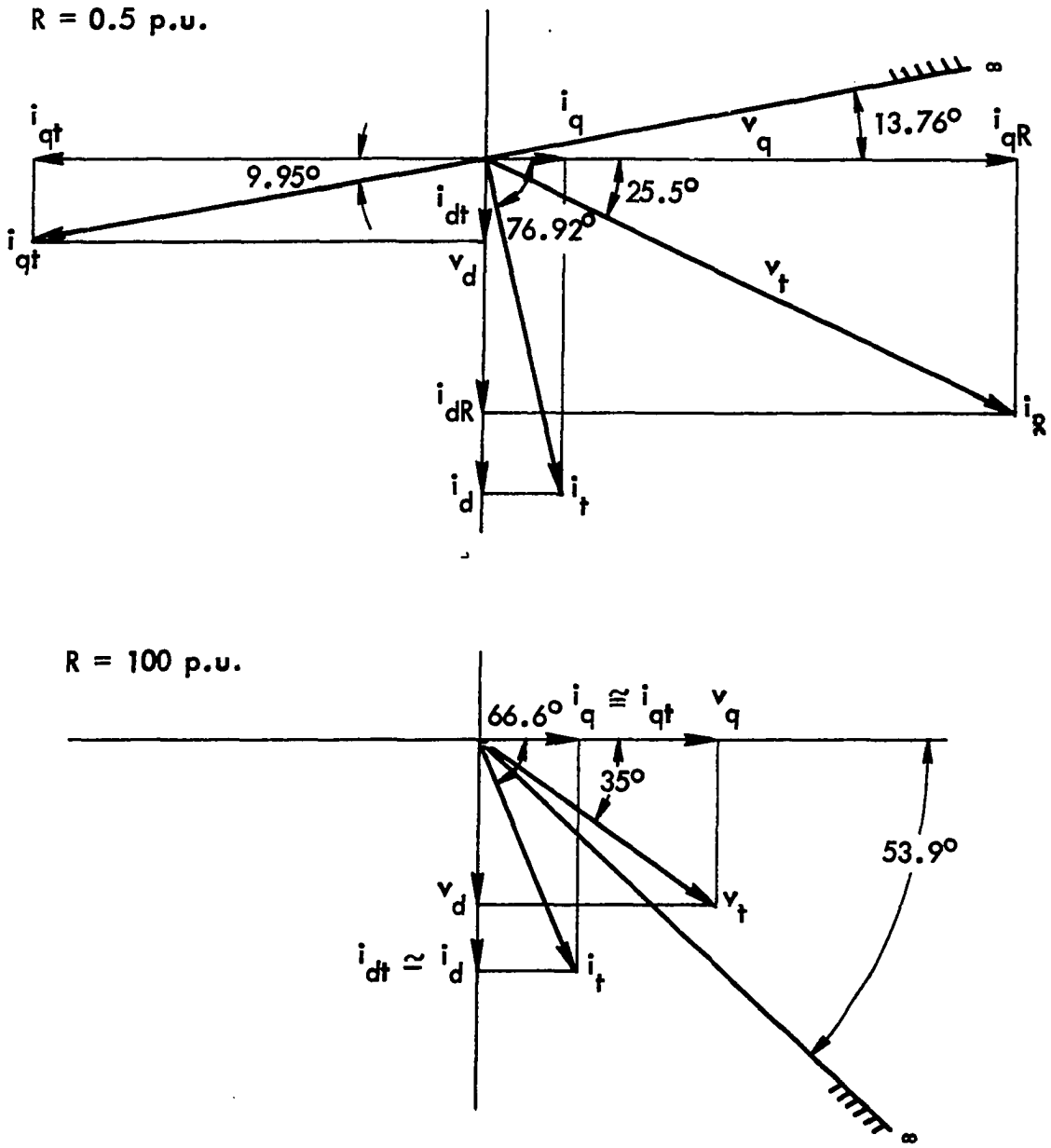

Figure 104. Phasor diagrams for the machine with and without local load

The odq quantities shown both in Table 28 and Figure 104 are converted to abc values as follows.

For R = 0.5 p.u.

$$v_{todq} = \sqrt{3}\, v_{tabc} = \sqrt{v_d^2 + v_q^2} \qquad [C-42]$$

$$v_{tabc} = \frac{1}{\sqrt{3}} v_{todq} = \frac{1}{\sqrt{3}}(2.0375) = 1.172$$

$$i_{tabc} = \frac{1}{\sqrt{3}}\sqrt{i_d^2 + i_q^2} = \frac{1}{\sqrt{3}}(2.36) = 1.348$$

$$i_{atabc} = \frac{1}{\sqrt{3}}\sqrt{i_{dt}{}^2 + i_{qt}{}^2} = \frac{1}{\sqrt{3}}(3.22) = 1.835$$

$$i_{Rabc} = \frac{1}{\sqrt{3}}\sqrt{i_{dR}{}^2 + i_{qR}{}^2} = \frac{1}{\sqrt{3}}(4.09) = 2.335$$

Similarly for R = 100 p.u.

$$v_{tabc} = \frac{1}{\sqrt{3}}(2.03) = 1.16$$

$$i_{tabc} = \frac{1}{\sqrt{3}}(1.732) = 1.00$$

$$i_{atabc} = \frac{1}{\sqrt{3}}(1.715) = 0.98$$

$$i_{Rabc} = \frac{1}{\sqrt{3}}(.0205) = 0.0117$$

Using the phasor diagrams and the abc quantities the values shown in Table 29 are computed as follows.

For R = 0.5 p.u.

$$P_G = v_{tabc}\, i_{tabc} \cos \theta$$

$$= 1.172(1.348) \cos (76.92 - 25.5)$$

$$= 1.58 \cos 51.42$$

$$= 0.985 \text{ p.u.}$$

$$Q_G = v_{tabc}\, i_{tabc} \sin \theta$$

$$= 1.58 \sin 51.42$$

$$= 1.235 \text{ p.u.}$$

$$P_R = R i_{Rabc}^2$$

$$= 0.5(2.335)^2 = .5(5.45) = 2.725$$

$$= 2.725 \text{ p.u.}$$

$$P_L = P_G - P_R = 0.985 - 2.725$$

$$= -1.740 \text{ p.u.}$$

$$Q_L = 1.235 \text{ p.u.}$$

Similarly for R = 100 p.u.

$$P_G = v_{tabc}\, i_{tabc} \cos \theta$$

$$= 1.16(1.0) \cos (66.6 - 35)$$

$$= 1.16 \cos 31.6$$

$$= 0.99 \text{ p.u.}$$

$$Q_G = v_{tabc}\, i_{tabc} \sin\theta = 1.16 \sin 31.6 = 0.61 \text{ p.u.}$$

$$P_R = Ri_{Rabc}^2 = 100(0.0117)^2 = 0.0136 \text{ p.u.}$$

$$P_L = P_G - P_R = 0.99 - 0.0136 = 0.9864 \text{ p.u.}$$

$$Q_L = 0.61 \text{ p.u.}$$

The foregoing considerations are summarized in Figure 105 and Table 29. The difference in the var output of the machine Q_G explains the differences in the field voltage v_f noted while comparing Figures 101 and 102, respectively, with Figures 59 and 61.

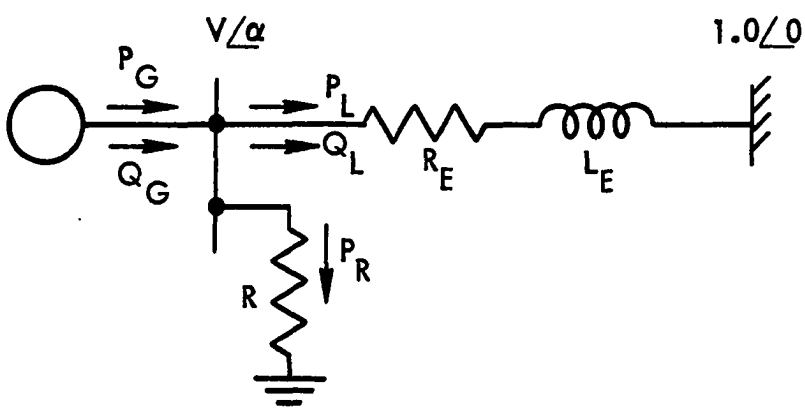

Figure 105. A machine connected to an infinite bus through a transmission line

Table 29. Comparison of variables shown in Figure 105 for R = 0.5 p.u. and R = 100 p.u.

R	V	P_G	P_R	P_L	α	δ	Q_G	Q_L
0.5	1.172	0.985	2.7250	-1.7400	-39.26°	-13.76°	1.235	1.235
100.0	1.160	0.990	0.0136	+0.9864	+18.9°	+53.94°	0.610	0.610